Effects of Bond Deterioration Due to Corrosion on Seismic Performance of Reinforced Concrete Structures

Thesis in partial fulfilment of the requirements for the degree of

Master of Engineering in Civil Engineering

By

Anton Kivell

Department of Civil and Natural Resources Engineering

University of Canterbury

New Zealand

2012

Abstract

Reinforced concrete structures deteriorate throughout their lifetime. This is particularly apparent in structures subjected to aggressive environments, which results in corrosion of reinforcing steel. Designers make allowances for accelerated deterioration in these environments in an attempt to ensure the durability of the structure. To combat corrosion, improved concrete characteristics and additional concrete cover are used to increase the protection provided by concrete to reinforcing. In spite of these measures, cracking of structures in service and from natural hazards can limit the effectiveness that these measures provide. Ultimately, this results in structures suffering from corrosion, which affects their strength, stiffness, and ductility. While strength reduction can be associated directly with a reduction in bar area, impacts on stiffness and ductility are associated with more complex mechanisms, one of which is bond deterioration. A key assumption in reinforced concrete design is that there is perfect bonding between steel reinforcing and surrounding concrete to allow for strain compatibility to be assumed. Perfect bond does not exist and diminished bond performance due to corrosion deterioration further violates this assumption, the effects of which are not fully understood.

This thesis investigates the effects of bond deterioration due to corrosion on the seismic performance of reinforced concrete structures. 60 monotonic and cyclic pull-out tests were undertaken on corroded reinforced concrete specimens, with corrosion levels ranging from 0% to 25% reinforcing mass loss. Additional tests were also conducted on specimens with variations in the amount of confining steel to simulate losses in confinement associated with corrosion of confining steel. Experimental results were used to develop corrosion and confinement dependent cyclic bond-slip model.

The proposed bond-slip model was then used to modelling pull-out of reinforcing bars detailed in accordance with New Zealand design standard NZS3101. Analyses were performed at a range of corrosion levels, levels of confinement, and uncorroded bond strengths. These showed that pull-out of reinforcement occurred at as little as 8% corrosion in low strength, unconfined conditions.

Multi-spring modelling of standard reinforced concrete columns, representing a bridge pier to foundation connection, was performed at the full range of deterioration with allowance for bond slippage. These analyses showed significant reductions in stiffness occurring with increased corrosion levels as well as reduced ductility and possible pull-out of reinforcement.

Acknowledgements

I would like to start by thanking my supervisory team of Dr Alessandro Palermo and Dr Allan Scott. You have shared your experience, knowledge, wisdom and time with me and I am grateful for everything you have done for me over the past two years. Over this time I feel like I have gained two friends along with many memories and experiences academically, socially, and on the sporting field.

I would also like to thank Prof Athol Carr for his assistance in implementing the Bond-slip hysteretic model within Ruaumoko and for sharing his wealth of knowledge and patience with me.

Throughout my postgraduate studies I have spent many hours in the University of Canterbury laboratories with the lab technicians, in particular Tim Perigo, Alan Poynter, Stuart Toase and John Maley. Without your help and practical know-how I would never have been able to design, construct and test any of my experimental programme.

Through post-grad I have meet many interesting people from many different walks of life and from around the world. Those who I have become closest to are those who I have shared E324 with. A few have come and gone but Joe Good, Job Byrne, Mark Hannah, Chris Lai have all become people who I would call my good mates. We have shared many awesome times in our little corner and out at BYO's and the experience would have been nothing without you all. While studying I also spent a lot of time with the Lads (and a Lass from time to time) of 2a Montana Ave. These are a special group of people who I have become particularly fond of and to say that I have a few memories from the place would be an understatement. Daz, Sturat, B.J, Nicky T, P. Don, LeeRoy, Wendy Dean, Tessa Jane, thanks for the memories, too many good times to count. To E324 and 2a Montana, cheers guys this is for you;

"You guys might not know this, but I consider myself a bit of a loner. I tend to think of myself as a one-man wolf pack. But when my sister brought Doug home, I knew he was one of my own. And my wolf pack... it grew by one. So there... there were two of us in the wolf pack... I was alone first in the pack, and then Doug joined in later. And six months ago, when Doug introduced me to you guys, I thought, "Wait a second, could it be?" And now I know for sure, I just added two more guys to my wolf pack. Four of us wolves, running around the desert together, in Las Vegas, looking for strippers and cocaine. So tonight, I make a toast!" *Allan, The Hangover*

Thank you to my girlfriend Tarryn who has kept me smiling every day and correcting my English.

Finally I would like to thank my parents. You have given me every opportunity I could hope for and all the support I needed. You have stopped at nothing to teach me about life and yet let me make my own mistakes (like post-grad). This Thesis is dedicated to you and all you have done for me. Thank you.

Anton Kivell

12th March 2012

Table of Contents

Table of Figures

List of Tables

Nomenclature

K	Percentage corrosion (%)
T_m	Monotonic back-bone curve
T_m*	Damage reduced monotonic backbone curve
T_R	Bond rupture stress
$T_{R,K}$	Bond rupture stress at corrosion level 'K'
$T_{R,\Omega}$	Bond rupture stress at confinement level 'Ω'
$T_{R,0}$	Uncorroded bond rupture stress
T_f	Ultimate frictional stress
$T_{f,K}$	Ultimate frictional stress at corrosion level 'K'
S_R	Bond rupture slip
S_P	Slip where the rupture stress plateau ends
S_f	Slip where purely frictional behaviour begins
Ω	Stirrup Index of Confinement
n_{st}	Number of stirrup legs,
A_{st}	Area of an individual stirrup leg,
n_p	Number of anchored bars,
A^*_p	Longitudinal section area of one anchored bar is the influence length.
Q	Concrete Index of Confinement
b	Width of the specimen
φ_p	Longitudinal bar diameter
Δz	Spacing between stirrups.
λ_n	Bond reduction factor
$\tau_{max}(n)$	Maximum stress in the 'n^{th}' cycle
$\tau_{max}(1)$	Maximum bond stress in the initial loading cycle
κ	Ratio of the maximum bond stress to that in the first cycle
n	number of loading cycles
ξ_K^N	Corrosion influence factor
m_t	Mass loss
I	Current (Amps)
M	Molar mass of element
z	Valency of the element
t	Time
F	Faraday's Constant
α	Frictional damage-energy constant
β	Rate damage-energy constant
α_K	Frictional damage-energy factor at corrosion level 'K'
β_K	Rate damage-energy factor at corrosion level 'K'
f'_c	Concrete compressive strength (MPa)
A	Sliding damage constant
B	Sliding damage constant
C	Sliding damage constant
E	Hysteretic energy
E_0	Energy under the monotonic pull out model curve prior to initiation of purely frictional behaviour
E_f	Frictional hysteretic energy
E_0	Ultimate frictional stress multiplied by the ultimate friction slip

T_0	Fully confined, undamaged bond rupture stress.
l_{sp}	Depth of strain penetration
ϕ	Diameter
n(x,t)	Concentration at depth ‘x’ and time ‘t’
n(0)	Surface concentration
erfc	Error function
x	Depth into cover concrete
D	Diffusivity constant
$i_{corr}(1)$	Corrosion current
$i_{corr}(t_p)$	Corrosion current after time t_p
t_p	Time after initiation of corrosion
w/c	Water to cement (binder) ratio
f_u	Ultimate steel stress
f_y	Yeild steel stress
ε_f	Fracture steel strain
d_b	Bar diameter
l_p	Plastic hinge length
r	post-yield stiffness (Takeda hysteresis)
α	Unloading constant (Takeda hysteresis)
K_u	Unloading stiffness (Takeda hysteresis)
β_1	Reloading constant (Takeda hysteresis)
K_p	Reloading stiffness (Takeda hysteresis)
β_2	Sliding constant (Takeda hysteresis)
K_s	Sliding stiffness (Takeda hysteresis)
α_a	Factor for reduced bond performance due to bleed water in fresh concrete (NZS3101)
L_{db}	Bond development length (NZS3101)
d_b	Reinforcing bar diameter (NZS3101)

1 Introduction

Reinforced concrete structures are subject to deterioration over their lifetime, particularly those subjected to aggressive environments. Corrosion of reinforcing due to ingress of aggressive agents results in damage to cover concrete and degraded reinforcing steel. In design, allowances are made for aggressive environments in an attempt to ensure the durability of the structure. Improved concrete characteristics and additional concrete cover are utilised to increase protection provided by concrete to reinforcing. However, variability in materials and construction accuracy can lead to structures deteriorating at higher rates than anticipated and corrosion becoming a threat to their longevity. In addition to this, cracking of structures in service and from natural hazards can limit the effectiveness that these measures provide.

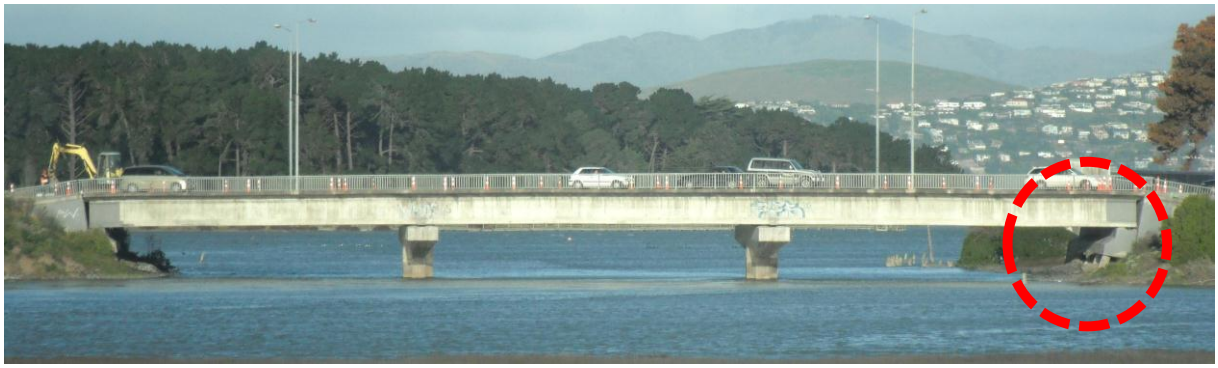

(a)

(b) **(c)**

Figure 1-1: Damage to bridges following the February 2011 Christchurch Earthquake; (a) Overview of the South Brighton Bridge, circle indicating the location of photo (b); (b) Cracking and spalling of concrete piles at South Brighton Bridge, Christchurch; (c) Spalling of cover concrete at the New Brighton Pier, Christchurch.

Two examples of such damage are shown in Figure 1-1 following the 2011 Christchurch earthquake (Palermo et al. 2011) where spalling of the cover concrete of a pile (b) and pier column (c) has left reinforcing steel exposed in marine environments. While these examples show severe damage, even minor cracking can significantly decrease the ability of concrete to protect reinforcing bars (Scott and Alexander 2007).

Ultimately, damage results in increased rates of corrosion deterioration, which affects strength, stiffness and ductility. Transverse reinforcement is particularly susceptible as it is afforded the least concrete cover. Loss of transverse reinforcement has a significant effect on confinement which is crucial in ensuring ductile behaviour in reinforced concrete members.

While strength reduction can be loosely associated with a reduction in bar area, the impacts on stiffness and ductility are associated with more complex mechanisms, one of which is bond deterioration. A key assumption in reinforced concrete is that there is a perfect bond between steel reinforcing and surrounding concrete. Even under perfect bonding conditions, minor elastic bond deformation occurs. With inclusion of diminished bond performance due to corrosion, bond deformation may become a significant factor in sectional and member response.

The interrelated effects of bond performance, corrosion of reinforcing and seismic performance will be examined in this thesis. This can be seen visually in Figure 1-2.

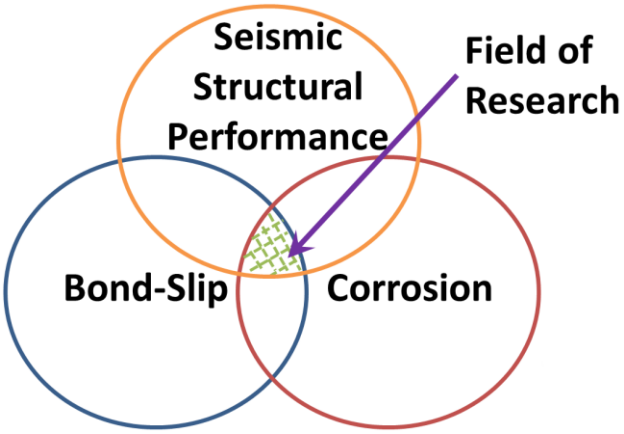

Figure 1-2: Field of research

Effects of corrosion are most commonly associated with a loss of cross section, however corrosion of reinforcement impacts a number of other factors, with some of these causing follow-on effects that accelerate degradation further. Figure 1-3 shows the relationship between corrosion and structural performance and each of their inter-related mechanisms.

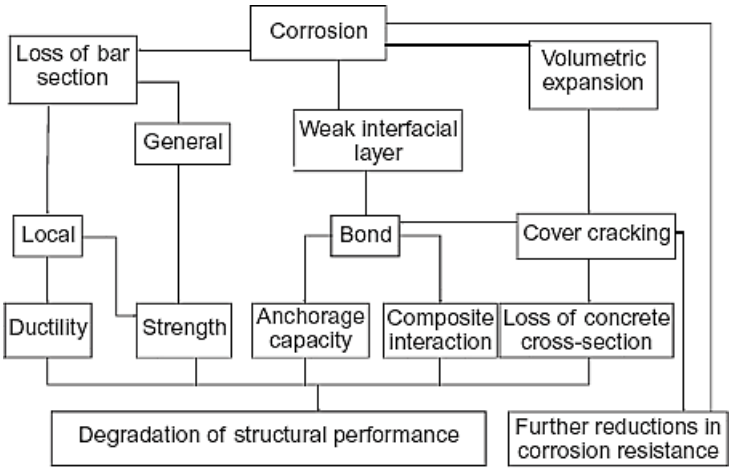

Figure 1-3: Effects of corrosion on structural capacity (Cairns et al. 2008).

Investigations into the effects of corrosion on bond performance provided evidence of the significant reductions in bond capacity that corrosion causes under monotonic loading (Almusallam et al. 1996; Al-Hammoud et al. 2010). In addition to this, limited investigations into cyclic performance have been undertaken which also showed large variations with increased corrosion (Fang et al. 2006a).

Research in the 1980's developed a comprehensive model for uncorroded cyclic bond performance (Eligehausen et al. 1983). This cyclic model will be used as the foundation for the analysis of the data gathered. The model uses energy encapsulated by the stress-slip hysteretic relationship to determine the level of bond degradation under repeated generalised cyclic loading.

The performance of corrosion affected structures can be impaired under seismic loading (Biondini et al. 2011), altering the deformation mechanism from that desired under capacity design principles (Park and Paulay 1975; Paulay and Priestley 1992). Degradation in bonding may also impact more recently developed design aspects that rely on bond development (slotted beams (Au 2010), precast frames) resulting in pull-out rather than rupture of embedded reinforcement. Recent experimental investigations such as those undertaken by Ou et al. (2010), have looked into corroded column performance and found that due to higher damage levels to transverse reinforcement, fracture of shear reinforcement rather than a ductile flexural failure governed that failure of specimens.

1.1 Description

This thesis investigated the effects of bond deterioration due to corrosion on the seismic performance of reinforced concrete structures. Sixty monotonic and cyclic pull-out tests were undertaken on corroded reinforced concrete specimens, with corrosion levels ranging from 0% to 25% mass loss of reinforcing. Some specimens included variations in the amount of confining steel to simulate losses in confinement associated with corrosion of confining steel. These experimental results were used in development of a corrosion and confinement-dependent bond-slip model. Numerical multi-spring modelling of reinforced concrete joints, mimicking a pier to foundation connection in plastic hinge

zones, was performed at the full range of deterioration with allowance for bond slippage. Findings from these were used to assess the expected impacts on seismic performance of degraded bonding of corrosion affected reinforcement in reinforced concrete structures.

This thesis is divided into six chapters, the first of which is the introduction. Chapter 2 outlines the existing research in each of the fields of research that is applicable to the thesis topic. Chapter 3 provides a full experimental methodology along with testing results and discussion on experimental findings. Chapter 4 analyses the experimental findings to determine trends and relationships. These were implemented within a cyclic bond model developed to allow for corrosion deterioration and altered confinement in determining bond performance. In Chapter 5, the proposed model from Chapter 4 is implemented within a multi-spring representation of a reinforced concrete section and analysed to determine the effects of bond deterioration on moment-curvature behaviour. Analysis is also performed on a model of a New Brighton Pier column with simulated deterioration for 50 years following the Christchurch earthquake, to determine its expected lifecycle performance. Finally, Chapter 6 summarises the conclusions of each chapter.

1.2 Objectives

The scope of this thesis was to improve understanding of corroded reinforced concrete structures under earthquake loading. The key areas of interest are;

- bonding performance of corroded (0%-25%) reinforced steel under monotonic and cyclic loading.
- effects of reduced confinement on bond performance of lightly (<5%) corroded bars.
- degradation effects to hysteretic properties of corrosion affected reinforced concrete sections.
- effects of bond deterioration on the seismic performance of reinforced concrete structures.

The outcomes of this investigation allowed for better prediction and assessment of the seismic lifetime for newly designed and existing reinforced concrete structures. Research into bond behaviour of corroded reinforcing under cyclic loading has been limited. This thesis builds upon existing data while assessing in greater depth, the effects of confinement on corroded cyclic bond. The ultimate outcome of this project was a corrosion level and confinement level-dependent model for bond slip under reversed cyclic loading. In addition, numerical analysis of concrete section behaviour provided an improved understanding of seismic behaviour on corroded reinforced concrete structures.

2 Literature Review

Existing research into corrosion of steel reinforcement in concrete has focused on the measurement, prevention and repair of damage. Research on the effect of corrosion on seismic performance began to be investigated in the late 2000's and is a field of increasing interest. Existing research can be divided into the following groups; bonding, corrosion mechanisms, methods recreating corrosion in the laboratory, and structural behaviour looking at both experimental work and numerical methods. The current body of knowledge on these subjects is outlined in this chapter.

2.1 Uncorroded Bonding between Steel Reinforcing and Concrete

It is critical that the reinforcing be detailed in such a manner that steel reinforcing yields before bond between steel and concrete ruptures allowing ductile behaviour. Because of this, bonding of reinforcement has been an area of much investigation. In regions where inelastic bar strains develop, demand on bond strength can be very high. A common area for this to occur is around beam column joints (Paulay and Priestley 1992). With the introduction of capacity based design in the 1970's (Park and Paulay 1975), ductile behaviour became a crucial component in design of structures in seismic environments. There have been numerous attempts made to model and evaluate bond strength (Rehm 1968; Semchenkov et al. 2009; Verderame et al. 2009) and performance is well understood for tradition construction methods.

Bond is provided through two mechanisms; cohesion and chemical adhesion at the concrete-steel interface, and mechanical interlocking between reinforcing ribs and concrete (Park and Paulay 1975). Chemical adhesion, shown as v_a in Figure 2-1, is the primary form of resistance in round bars, which also resist through limited mechanical interlock due to bar surface roughness. Mechanical interlock acts to resist bar movement through providing stresses normal to the interface surface at rib locations. These forces, f_b in Figure 2-1, are transferred to surrounding concrete, which then must resist through concrete cohesion, v_c, the combined adhesion and mechanical interlock forces.

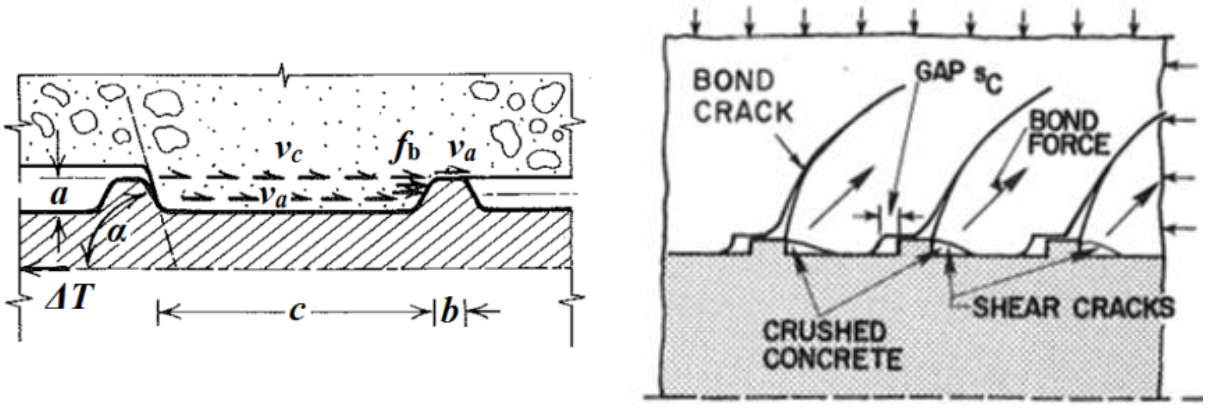

Figure 2-1: Bonding mechanisms, Left: (Park and Paulay 1975), Right: (Eligehausen et al. 1983)

Eligehausen, Popov et al. (1983) showed how initial elastic bonding response was associated with formation of bond cracks, shown in Figure 2-1. As loading increases, concrete crushing begins to occur at the compressed face of ribs, producing minor inelastic deformation. After further loading, arced shear cracks occur between the lug top and flat bar surface, initiating sliding accompanied by additional crushing. Under cyclic loading this process is reversed with bond cracking in the opposite direction.

Plizzari et al. (1998) provided a relationship between confinement and bond rupture stress. This relationship specifically noted that additional confining steel above a certain level has little effect on rupture stress. The index of confinement used by Plizzari et al.(1998) consists of two components relating to confinement from stirrups and concrete. The 'Stirrup Index of Confinement', Ω, was used to quantify the level of confinement provided by stirrups used in specimens. The equation for this is shown as Equation 2-1, which relates the total area of stirrups, $n_{st}A_{st}$, to the area of the longitudinal section of anchored bars, $n_pA^*_p$.

$$\Omega = \frac{n_{st}A_{st}}{n_pA_p^*} \qquad \text{Equation 2-1}$$

n_{st} represents the number of stirrup legs, A_{st} is the area of an individual stirrup leg, n_p is the number of anchored bars, A^*_p is the longitudinal section area of one anchored bar in the influence length. The 'Concrete Index of Confinement', Q, is the ratio between the net cross-sectional area of concrete between stirrups and the cross-sectional area of stirrups. This is given in Equation 2-2;

$$Q = \frac{(b - n_p\varphi_p)\Delta z}{n_p\varphi_p\Delta z} \qquad \text{Equation 2-2}$$

where b is the width of the specimen, φ_p is the longitudinal bar diameter, n_p is the number of longitudinal bars, and Δz is the spacing between stirrups. These indices provide a measure of the level of confinement provided to a developing reinforcing bar.

2.2 Corrosion

Corrosion mechanisms are generally well understood and structural design that allows for the likelihood of corrosion is common in design codes in most countries (Hansson et al. 2006). Corrosion is an electrochemical process which results in the oxidation of iron in steel reinforcing bars. Iron oxides lose their metallic properties of strength and ductility, diminishing the performance of steel reinforcing. The iron-oxide products have a lower density than the pure metal, causing expansive pressure to be exerted on surrounding concrete, resulting in damage to the concrete. The expansive properties are exacerbated by any moisture available to the products of corrosion.

Design codes focus on maintaining reinforcing steel integrity by protecting it from its environment with cover concrete. Concrete is very well suited to this application, as it can be durable, impermeable, and provides passivation for steel reinforcing. In NZS3101 (Standards New Zealand 2006), durability is dictated by four factors; depth of cover concrete, concrete strength (water/cement ratio), admixtures or use of supplementary cementicious material, and the environment in which the structure is to stand. There are situations though, where the protection provided by covering concrete is not sufficient, or damage to cover concrete results in the onset of corrosion, limiting its durability.

As well as loss of steel section, the expansive nature of steel corrosion can cause delamination and spalling of cover concrete that in turn accelerates the corrosion process further. Accelerated deterioration also occurs in areas that are subjected to repeated wetting and drying cycles of salt water. These areas have regular replenishment of high concentrations of chloride ions on the surface along with a regular supply of oxygen (Costa and Appleton 2002).

While concrete provides a good protective barrier against deterioration of steel reinforcing its low tensile strength makes it prone to cracking. Cracks in concrete can leave reinforcing directly exposed to the environment, allowing accelerated ingress of aggressive agents. This was confirmed by Mohammed et al. (2003) and Raupach (1996) who found significant increases in micro and macro cell corrosion and also oxygen permeability in cracked areas of specimens tested in the laboratory.

2.2.1 Corrosion Mechanisms

Concrete provides a passive environment for reinforcing steel, preventing oxidation by allowing the formation of a gamma-ferric oxide layer on the steel surface which is reliant on an alkaline environment. Over time, aggressive agents can penetrate cover concrete resulting in activation of corrosion of reinforcing steel. External agents are primarily chlorides and carbon dioxide. Chlorides break down the insoluble gamma-ferric oxide protective surface into a soluble iron chloride which forms on reinforcement. Carbonation results in the neutralisation of alkaline conditions in the concrete, which are required for the formation for the gamma-ferric oxide layer. These who

mechanisms work in different ways, but achieve the same result which is loss of the protective gamma-ferric oxide layer, initiating the oxidation of iron.

Corrosion is an electro-chemical process in which iron is oxidised. It requires the presence of iron and oxygen, along with a conductive medium to allow for ion exchange. Cover concrete not only provides an alkaline environment that maintains a protective oxidised layer, it limits access of oxygen to steel due to its dense micro structure.

Corrosion occurs through two mechanisms, micro-cell corrosion and macro-cell corrosion, each with different characteristics. Micro-cell corrosion is a term that describes the active dissolution and corresponding cathodic half-cell reaction that takes place on adjacent locations of the same metal (Hansson et al. 2006), this is shown in Figure 2-2. It commonly occurs in reinforced concrete structures due to carbonation of cover concrete, where ingress of carbon dioxide from the environment neutralises alkaline cover concrete. Under micro-cell corrosion, steel corrodes in a uniform manor with a layer of corrosion product forming on its surface. Because of this uniformity and the slow rate at which carbonation progresses, micro-cell corrosion is the more benign of the two mechanisms (Hansson et al. 2006).

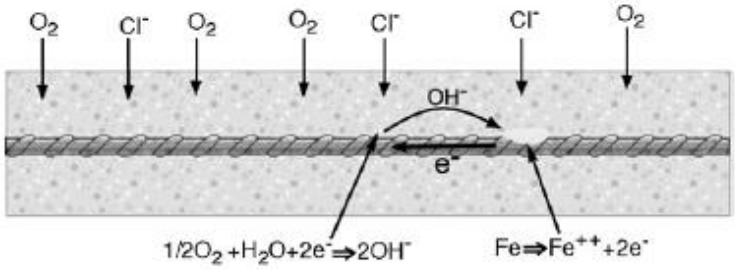

Figure 2-2: Illustration of micro-cell corrosion. (Hansson et al. 2006)

In macro-cell corrosion, large regions of reinforcing will act as a cathode in the oxidation reaction, removing electrons from the isolated anodic regions, thereby driving the corrosion process. Anodic regions do not have to be in close proximity to oxygen, as electrons can travel from the area of dissolution to the cathodic site through reinforcing steel. The cathodic area will be in a position where there is oxygen available to supply the reduction reaction, as shown in Figure 2-3. This mechanism causes concentrated corrosion in steel reinforcing known as pitting, which results in rapid loss of cross-sectional area of reinforcement. Loss of steel cross-section reduces the tensile capacity of reinforcement and the pitting nature of macro-cell corrosion causes stress concentration at locations where pitting occurs, resulting in isolated losses in capacity.

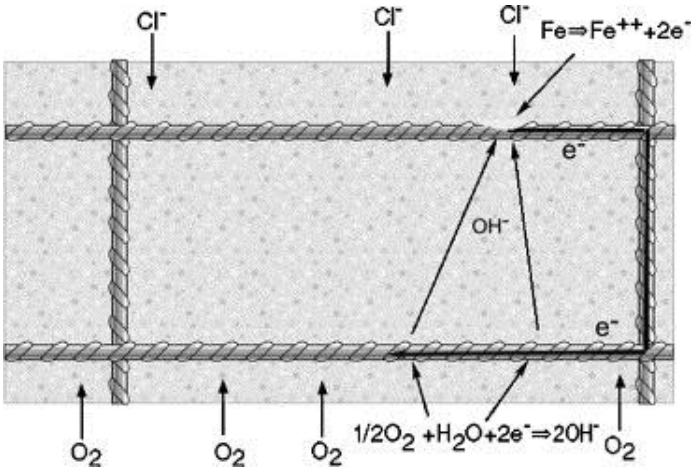

Figure 2-3: Illustration of macro-cell corrosion. (Hansson et al. 2006)

2.2.2 Prediction

While corrosion mechanisms are understood, prediction and measurement of corrosion through depassivation of steel and initiation of corrosion itself is far from precise. Due to numerous uncertainties involved, a probabilistic approach is the most appropriate and this is what has been used by Darmawan (2010) in modelling pitting corrosion. For many structures, signs of their distress are only apparent after significant internal damage has already occurred. Because of this, structures that are exposed to aggressive environmental conditions often require repair over their lifetime.

Probabilistic approaches have been adopted that focus on two transport mechanisms; diffusion and convection (Val and Trapper 2008). It is noted that humidity also plays a role in the rate of chloride ion ingress and so modelling of structures in the tidal zone is likely to be problematic. Results showed large discrepancies between the 1D and 2D modelling approach and it was recommended that 2D modelling be used for members of similar sectional dimensions such as columns and beams.

One of the more advanced prediction methods is known as cellular automata, in which finite regions (cells) are subjected to external aggressive agents over time and their spread through a section is determined through probabilistic methods based on the concentration of adjacent cells. This method has been used by Biondini et al (2004) in analysis of reinforced concrete members in 2D and 3D, in a bid to determine their future, deteriorated performance.

All these models provide an indication of the expected concentration of aggressive agents at a particular position or depth within a concrete section. In many cases the concentration that initiation of corrosion occurs, when steel reinforcements protective gamma ferric oxide layer breaks down, is not well defined. Furthermore, durability models do not provide an accurate indication for the rate of deterioration after initiation occurs.

Scott and Alexander (2007) published a paper investigating the effects of cracking, supplementary cementitious material (SCM), and cover depth on corrosion rate. Findings from the paper showed that

cracking, SCM's, and cover all play a role in corrosion rates. The reasons for this are associated with concrete resistivity and oxygen availability. From their results, an indication of the mass loss density, or percentage mass loss, can be determined using Faraday's law. Unfortunately, determining the exact location and bar area over which this mass loss occurred proved difficult to determine and somewhat subjective.

2.2.3 Corrosion Product Properties

Corrosion products of steel display lower density than the iron from which they come. This results in a tendency for expansion of reinforcement as corrosion propogates. Oxidation of iron produces a number of different products depending on the availability of oxygen and water. Weizhong et al. (2010) produced a table that determines the expansive nature of each common corrosion product when compared to metallic iron (Table 2-1). From this it can be seen that expansion of the most common corrosion product, Fe_2O_3, is highly dependent on the level of hydration. When hydrated by 3 : 1 ratio of H_2O molecules (H_2O:Fe_2O_3) , the volume factor triples, making the moisture content of corrosion products a critical factor in determining their expansive pressure.

Table 2-1: Parameters of relevant iron oxides and -hydroxides. Adapted and translated from Weizhong et al. (2010)

Chemical Formula	Molar Volume (cm^3/mol)	Volume Factor (Fe)	Colour
Fe	7.11	1.00	Silver
Fe0	12.61	1.77	Black
Fe_20_3	15.24	2.14	Auburn
Fe_20_3 . H_2O	22.21	3.12	Yellow
Fe_30_4	14.9	2.10	Black
$Fe(OH)_2$	26.4	3.71	White
$Fe(OH)_3$	34.25	4.82	Reddish Brown
a-FeOOH	20.76	2.92	Yellow
γ-FeOOH	21.73	3.06	Orange
Fe_20_3 . $3H_2O$	46.22	6.50	Reddish Brown

.

Zhao et al. (2011), used x-ray diffraction to determine the chemical composition of corrosion products and their associated expansive coefficient. Samples were taken from three environments: (a) a steel plate which was near to or on the coast, (b) reinforcement of a R.C port structure, and (c) a reinforcing bar that had been electrochemically treated in a NaCl solution. The coefficients of expansion for these samples are shown in Table 2-2.

Table 2-2: Expansion coefficients for rust products (Zhao et al. 2011)

Sample	Rust Expansion Coefficient
(a) Near to or on the coast	2.85
(b) Splash zone	3.02
(c) Electrochemical treatment in NaCl solution	2.64

Based on the environmental exposure to oxygen, Zhao (2011) proposed the following factors that can be used to determine the likely expansion of rust products depending on oxygen availability, humidity, and presence of chlorides, which are shown in Table 2-3.

Table 2-3: Rust expansion coefficients for differing environments (Zhao et al. 2011)

	Humidity		
Oxygen Availability	**High –** long term water contact/submerged	**Medium-** tidal/splash zone	**Low-**normal atmosphere
High- exposed to air directly	3.3	3.1	2.9
Medium- After cover cracking	3.2	3.0	2.8
Low- Immersed in water of before cover cracking	3.1	2.9	2.6

2.3 Accelerating Corrosion

Several methods have been adopted by researchers to reproduce deterioration due to corrosion in a reasonable time frame. Some of these are outlined in the following section.

2.3.1 Electrochemical Corrosion

Electrochemical acceleration of corrosion is the most common method used to accelerate corrosion in research investigating corroded bond strength. This method has been widely used in literature (Almusallam et al. 1996; Cabrera 1996; Lee et al. 2002; Fang et al. 2004; Fang et al. 2006a). Accelerated corrosion causes uniform corrosion along reinforcing, however, it has also been used in modelling of pitting corrosion through the inclusion of chlorides (Darmawan 2010) and after cracking corrosion occurs preferentially at crack locations.

The most common apparatus for electrochemical accelerated corrosion can be seen in Figure 2-4, taken from Fang et al. (2004) which uses partial submersion of the reinforcing steel in a 5% NaCl solution. Fang (2004) submerged specimens for 3 days prior to testing to ensure a uniform moisture distribution, after which an electrical current was passed through the solution and the specimen via a

stainless steel plane (unreactive conductor). Current was supplied at a rate between 0 and 2A. To support more realistic, non-uniform corrosion, a small (unspecified) amount of NaCl was added to the concrete during mixing. The submerged protruding steel was coated in paraffin and wrapped with an insulating plastic membrane.

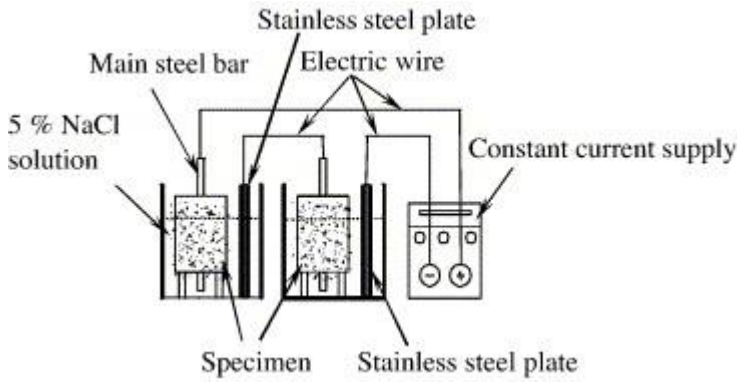

Figure 2-4: Electrochemical corrosion system as used by Fang et al. (2004).

The electrochemical method was also used to accelerate the corrosion of reinforcing bars encased in concrete to test the properties of the corroded steel bars (Almusallam 2001; Du et al. 2005), and used in conjunction with mechanical section reduction in reinforced concrete columns (Saito et al. 2007). Earlier research by Lee et al. (2002) used a similar apparatus with a 3% NaCl solution and copper plates as unreactive conductors. Prior research used a slight variation on this method, choosing to leave the reinforcing steel above the water level due to concerns that the electrolyte solution would remove some of the corrosion products from the bonding interface(Almusallam et al. 1996; Cabrera 1996). Cabrera (1996) included a reference electrode to allow for measurement of the difference in potential between the solution and the steel bar.

Yingshu et al. (2007) found advantages in keeping the corroding steel bar above the solution level as to avoid the dissolution of oxidation products; this provided a more realistic surface around the reinforcing bar. Yingshu et al. (2007) tested large scale models and due to the increased size of the specimens, the researchers elected to incorporate a stainless steel cathode at the centre of the reinforcing cage to act as an additional electrode.

Lee et al. (2000) tested seven columns subjected to accelerated corrosion. In order to limit corrosion to the desired section of the columns and eliminate any end effects, regions outside the test area were epoxy coated. In addition to this, the concrete was intentionally contaminated with NaCl (2% by mass) to help depassivate steel reinforcing. Slow initiation of corrosion was observed, along with low corrosion rates. This was attributed to the central location of the stainless steel cathode in the column, requiring ions to travel large distances between electrodes and oxygen to diffuse nearly 150mm to the reaction site. In later testing, columns were cast with a hollow, perforated, stainless steel pipe as the internal cathode. Optimum levels of corrosion were observed with a cycle of 1 day wet and 2.5 days

dry. The greatest amount of cracking was observed just above the level of the wet dry cycling suggesting increased corrosion due to better access to oxygen.

2.3.2 Salt Spray Exposure

One system to simulate the effects of marine environments is the salt spray (fog) test performed in accordance with ASTM B117. This system was used by Papadopoulos (2007) to corrode steel reinforcing bars with the hope that the spray method would mimic the natural environment better than other methods. The spray used was 5% NaCl and the test was performed under controlled conditions in a salt spray chamber.

2.3.3 Artificial Climate

Repeated wet-dry cycling in a NaCl solution was adopted by Tsai et al. (2008) who submerged steel samples in a solution of 10 times the concentration of seawater for 24 hours and then dried them for 24 hours at 70^{o}C repeatedly. This was found to reduce the testing time by 75%, but the increased temperature increased the equivalent age of the concrete, resulting in increased strength and reducing corrosion of the reinforcing. A similar method was adopted by Yingshu et al. (2007) where beams were kept at 40^{o}C with high humidity (80%) and a 5% NaCl solution was sprayed over them for 1 hour, followed by 7 hours of infrared light shining upon them with limited success.

2.3.4 Mechanical Section Reduction

Mechanical section reduction has been found to be a suitable method of recreating pitting corrosion in steel reinforcing bars (Cairns et al. 2005). Cairns et al. (2005) used a hemispherical end to a milling cutter to drill out some of the section, as shown in Figure 2-5. The reduction in maximum tensile load that the section could carry was proportional to the change in section area, though the reduction in yield load was slightly less than expected, and there was a significant reduction in ductility due to limiting of yielding to the defect area (Cairns et al. 2005).

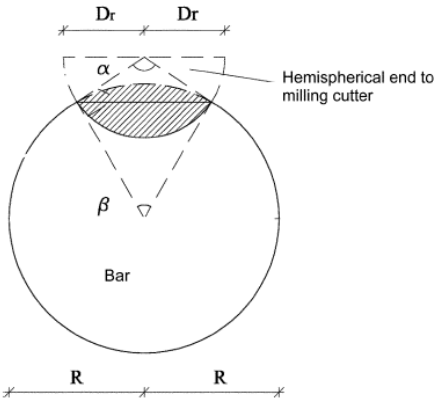

Figure 2-5: Machined defect geometry (Cairns et al. 2005).

This method has also been used to mimic isolated section reduction (pitting) in recent research (Saito et al. 2007). Instead of hemispherical milling, Saito et al. (2007) opted to scrape the section of bars in the region where corrosion was desired over a 200mm length of bar. Included in this region were roundly scraped portions to simulate heavily pitted sections of bar. While this method is suitable for recreating the mechanical behaviour of reinforcement, the usefulness of it in recreating bond damage is limited.

2.3.5 General

Yingshu et al. (2007) assessed the comparative performance between the artificial climate and electrochemical methods. Testing of beams found that the electrochemical method resulted in a sudden failure in the beam due to bond failure in the main corroded tension bars. The electrochemical method provided macro-cell corrosion on the entire bar surface, whereas the artificial climate provided corrosion only on the surface facing the concrete cover. It was also noted that the chemical composition of the corrosion products differed depending on the test method (Yingshu et al. 2007). The time to reach cracking took 3 months for the artificial climate but only 3 days for the electrochemical approach (using 1 Amp applied current), this fast reaction is suspected to lead to insufficient supply of oxygen to the anodic region thus differing the chemical composition of the corrosion products. The paper concludes that the corrosion product produced by an artificial climate gives a more realistic representation of corrosion in the natural environment.

A similar study concluded that the electrochemical method was an effective way to study deterioration of reinforcing (Zhang et al. 2006). Zang et al. (2006) found that the natural environment impacted the ultimate deformation ability of beams, whereas the electrochemical method affected the degradation of stiffness more significantly.

2.4 Corroded Bond Performance

2.4.1 Corroded Monotonic Bond

The effects of corrosion on bond have been experimentally investigated by several researchers (Almusallam et al. 1996; Lee et al. 2002; Fang et al. 2004; Fang 2006a; Fang et al. 2006b; Lundgren 2007). This research has focused primarily on the performance under monotonic loading of round and deformed bars corroded using electrochemical techniques.

Findings from these papers were that bonding strength of round and deformed bars increases under mild corrosion (< 5% loss in cross-sectional area). Larger increases in bond strength were observed for round bars when compared to deformed bars, and was attributed to their reliance on friction to resist sliding as opposed to deformed bars where mechanical interlock provides the primary form of resistance. The expansive nature of corrosion products increased radial stresses and with them frictional resistance. Post rupture behaviour of round bars was found to be poor with a rapid loss of

capacity, whereas deformed bars showed only a slight decrease in sliding resistance provided adequate confinement was provided. Almusallam (1996) found that once corrosion reached high levels (>12%), effects of the deformed bars ribs, which provide interlock with the surrounding concrete, was lost and the corrosion products had a lubricating effect, significantly reducing bond capacity.

Effects of bar type and confinement can be seen in Figure 2-6 (Fang et al. 2004), where confinement provided by transverse reinforcement significantly increased the ultimate and post ultimate performance of the two samples shown. It is also clear that deformed bars have a greater bond capacity, though when unconfined, their post ultimate performance tends to be similar, with significant bond degradation.

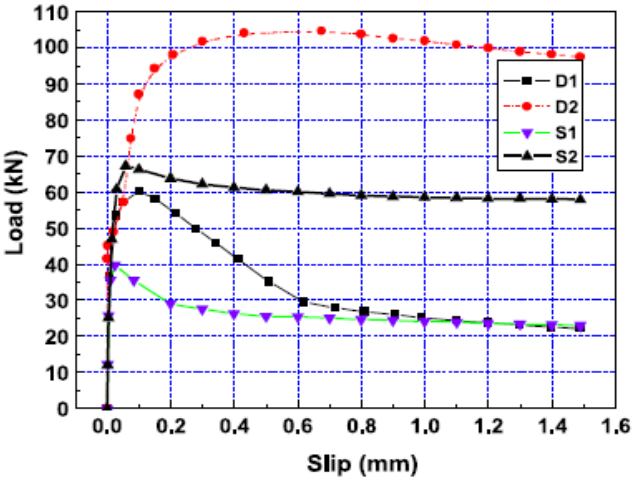

Figure 2-6: Effects of steel bar profile and stirrups on slip with a corrosion level of around 3%. (Fang et al. 2004) D refers to 'deformed bar', S refers to 'smooth bar' or 'round bar', 1 refers to 'without stirrups, 2 refers to 'with stirrups'.

Testing of corroded bond performance under monotonic loading was also performed by Kim et al. (2008). Specimens were unreinforced and effects of corrosion of bars prior to specimen construction and corrosion within concrete was investigated. Corrosion prior to construction was found to have little effect, though corrosion was limited to low levels (2%).

Internal corrosion was found to have negligible effects when less than 2%, but noticeable decreases in strength were observed beyond this, with 40% reduction in bond rupture stress observed at 5% corrosion. Variation was also observed in rupture slip as shown in Figure 2-7, with increased rupture slip observed at higher levels of deterioration.

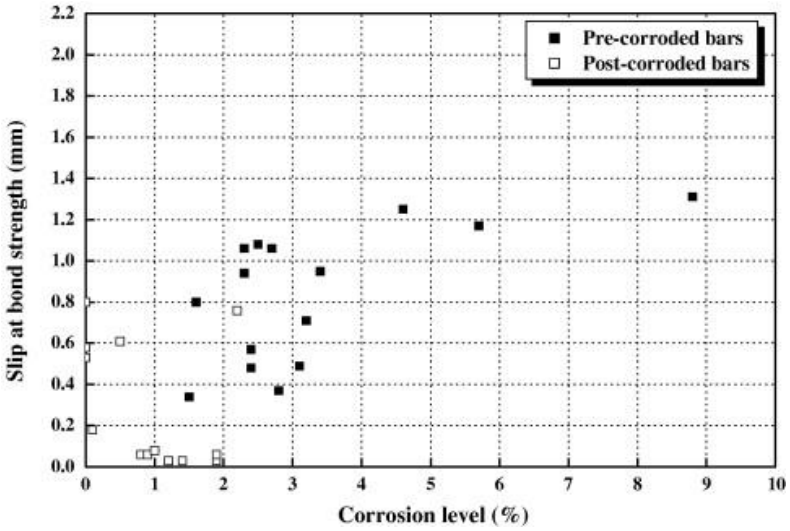

Figure 2-7: Slip at bond rupture with increasing bar corrosion (Chung et al. 2008).

2.4.2 Corroded Cyclic Bond

The effects of corrosion on bond-slip behaviour under cyclic loading have not been extensively investigated. Based on a limited number of tests Fang (2006b) it was concluded that corrosion of approximately 5% displayed the greatest level of bond reduction under cyclic loading. This level of corrosion has also been associated with giving the maximum bond strength capacity under monotonic loading (Fang et al. 2006a). The experiment set up used by Fang et al. (2006a) used small specimens with bonded bar lengths of only 80mm in an attempt to ensure uniform bond stresses occur along the bar. A drawing of the specimens used by Fang et al. (2006a) is shown below in Figure 2-8. The specimens tested by (Fang 2006b) were either 'confined', with two 6mm stirrups, or 'unconfined' where no stirrups were used. When cyclic testing under constant maximum displacement was performed the trend is as shown in Figure 2-9.

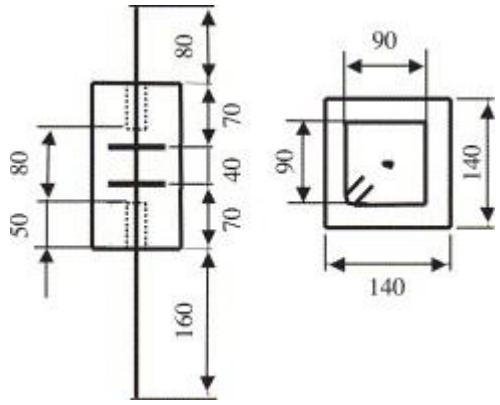

Figure 2-8: Specimen tested by Fang et al. (2006a) Left: Cross-section side, Right: Cross-section front

Confinement was shown play a critical role in maintaining bond strength under cyclic loading (Fang 2006b; Fang et al. 2006a; Al-Hammoud et al. 2010). It was also shown that performance is significantly reduced under cyclic loading once loading is reversed (Fang et al. 2006a). Cracking in concrete due to previous loading and unloading resulted in deterioration of bond stiffness in

uncorroded bars (Park and Paulay 1975) with similar behaviour also observed in corroded bars (Fang et al. 2006a). Cracking of specimens prior to testing was shown to reduce the stiffness and strength of bond for corroded bars. Round bars displayed a greater decrease in bond strength than deformed bars under initial load cycle. However, after 10 cycles, the reduction was much the same as that in deformed bars (Fang 2006b). An example of bond-slip behaviour under cyclic loading taken from Fang, Gylltoft et al. (2006a) is shown in Figure 2-9.

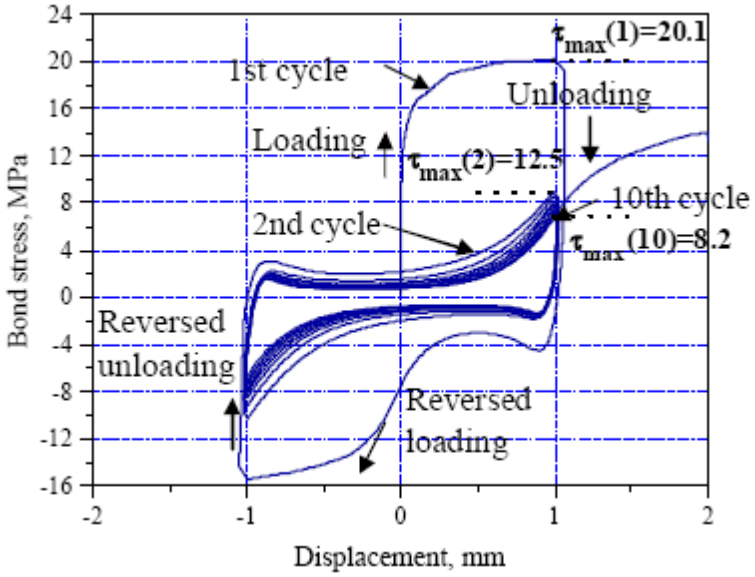

Figure 2-9: Typical bond-slip behaviour under constant displacement (Fang 2006b; Fang et al. 2006a)

Fang et al. (2006a) used a bond reduction factor, λ_n, to quantify the reduction in bond strength between various cycles, which is shown below in Equation 2-3.

$$\lambda_n = 1 - \kappa = 1 - \frac{\tau_{max}(n)}{\tau_{max}(1)} \qquad \text{Equation 2-3}$$

Where λ_n is the bond reduction factor, $\tau_{max}(n)$ refers to the maximum stress in the 'n^{th}' cycle, $\tau_{max}(1)$ refers to the maximum bond stress in the initial loading cycle and κ is the ratio of the maximum bond stress in that cycle to that in the first cycle. Larger values of λ_n indicate a greater reduction in bond. This equation was developed for use in constant displacement testing, thus behaviour under generalised loading is not investigated.

Fang (2006b) includes the effects of corrosion on the cyclic performance using ξ, the corrosion influence factor (CIF). This is defined in Equation 2-4;

$$\xi_K^N = \lambda_0^N - \lambda_K^N \qquad \text{Equation 2-4}$$

Where ξ_K^N is the CIF for corrosion level 'K' at the N^{th} cycle, λ_0^N is the uncorroded bond reduction factor and λ_K^N is the bond reduction factor for corrosion level 'K' at the N^{th} cycle. Figure 2-10 displays the results from four specimens of various corrosion levels. From Figure 2-10 it was concluded that

corrosion of ~5% displayed the greatest level of bond reduction under cyclic loading. This level of corrosion has also been associated with giving the maximum bond strength capacity under monotonic loading (Fang et al. 2006a), the relevance or reason for this is not discussed in this paper.

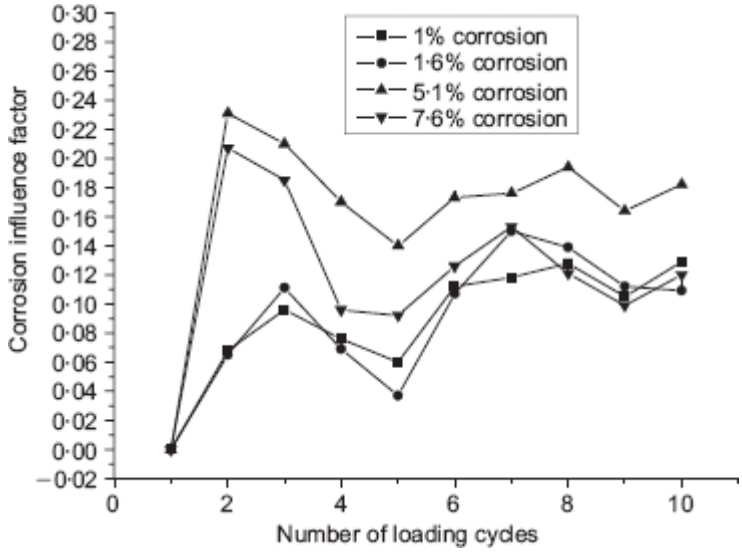

Figure 2-10: Corrosion influence factor (CIF) for different corrosion levels over 10 loading cycles. (Fang 2006b).

2.5 Experimental Performance of Corroded Structural Elements

A limited number of tests on structural members subjected to aggressive environments and under simulated earthquake or cyclic loading have been undertaken. Saito et al. (2007) investigated a series of corroded scale columns and found that electrochemical corrosion caused a reduction in the deformation capacity. Corrosion was induced on isolated sections of reinforcement in columns at the anticipated location of plastic hinges. Induced corrosion resulted in premature buckling of the longitudinal bars under testing due to reduced confinement.

Cairns et al. (2008) tested corroded simply supported beams, built with round bars and corroded to between 4% and 12%, under monotonic loading. It was found that both capacity and ductility of the beams increased with corrosion, as a consequence of decreased bond slip in the corroded beams. Similar testing was undertaken by O'Flaherty et al. (2010) on simply supported beams using deformed bars. It was observed that increased corrosion caused decreased stiffness with a change in failure mechanism from flexure to shear, observed at approximately 20% corrosion. This showed how corrosion differently affects bond behaviour differently depending on whether the reinforcing bars were round or deformed.

Rinaldi et al. (2010) also carried out prestressed beam testing, results are shown Figure 2-11. Rinaldi et al. (2010) also measured slip of the prestressing tendons, some of which slipped 30mm before

ultimate load was reached. From this it was concluded that simple reduction of reinforcement area to account for corrosion provided erroneous prediction of true behaviour, which matched findings from testing by Saito, Oyado et al. (2007).

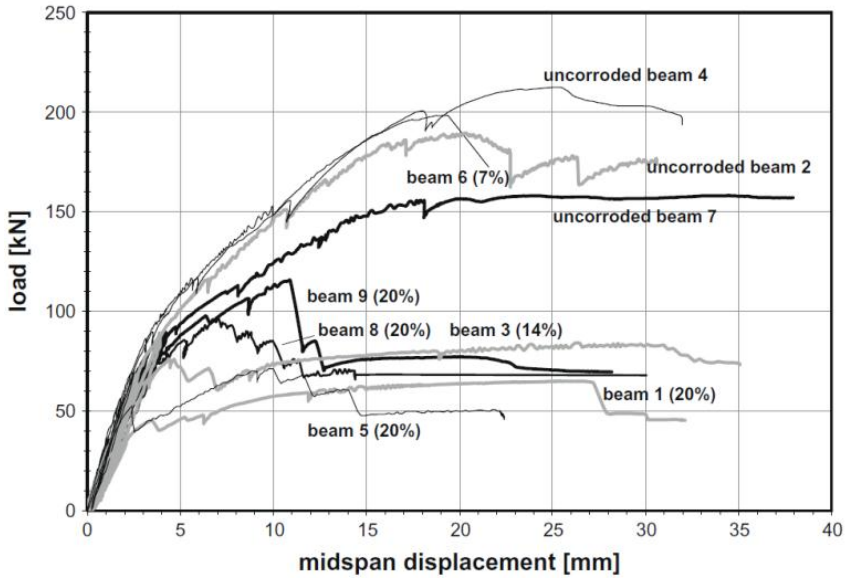

Figure 2-11: Load deflection plot for uncorroded and heavily corroded pre-stressed beams. (Rinaldi et al. 2010).

Yamakawa (1998) tested naturally corroded wall elements subjected to axial and cyclic lateral loading. It was concluded that while specimens showed outward signs of distress through cracking, deterioration of their cyclic performance was slight or not observed.

Ou et al. (2010) investigated the cyclic behaviour of corroded beams and found that transverse reinforcement, due to its smaller diameter, received higher levels of deterioration under their electrochemically accelerated corrosion set-up. Increased deterioration of transverse reinforcement, and its associate reduced reinforcement area, prompted a change in failure mechanism from flexure to shear. Prior to the complete shift to shear dominated failure, it was observed that there was a tendency for buckling of longitudinal reinforcement under flexural failure. This highlighted the role of confinement that transverse steel plays in producing ductile behaviour through buckling resistance. At lower level of deterioration, debonding of reinforcement was observed and attributed to increases in ultimate deformation capacity.

2.6 Micro-Modelling: Bond-slip

Several bond slip models have been proposed; those used in numerical modelling are usually monotonic, while no corroded cyclic bond models have been found in literature.

2.6.1 Uncorroded

Most monotonic bond-slip models follow a similar format as that used by Coronelli and Mulas (2001), which is shown in Figure 2-12, and allows for consideration of confined and unconfined bonding conditions. Similar models were also used by Oliveira et al. (2008) in finite element modelling of reinforced concrete beams. More simplified models using bilinear relationships with and without degrading stiffness were used by Sanchez et al. (2010) in finite element modelling of reinforced concrete beams. Kwak and Kim (2001) adopted a tri-linear monotonic model as shown in Figure 2-12.

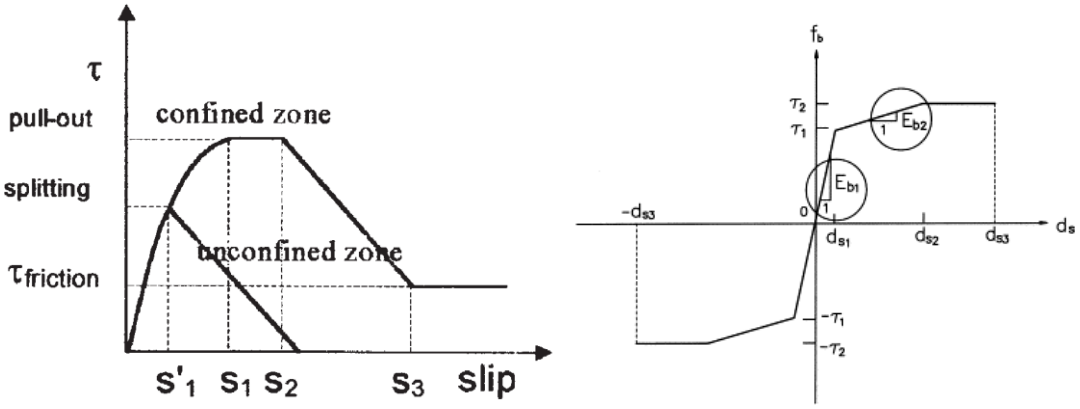

Figure 2-12: Monotonic bond-slip models, Left: Coronelli and Mulas (2001); Right: Kwak and Kim (2001)

An earlier piecewise linear bond-slip model proposed by Yankelevsky (1985), shown in Figure 2-13, was used for theoretical modelling of bar pull-out using simultaneous transcendental equations. Linear approximations were necessary due to limited computing power at the time.

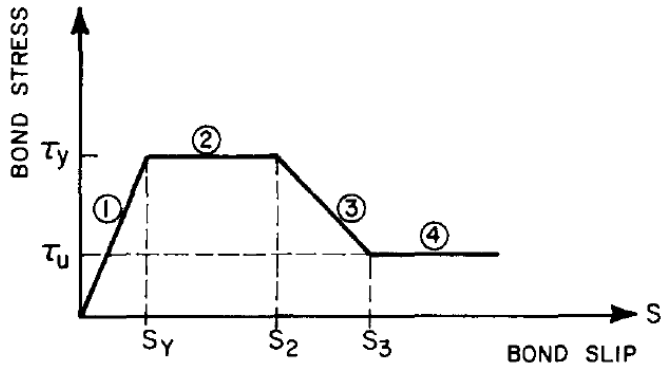

Figure 2-13: Monotonic bond-slip model. (Yankelevsky 1985)

One of the most widely used bond-slip hysteretic models was developed in 1983 (Eligehausen et al. 1983). This was based on the experimental results from 125 pull-out tests under reversed cyclic and monotonic loading. Specimens were constructed with various bar arrangements, sizes, and concrete strengths to recreate similar conditions to that around beam column joints. Results from testing produced a format for general hysteretic bond behaviour which can be seen in Figure 2-14. A significant drop in stress occurs when being reloaded along with slipping at constant stress along previously loaded sections. Experimental data showed decreasing bond stresses when reversed loading

is continued but with decreasing reductions in stress with each cycle. Provided that maximum slip remains less than rupture slip, the undamaged monotonic envelope (1 in Figure 2-14) can still be attained. When cycling exceeds the rupture slip, when reloaded, the monotonic envelope is reduced (5 in Figure 2-14).

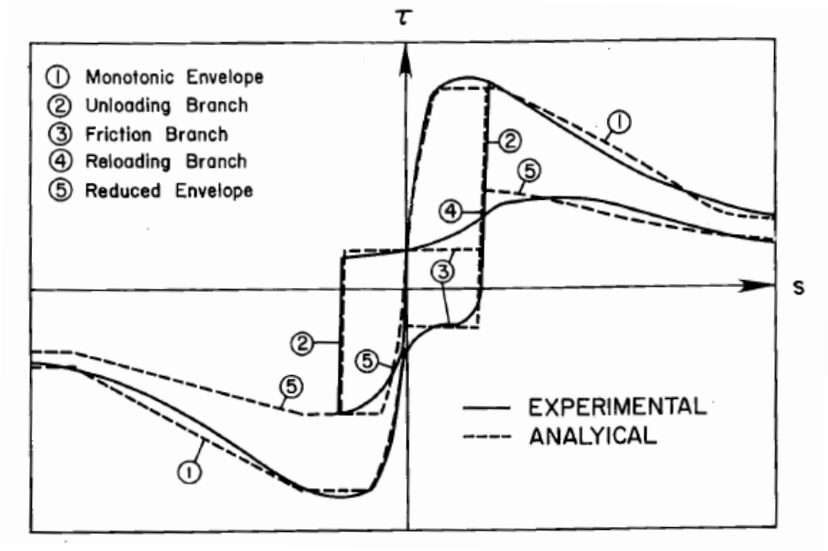

Figure 2-14: General relationship between bond stress and slip for monotonic and cyclic loading comparing experimental data with the analytical model. (Eligehausen et al. 1983)

Included within their model, Eligehausen et al. (1983) utilised relationships between dissipated bond energy and damage in order to determine the reduction in the monotonic envelope due to cyclic loading, as well as determining stress reductions to the frictional branch (3 in Figure 2-14). This allowed their model to capture generalised cyclic behaviour very effectively. It is acknowledged that this is a very simple model compared to the real behaviour, but it was believed to provide satisfactory agreement with experimental results and provides the most comprehensive cyclic model found in literature.

2.6.2 Corroded

Based on experimental testing, equations for reduction of bond rupture stress with corrosion have been proposed by Cabrera (1996), Lee et al. (2002), Stanish et al. (1999), Chung et al. (2004), Bhargava et al. (2007) and Chung et al. (2008).

These equations are displayed in Table 2-4. Effects of corrosion on bonding were represented by a curve through stress values or by normalising stress by uncorroded rupture stress values to show strength reduction.

Table 2-4: Existing equations proposed to account for the effects of corrosion (K) on rupture bond stress ($T_{R,K}$).

Paper	Equation
(Cabrera 1996)	$T_{R,K}$=23.478-1.313K (MPa)
(Lee et al. 2002)	$T_{R,K}=5.21e^{(-0.0561K)}$ (MPa)
(Stanish et al. 1999)	$T_{R,K}=\sqrt{f'_c}(0.77 - 0.027K)$ (MPa)
(Chung et al. 2004)	$\frac{T_{R,K}}{T_{R,0}} = 2.09K^{(-1.06)} \leq 1.0$
(Bhargava et al. 2007)	$\frac{T_{R,K}}{T_{R,0}} = 1.192K^{(-0.117K)} \leq 1.0$
(Chung et al. 2008)	$T_{R,K}=24.7K^{-0.55} \leq 16.87$ (MPa)

Lee et al. (2002) experimentally developed a relationship between corrosion level and bond rigidity, which can be seen in Figure 2-15. Bond rigidity was seen to decrease significantly even at low levels of corrosion (2%) which coincided with cracking of the unconfined specimens.

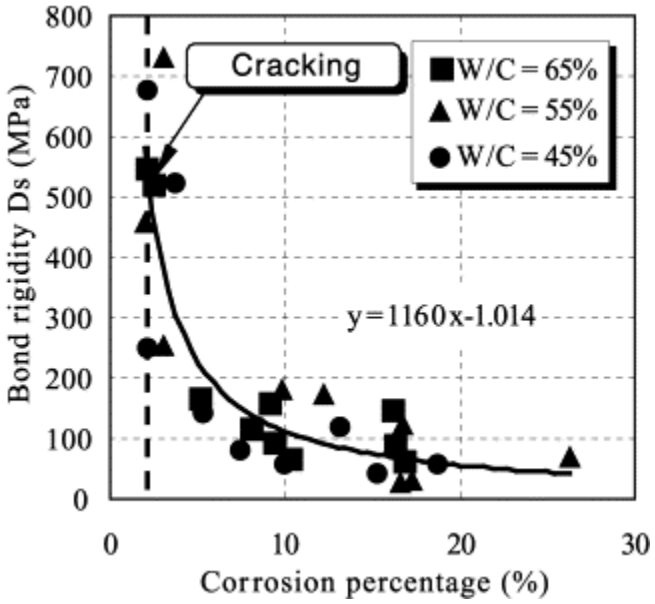

Figure 2-15: Bond rigidity with increasing corrosion (Lee et al. 2002)

No expressions were found in literature to account for corrosion effects of other characterisation points along the monotonic curve.

No cyclic bond-slip models were found within literature that included effects of corrosion.

2.7 Meso-Modelling: Structural Components

Coronelli and Mulas (2001) used finite elements to model the behaviour of a beam-column joint including effects of bond-slip. These effects were included through use of an interface element between the concrete and steel elements, which are shown in Figure 2-16. This was subsequently included in the global finite element model of the joint shown on the right in Figure 2-16. The results from this were found to have a very close correlation with experimental testing that was conducted. From the results of the experimental and finite element testing, a rotational spring model was produced for the global behaviour of the joint including bond-slip effects. When this was implemented into a lumped plasticity frame model, significant increases in the lateral deformability of the structure were observed as well as an altered distribution of ductility requirements, both attributing to reduced stiffness due to inclusion of bond-slip effects.

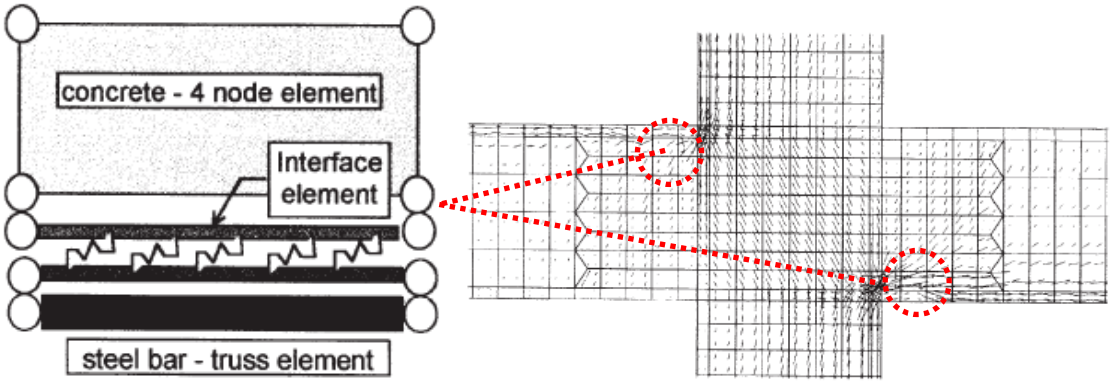

Figure 2-16: Left: Bond slip element used in global FEM model (Coronelli and Mulas 2001). Right: FEM mesh used to model a beam-column joint (Coronelli and Mulas 2001).

Recent work carried out at the University of Canterbury (Leung 2011) used discrete element modelling to model pull-out of corroded reinforcing based on experimental results (Kivell et al. 2011a; Kivell et al. 2011b). Models replicated experimental specimens and investigated effects of uniform and localised corrosion over the bonded length as shown in Figure 2-17. It was found that the corrosion pattern influenced reduction of bond strength, with uniform corrosion providing a larger reduction than localised corrosion for a given average percentage reduction in cross-section. Localised corrosion was found to induce a higher number of micro-crack in the reinforced concrete than uniform corrosion for the same average level of corrosion along the bonded length.

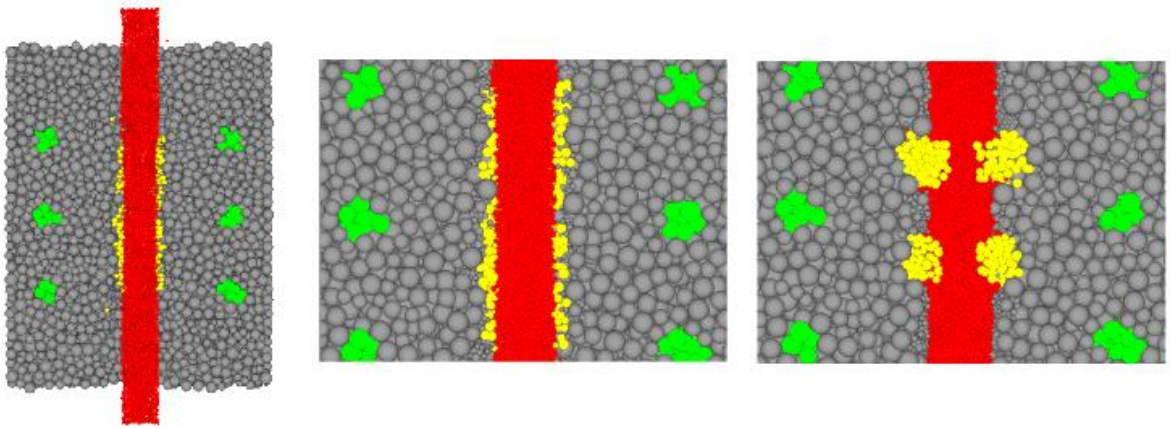

Figure 2-17: DEM model of experimental specimen monotonic pull-out testing, Left: Overview, Right: Uniform corrosion, Left: Pitting/localised corrosion. (Leung 2011)

2.8 Macro-Modelling: Global Structure

In addition to Coronelli and Mulas (2001), who looked at the effects of uncorroded bond-slip on structural performance, investigations into deteriorated structural behaviour have been undertaken. Berto et al. (2009) accounted for deterioration through reduced bar section, reduction in transverse and longitudinal reinforcing, reduced confinement, reduced bar ductility and degraded cover concrete properties. Based on the deteriorated section, revised moment-curvature behaviour was determined then implemented initially within a lumped plasticity model of a two storey, two bay, frame. Locations of deterioration were limited to an exterior column in one model and all ground floor columns in another. Deterioration resulted in reduced strength (~10%) and reduced displacement ductility (~30%). It was noted that even in sound condition, a soft storey deformation mechanism formed under pushover analyses. The same concept was then applied to a three-dimensional, four storey, five bay, R.C frame structure. Here there was a change in deformation mechanism from 'beam-sway' to 'soft-storey' when deterioration was limited to the ground floor. A three-dimensional model combined with isolated regions of deterioration caused a torsional response of the structure. Berto et al. (2009) acknowledged that "effects due to rebar slippage becomes of primary importance and cannot be neglected in the case of particularly aggressive attacks (high levels of corrosion)".

The effects of corrosion on bond strength are likely to have flow-on effects to the hysteretic performance of ductile frames. A reduction of bond strength of as little as 15% may result in a 30% reduction in total energy dissipation of a beam column joint (Filippou et al. 1983). Park and Paulay (1975) state that bond loss contributes to an overall loss of stiffness in reinforced concrete structures. Loss of bond can result in penetration of yielding into the anchorage zone, diminishing the available development length and reducing anchorage capacity.

Biondini et al. (2011) investigated the effects of deterioration due to corrosion on seismic performance. This was done through numerical modelling of aggressive agent ingress and damage caused using a process called cellular automaton (Biondini et al. 2004). Damaged sections were analysed and their moment curvature behaviour determined, then implemented in lumped plasticity models. Figure 2-18 displays findings of Biondini et al. (2011) from push-over analysis where, due to localised deterioration, the deformation mechanism was altered. After 30 years of simulated deterioration the deformation mechanism altered from 'beam-sway' to 'column-sway' resulting in significant reduction in displacement ductility of the structure and reduced energy dissipation. In addition to this, the ultimate base shear showed a gradual reduction to around 20% of undamaged capacity after 50 years.

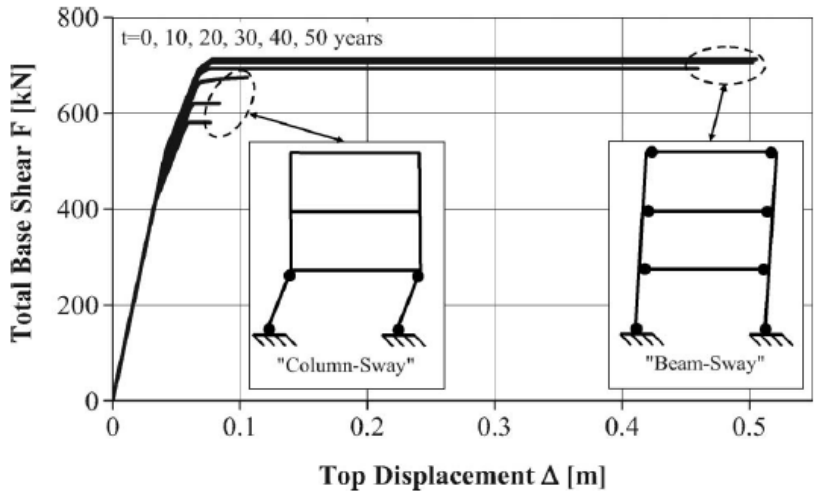

Figure 2-18: Effects of corrosion over 50 years on structural performance (Biondini et al. 2011).

2.9 Motivation

From the literature review it can be seen that there has been a significant amount of research carried out on bond-slip and corrosion separately. Gaps in knowledge lie in the effects of corrosion on cyclic bond-slip behaviour. Fang (2006a; 2006b) and Fang et al. (2004; 2006a; 2006b) have performed a limited number of tests on corroded bars under cyclic loading, but of these only 10 included confinement and all of these were tested under constant maximum displacement. In order to produce a robust model, more experimental data is required with a more in-depth focus on the levels of corrosion and varying amounts of slip. In addition to this, Fang's specimens were constructed with either stirrups or without stirrups and results showed large differences between the behaviour of these but it is not clear what the effects of intermediate levels of confinement are. This is critical as when a structure deteriorates, transverse reinforcing, which provides confinement to longitudinal bars, is likely to be the most affected as it has the least cover.

In order to assess the global effects, micro-scale behaviour must be extrapolated into models for the behaviour of structural components and furthermore the entire structure. This was done using FEM's by Coronelli and Mulas (2001) when looking at uncorroded reinforcing. Diminished bond performance due to corrosion is expected to amplify the stiffness reductions observed by Coronelli and Mulas (2001) in their modelling, which allowed for uncorroded bond-slip effects and may also provide altered strength and ductility.

Degradation of structural stiffness through corrosion and seismic loading can lead to increased damage and a risk to life. This makes the ability to assess the seismic behaviour of corroded structures critical in determining the risk of degraded structures situated in seismically active regions.

3 Experimental Corroded Pull-Out Testing

The experimental research programme consisted of testing sixty reinforced concrete specimens with different levels of corrosion. The specimens were constructed and corroded as shown in Table 3-1 with a focus on monotonic and cyclic bond performance under various levels of corrosion and confinement. Corrosion level refers to the targeted reduction (%) in mass of reinforcing in the bonded region.

Table 3-1: Specimen details.

Series	Target Corrosion Level	Loading	Stirrups	Surface	Number
1	0%, 15%, 20%, 25%	Monotonic	6mm	Deformed	12
	0%, 15%, 20%, 25%	Cyclic	6mm	Deformed	12
2	4%, 8%, 11%	Monotonic	6mm	Deformed	9
	4%, 8%, 11%	Cyclic	6mm	Deformed	9
3	2%	Monotonic	4, 2.15, 0 mm	Deformed	9
	2%	Cyclic	4, 2.15, 0 mm	Deformed	9
				Total	**60**

This programme examined corrosion levels ranging from 0%-25% and also investigated the effects of reduced confinement at low levels of corrosion. Bond strength in this range of corrosion testing has been investigated in existing literature under monotonic loading (Fang et al. 2004), however, studies of cyclic (seismic) bond performance have been extremely limited with only a few published results (Fang et al. 2006).

Reduced confinement has been identified in literature as a key area of importance Plizzari et al. (1998) as confining steel often has the least cover concrete and so is the most susceptible to deterioration. Existing research into confinement and corrosion has tested either ‘fully confined’ or ‘unconfined’ specimens, when in reality deterioration of confinement is likely to exist somewhere in between. In light of this, specimens with reduced confinement were lightly corroded (2%) to limit splitting of unconfined (no confining steel) specimens prior to testing.

3.1 Methodology

3.1.1 Test Specimens

Test specimens consisted of a steel reinforcing bar set in a concrete prism with three stirrups held around it. PVC pipe was used to limit the bonded length to four times the bar diameter (80mm), as shown in Figure 3-1. The bonded length was far less than the development length ensuring no yield of primary reinforcement in testing, in addition to producing relatively uniform bond stress along the bar.

Stirrups at close spacing provided confinement along the bonded length and helped to remove any end effects. In Series 1 and 2, round stirrups of 6mm diameter were used. In Series 3 the diameter was reduced to 4mm, 2.15mm and unconfined to assess the impact that confinement has on bond. Full details of the test specimen, with 6mm stirrups, are shown in Figure 3-1.

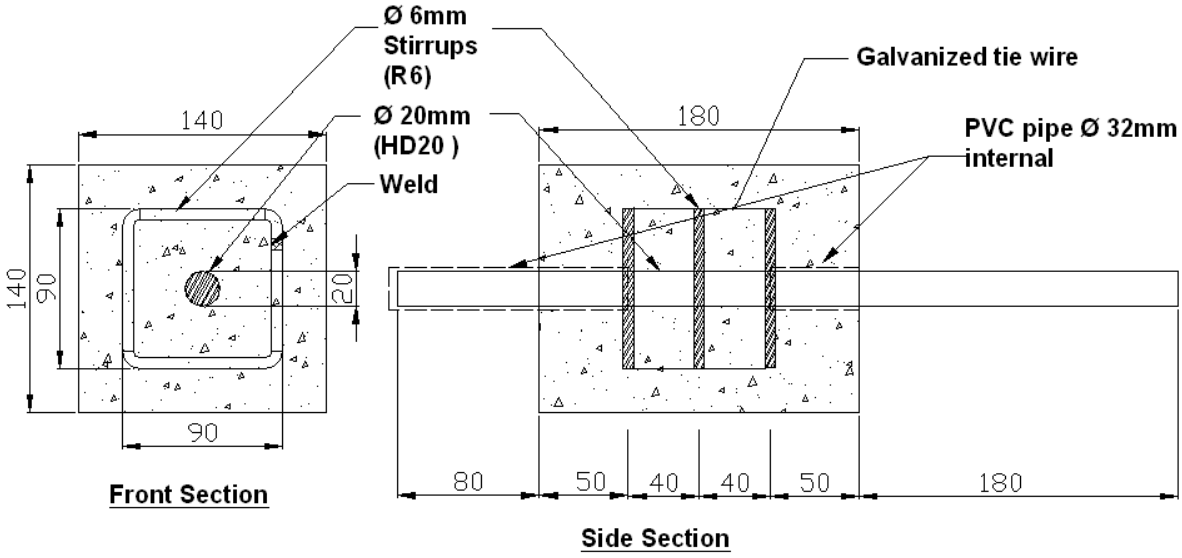

Figure 3-1: Test specimen (using 6mm stirrups), Left: Cross-section front, Right: Cross-section side.

To ensure that the bars did not yield, Grade500E (Nominal yield strength of 500 MPa) steel was used for the main reinforcing bar, while Grade300 (Nominal yield strength of 300 MPa) was used for stirrups; these have the designation HD and R respectively. The concrete used was designed for a 50 MPa compressive strength. This was selected to match the strength requirements from NZS3101:2006 (Standards New Zealand 2006) for a 'C' class aggressive environment which is related to structures exposed to marine conditions which required a binder content of 350kg/m^3 or greater and a water/binder ratio of less than 0.45.

Due to large gaps being left in the data from Series 1 to be subsequently discussed, further investigation was required into the performance of specimens with lower levels of corrosion. To do this a further 18 specimens were cast. The additional 18 specimens were constructed using improved techniques in order to limit corrosion to the bonded region. Corrosion of stirrups and the galvanised tie wire used to hold them, was seen as key reasons for the inaccuracies observed in the earlier series of corroded specimens.

3.1.2 Materials Testing

It is important for numerical validation reasons that the physical properties of the materials used in the experimental testing are well known. Material characterisation is outlined in the following section.

3.1.2.1 Steel

The steel reinforcing used in the specimens is of standard commercial quality with testing details provided in Appendix A. Grade500E steel was found to have an average yield stress of 571 MPa, an average ultimate strength of 689 MPa, and a ultimate elongation of 12.0%. Grade300 steel was found to have an average yield stress of 389 MPa and an ultimate elongation of 12.0%.

3.1.2.2 Concrete

The 28 day concrete strength targeted was 50 MPa using a water to binder ratio of 0.4. After a number of trial mixes were cast to assess the fresh properties of the mix, the mix design shown in Table 3-2 was selected.

Table 3-2: Concrete mix design.

Material	Amount / m^3
General Purpose Cement	387 kg
13mm Greywacke	1136 kg
Natural River Sand	744 kg
Water Reducer (RMC01)	2100 ml
Water	155 lt

As concrete is a variable material a number of its hardened properties were tested at 7, 28, and 90 days. The most common defining property of a concrete mix is its compressive strength at 28 days. Whilst this is important it is also essential to know its strength over a broader time fame given that final testing of the specimens did not occur until 2-3 months after pouring. The average results found from testing for compressive strength (f'_c), tensile strength (f'_t) and elastic modulus (E) are shown in Table 3-3.

Table 3-3: Summary table of average values over time of selected concrete mix design.

Property	7 Day	28 Day	90 Day
f'_c (MPa)	42.0	50.8	64.4
f'_t (MPa)	6.3	7.1	7.5
E (GPa)	35.1	35.2	40.2

Testing of compressive strength was carried out in accordance with ASTM C873 / C873 -04el *(2004)*. The results from this testing (Figure 3-2) show that 7 day strengths observed were higher than might be expected in relation to those at 28 and 90 days.

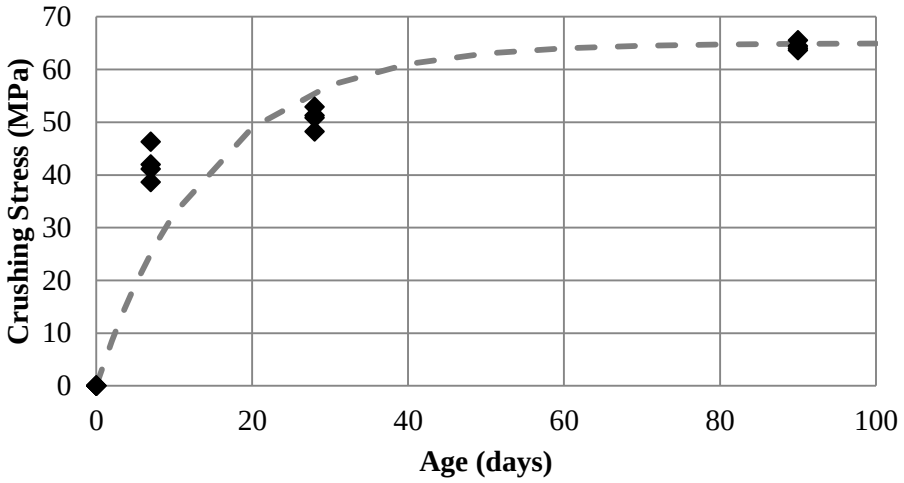

Figure 3-2: Compressive strength of concrete mix used in specimens.

The modulus of rupture was also determined using the method outlined in ASTM C78-09 (2009). Results from this testing can be seen in Figure 3-3.

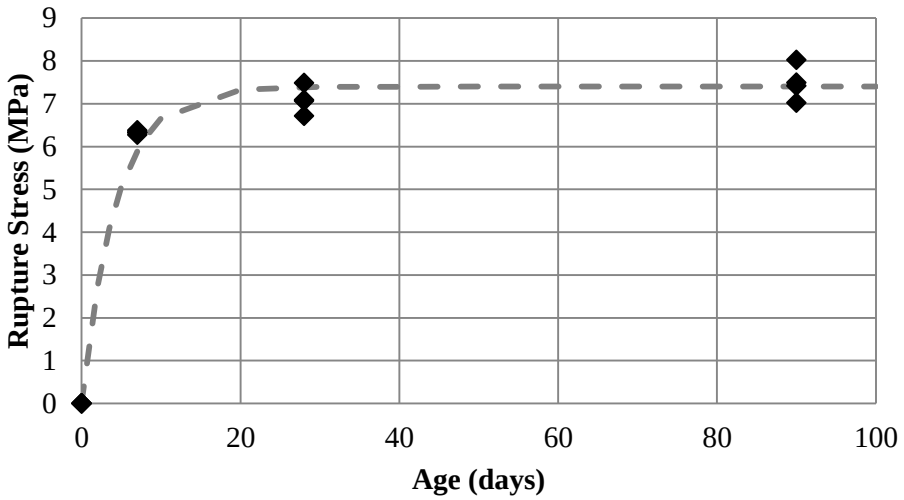

Figure 3-3: Tensile concrete strength over time (determined through modulus of rupture).

The elastic modulus was determined using *ASTM C469 - 02e1 (2002)*. Results for this testing can be seen in Figure 3-4.

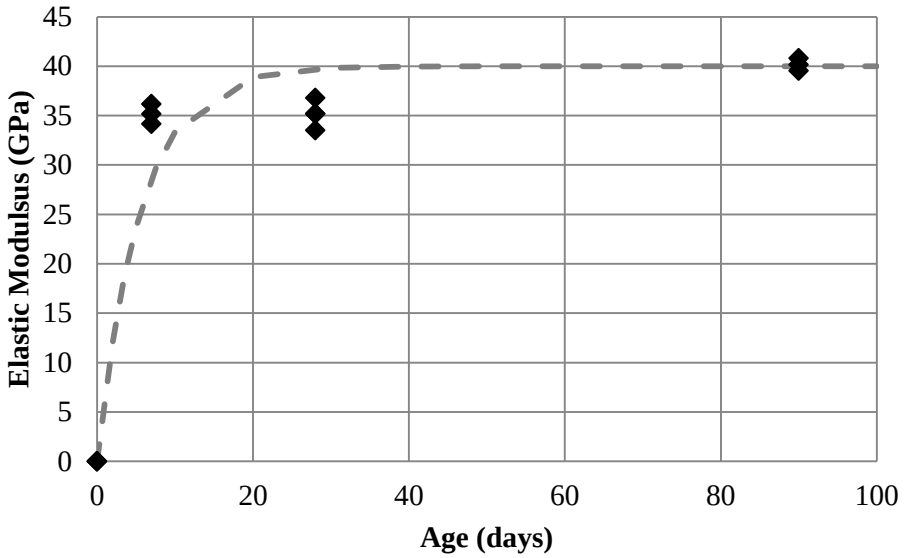

Figure 3-4: Elastic Modulus of design concrete mix cylinders over time.

While all characteristics followed a similar trend, when compared with exponential trend lines, variation was apparent, especially at the 7 day point, with characteristics being higher than what would be expected under regular hardening. Regardless, 90 day values were consistent, providing reliable values for concrete strength at the time of pull-out testing.

3.1.3 Construction

All specimens were constructed using the same sequence and materials in order to minimise variation. The testing regime dictates that each set of specimen type will have three specimens for each monotonic and cyclic loading. Therefore, specimens were constructed in batches of six so that concrete strength would be identical for similarly corroded specimens at the time of testing. The construction sequence is outlined in the following section.

3.1.3.1 Moulds

Reusable moulds were constructed from standard 18mm thick formwork plywood and held together with screws, allowing the easy removal of the specimens once hardened. The interior dimension of the mould matched that of the exterior of the specimen with the holes drilled to match the exterior circumference (34 mm) of the PVC piping used to limit bond length. The reinforcing cages were suspended either from the top of the moulds using nylon string or, in phase two, using cable ties threaded through holes on the faces of the moulds. Prior to each batch, formwork sealant was applied to the corners and interfaces between plywood sheets to stop seepage of fresh concrete and allow for easy removal of the specimens. The specimens were poured on their side i.e. with the main reinforcing bar horizontal. It is known that bleed water building up of the underside of the bar can have an adverse effect on bond strength. However, it was assumed that this effect would be negligible given that the depth of concrete below the bar at pouring was only 70 mm.

3.1.3.2 Concrete

The mix design adopted for the test specimens was shown earlier in Table 3-2. As the specimens were being poured six at a time, every effort was made to ensure that the mix used was constant throughout the experimental phase. Mixing was carried out in a 90lt drum mixer, which was used for all mixes along with the following mixing procedure:

1. stone and sand were mixed for 60 seconds,
2. cement was added and mixed for 60 seconds,
3. water and water reducer were slowly added,
4. mixing was continued for three minutes until the mix was homogenous in consistency.

Once mixed, the fresh concrete was poured in three layers into the moulds with vibration between the pouring of each layer. In the mix that was used to determine the physical properties of the concrete, the cylinders were also poured and vibrated at thirds to match the specimens.

3.1.3.3 Reinforcing Cages

The steel cages that provide confinement to the main reinforcing bar consisted of three square stirrups with a centre to centre dimension of 90mm. The ends of the bars were bent square to match the profile of the rest of the stirrup and avoid an electrical connection between the stirrup and the main reinforcing bar. To prevent opening of the stirrups under internal expansive pressures, they were welded at the overlapping section.

Initially each of the three stirrups in each cage was held 40mm from each other using galvanised steel tie wire. After problems were encountered with corrosion of the reinforcing cage affecting the ability to determine the corrosion level of the bar, it was elected to have the confining stirrups epoxy coated using a powder coating method to limit access of electrical current and moisture. In addition to this, the galvanised tie wire was replaced by plastic cable ties and glue to support the stirrups in fresh concrete.

3.1.3.4 Bars

The reinforcing bars used in the specimens were Grade500E, seismic steel, deformed, reinforcing bars. These required some preparation before they could be used in the specimens. First the bars were cut to a length of 440mm, with care taken to ensure that the grade stamp did not coincide with the region of the bar that would be bonded to the concrete. Following this, a 40mm long, 20mm tread was cut onto the required end of the bar. Since the treading process involved the use of cutting oil, the region of the bar where bonding would occur was degreased and thoroughly washed to remove any oil residue. After washing, the bars were dried and a layer of silicon applied to either side of the bonded section to coincide with the location of the PVC piping and create a waterproof seal.

3.1.3.5 Construction

PVC pipes were cut and smoothed as well as having a ring of silicon applied to the interior of one of their ends. Once hardened the silicone ring and the silicon already applied to the main reinforcing bar were joined with additional silicon to create a watertight seal. A reinforcing cage was then placed into each mould and suspended by nylon thread (plastic cable ties) from the sides of the mould. The cage was held in position such that it was in the centre of the mould and the reinforcing bar ran through the centre. The reinforcing bar, with the PVC pipe attached, was inserted into the mould through the holes on its sides so that the bonded region was situated in the middle. Silicon sealant was used to seal the internal interface between the PVC and formwork. Small pieces of foam were inserted into the external gap between the reinforcing bar and the PVC pipe to ensure that the reinforcing was centred in the hole.

Once the silicon had set the concrete was mixed to the specifications outlined in Table 3-2. Concrete was then poured into the moulds in thirds and vibrated between each pour. It was ensured that the reinforcing cages remained in the correct orientation whilst vibration was taking place. Once pouring was completed the moulds were covered in damp hessian and left to harden for 2 days at which time the specimens were removed. Specimens were then kept in the fog room at constant temperature and moisture until 28 days after they were poured, at which time the accelerated corrosion process began.

3.1.4 Accelerated Corrosion

Specimens were corroded using an electrochemical accelerated corrosion technique that involved impressing a current through the specimens, which were semi-submerged in a 5% NaCl solution to accelerate the oxidation process. The maximum current was 0.1A per specimen, which allowed the required reduction in cross sectional area to take place over approximately 10-50 days.

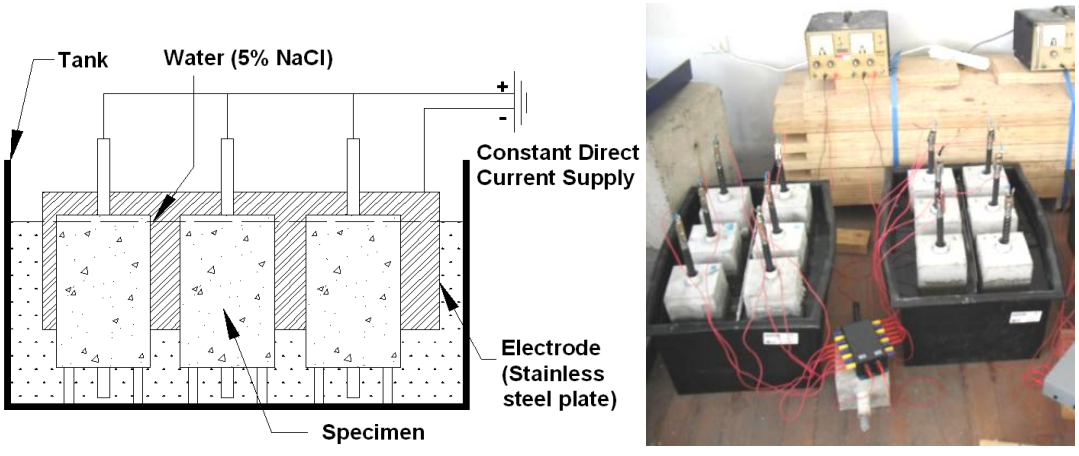

Figure 3-5: Electrochemical corrosion system; a) Schematic drawing b) Photograph of set-up in the lab.

Specimens were soaked in the solution for three days prior to application of the current. The accelerated corrosion set up is shown in Figure 3-5. A similar set up has been adopted by several researchers (Fang et al. 2004; Fang 2006b; Fang et al. 2006a; Yingshu et al. 2007; Cairns et al. 2008). Rough predictions of the level of corrosion were made using Faraday's Law as shown in Equation 3-1, which states that the mass loss is proportional to the number of electrons exchanged and the molar mass of the element.

$$m_t = \frac{t \times I \times M}{z \times F} = \frac{t \times I \times 55.847}{2 \times 96487} \qquad \text{Equation 3-1}$$

Where m_t= mass loss, I = current, M = molar mass of element, z = valency of the element, t = time and F = Faraday's Constant. The current flowing through each specimen (I) was measured at daily intervals to track the mass loss. This current was maintained at 0.6A by the power supply, which gave an approximately even distribution between six specimens. This was found to be correct with the majority of specimens receiving 0.1 +/- 0.005A throughout the process. By linking the specimens in parallel it is possible to corrode more than one specimen at a time.

After the accelerated corrosion process was completed, and the specimen had been tested, the true reduction in cross section was measured. This was done by weighing the corroded reinforcing section after corrosion products were removed, and comparing it with its weight prior to being corroded. Bars, before and after applied corrosion, were cleaned using a weak acidic solution to remove scale and rust products and then weighed.

3.1.5 Loading Protocol and Instrumentation

Once corroded, specimens were tested under either monotonic or cyclic loading in a purpose built frame; shown in Figure 3-6. Testing was performed using the Instron Loading frame at the University of Canterbury which had a capacity of 250 kN, well in excess of the anticipated maximum failure loads of approximately 150 kN, and with controlled displacement capabilities. The load was measured through a load cell and displacement (slip) measured using a potentiometer measuring movement at the free end of the reinforcing bar. Monotonic testing was performed to determine the bond rupture slip.

Cyclic loading was determined and calibrated on the monotonic force-slip displacement curve that was found in the monotonic testing of the uncorroded specimens. The monotonic rupture displacement was divided by two and used as the increment of slip increase for initial cycling, shown in Figure 3-7.

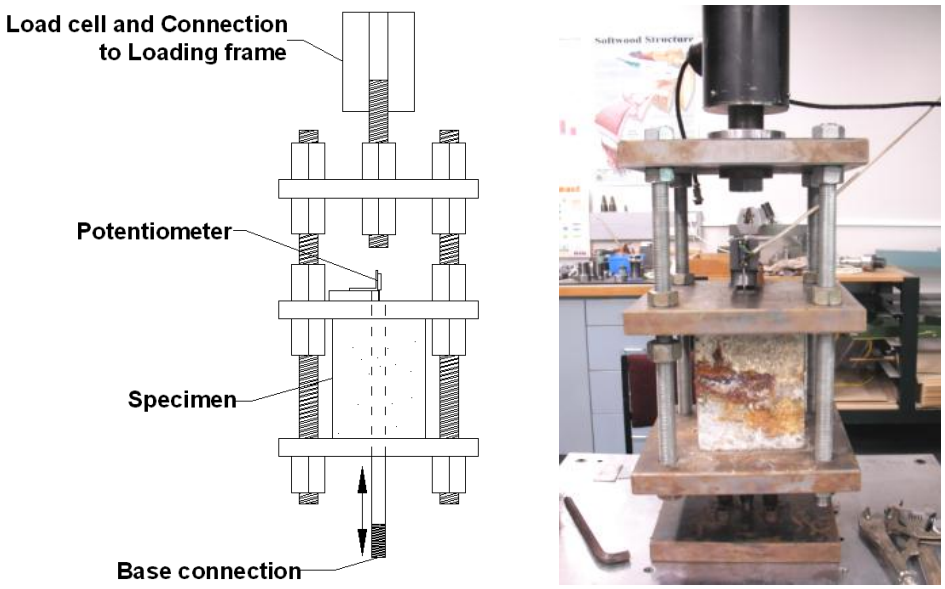

Figure 3-6: Schematic (left) and picture (right) of the testing frame set up.

At each level of maximum slip, the bar was cycled three times before the maximum slip was increased further. Beyond bond rupture, the slip increment was also increased until maximum travel of the potentiometer was reached (±6.0mm).

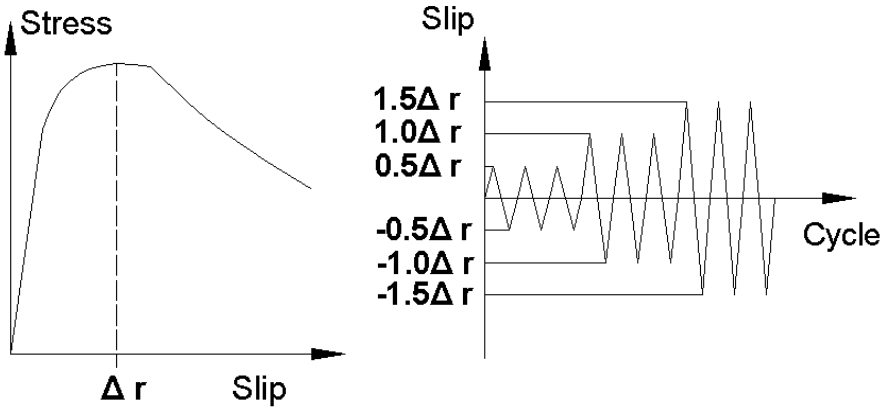

Figure 3-7: Left: Monotonic test results, Right: Cyclic Loading protocol, showing displacement (slip) over several cycles as determined from monotonic test.

3.1.6 Terminology

Figure 3-8 shows a model of the stress-slip curve for monotonic pull-out. The terms shown will be used to describe behaviour observed within the experiments and also later in analysis. T_m refers to the 'Monotonic back-bone' curve; T_R, to the bond rupture stress; T_f, to the ultimate frictional stress; S_R, to the slip at which bond rupture occurs; S_P, to the slip where the rupture stress plateau ends, and S_f, to the slip where purely frictional behaviour occurs.

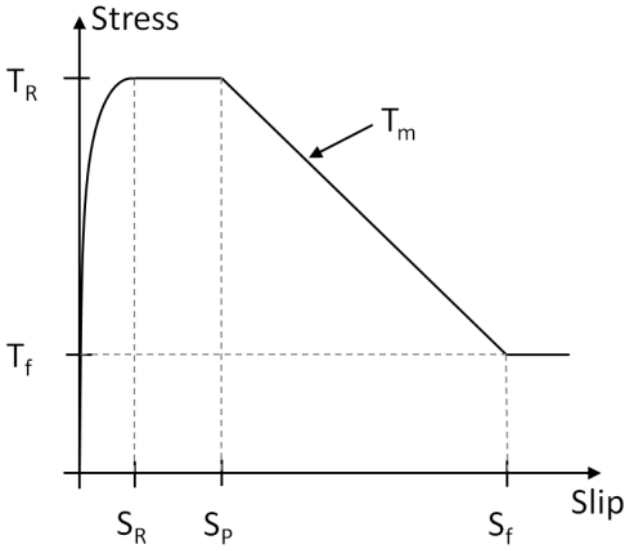

Figure 3-8: Terminology used in describing stress-slip behaviour.

3.2 Results (Series 2 – 0% -12% Corrosion)

Series 2 targeted 0% to 12% corrosion and was conducted following Series 1 in which significantly higher levels of deterioration were observed that was anticipated. This series was constructed using powder coated stirrups and used plastic cable ties, to support the reinforcing cage while concrete was fresh. These measures were not taken in any of the other series.

3.2.1 General Comments

Corrosion levels of specimens were found to range from 0% to 11.9%, although the majority were less than 7.5%, highlighting the limitations of corrosion prediction even when empirical methods are used. Four specimen bars at various levels of corrosion are shown in Figure 3-9.

(a) **(b)**

(c) **(d)**

Figure 3-9: Corroded bars after cleaning; (a) 3.5% corrosion, (b) 6.1% corrosion, (c) 8.7% corrosion, (d) 11.9% corrosion.

At lower levels of corrosion (< 7%) mass loss was relatively uniform along the bonded section with regular, random pitting occurring. At higher levels of corrosion, damage became more localised with

isolated regions sustaining heavy losses in cross-section (~10%) accompanied by random minor pitting, thus introducing non-uniform bond deterioration in the bonded section.

3.2.2 Monotonic Response

Non-uniformity of bond degradation was apparent from monotonic testing with variation of rupture stresses occurring even in similarly corroded specimens. Lightly corroded specimens (<1%) displayed a distinguishable and abrupt peak at rupture. This was unlike those with higher levels of corrosion, where rupture was followed by gradual degradation in bond stress with increased slip. Increases in ultimate frictional stress (T_f) once full bond failure occurred were also observed with increasing levels of corrosion. Increased frictional stresses are attributed to increased confining stresses due to radial expansive pressures exerted by corrosion products, along with reduced damage to surrounding concrete due to bar movement. Reduction of bar section resulted in reduced mechanical interlock between bar lugs and surrounding concrete. This in turn caused a gradual change in failure mechanism from shearing of concrete between lugs to frictional slippage, however, this mechanism was not fully developed until higher levels of corrosion. The portion of resistance provided through mechanical interlock was represented by stresses greater than the purely friction stress. Figure 3-10 shows how this reduced as the level of corrosion increased. At 11.9% corrosion, rupture stress is composed of ~20% mechanical interlock with the rest being frictional resistance. Complete analysis of the effects of corrosion on bonding mechanisms is covered in Section 4.2 and all monotonic graphs can be seen in Appendix B.

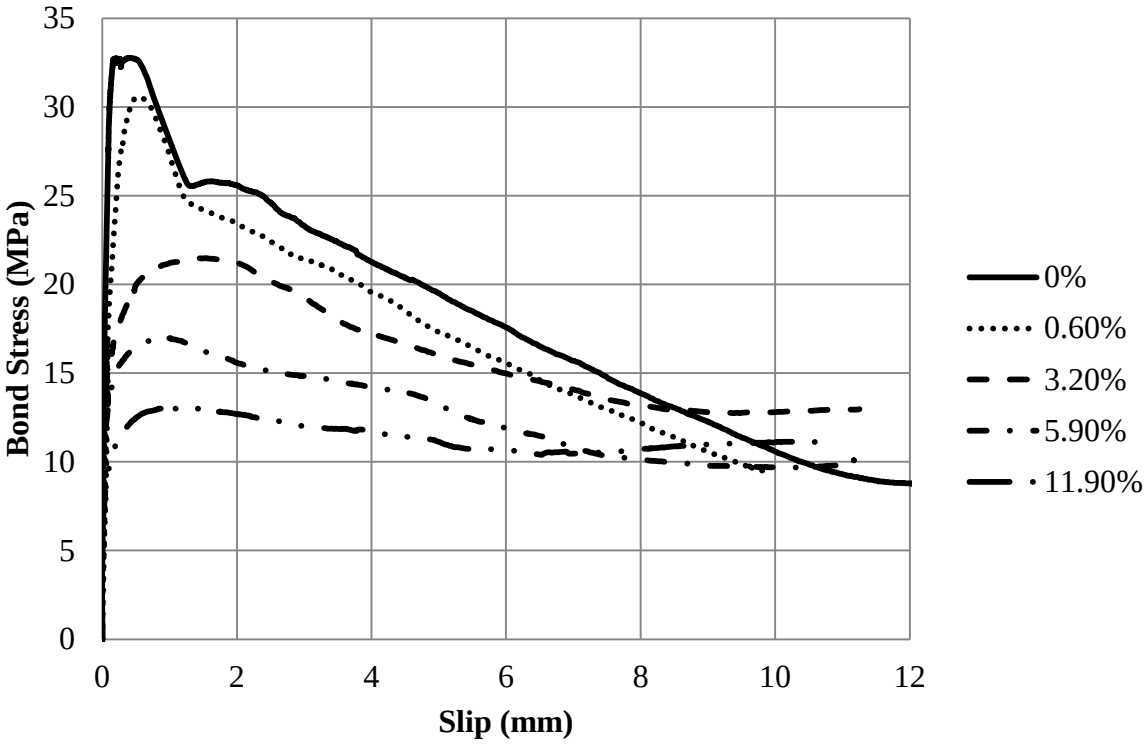

Figure 3-10: Monotonic pull-out stress-slip behaviour for bars corroded from 0%-12%.

When bond rupture stress values from monotonic testing were compared with the level of corrosion in reinforcing a trend of decreasing stress with increasing corrosion was apparent, as shown in Figure 3-11. Experimental data displayed significant scatter and when an exponential regression line was implemented a moderate correlation of $R^2 = 0.56$ was found, showing variability of corrosion effects.

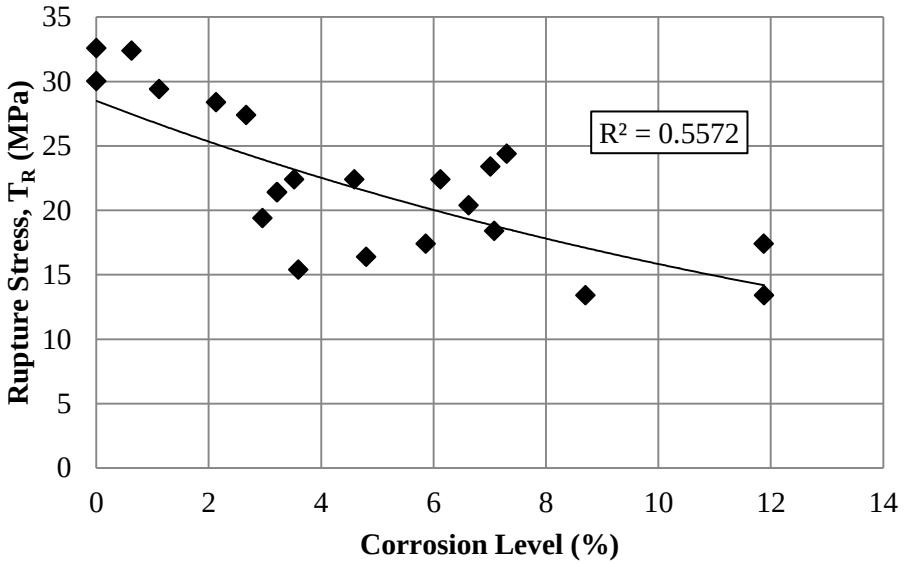

Figure 3-11: Plot of bond rupture stress against corrosion level for monotonic pull-out of specimens with corrosion levels between 0% and 12%.

3.2.3 Cyclic Response

Nine cyclic tests were carried out at a range of corrosion levels from 0% to 7%, unfortunately no cyclic tests were carried out on specimens in the 7% to 12% range. Individual tests are displayed in Appendix C. Dimensionless bond stress (T/T_m) and dimensionless energy (E/E_0) were used to characterise behaviour using a similar method to Eligehausen et al. (1983). The peak stress at each cycle (T) was divided by the monotonic envelope value at the same slip (T_m), given from monotonic testing of a similarly corroded test specimen.

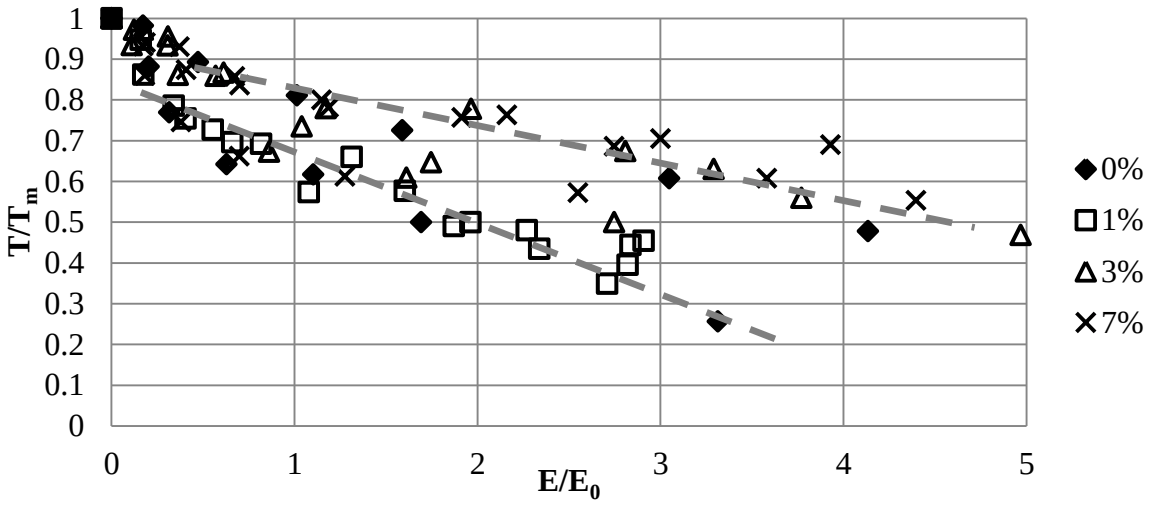

Figure 3-12: Damage-energy relationship for cyclic testing of specimens corroded between 0% and 7%.

The cumulative energy (E) was divided by the energy encapsulated by the monotonic envelope prior to a purely frictional response being reached (E_0). Results using this technique are shown in Figure 3-12.

While there was some variability in the results, two general trends, demonstrated by dashed lines, can be observed in Figure 3-12. These are not associated with corrosion effects and in fact often there are points from each level of corrosion in both, with data from one specimen following a different line to an equally corroded counterpart. The likely reason for such variation lies in the use of the monotonic back-bone curve, T_m, in the dimensionless term T/T_m. The model for T_m did not allow for 'peaking', which occurred in specimens at low levels of corrosion due to higher stresses causing splitting failure through the concrete prism, rather than sliding, as shown in Figure 3-13. As a result of this 'peaking' behaviour, damage due to cyclic loading appeared more severe on the dimensionless scale than in reality due to the model over predicting the undamaged monotonic envelope beyond bond rupture. As peak height is variable and depends on pre-rupture loading and confinement, specimens that do not display 'peaking' behaviour or which only had minor peaks, better fit the monotonic model and appear to have damage applied at a lower rate of dimensionless energy. Full analysis of the cyclic trends and models will be covered in Section 4.3, all cyclic test graphs are displayed in Appendix C.

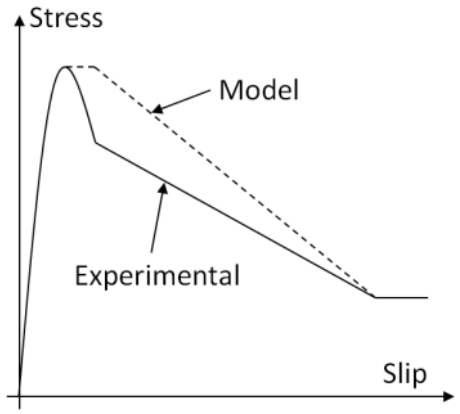

Figure 3-13: Variations in representation of the monotonic model and experimental behaviour.

3.3 Results (Series 1 – 15% -25% Corrosion)

The first series of testing was intended to target a level of corrosion ranging from 0% to 11% reduction in bar cross-section. Testing of the specimens initially intended to be at 10% found them to be closer to 1% and so the remaining twenty four specimens were returned to the corrosion bath and left to corrode until they were expected to reach their target levels of corrosion. The target was based on the time in Ampere-hours taken to reach the 1% corrosion level in the initially tested specimens.

Testing of these twenty four specimens revealed that they had all sustained far greater levels of corrosion than anticipated with corrosion levels found to range between 15%-25% reduction of cross-section. As would be expected the comparison between the uncorroded and highly corroded specimens showed distinct differences. The results and trends are shown in the following section with an in depth assessment of the accelerated corrosion process undertaken in Section 3.5.1.

3.3.1 General Comments

The level of bar reduction in the bonded area was typically far greater than that observed on the rest of the bar with most of the unbonded regions showing little to no signs of corrosion. The severity of corrosion along the bonded section was not uniform in the majority of the specimens. It was commonly seen that a 10-30mm section of the bonded region would display reduction of cross-section in excess of 30% with far less reduction found in other regions, as shown in Figure 3-14. However, lack of uniform corrosion over the length of the bar is typical of that associated with chloride induced corrosion.

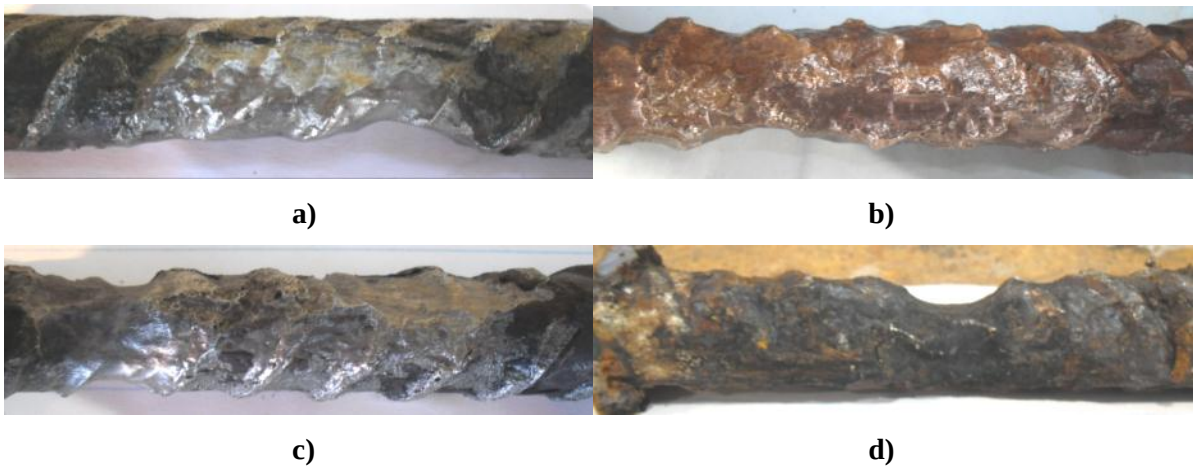

Figure 3-14: The bonded sections displaying the reduction in cross section observed. a) 21% corrosion, b) 20% corrosion, c) 16% corrosion, d) 21% corrosion prior to cleaning.

It should be noted that when preparing the specimens for testing at levels of corrosion greater than 20%, some rotation of the bar was observed in a few specimens due to differential movement between the loading frame and the test specimen. While care was taken to stop rotation from happening, the smallest applied moment may have jeopardised the bond integrity. It follows therefore, that if the forces required to twist the bar were this low and can be compromised with minimal handling, then the bond had already been severely degraded by the corrosion products.

Moderate levels of corrosion were observed in the stirrups. This was predominantly located in just one of the three stirrups in each specimen. It was noted that deterioration was focused at the corners of stirrups. Similar behaviour was observed by Ou et al. (2010). It was unclear whether this was associated with two dimensional ion ingress at corners, yielding through bending of stirrups, or a combination of both. Since the deterioration was generally limited to the one stirrup at the edge of the

bonded section of primary reinforcement, it is assumed that the overall confinement was not significantly affected, but further investigation was required to determine the confinement effect.

Under regular conditions, the corrosion products would have been expected to produce a red-orange colour of iron (III) oxide. Some red orange oxide was produced under accelerated process but the bulk of the corrosion product was black in colour suggesting the formation of an iron (II) oxide with somewhat lower expansive properties.

3.3.2 Monotonic Response

The results from the monotonic testing displayed a reasonable level of variability across the range of corrosion levels and can be seen in Figure 3-15, where several indicative pull out test stress-slip relationships are shown. The full plots of all monotonic testing are presented in Appendix B. Stresses were calculated by dividing the total load applied to the bar by the uncorroded surface area in the bonded section. The uncorroded control specimens had a rupture stress of 32.6 MPa and 30.1 MPa, far greater than the corroded specimens. Their rupture was followed by a decrease in stresses until a frictional response was reached. Roughly constant stress of 8 MPa was reached at a slip value of 12 mm, which corresponds to the rib spacing on the HD20 reinforcing bar used in the specimens and purely friction stresses.

In tests of specimens with similar levels of corrosion, similar bond characteristics might be expected. At 16% corrosion, this was found with two of the three tests which had rupture stresses of 12 -13 MPa, but the third reached 20.2 MPa. Such behaviour was attributed to differing corrosion patterns in the bonded section. At 16% corrosion there was not a significant reduction in initial stiffness of the specimens, but it was apparent that the nature of the rupture mechanism changed with a clearly defined peak no longer being displayed. The change in mechanism is attributed to the removal of the ribs on the bar through corrosion. This significantly reduced mechanical inter-lock between the bar and concrete, which left predominantly frictional forces to resist loading. One test did display a small peak, which was attributed to the non-uniform loss of cross-section along the bar, meaning that some sections retained their ribs and still offered mechanical inter-lock (Fang, 2004).

At corrosion levels greater than 20% all specimens reached a similar bond stress of 6 MPa by 1 mm of slip. Beyond 1mm the specimens followed roughly the same path, despite one of the specimens having 28% bar reduction. This single specimen did however display a significantly reduced initial stiffness. This suggested that for greater than 20% reduction of cross-section the bond is so heavily damaged that the effect on rupture stress of additional corrosion will be negligible, although the initial stiffness may further diminish.

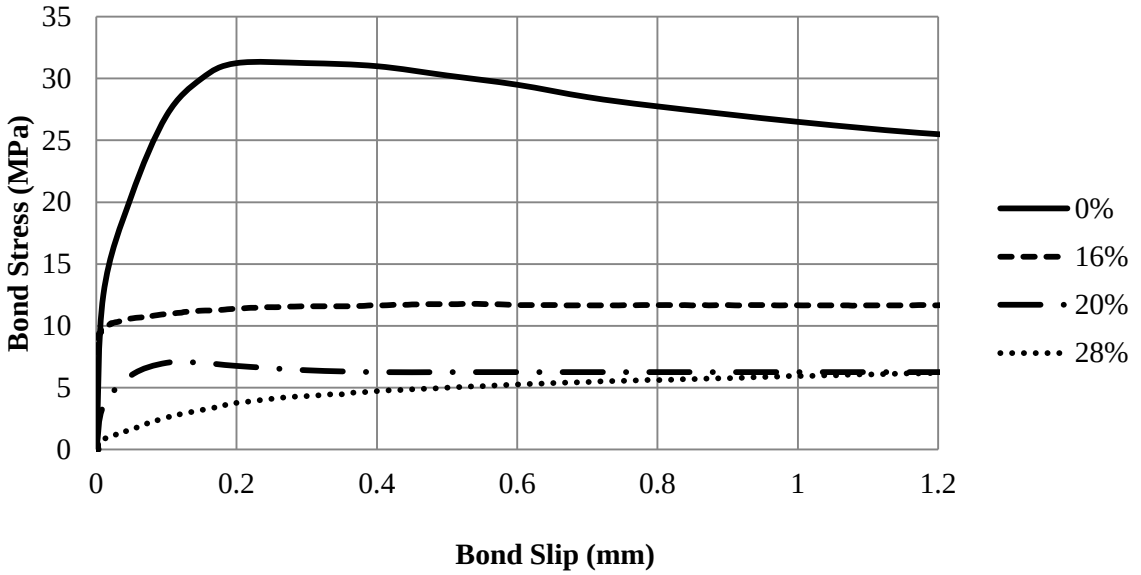

Figure 3-15: Average monotonic pull-out test results for each corrosion level.

The uncorroded tests showed rupture occurring at approximately 0.2 mm, whereas the corroded tests at 16% corrosion displayed a rapid reduction of stiffness to near zero in the 0.02 - 0.1 mm region. At corrosion levels greater than 20% the stiffness reduction occurred in the range of 0.05 – 0.2 mm, with lower initial stiffness. A more in depth analysis of corrosion effects on initial stiffness is undertaken in Section 4.2.3.1.

In Figure 3-16 the rupture stress of all the monotonic, and a number of the cyclic tests that reached rupture in their initial cycle, were graphed against the level of corrosion found in each of the test specimens. There is a sound correlation between the factors, with 15% corrosion resulting in 50% reduction in bond strength. Based on this relationship, it would be expected that by 30% corrosion there would be close to 100% loss in bond strength. This seems unrealistic and the evidence is insufficient to extrapolate the trend further than 25% corrosion.

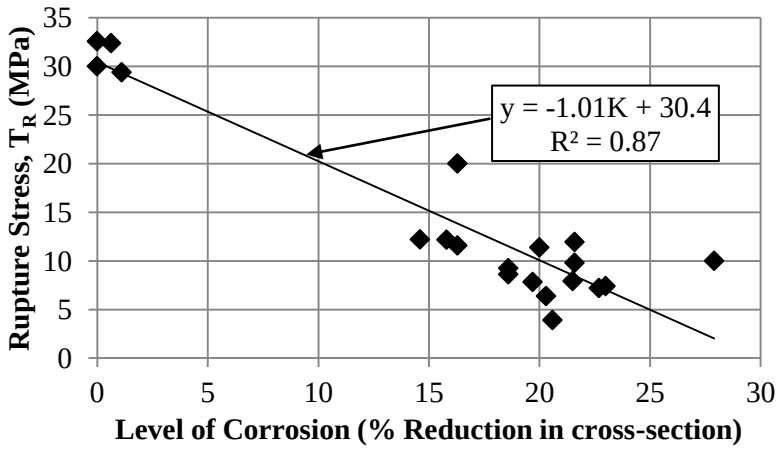

Figure 3-16: Peak bond stress against the level of cross-section reduction for the reinforcing bar.

3.3.3 Cyclic Response

Twelve cyclic tests were carried out at a range of corrosion levels matching the monotonic testing. Individual tests are displayed in Appendix C. All tests followed a similar loading regime to that shown in Figure 3-17 with each increase in slip increment being followed by three full reversed cycles before the maximum slip increment was increased. The general behaviour was similar to the monotonic tests, with higher levels of corrosion providing higher reduction in bond stresses.

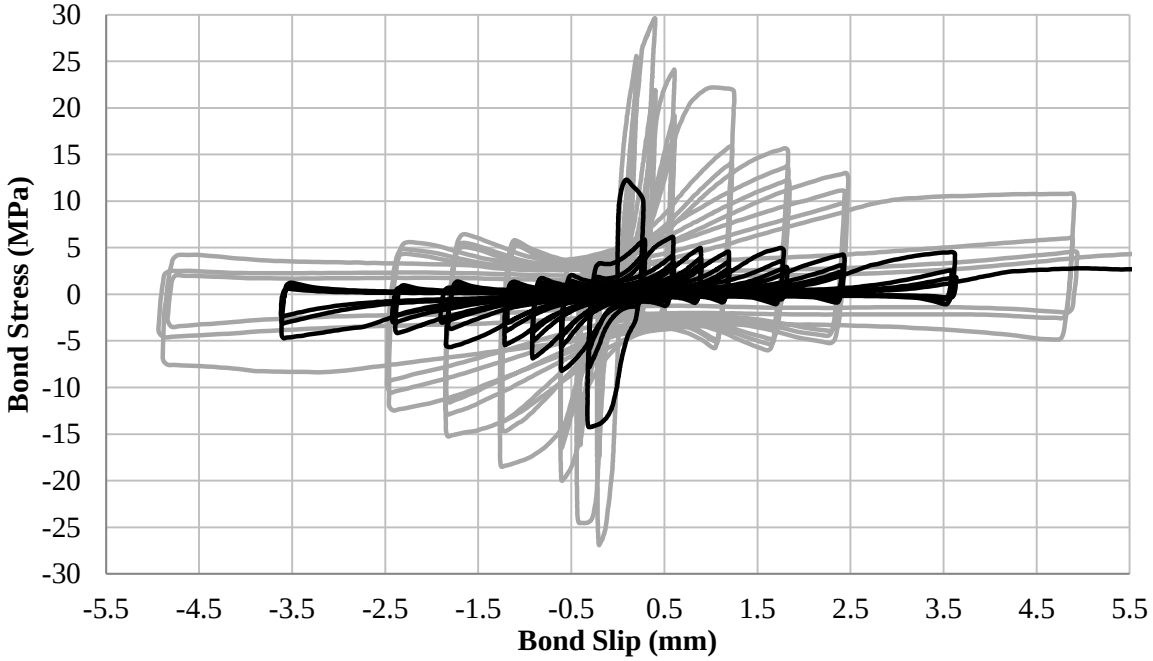

Figure 3-17: Cyclic stress-slip relationship for 0% corrosion (grey) and 18.6%(black)

Moreover, bond stresses associated with the sliding sections in the friction branch, displayed in Figure 3-17, when the bar is not near maximum slip, were initially higher in the corroded specimens but diminished quickly. In contrast to this, the uncorroded specimens tended to show an increase in stress with the increase in displacement associated with the fourth cycle where the maximum displacement increased from 0.2 mm to 0.4 mm. At the end of testing, after 18 cycles, the sliding stress was between 1.0 and 2.0 MPa the non-corroded specimens, whereas it was only 0.1 MPa for their corroded counterparts. This suggests that the corrosion products initially increase the confining stresses on the bar due to their expansive nature but, once disrupted, have a lubricating effect on the sliding process.

In the analysis of the cyclic data both dimensionless bond stress (T/T_m) and energy (E/E_0) were used to characterise behaviour using a similar method to Eligehausen et al. (1983). The peak stress at each cycle (T) was divided by the monotonic envelope value at the same slip (T_m) given from monotonic testing of a similarly corroded test specimen. The cumulative energy (E) was divided by the energy encapsulated by the monotonic envelope prior to a purely frictional response being reached (E_0). Using

this process it might be expected that the effect of corrosion on reducing bond performance would not affect the dimensionless energy. The results from this series of testing suggest otherwise.

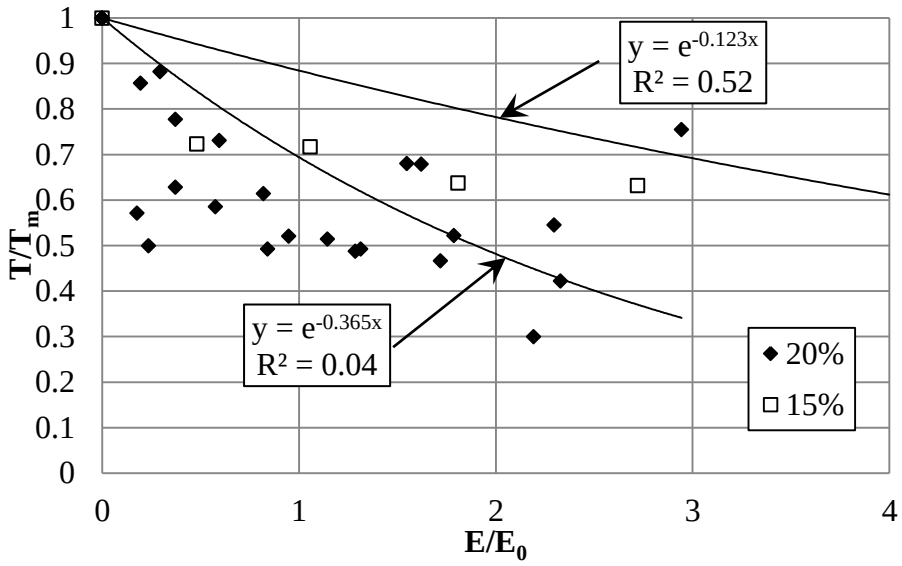

Figure 3-18: Maximum stress / Monotonic stress envelope against non-dimensional energy displayed for 15% and 20% reduction in bar cross-section due to corrosion.

Figure 3-18 shows a greater reduction in stresses due to cyclic loading in 20% corroded specimens when compared to the 15% corroded specimens. As it can be seen, the correlation between the trend lines used and experimental results is not strong. A more in depth investigation into this will be performed in Section 4.3 using the full data set. Unfortunately, only a single cyclic test was performed on a 15% corroded specimen so data is limited.

3.4 Results (Series 3 – 2% Corrosion, Reduced Confinement)

3.4.1 General Behaviour

The level of corrosion observed in these tests also varied from that expected, while 3% was targeted, the reality was that specimens were mostly between 0.1% and 2.5%, with an average of approximately 1%. Despite this, all of the un-reinforced specimens displayed cracking primarily in the longitudinal direction (parallel to the main reinforcing bar) so cracking was also observed in the transverse direction (due to stirrup corrosion).

3.4.2 Cracking Damage

As steel oxidises, rust products exert radial expansive pressures on surrounding concrete. These pressures result in build-up of tensile forces within the concrete, which can result in cracking. Confining steel helps to resist these tensile stresses, although in some cases corrosion of the confining steel can in itself produce cracking as shown in Figure 3-19. This was a common cracking pattern seen

in many specimens where corrosion of stirrups and primary reinforcing occurred. The effects of these transversal cracks were unclear but are likely to impact on the apparent bond stiffness due to opening and closing of the crack under loading.

Figure 3-19: Transversal cracking (0.5mm) in specimen 1.

Lack of confining steel allowed the formation of longitudinal cracks in the unreinforced specimens at the completion of the corrosion process and prior to testing. Examples of these cracks are shown in Figure 3-20 where image (a) shows a 'split' specimen where the cracking is significant and runs through the entire section to the bar, whereas in (b) the longitudinal crack is still moderate leaving the section somewhat intact. Longitudinal cracks were also present in specimens when using 2.15mm stirrups, although the severity of cracking was not as great.

(a) **(b)**

Figure 3-20: Damage to specimens prior to testing; (a) Specimen 2b, split (3mm crack); (b) Specimen 3b, Intact with moderate (1mm) cracking.

Specimens constructed with no confining steel or 2.15mm confining steel that were intact prior to testing failed in a brittle manner through longitudinal splitting of the concrete. Cracks can be seen in Figure 3-21 where (a) shows a specimen immediately after splitting occurred and (b) shows the unloaded specimen after testing in which splitting failure occurred.

Split and intact specimen performance will be covered in greater detail in section 3.4.4.

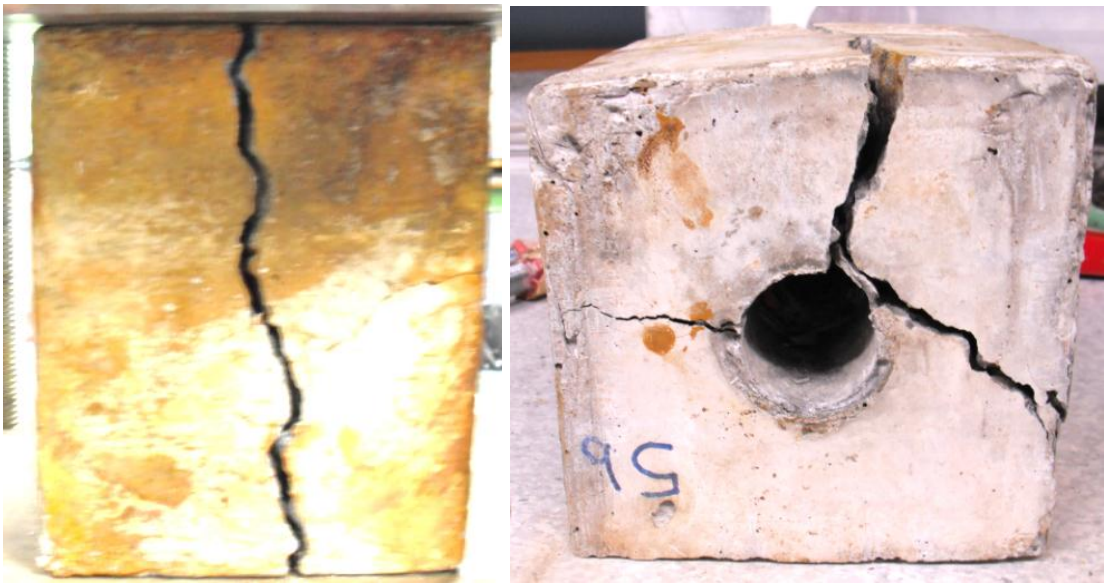

(a) **(b)**

Figure 3-21: (a) 5mm crack in Specimen 3b after splitting failure occurred; (b) Splitting damage in Specimen 5b after testing.

3.4.3 Index of Confinement - Stirrups

The index of confinement used has been adopted from Plizzari et al. (1998). It consists of two components relating to confinement from stirrups and concrete. The 'Stirrup Index of Confinement', Ω, was used to quantify the level of confinement provided by stirrups used in specimens. The equation for this is shown below in Equation 3-2. It related the total area of stirrups, $n_{st}A_{st}$, with the area of the longitudinal section of anchored bars, $n_pA^*_p$.

$$\Omega = \frac{n_{st}A_{st}}{n_pA_p^*} \qquad \text{Equation 3-2}$$

n_{st} represents the number of stirrup legs (4, only counting half of the end two stirrups), A_{st} is the area of an individual stirrup leg, n_p is the number of anchored bars (1), A^*_p is the longitudinal section area of one anchored bar in the influence length (1600 mm^2). The Stirrup Index of Confinement for specimens of varied confinement are shown in Table 3-4 below.

Table 3-4: Stirrup Confinement Index for specimen arrangements tested.

Stirrup Diameter (mm)	Stirrup Index, Ω
0.00	0
2.15	0.0091
4.00	0.0314
6.00	0.0707

Plizzard et al. (1998) found that bond rupture stress increases with confinement until the Stirrup Index of Confinement reaches 0.03. This was the equivalent of the specimens constructed using 4 mm stirrups under this series of tests.

3.4.4 Monotonic Testing at Varying Levels of Confinement

The level of confinement provided to lightly corroded specimens proved to affect strength and post rupture bond behaviour, which was consistent with the findings from uncorroded investigations (Plizzari et al. 1998). The rupture stress results from cyclic tests in which bond rupture occurred prior to cyclic unloading were also included. Trends observed in rupture stresses with various levels of confinement are shown in Figure 3-22, with rupture stress increasing as the level of confinement increases. All monotonic tests are shown in Appendix D. Prior to testing, several of the less confined specimens displayed splitting failure due to corrosion, parallel to the primary reinforcing. Tests in which splitting occurred prior to testing are shown in Figure 3-22. The hollow diamonds display much lower maximum stresses compared to their intact counterparts with approximately 60% reduction in unconfined specimens and approximately 30% reduction for specimens with 2.15mm confining steel.

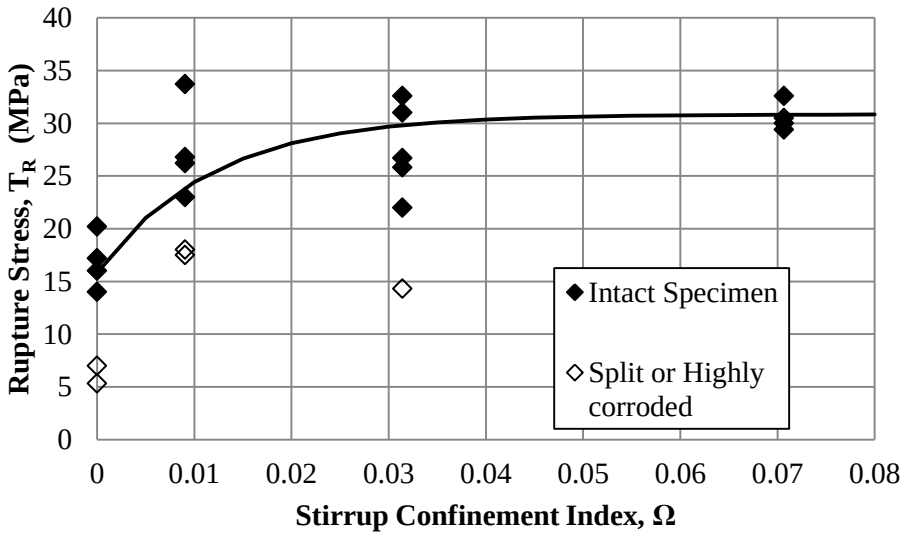

Figure 3-22: Plot of rupture stress against Stirrup Confinement Index for monotonic pull-out testing of ~1% corrosion reinforcing bars.

The relationship found from this series of testing relating Stirrup Confinement Index and rupture stress for intact specimens is shown in Equation 3-3;

$$T_R = 15.85 + 15(1 - e^{-85\Omega}) \qquad \text{Equation 3-3}$$

Increased corrosion, as occurred in specimens with Ω=0.0314, resulted in the effects of stirrup confinement becoming more apparent with a significant drop on rupture stress achieved. The severity of specimen splitting prior to testing increased, causing reduced bond rupture stresses. In light of this, the proposed equation is only applicable for bars with low levels of corrosive deterioration. Specimens with 4mm stirrups (Ω = 0.0314) were unintentionally subjected to higher levels of corrosion ranging from 0% to 6.5%. Effects of this can be seen in the significantly lower rupture stress displayed by the 6.5% corroded specimen (hollow diamond), which was approximately 10 MPa lower than similarly reinforced specimens. Rupture of confining steel was not observed; although complete loss of section due to corrosion was observed in some specimens constructed using only 2.15mm stirrups.

Post-rupture behaviour was also significantly affected by level of confinement and whether specimens were intact or split prior to testing. Intact specimens containing low levels of confinement (Unconfined and 2.15mm stirrups) still developed substantial rupture stress, but upon rupture displayed an instantaneous slip of 1-2mm, accompanied by a large or complete reduction in stress, as shown in Figure 3-23. Failure of these specimens was through a splitting mechanism inducing brittle behaviour and was accompanied by formation of a longitudinal crack, often 1-5mm in width. In the case of the unconfined specimens, bond capacity was completely lost upon rupture for all intact specimens. Inclusion of reinforcing steel allowed residual bond capacity to be maintained upon concrete splitting, even after yield stress of confining had been exceeded. Specimens that were split prior to testing performed poorly. Split unconfined specimens behaved in a similar manner to the intact specimens after they had split under testing.

In specimens with higher levels of confinement (4mm and 6mm stirrups), the failure mechanism moved away from splitting of the concrete prism, to sliding of bars along the concrete failure plane (at the top of ribs). Rupture stresses were only maintained for 2-5 times yield slip but failure was not abrupt and was followed by the slow degradation of bond.

Specimens containing 4.0mm stirrups were subjected to higher levels of corrosion on average. This can be attributed to increased corrosion time, which was intended to account for stirrup corrosion. The average level of corrosion was 3.6%, with levels ranging from 0.2% to 6.4% corrosion. Large variations were seen in the behaviour of the three monotonic tests using 4.0mm stirrups as shown in Figure 3-23, denoted with (a), (b) and (c). (a) represents the monotonic pull-out of a 0.2% corroded bar, failure was through concrete splitting, which was accompanied by an instantaneous slip of 1.1mm. Thus in spite of being moderately well confined, the failure mechanism was still brittle. This failure

mechanism was not seen in (b) and (c), where instead failure occurred through sliding of the bar. These bars were more corroded with 2.8% and 6.4% for (b) and (c) respectively, resulting in a significantly altered response. (b) displays some interlocking behaviour creating a small peak at rupture, whereas (c) displays purely frictional behaviour.

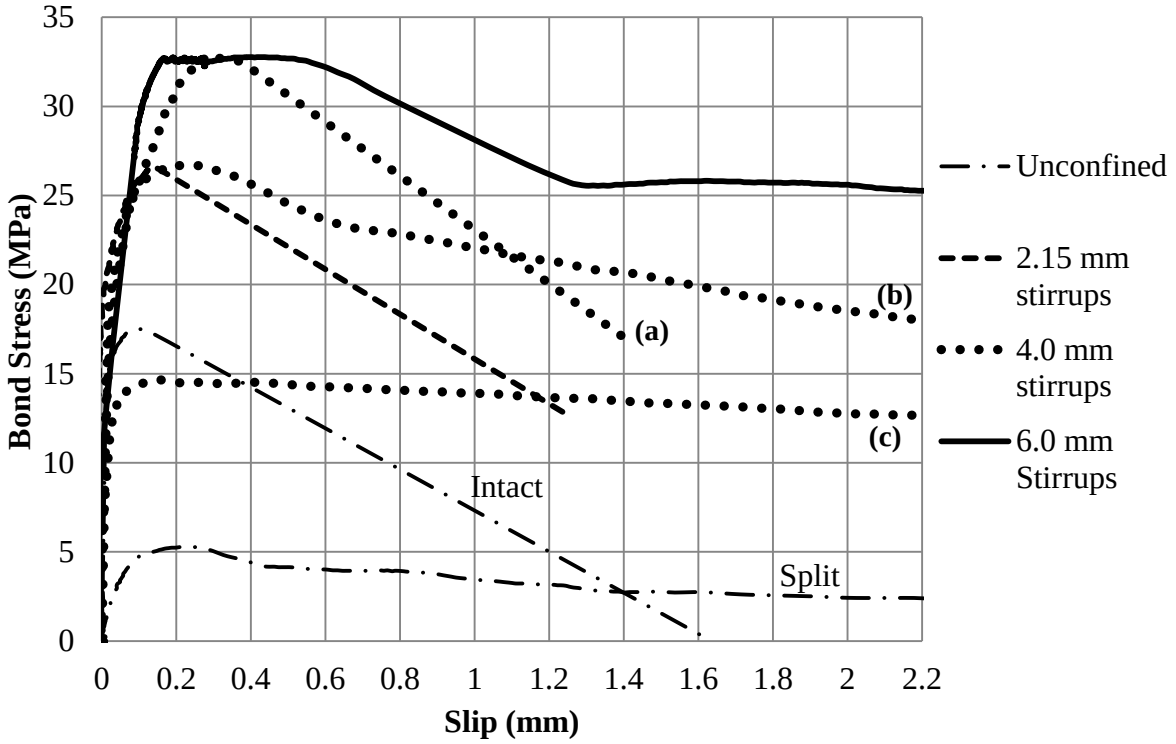

Figure 3-23: The stress-slip behaviour of monotonic pull-out of ~1% corroded bars with varying levels of confinement.

All specimens that displayed splitting show similar splitting stiffness. This was attributed to the experimental data collection devices being unable to gather intermediate points between peak rupture stress and residual stress, due to its instantaneous nature. While better confined specimens were able to arrest strength loss through increased activation of stirrups, the amount of strength loss before this occurred was highly variable.

The effect of axial compression provided by the loading frame was unclear. Friction provided by the steel plates increased confinement to the end sections of the specimens. It is assumed that the debonded regions will assist in reducing these effects. Compression provided through tightening of the plates will have induced perpendicular tensile stresses in the concrete prism, reducing the additional lateral stress the concrete is able to withstand when the bar is pulled out. These effects were beyond the scope of this investigation have not been included.

3.4.5 Cyclic Testing at Various Levels of Confinement

Brittle behaviour of less confined specimens meant that in cyclic testing bond rupture on the initial cycle was avoided. In turn, cycling of the bar at sub-rupture slips resulted in damage and dissipation of bond stresses, creating more gradual bond failure through bar slippage opposed to splitting in most cases. At low levels of confinement, splitting, even if only moderate, resulted in almost complete loss of sliding forces under cycling, which can be seen in Figure 3-24. All individual cyclic tests are shown in Appendix E.

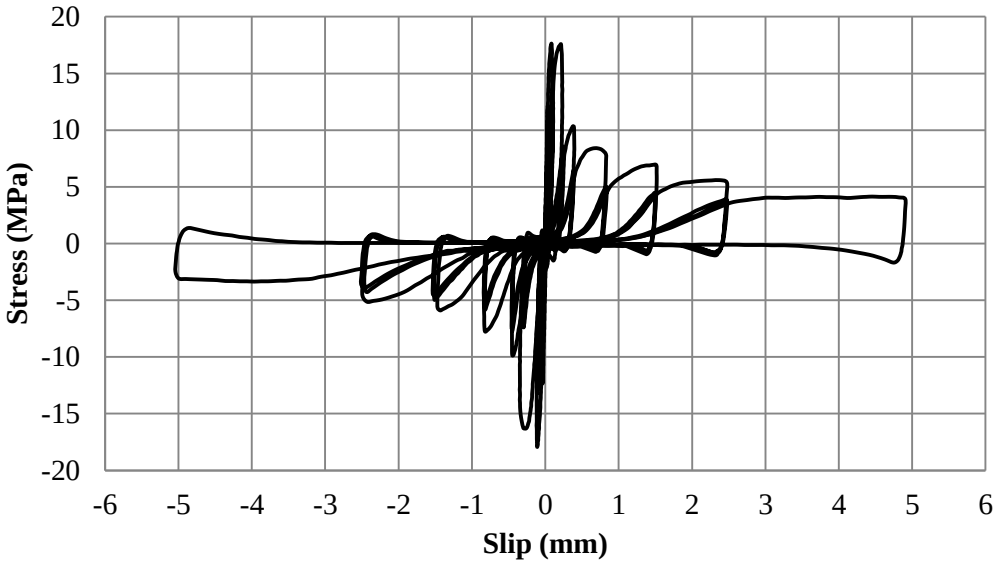

Figure 3-24: Cyclic pull-out, 0.6% corrosion, 2.15mm confinement.

In light of the altered failure mechanism between monotonic and cyclic tests it was decided to compare cyclic results with a scaled representative test in which slipping failure occurred. Local bond damage due to cycling at sub-rupture stresses reduces the peak bond rupture stress. However, splitting failure can be avoided as radial stresses applied through mechanical interlocking between concrete and reinforcement reduce with damage to local concrete and frictional stresses become more prevalent. Due to the avoidance of splitting, complete loss of bond stress can be avoided. This meant that when cycling was kept less than rupture, higher bond capacity was available at slip values greater than the monotonic rupture envelope. For this reason it was deemed most suitable to use the well confined monotonic values in determining damage-energy behaviour. This highlights the variable, and often erratic bond behaviour displayed under unconfined conditions.

The damage-energy relationship that is shown in Figure 3-25 was created in the same manner described earlier in Section 3.3.3. Specimens were grouped based on their confinement; 'Well confined' specimens with 6.0mm stirrups (Ω=0.0707) approximately representing regions detailed for plastic behaviour under modern seismic design (NZS3101, 2006), 'Moderate confinement' specimens with 4.0mm stirrups (Ω=0.0314) representing elastically detailed members and 'Poor confinement'

specimens with 2.15mm stirrups and no confinement (Ω = 0.0 to 0.0091). This was based on the similarity in performance of each of the specimen groups.

Figure 3-25 shows that the level of confinement contributes to the rate of bond degradation of lightly corroded bars. As in monotonic testing, poorly confined specimens rely on surrounding concrete to confine them. Once cracking occurs concrete was unable to act in tension, removing confining stresses, and bond damage occurred more rapidly. Further analysis into the effects of confinement, also linked with corrosion is provided in Section 4.4.

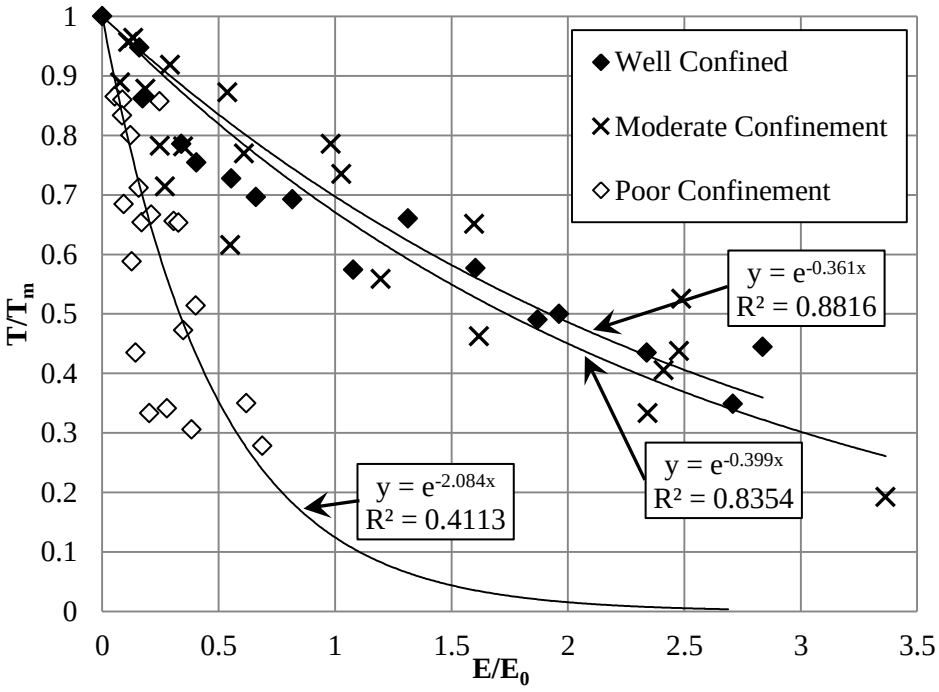

Figure 3-25: Damage-Energy relationship for differing levels of confinement at low (~1%) levels of corrosion. 'Well Confined' – 6mm stirrups, 'Moderate Confinement' – 4mm stirrups, 'Poor Confinement' – 2.15mm and Unconfined specimens.

3.5 Analysis of Overall Trends

3.5.1 Recreation of Corrosion using Electrochemical Methods

Large variations were observed in corrosion levels when using the electrochemical technique adopted to recreate corrosion at an accelerated rate. Figure 3-26 shows the difference between the theoretical relationship (dashed line) and the experimental results. This shift was attributed to corrosion of stirrups and galvanised steel ties. In addition to this, there were large variations in the level of deterioration for specimens that had similar amounts of current applied. Corrosion of stirrups was observed in almost all specimens subjected to induced corrosion, with some extreme cases of deterioration shown in Figure 3-27. Deterioration such as this is the primary source of observed

variation in corrosion of the main reinforcing bar. In some instances complete loss of stirrup cross-section was observed, as shown in Figure 3-27b.

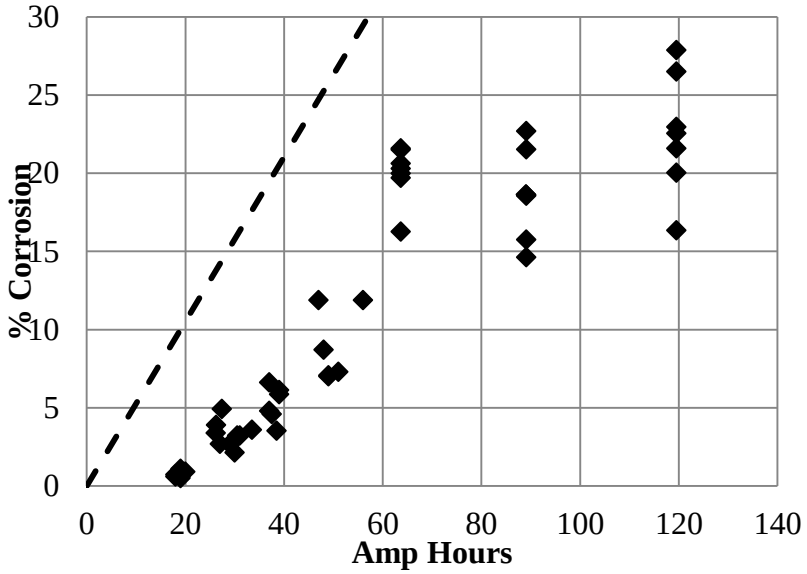

Figure 3-26: Relationship between applied amp-hours and level of corrosion, dashed line represents the theoretical relationship when using Faraday's law.

(a) **(b)**

Figure 3-27: Corrosion damage to confining stirrups, (a) partially corroded stirrup (b) complete loss of section of corroded stirrup

Use of imposed current to accelerate what is a slow electrochemical process in nature proved to be effective but erratic. For the final series of testing an approximate relationship, established from Phase 1 of testing, was adopted. This proved to be more reliable than theoretical calculations, though still produced large variations between specimens and slightly underestimated final corrosion levels.

Epoxy powder coating was used along with plastic adhesive, in place of galvanised wire, for the final series of specimens in an attempt to limit stirrup corrosion. This was found to have only limited

success with specimens still corroding in a similar manner to those without epoxy coating. Damage was again focused at the corner of stirrups (Figure 3-28), and while damage was less than that observed in highly corroded specimens, it was proportional to damage associated with the main reinforcing bar.

Figure 3-28: Corrosion damage to epoxy coated stirrups.

3.5.2 General Corrosion Effects (Monotonic)

Selected monotonic test results have been plotted in Figure 3-29 to show the general behavior of specimens as corrosion level increased. As corrosion levels increased, rupture stress, T_R, decreased and the presence of a well defined 'peak' at rupture diminished. Low to moderate levels of corrosion (<13%) were found to improve frictional stresses, T_f, which was attributed in increased radial pressures exerted on reinforcemnt due to its corrosion.

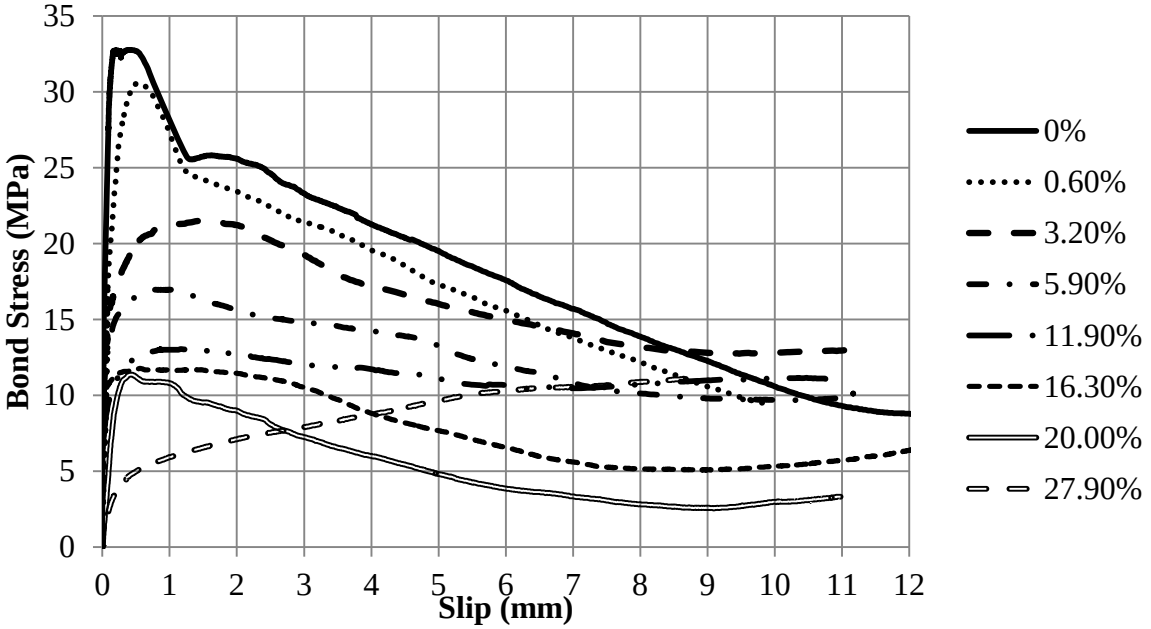

Figure 3-29: Selected indicative monotonic pull-out tests at various levels of corrosion.

Friction stresses decreased as corrosion level, and associated bond damage, inceased further. Reduction of frictional stresses was attributed to loss of mechanical interlock and lubricating effects provided by corrosion products which became more predominant at higher levels of deterioration.

In the majority of cyclic tests the equivalent monotonic rupture stress was able to be inferred based on initial cyclic performance. These were in general accordance with standard monotonic tests and allowed the data set to be expanded two-fold to 44 samples. Specimens from Series 3 with 4mm confining stirrups were also included and found to be complementary, though were slightly more erratic. Data from these tests was plotted in Figure 3-30 where two exponential trend lines were applied, one to the entire 44 specimen data set (top) the other to monotonic test data only (bottom). As shown by the regression values, these trend lines provided good correlation with the experimental data.

From Figure 3-30 it is clear that bond capacity is highly sensitive to the level of corrosion with 20% corrosion resulting in more than 65% loss in capacity, while 10% corrosion resulted in approximately 50% loss in bond capacity. Prediction of bonding performance at corrosion levels greater than 25% is difficult to determine with any sort of certainty and extrapolation is not advised.

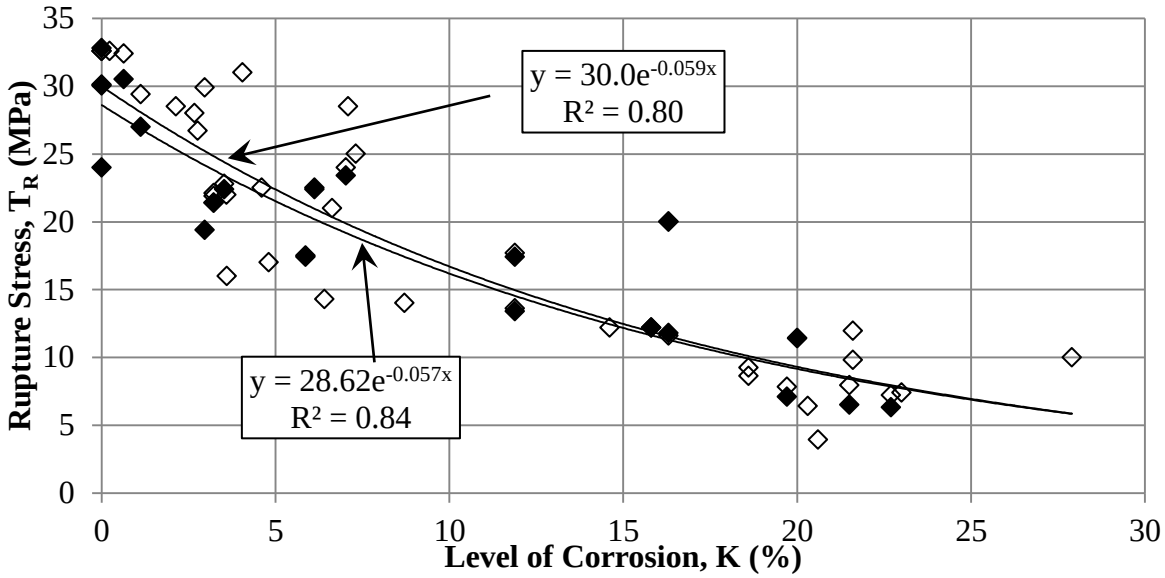

Figure 3-30: Plot of bond rupture stress under monotonic pull-out against level of corrosion including values from cyclic testing (hollow diamonds).

These results have been compared to results found by: Fang et al. (2004), Cabrera (1996), Almusallam et al. (1996), Al-Sulaimani et al. (1990), and Lee et al. (2002), who also investigated the effects of corrosion on bond performance. Figure 3-31 show the combined data set where it can be seen that uncorroded bond stresses observed were in the order of 50% higher than those observed by other researchers.

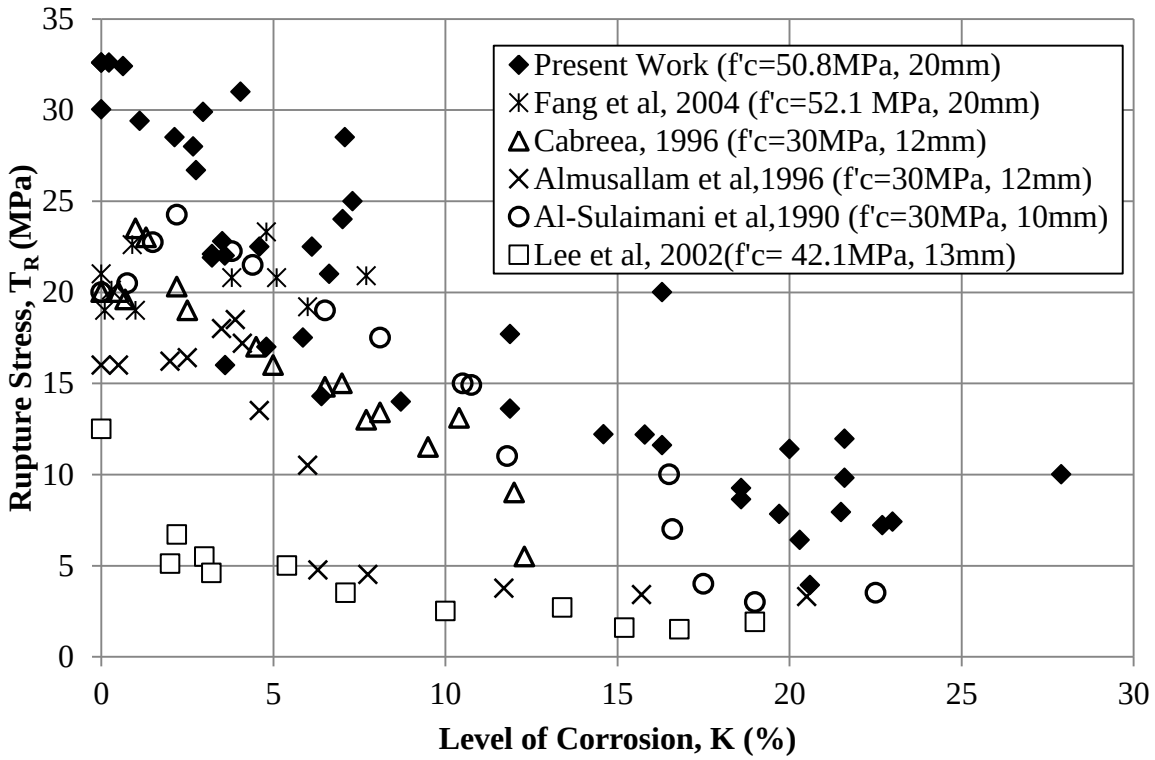

Figure 3-31: Comparison between experimental results gathered in this thesis and existing research.

Many different factors influence bond rupture strength and could be attributed to these differences. Firstly, all researchers, except for Fang et al. (2004), used different specimen geometry from those tested in this investigation. The level of confinement, bonded length and general dimensions differ between all other series tested. Even specimens of Fang et al. (2004) differ in confinement with their use of only two 6mm stirrups for confining steel as opposed to three used in these series of testing. Confinement plays a role in bonding performance but this may only be associated with approximately 10% of the difference to the results of Fang et al. (2004). The differing geometry of all the other specimens makes them difficult to compare in this regard.

Secondly, the strength and type has been shown to be a key parameter in bond strength (Eligehausen et al. 1983). All other specimens, other than those tested by Fang et al. (2004), were constructed using 30MPa concrete. It is widely acknowledged in design standards (Standards New Zealand 2006) that concrete strength plays a key role in bond strength, in particular its tensile strength, which is taken to be a function of the square root of its compressive strength. Based on this, using 50MPa concrete as opposed to 30MPa concrete, 30% out of the total 50% difference can be accounted for. In addition to this, at the time of testing, concrete in the specimens was in the order of 90 days old, at which time it was reaching compressive strengths of 65MPa. This may have impacted on the differing performance, although the age or strength at testing of concrete used in the other research was not published.

Thirdly, the deformation patterns were not described in more detail than ‘deformed’ or ‘ribbed’ leaving their exact dimension unknown. Deformations provide mechanical interlock, which is the primary component of resistance at bond rupture.

Fourthly, the bar size used by all other researchers differed from that used in this investigation, except for Fang et al. (2004, 2006). Increasing bar size has been found to reduce bond capacity (Eligehausen et al. 1983). Eligehausen et al. (1983) who found that an increase from 19mm bars to 32mm bars resulted in a 15% reduction in bond rupture stress.

Fang et al. (2004) developed 20MPa bond strength before rupture with specimens that were virtually identical to those used in this series of experiments. The final possible point of difference is the testing method. There may have been differences in testing associated with loading of specimens into the frame. In this series of tests it was acknowledged that opening of gaps between the concrete specimen and steel plates, which make up the loading frame would cause altered slip values to be recorded. In light of this, when specimens were loaded into the frame, the plates were tightened as much as possible using the nuts on the frame rods, clamping the specimen. This would have contributed to confining of the specimen and may have been a factor in the differing results.

3.5.3 General Corrosion Effects (Cyclic)

In general, corrosion was found to reduce the peak cyclic stresses and frictional sliding stresses. Comparison between cyclic results is difficult without more in depth analysis due to the complexity of variables present in cyclic test. This analysis is described in Section 4.3.

General stress-slip behaviour under positive and negative slip (bar in tension and compression respectively) was in general similar, although there were some points of difference. Peak stresses differed for each direction of loading. Specimens were always loaded under positive slip initially when cycling. For low levels of corrosion, stresses tended to be greater under positive slip, as shown in Figure 3-32 in the case of 0% corrosion, which may be associated with bond damage under elastic cycling.

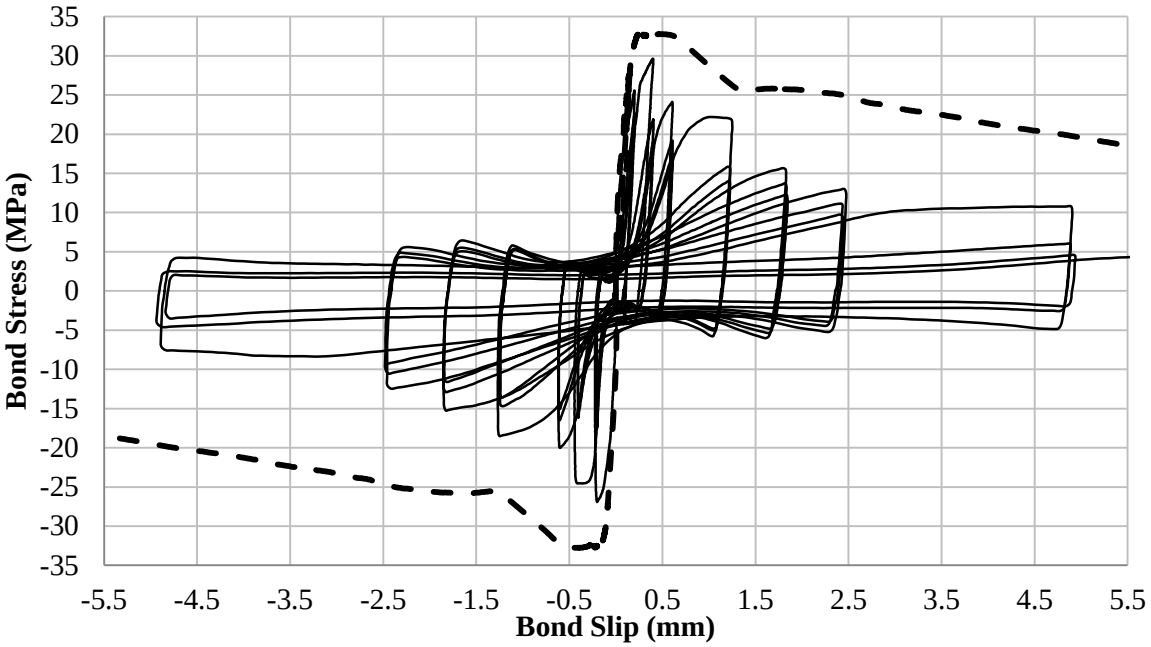

Figure 3-32: Stress-slip relationship for cyclic (0%) and monotonic (0%)

From Figure 3-32, the initial cycles reach equal stresses. Beyond this, damage occurs in the 4th cycle (first cycle of the second slip increment), resulting in reduced bond capacity when loading is reversed. This meant that stresses on the negative cycles had consistently half a cycle more damage and thus lower stress capacity. Counteracting this improved mechanical interlock between lugs and concrete, and higher friction would be expected under negative slip (bar in compression) due to the Poisson effect exhorting increased radial stresses, though this is likely to be a minor effect.

Elastic deformation of the specimen's concrete prism and loading frame may have also caused discrepancies in the bar slip. Bar slip was measured from the unloaded end, thus when the bar was in tension, the bonded region within the concrete prism would have moved away from the potentiometer which was fixed to the top steel plate. The opposite occurred when the bar was under compression. Elastic elongation of the steel rods under 150kN was in the order of 0.05mm with a similar amount attributed to concrete shortening. Raw data was manipulated to account for these effects, but displacements under testing were dictated based on the unadjusted slip values. As a result of these deformations, there was often a disparity between positive and negative slip values and stresses, especially under low slip (<0.5mm), where 0.05mm of specimen deformation provided a more significant difference. These effects were more prevalent in lightly corroded specimens where higher loads were reached and may be responsible for some of the variation, also played a role in stiffness under initial loading and when specimens were unloaded.

3.6 Experimental Limitations

Within the experimental programme a number of assumptions and simplifications were made to achieve results within time and resource constraints. These were assumed to have negligible effects on results, but their true impact was often unclear.

Use of 80mm bonded length was made to allow for assumption of uniform bond stress along reinforcement. Corrosion of reinforcing proved highly non-uniform, especially in heavily corroded specimens, causing non-uniform stress distribution. Non-uniformity would be expected in real structures where one region of heavy pitting is accompanied by a much larger region on lesser damage under macro-cell corrosion. This can be accounted for through application of differing levels of corroded bond represented within the numerical application the bond-slip model. Secondly, under testing condition, reinforcement was not yielded which would be expected to occur in seismic, ultimate limit state conditions, where cyclic bond-slip becomes a factor. Yield, or even differing bar stresses at pull out due to differing bond condition, affects the cross-section of reinforcing due to Poisson's effect and were not considered (Ashtiani et al. 2011).

In structures, reinforcement is never in tension while its surrounding concrete is in compression. While recent in research (Ashtiani et al. 2011), mechanically jointed beams have been used to remove these errors, these were seen to be too labour intensive, too bulky to corrode efficiently and accurately, and not seen to provide a justifiable level of increased accuracy in a process which is already fraught with inherent variation.

Bar size, cover, concrete strength and deformation patterns have all been round to play a role in bond performance (Eligehausen et al. 1983). These factors were kept constant to allow for assessment of only corrosion and confinement effects. In addition to this, a complete experimental investigation into all for mentioned factors and their effects when combined with corrosion would see a dramatic increase in demand on time and material resources.

Finally, use of accelerated corrosion techniques to allow timely recreation of corrosion electrochemically created corrosion products that differed slightly from those observed in natural corrosion. Submersion in water limits oxygen availability, causing formation of lesser oxygenated iron oxides with differing expansive characteristics. Presence of moisture also impacts the swelling properties though these variations have been shown in to only vary in the order of 10% (Weizhong et al. 2010; Zhao et al. 2011) but would have altered internal radial pressure to some degree.

4 Corrosion Dependent Bond-Slip Model

Experimental data was analysed and analytical trends observed were implemented within a hysteretic model of corrosion and confinement dependent cyclic bond-slip behaviour. The model was developed in such a way that it would be suitable for implementation within numerical modelling of the interface between steel reinforcement bonded to concrete.

4.1 Methodology

The model developed by Eligehausen et al. (1983), shown in Figure 2-14 and discussed in Chapter 2.1, has been widely used since its development and was the starting point for development of the corrosion dependent model. The developed model accounted for: bond strength degradation under cyclic loading, the effects of corrosion, and the effects of reduced confinement. Bond stresses return to the monotonic 'back-bone' if loading has not reached 90% of the rupture stress in cycling. If cyclic stress exceeds 90% of rupture stress point, damage to the bonding surface will result in diminished bond performance which aggregates with continued cycling.

Impacts of corrosion and confinement were included, in addition to the existing curve. Corrosion was measured in the percentage mass-loss along the bonded section and confinement was determined based on the corrosion reduced 'Stirrup Index of Confinement', Ω (Plizzari et al. 1998) which relates the bonded areas within the area of confining steel. When applied to a structural component it may be appropriate to have differing confinement values based on whether the surrounding concrete is enclosed by stirrups or is only cover concrete. The same principle may also be applied to corrosion, with bars nearest to the exposed concrete surface generally experiencing the greatest amount of deterioration.

4.1.1 General Behaviour

The proposed cyclic bond model consisted of two main sections: the monotonic 'back-bone' curve which is shown in Figure 4-1, and the cyclic component, which is shown in Figure 4-2. Relationships for the backbone curve were determined from experimental testing described in Chapter 3. The relationships used within the proposed model for determining; Rupture stress, T_R, Ultimate frictional stress, T_f, and Ultimate friction slip, S_f, for various levels of corrosion and confinement are described in the following sections.

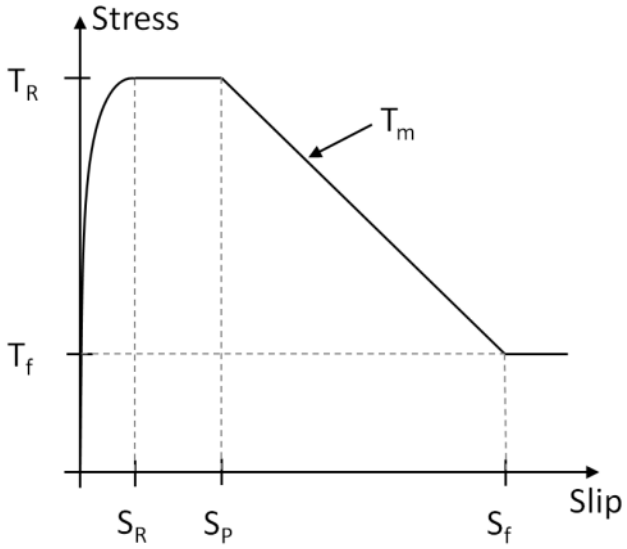

Figure 4-1: Monotonic 'back-bone' model, T_m*

The monotonic back-bone, T_m, consists of four regions. The initial loading section before rupture, T_R, is determined using Equation 4-1;

$$T_m = T_R \left(\frac{Slip}{S_R}\right)^n \qquad \text{Equation 4-1}$$

'n' was taken as 0.2 to match experimental behaviour. The other three regions consist of straight lines linking critical points with the final section, where slip is greater than S_f having a constant value of T_f. Values for the monotonic backbone, T_m, follow Equation 4-2 which matches the Eligehausen et al. (1983) model.

$$T_m = \begin{cases} T_R \left(\frac{Slip}{S_R}\right)^n & 0 \le Slip < S_R \\ T_R & S_R \le Slip < S_P \\ T_R + \frac{\left(T_f - T_R\right)}{\left(S_f - S_P\right)}(Slip - S_P) & S_P \le Slip < S_f \\ T_f & S_f \le Slip \end{cases} \qquad \text{Equation 4-2}$$

The cyclic model can be broken down into five main sections, as can be seen in Figure 4-2. Description of these sections and their computation follows.

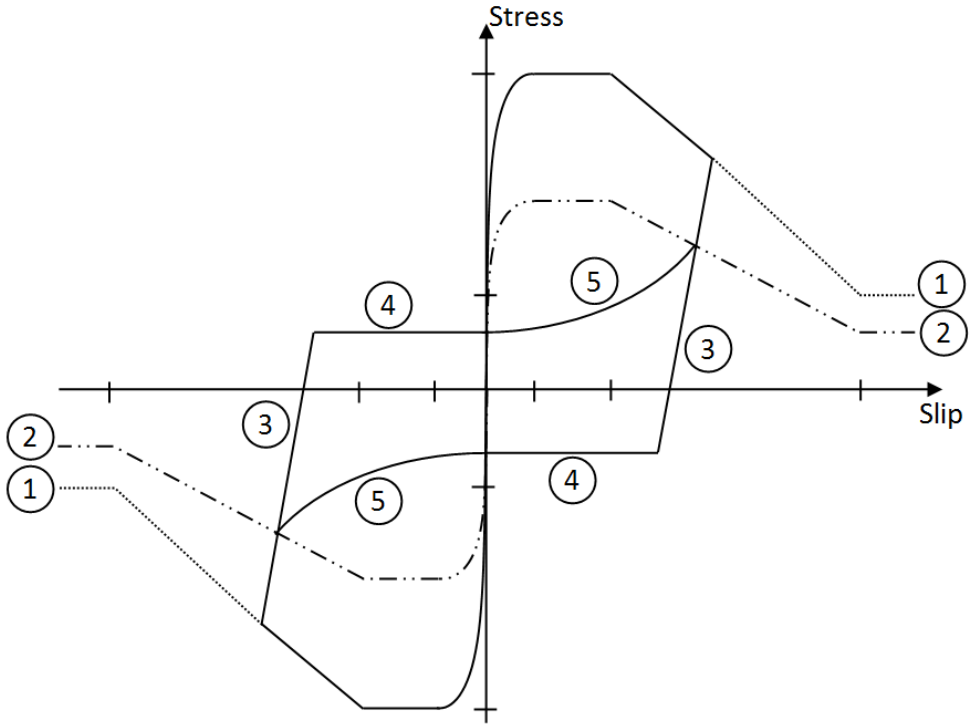

Figure 4-2: General make up of the proposed cyclic bond model

1. *Monotonic 'Back-bone' Curve, T_m:* Represents monotonic pull-out behaviour and provides the largest bond stress that can occur at a given slip. The 'back-bone' curve is dependent on concrete, steel and geometric properties of the longitudinal reinforcing bar and its surroundings. Included in this document are allowances for alteration of the initial 'back-bone' values depending on; level of corrosion deterioration (Section 4.2) and level of confinement (Section 4.4).
2. *Damage Affected Monotonic Envelope, T_m*:* When bond stresses exceed 90% of rupture stress and loading is reversed, damage begins to accrue due to crushing and cracking of concrete surrounding the reinforcing bar. Damage to surrounding concrete reduces the stress that the bond is able to attain for a given slip, reducing the monotonic back-bone envelope. The method of determining the damage affected monotonic envelope for differing levels of corrosion and confinement is outlined in Section 4.3.1 and Section 4.4.4, respectively.
3. *Initial Unloading Phase:* When loading is reversed there is an initial elastic rebound phase caused by compressed concrete in front of the reinforcing rib. The stiffness, k, of this phase is very large with suitable stiffness values ranging from 180 MPa/mm to 1000 MPa/mm. In numerical modelling the stiffness associated with section 3 of the cyclic curve will be taken to be 250 MPa/mm. This behaviour occurs when reversing occurs in any of the other phases and continues with a stiffness of 'k' until the value of phase 1, 2, 4 or 5 are met. Similarly, if complete unloading does not occur then loading will remain on this path until phase 1, 2, 4 or 5 are met.

4. *Unloading Sliding Phase, T_S:* Represents sliding of reinforcement against surrounding concrete. The stress values for this section are closely related to the Ultimate friction stress, T_f, in Figure 4-1. Sliding stress depends on concrete, steel and geometric properties of the reinforcing bar and surroundings, as well as the maximum slip. Allowance for corrosion and cyclic damage effects are also included and are further described in Section 4.3.2.
5. *Loading Sliding Phase:* Experimental results displayed a phenomenon where bond stresses increased as maximum slip was approached. In order to capture this behaviour a power function was adopted. This function is shown as Equation 4-3 ;

$$T = T_S + (T_m * - T_S)(\frac{Slip}{|Slip_{max}|})^{2.5} \quad \text{Equation 4-3}$$

Where T_m* is the value of the damaged monotonic envelope at the current slip and $|Slip_{max}|$ is the maximum previous slip in the direction that loading is moving towards.

Coding of the hysteretic model from Ruaumoko3D (Carr 2010b) can be seen in Appendix G.

4.2 Modification Factors for Level of Corrosion (Monotonic)

4.2.1 Rupture Behaviour, T_R

Due to the large variations in uncorroded rupture strength found in previous research (Fang et al. 2004; Cabrera. 1996; Almusallam et al. 1996; Al-Sulaimani et al. 1990; Lee et al. 2002) it was elected to normalise all data by each series' uncorroded rupture stress, known as the stress ratio ($T_{R,K}/T_{R,0}$), the results of which can be seen in Figure 4-3.

From the experimental data Equation 4-4, the relationship for corrosion dependent stress ratio was determined.

$$\frac{T_{R,K}}{T_{R,0}} = 1.2e^{-0.076K} \leq 1.0 \quad \text{Equation 4-4}$$

Where K is the percentage corrosion of the bonded region. This equation gives a regression (R^2) value of 0.77 for the global data set giving confidence in its validity.

Similar equations have been proposed by other researchers to account for effects of corrosion on bond rupture stress. Bhargava et al. (2007), presented a number of these alternative equations while proposing their own. These are shown in Table 4-1, some of the expressions have been normalised to match the 'stress ratio' concept.

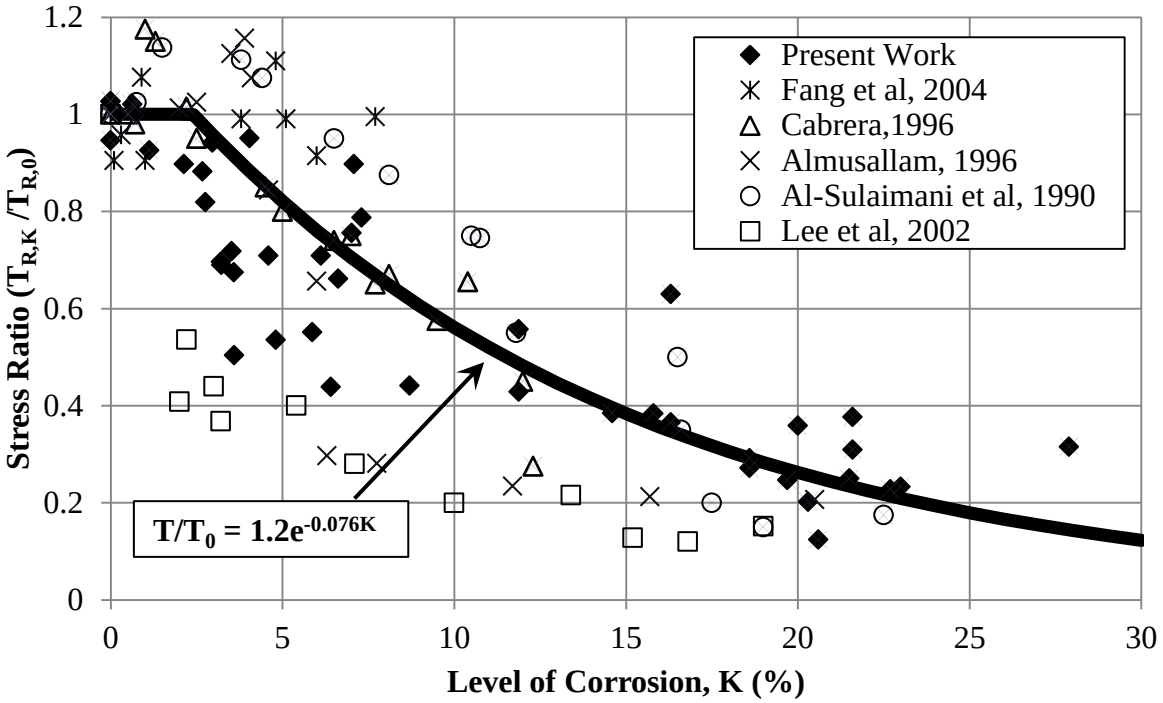

Figure 4-3: Normalised rupture stress (Stress Ratio) against level of corrosion comparing result with other published test data.

When the equation proposed within the present work was compared to that proposed by Bhargava et al. (2007) similar behaviour was observed. Differences between the two relationships may be attributed to differing confinement used in the experimental data, as highlighted earlier in Section 3.5.2.

Table 4-1: Existing equations proposed to account for the effects of corrosion on rupture bond stress.

Paper	Equation	Normalised Equation	Comments
(Cabrera 1996)	$T_{R,K}$=23.478-1.313K (MPa)	$\frac{T_{R,K}}{T_{R,0}} = 1 - 0.056K$	Pull-out, d_b=12mm, w/c=0.55, 0%-12.6% corrosion
(Lee et al. 2002)	$T_{R,K}=5.21e^{(-0.0561K)}$ (MPa)	$\frac{T_{R,K}}{T_{R,0}} = e^{(-0.0561K)}$	Pull-out, d_b=13mm, f'_c=24.7-42.1 MPa, w/c=0.45-0.65, 0%-12.6% corrosion
(Stanish et al. 1999)	$T_{R,K}=\sqrt{f'_c}(0.77 - 0.027K)$ (MPa)	$\frac{T_{R,K}}{T_{R,0}} = 1 - 0.035K$	Flexural, d_b=10mm, f'_c=35MPa and 43 MPa, 0%-20.7% corrosion
(Chung et al. 2004)	$\frac{T_{R,K}}{T_{R,0}} = 2.09K^{(-1.06)} \leq 1.0$		Flexural, d_b=10mm, f'_c= 18.8 MPa, 0%-15% corrosion
(Bhargava et al. 2007)	$\frac{T_{R,K}}{T_{R,0}} = 1.192K^{(-0.117K)} \leq 1.0$		Derived from experimental data-base

In Figure 4-4 a comparison between the five models is shown: the present work and results from the four other papers. The models proposed by Stanish et al. (1999) and Lee et al. (2002) follow the present data closely, whereas other models display a greater and more rapid deterioration of bond capacity.

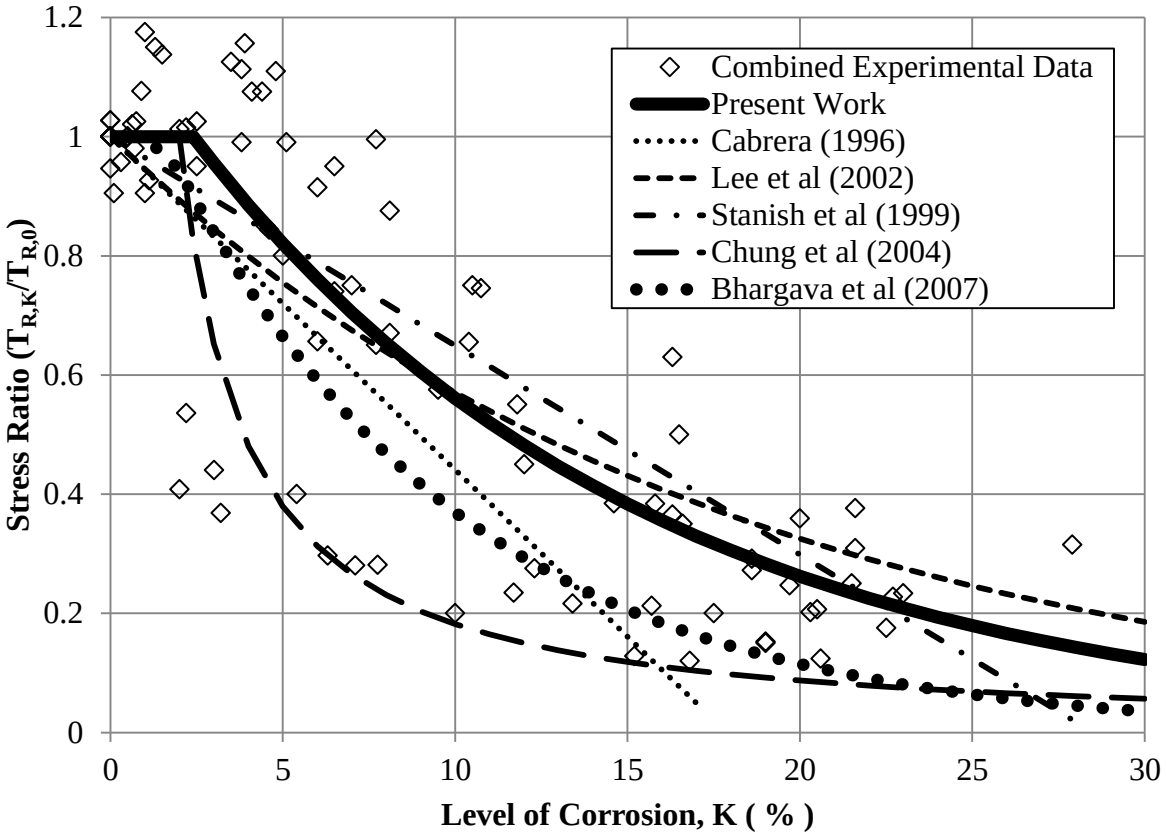

Figure 4-4: Comparison of proposed bond degradation model: existing models and experimental results.

4.2.2 Ultimate Frictional behaviour, T_f

Once purely frictional behaviour was reached, stress was measured and plotted against the level of corrosion, as shown in Figure 4-5. It can be seen that under low levels of corrosion (< 7%) additional corrosion enhances frictional stress capacity, which was attributed to increased radial stresses on corroded reinforcing due to the expansive nature of corrosion products. Following this, additional corrosion provided a lubricating effect and ultimate frictional stresses declined until they plateaued after 21%. This plateau was assumed due to limited availability of data at corrosion levels in excess of 21%.

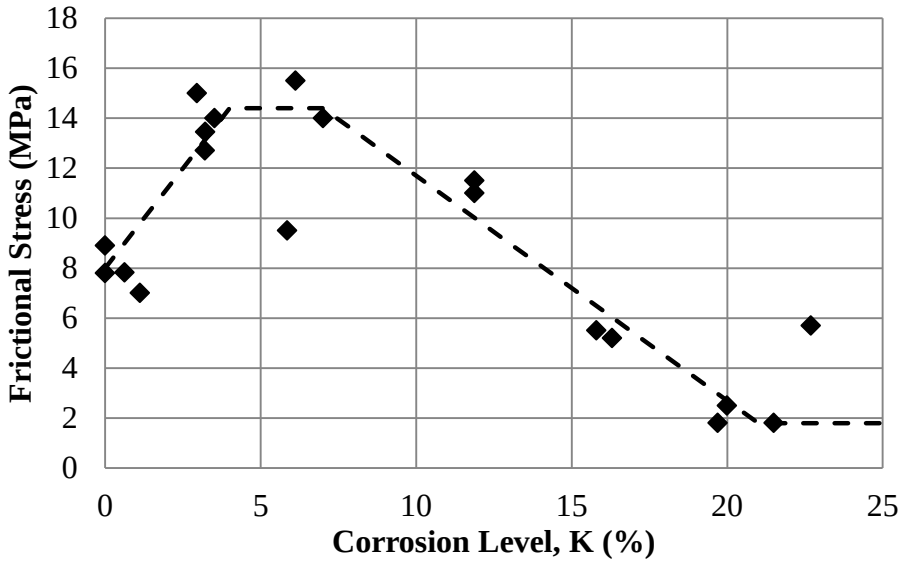

Figure 4-5: Relationship between ultimate frictional bond stress and the level of corrosion

In order to develop a generalised equation it was elected to adopt a dimensionless approach by dividing the ultimate frictional stress, $T_{f,K}$, by the monotonic rupture stress, $T_{R,K}$. $T_{f,K}/T_{R,K}$ was plotted against corrosion level, K, as shown in Figure 4-6. From these data points Equation 4-5 has been proposed.

$$\frac{T_{f,K}}{T_{R,K}} = \begin{cases} 0.26 + 0.13K & 0\% \leq K < 3\% \\ 0.65 & 3\% \leq K < 13\% \\ 0.65 - 0.06(K - 13) & 13\% \leq K < 20\% \end{cases}$$

Equation 4-5

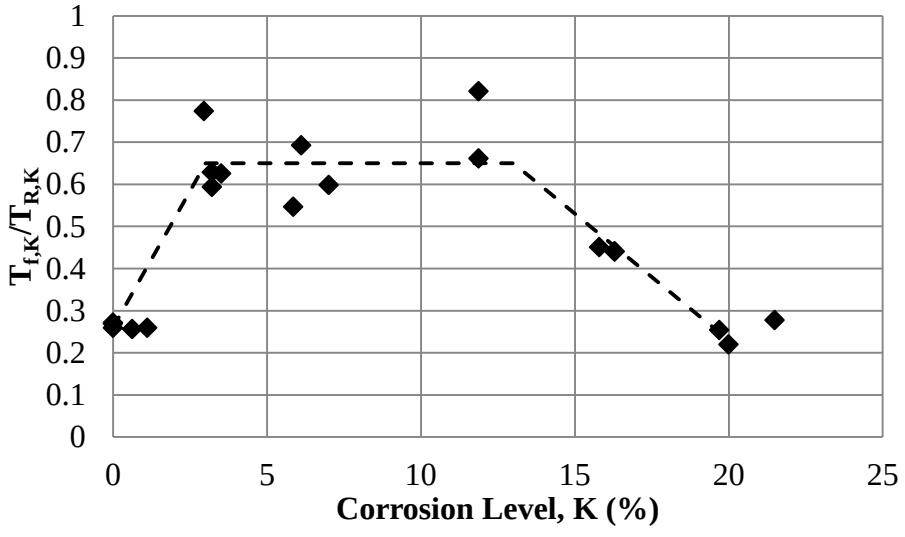

Figure 4-6: Bond stress after purely friction behaviour has been reached as a function of monotonic rupture stress at various levels of corrosion.

No comparative relationships linking level of corrosion and ultimate frictional bond stress were found in literature.

4.2.3 Ultimate Frictional Slip, S_f

Slip at the point where ultimate frictional behaviour occurs, S_f, was found to range between 12mm and 6mm. As shown in Figure 4-7, the value of ultimate frictional slip decreased quickly with corrosion until plateauing around 8mm after ~5% corrosion. Equation 4-6 has been proposed to represent this and is shown below and within Figure 4-7.

$$S_f = 4.5e^{-0.3K} + 7.5 \qquad \text{Equation 4-6}$$

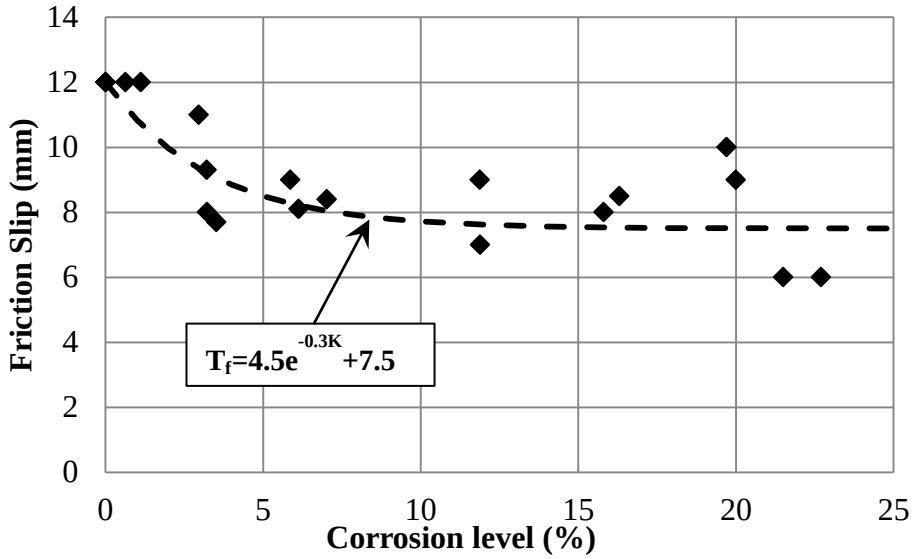

Figure 4-7: Bar slip at which purely friction behaviour is reached for an HD20 bar at various corrosion levels.

It would be inappropriate to utilise this relationship for reinforcement other than deformed 20mm diameters bars. For this reason it was decided not to normalise the friction slip value. It has been suggested by other researchers that the value at which bar resistance becomes purely frictional is largely dependent on the reinforcing rib spacing and geometry (Eligehausen et al. 1983). No comparative relationships linking level of corrosion and ultimate frictional bond slip were found in literature.

4.2.3.1 Rupture Slip and Plateau End Slip, S_R and S_p

Bond rupture was taken to be when the maximum load was attained. There was no definitive relationship found between rupture slip and level of corrosion. As shown in Figure 4-8, rupture slip values were extremely erratic and were found to be sensitive to minor differences in testing arrangement and minor specimen defects. They may have also been affected by non-uniform corrosion of the reinforcing bar in the bonded region. Suitable values range from 0.25mm, as found for the uncorroded specimens, up to 1.5mm. An average of around 0.3mm was deemed suitable for most numerical investigations.

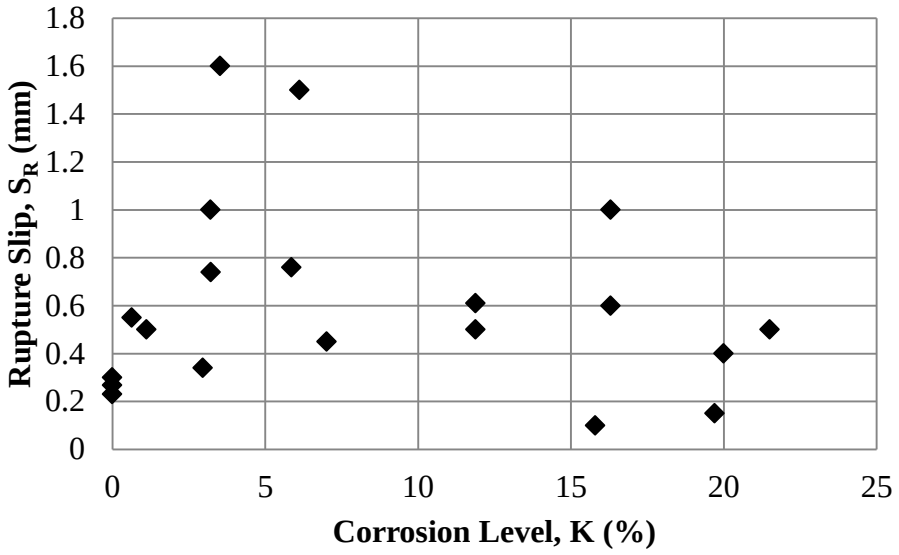

Figure 4-8: Relationship between rupture slip and corrosion level

In many tests no definitive end of plateau was observed, with instead a gradual reduction in bond stiffness. Because of this, a generalisation of 'rupture slip + 1.0mm' was used within further analysis. This value fits well with the majority of tests, though may be reduced to a 0.5mm plateau for specimens where 'peaking' might be expected. (Refer to Section3.2.3 for 'Peaking' description)

Combining the aforementioned monotonic back-bone factors, a stress-slip surface was created for corrosion levels between 0% and 20% as shown in Figure 4-9.

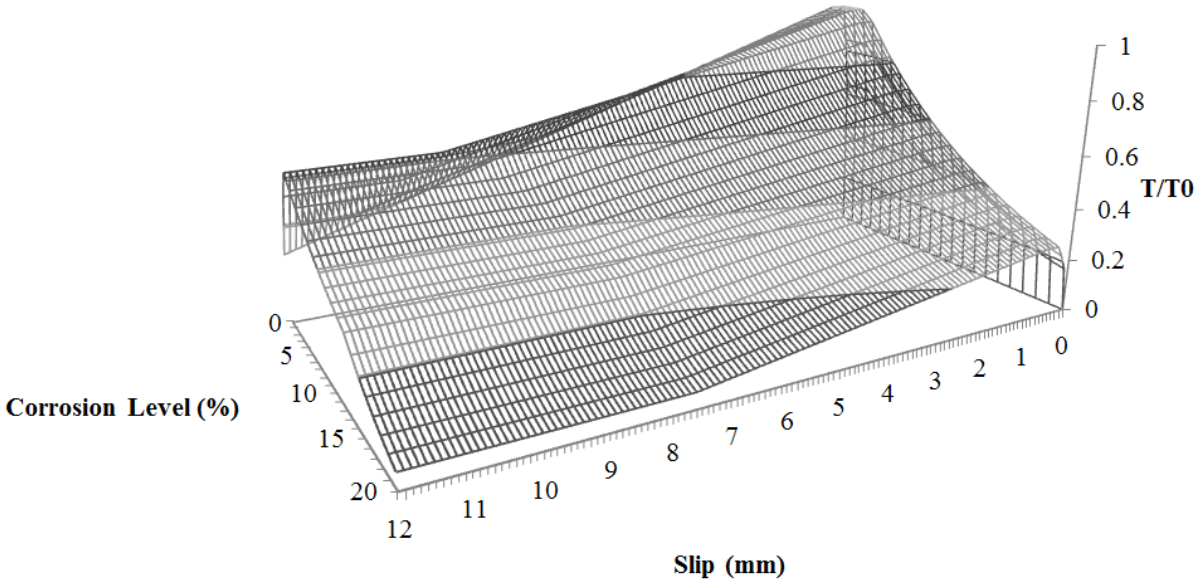

Figure 4-9: Surface model of the normalised proposed monotonic stress-slip relationship.

4.3 Modification Factors for Level of Corrosion (Cyclic)

Under cyclic loading, a number of additional variables were introduced to capture specific phenomena. When bond stresses were near rupture under cyclic loading, damage to surrounding concrete occurred, reducing bond stresses at maximum slip. This reduced the monotonic envelope from T_m to T_m* as shown in Figure 4-10.

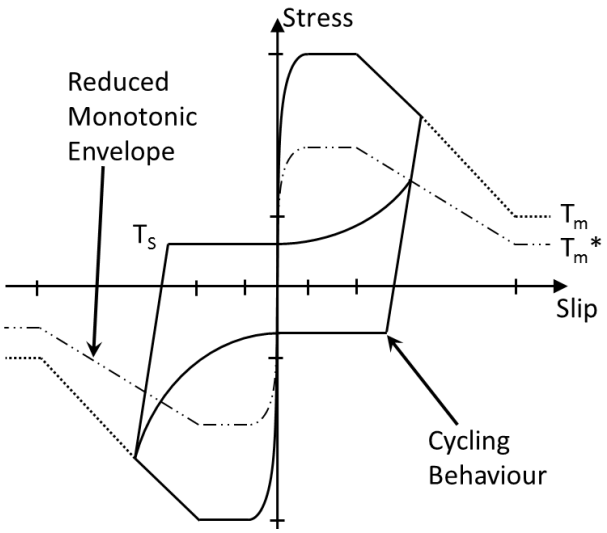

Figure 4-10: Generic cyclic behaviour diagram.

The model was structured such that when slip was not near its maximum value, sliding behaviour occurred. This is shown in Figure 4-10 by the central horizontal regions denoted with T_S. When load was applied in these regions, stresses display a graduated increase until the monotonic envelope was reached at the previous maximum slip. Damage to sliding stress, T_S, was dependent on sliding energy dissipated and maximum slip. The initial unloading portion of the curve, representing elastic rebound of compressed concrete in front of bar ribs occurred in approximately the first 0.05mm of unloading and was unaffected by repeated cycling.

4.3.1 Cyclic Damage, T_m/T_m*

Based on the general trends observed in Sections 3.2.3 and 3.3.3 on cyclic behaviour, Equation 4-7 has been proposed to determine the generalised 'Damage-Energy' relationship allowing for the inclusion of corrosion effects;

$$\frac{T_m^*}{T_m} = \alpha_K e^{\beta_K \frac{E}{E_0}} + (1 - \alpha_K) \qquad \text{Equation 4-7}$$

Where T_m*/T_m represents the damage or fraction of the monotonic envelope that can be achieved after cycling (i.e. Slip = minimum or maximum slip). α_K and β_K are empirically determined constants dependent of the level of corrosion, which can be found from charts/equations in Section 4.2, and E/E_0

is the fraction of dissipated energy over the energy under the monotonic stress envelope, as shown in Figure 4-11.

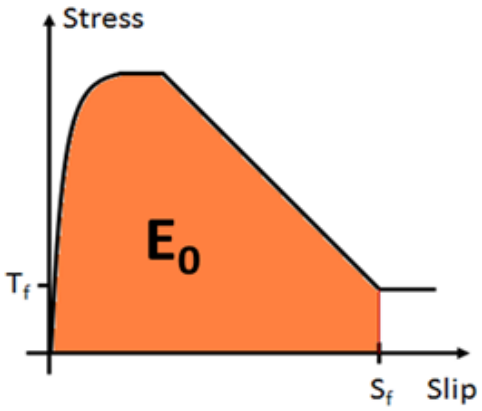

Figure 4-11: Definition of E_0, the area under the monotonic bond stress-slip curve before purely frictional behaviour is reached.

From experimental results it was found that one minus the ratio of ultimate frictional stress, T_f, to the rupture stress, T_R, (Equation 4-8), gave very good correlation with the ultimate damage due to cycling as shown in Figure 4-12. However, at higher levels of corrosion (>20% corrosion) the relationship breaks down and a value of α=0.6 was more suitable.

$$\alpha_K = 1 - \frac{T_{f,K}}{T_{R,K}} \qquad 0 \le \alpha_K \le 1$$

Equation 4-8

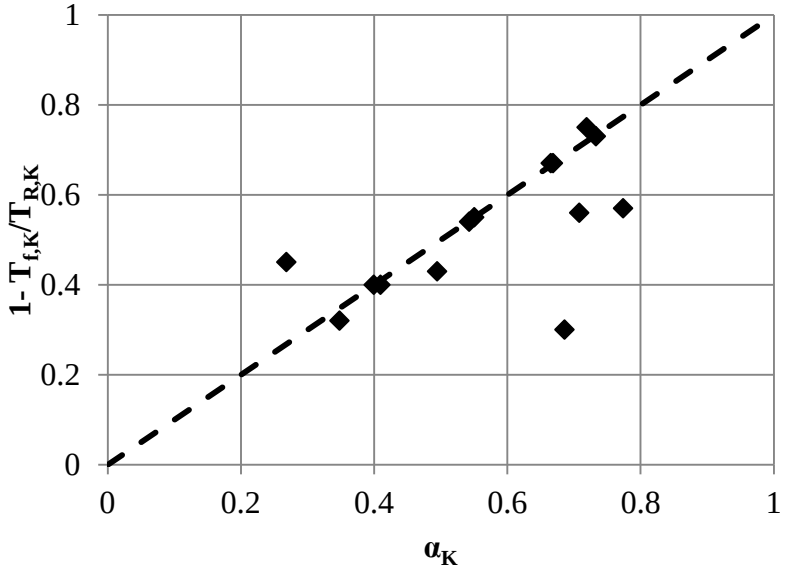

Figure 4-12: Relationship between the monotonic frictional ratio and α used in damage-energy relationship.

Hence when T_f/T_R is substituted into the α_K equation, Equation 4-9 was formed;

$$\alpha_K = \begin{cases} 0.75 - 0.13K & 0\% \leq K < 3\% \\ 0.35 & 3\% \leq K < 13\% \\ 0.35 + 0.06(K - 13) \leq 0.6 & 13\% \leq K < 20\% \end{cases} \quad \text{Equation 4-9}$$

The plot for the Equation 4-9 is shown in Figure 4-13.

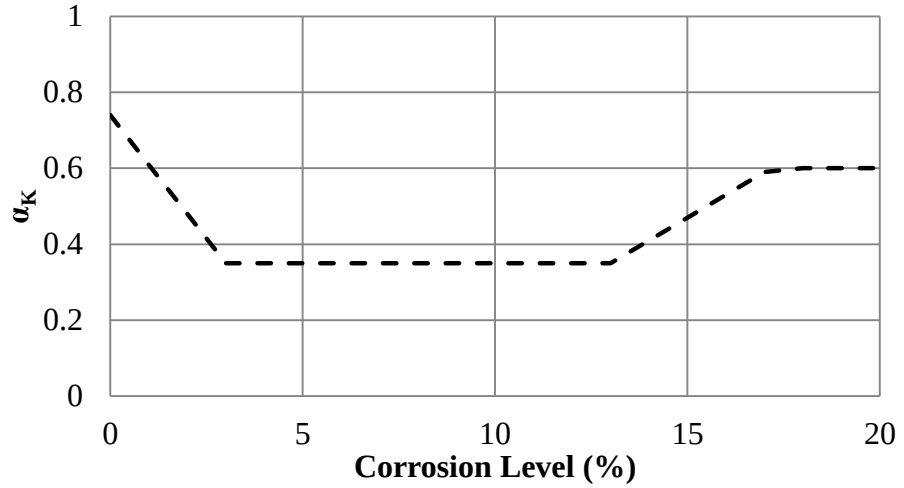

Figure 4-13: Relationship between α and corrosion level for Damage-energy model.

The second factor, β_K, was more erratic, as can be seen in Figure 4-14, where the regression value (R^2) was only 0.49, indicating only a moderate correlation between the data. However, removal of the two outlying values, where β_K<2.0, saw this value increase to 0.73. The final equation representing β_K is shown as Equation 4-10;

$$\beta_K = -0.58 - 0.046K \quad \text{Equation 4-10}$$

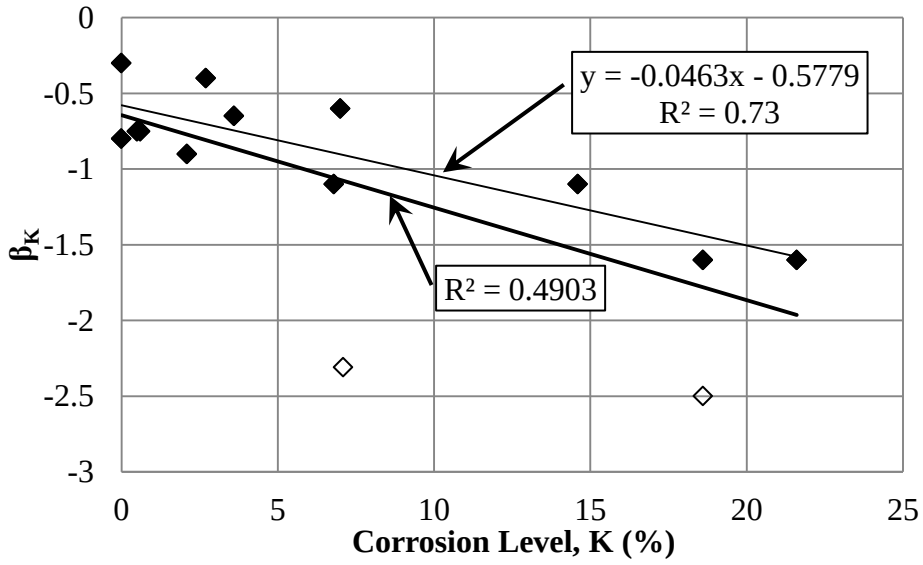

Figure 4-14: Relationship between beta and level of corrosion for use in damage-energy relationship.

Figure 4-15 shows the model's behaviour at low levels of corrosion ranging from 0% to 5%. It can be seen that damage to bond decreases with increasing corrosion up to 3% corrosion, and then remains approximately constant up until 5% corrosion.

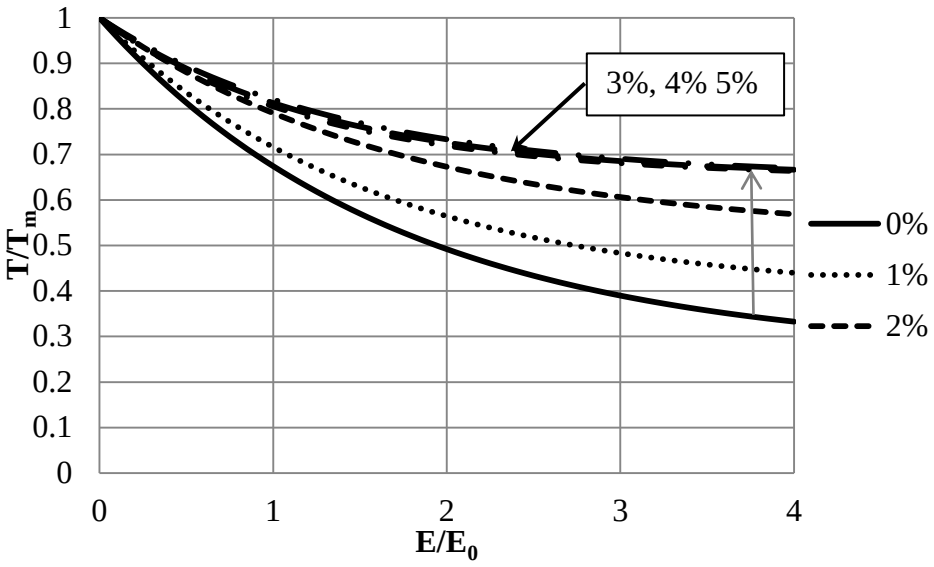

Figure 4-15: Damage energy model for corrosion levels between 0% and 5%.

The second graph, Figure 4-16, shows the model from 5% to 20% corrosion, where it can be seen that between 5% and 10% there is little change in damage behaviour. At 15% and 20% corrosion there are significant increases in the amount of damage for the equivalent amount of dimensionless dissipated energy. This trend is primarily dependent with the α_K factor which is closely associated with the Rupture stress, T_R, and Ultimate frictional stress, T_f from the monotonic envelope.

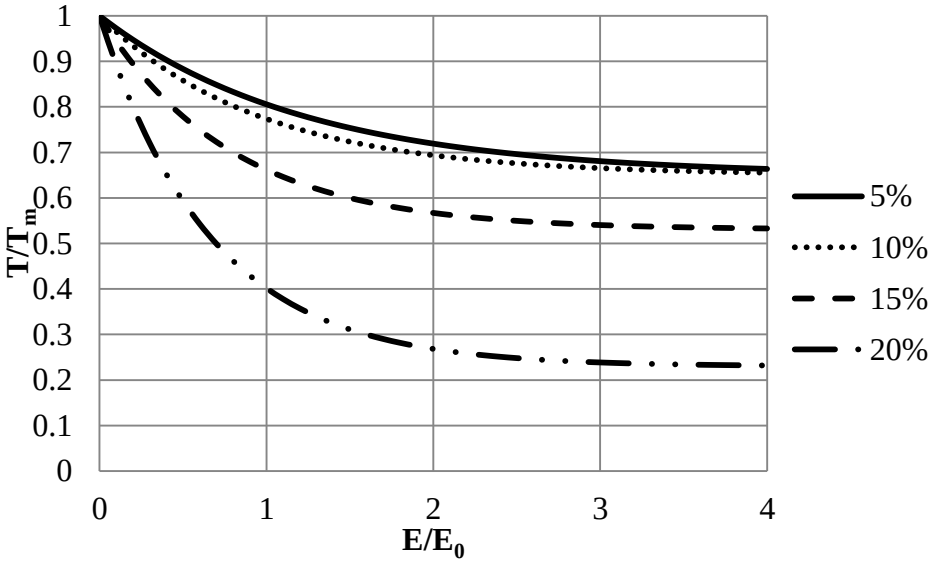

Figure 4-16: Damage-Energy model for corrosion level between 5% and 20%.

Figure 4-17 gives a graphic representation of the overall damage-energy model looking at corrosion levels between 0% and 20%. The effects of corrosion on bond degradation are highlighted through

increases in ultimate frictional stresses at ~3% corrosion, where the least reduction of bond stress, due to cyclic loading is observed. No comparative relationships linking level of corrosion and bond damage due to cyclic loading were found in literature.

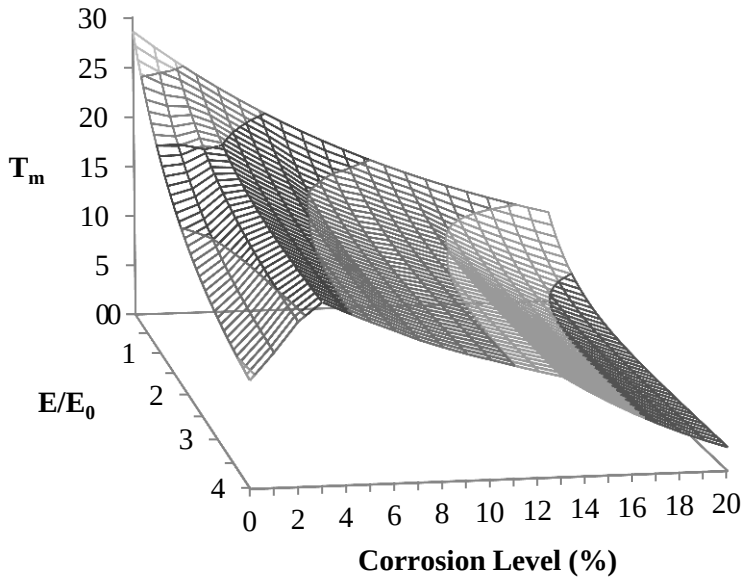

Figure 4-17: Surface representation of damage-energy model at various levels of corrosion.

As shown in Figure 4-18, friction stresses at rupture increase markedly with low levels of corrosion while mechanical interlock decreases rapidly. Friction increases due to formation of corrosion production on the bar surface until radial stresses overcome the tensile strength of surrounding concrete and cracking is initiated, reducing radial stress on reinforcement due to movement of corrosion products into the newly formed cracks. This causes the frictional resistance to reduce, and continue to reduce as the level of corrosion increases.

Mechanical interlock reduces with increasing corrosion level due to build up of corrosion products at the concrete-steel interface. Build up of corrosion products caused damage to the bonded concrete surface through micro cracking, as well as breaking any chemical adhesion between steel and concrete. As corrosion increased, loss of reinforcement ribs increased, which further impaired interlock as well as damaging surrounding concrete.

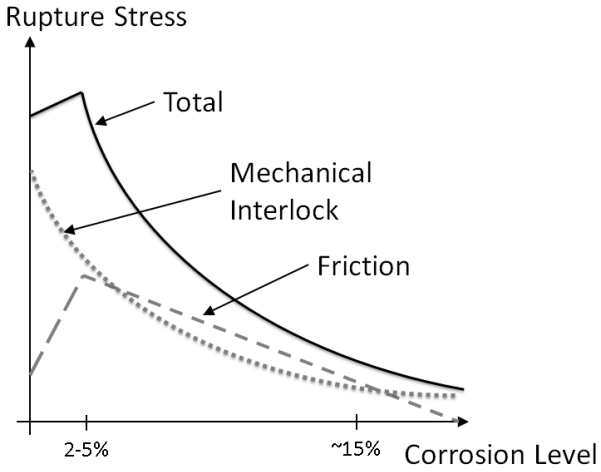

Figure 4-18: Changes in rupture resistance contributions of mechanical interlock and friction with increasing corrosion levels.

It can be assumed that throughout the pull-out process, at any given level of corrosion, frictional stresses remain roughly constant, provided splitting does not occur. Based on the above statement being true, then it is loss of mechanical interlock that is primarily responsable for reduction in resistance as pull-out progresses. For this reason, the relationship between the relative magitudes of these two resistance mechanisms is primarily responsible for behaviour of the damage-energy relationship developed for cyclic loading of corroded reinforcment.

4.3.2 Sliding Stress, T_S

Bond sliding is the portion of the hysteretic loop where stresses remain approximately constant and slip is not at a maximum or minimum. Sliding stresses under cyclic loading were found to be dependent on two variables; energy dissipated through sliding, and maximum bond slip. These variables are in turn, dependent on a number of factors, of which all, other than corrosion level, were maintained constant in experimental testing. Figure 4-19 shows the generalised trend between sliding stresses and maximum slip under cyclic loading. It can be seen that the first cycle of each increased maximum slip increment produced higher sliding stresses than the last cycle at the reduced maximum slip increment.

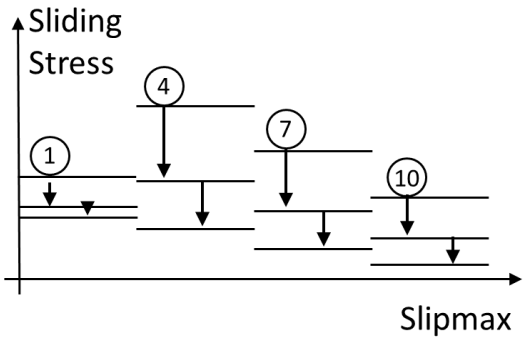

Figure 4-19: Diagram of generalised sliding stress over twelve cycles at increasing maximum slip.

Equation 4-11 was selected to represent sliding stresses found from experimental testing for specimens at various levels of corrosion, where A, B and C are corrosion dependent factors. Also included was the absolute maximum slip, *Slipmax*, and dimensionless dissipated frictional energy, E_f/E_{0f}, to capture the phenomenon described in Figure 4-19.

$$\frac{T_S}{T_{f,K} \times Slipmax} = Ae^{B(\frac{E_f}{E_{of}})^C} \qquad \text{Equation 4-11}$$

T_S represents sliding stress, $T_{f,K}$ represents the ultimate frictional stress at corrosion level K, *Slipmax* represents the absolute maximum slip value, E_f represents the energy dissipated through sliding and E_{0f} represents the ultimate frictional stress ($T_{f,K}$) multiplied by the ultimate friction slip (S_f). A, B and C were determined for each experimental test and their values plotted against corrosion level in Figure 4-20, Figure 4-21 and Figure 4-22.

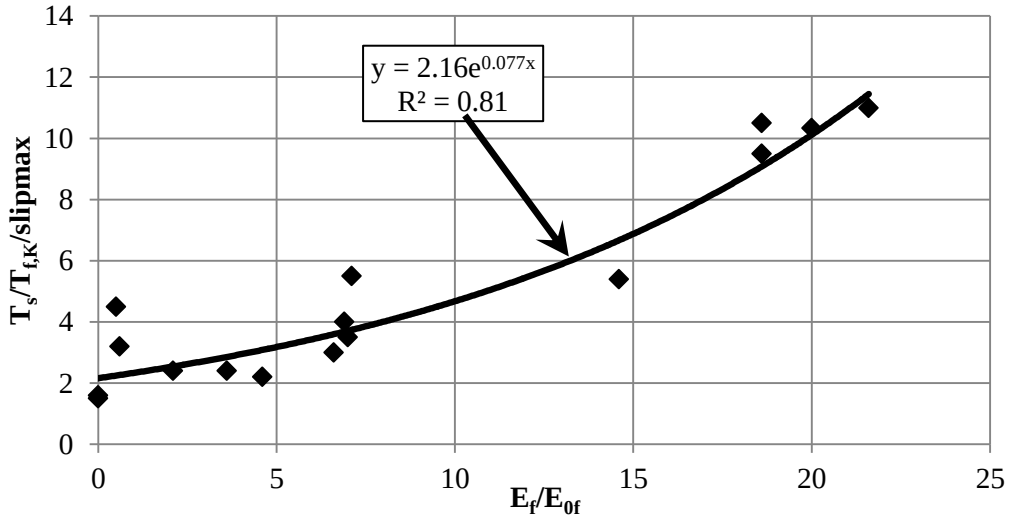

Figure 4-20: Plot of 'A' found from experimental results including model trend.

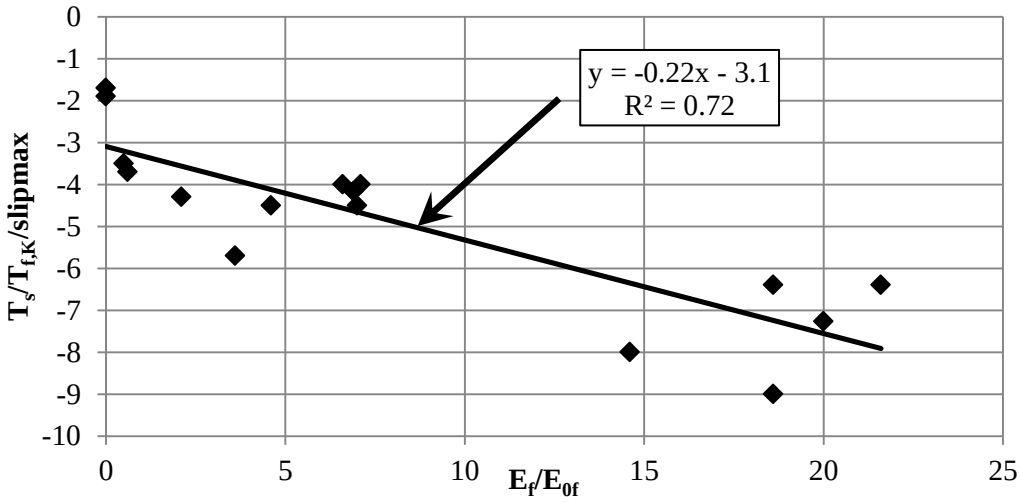

Figure 4-21: Plot of 'B' found from experimental results including model trend.

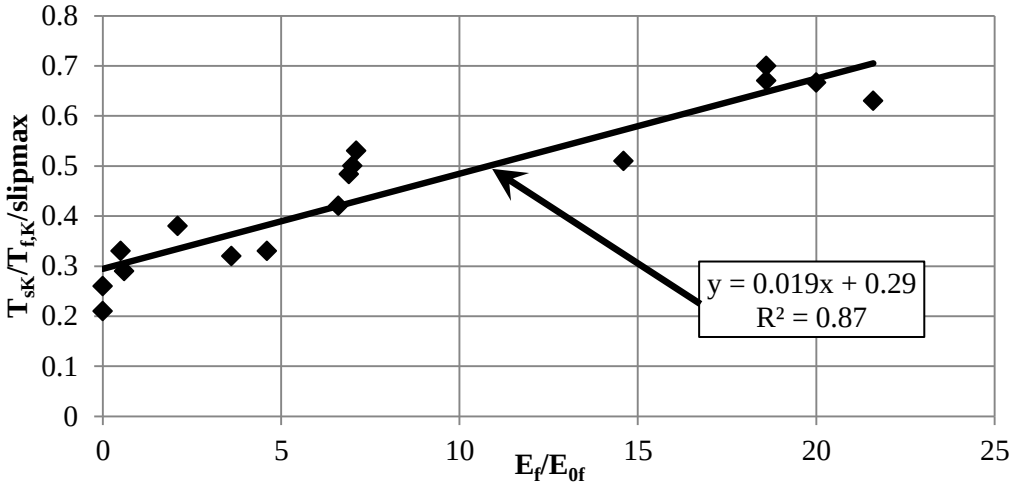

Figure 4-22: Plot of 'C' found from experimental results including model trend.

All trends displayed a strong correlation with R^2 values ranging from 0.72 to 0.87. From the equations displayed within the above figures, the relationships for, A, B and C are shown as Equation 4-12, Equation 4-13 and Equation 4-14;

$$A = 2.16e^{0.077K} \quad \text{Equation 4-12}$$

$$B = -0.22K - 3.1 \quad \text{Equation 4-13}$$

$$C = 0.019K + 0.29 \quad \text{Equation 4-14}$$

where 'K' is the percentage corrosion. Using these values, the original equation can be rearranged to determine the sliding stress, T_S, dependent on corrosion level, maximum slip, and sliding energy dissipated, as shown by Equation 4-15;

$$T_{s,K} = A(T_{f,K} \times Slipmax)e^{B(\frac{E_f}{E_{0f}})^C} \leq T_{f,K}(\frac{T_m^*}{T_m}) \quad \text{Equation 4-15}$$

This equation is limited to values less than the damaged ultimate frictional stress value ($T_{f,K}$ (T_m*/T_m)). When this relationship was plotted in its original form at different levels of corrosion, as shown in Figure 4-23, it can be seen that increasing corrosion levels resulted in larger decreases in sliding stresses.

To better show trends and understand sliding behaviour, corrosion adjusted values for the Ultimate frictional stress, $T_{f,K}$, were included from the corrosion dependent monotonic model described in Section 4.2.2. The altered model is shown in Figure 4-24 which displays stress divided by maximum slip, T_S/slipmax, against dimensionless dissipated energy.

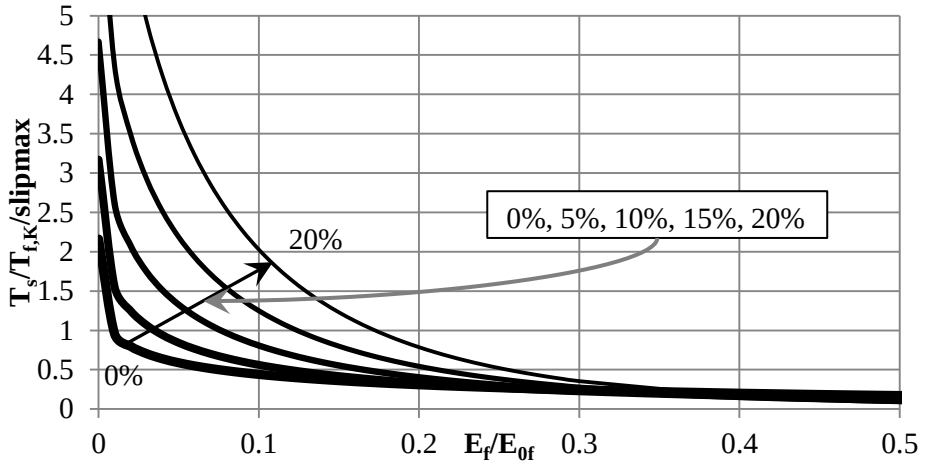

Figure 4-23: Plot of sliding stress damage relationship.

It can be seen that in a similar way to the Ultimate frictional stress, sliding stresses under the same maximum slip displayed an initial increase with increasing corrosion (up to 5%) followed by a decrease at corrosion levels greater than 5%. Sliding is a frictional mechanism and thus dependent largely on radial stresses experienced by the bar.

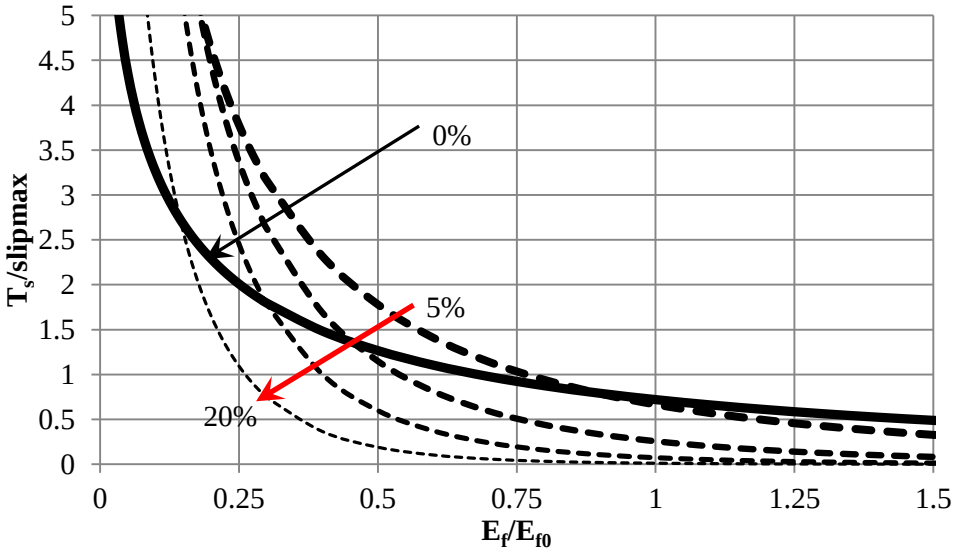

Figure 4-24: Sliding stress damage (over maximum slip) against dissipated sliding energy.

No comparative relationships linking level of corrosion and bond damage due to cyclic loading were found in literature. Fang et al. (2006a) did present a general trend that described reduction of sliding stress when cycling at constant maximum displacement. It was noted that 5% corrosion resulted in the largest reduction in sliding stresses over ten cycles at a fixed maximum displacement (Fang et al. 2006a), though this was determined from testing of only four specimens. This statement matches the what is described within the proposed model with 5% corrosion resulting in higher stresses initially but then decreasing beyond E_f/E_{f0} =0.9.

4.4 Modification Factors for Reduced Confinement

4.4.1 Splitting (Confinement)

As confinement decreased, a change in the bond failure mechanism from sliding to splitting of surrounding concrete was observed. This required an alteration in monotonic envelope to capture the instantaneous drop in bond strength that occurs in splitting failure as shown in Figure 4-25. To avoid computational issues associated with infinite stiffness S_f was set as $2S_R$, beyond which point bond stresses are equal to sliding stresses.

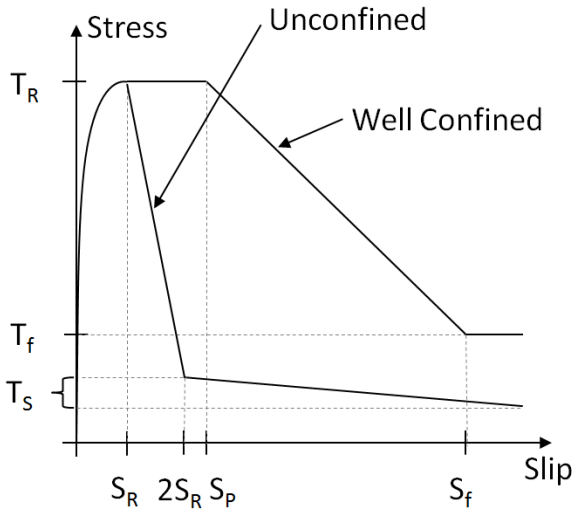

Figure 4-25: Difference in behaviour between well confined and poorly confined, splitting bond failure mechanisms.

4.4.2 Rupture Stress, $T_{R,\Omega}$

As discussed in Section 3.4, a clear relationship was displayed between confinement and bond rupture stress. To allow for the effects of confinement to be applied to scenarios where bar corrosion levels were not equivalent to those tested, a confinement stress ratio, $T_{R,\Omega}/T_{R,0}$, similar to that used for corrosion level, was adopted. Equation 4-16 was derived empirically from data shown in Figure 4-26.

$$\frac{T_{R,\Omega}}{T_{R,K}} = 0.55 + 0.45(1 - e^{-65\Omega}) \qquad \text{Equation 4-16}$$

The likelihood of concrete splitting prior to testing increases as corrosion increases and confinement decreases. Because of this, if surface cracking running parallel to reinforcement is apparent, expected capacity should be reduced. The relationship between cracking and bond strength reduction is outside the scope of this thesis, though data from existing research provides a series of proposed formulations (Tang et al. 2007). This model has been based only on experimental data gathered within the current experimental programme and is likely to be highly sensitive to the dimensions of specimens tested. Results matched the general trend observed by other researchers (Plizzari et al. 1998), though inclusion of corrosion provided additional variability.

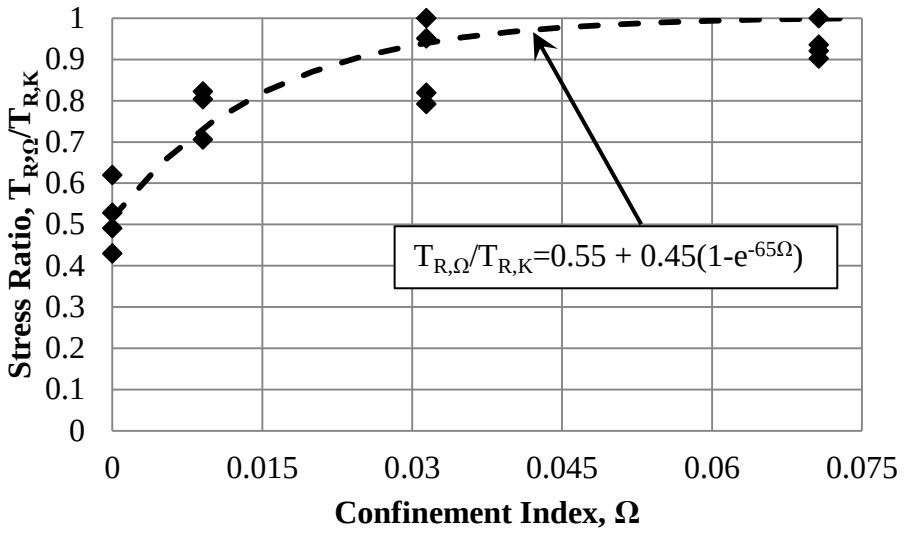

Figure 4-26: Graph of confinement index dependent stress ratio factor. Solid markers are intact specimens.

4.4.3 Ultimate Frictional Stress, T_f

For poorly confined specimens that prone to splitting failure, it is prudent to assume that complete bond strength is lost after rupture. While many specimens did regain limited strength after an instantaneous loss of strength, the magnitude of this was highly variable. In light of this, a piecewise model has been proposed based on experimentally gathered data. This model is displayed in Figure 4-27 below and fits Equation 4-17 (based on f'$_c$=50MPa);

$$T_{f,\Omega} = 1.2\sqrt{f_c'(1 - e^{-40(\Omega-0.01)})} \qquad \geq 0\ MPa$$

Equation 4-17

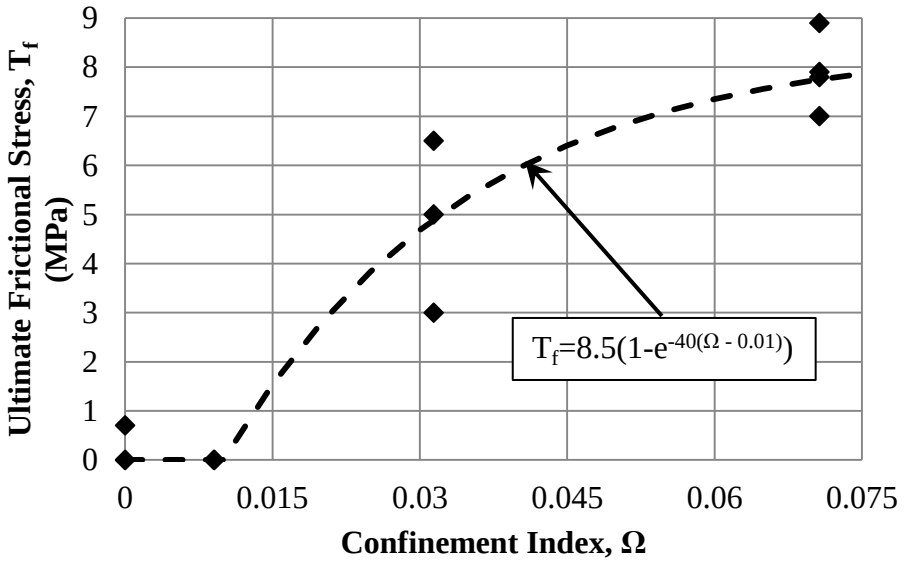

Figure 4-27: Relationship between ultimate frictional stress and confinement index.

From Figure 4-28 it can be seen that the dimensionless equation, Equation 4-18, for ultimate frictional stress did not produce a strong agreement with the experimental data. High levels of variability were present around Ω=0.03 where the failure mechanism for some specimens was through splitting and for others the concrete prism remained intact.

$$\frac{T_{f,\Omega}}{T_{R,\Omega}} = 0.29\left(1 - e^{-40(\Omega - 0.01)}\right) \quad \geq 0 \qquad \text{Equation 4-18}$$

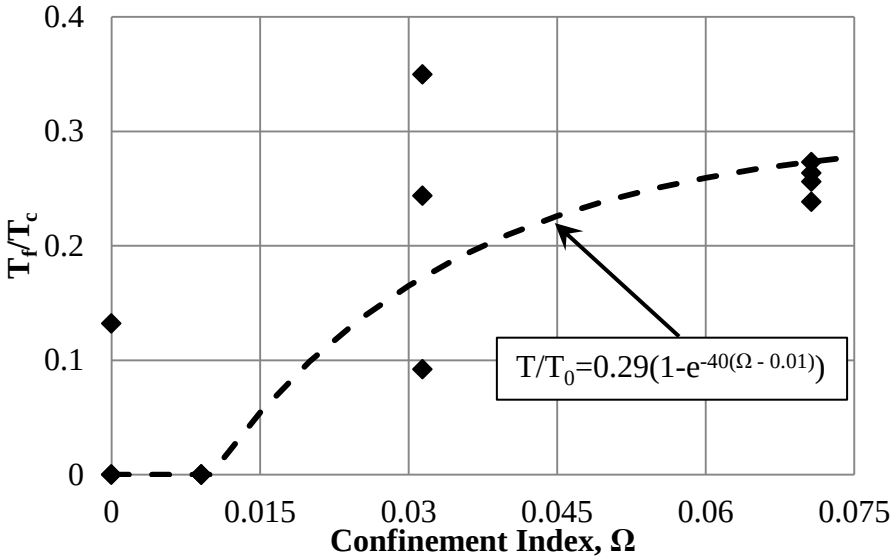

Figure 4-28: Dimensionless relationship between ultimate frictional stress and confinement index.

4.4.4 Damage-Energy Relationship

Experimental results from cyclic testing revealed that while brittle failure occurs under monotonic loading, if cycling remined at less than rupture stress, failure was less brittle. In fact, provided peak stress was not attained, splitting did not occur and damage was limited to the bonding interface as opposed to global splitting of the specimen. This allowed for a damage-energy relationship to be applied to confinement in a similar way to that used for corrosion level. To account for differing confinement the following adjustment factors for α_c and β_c have been proposed and are shown as Equation 4-19 and Equation 4-20;

$$\alpha_c = \frac{\alpha}{\alpha_K} = 1.58 - 8\Omega \quad \geq 0.0 \qquad \text{Equation 4-19}$$

$$\beta_c = \frac{\beta}{\beta_K} = 6.4 - 180\Omega \quad \geq 1.0 \qquad \text{Equation 4-20}$$

The factors were combined with the α_K and β_K factors, determined from the corrosion level in the reinforcing, to determine the combined effects for corrosion and confinement. Graphs displaying these equations and their associated experimental data points are shown in Figure 4-29 and Figure 4-30

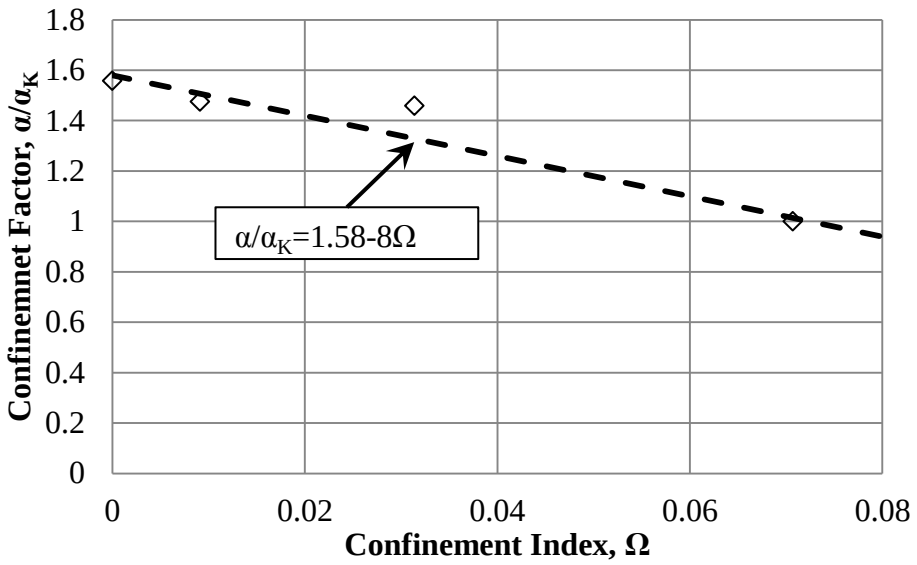

Figure 4-29: Adjustment factor for α accounting for confinement index including experimental data (diamonds).

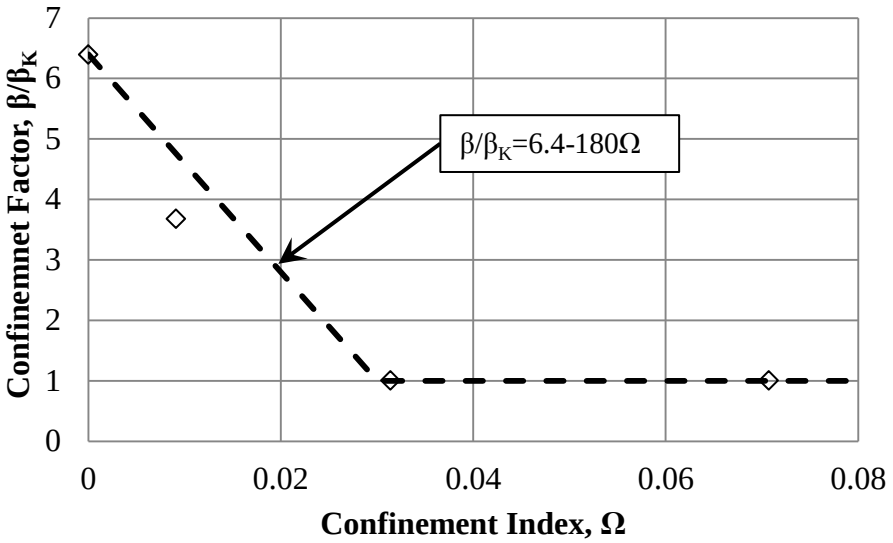

Figure 4-30: Adjustment factor for β accounting for confinement index including experimental data (diamonds)

Comparisons between the model and experimental data are shown in Figure 4-31 where it can be seen that the model follows the experimental data. It is important to note that due to the brittle nature of unconfined monotonic testing, the monotonic envelope used in determining damage was compared to a well confined specimen, scaled to the rupture stress of the tested specimen. It must also be reiterated that this model is only suitable provided that poorly confined specimens, prone to splitting failure, do not rupture, as rupture generally resulted in complete loss of bond stress and thus T_m^*/T_m would drop to zero.

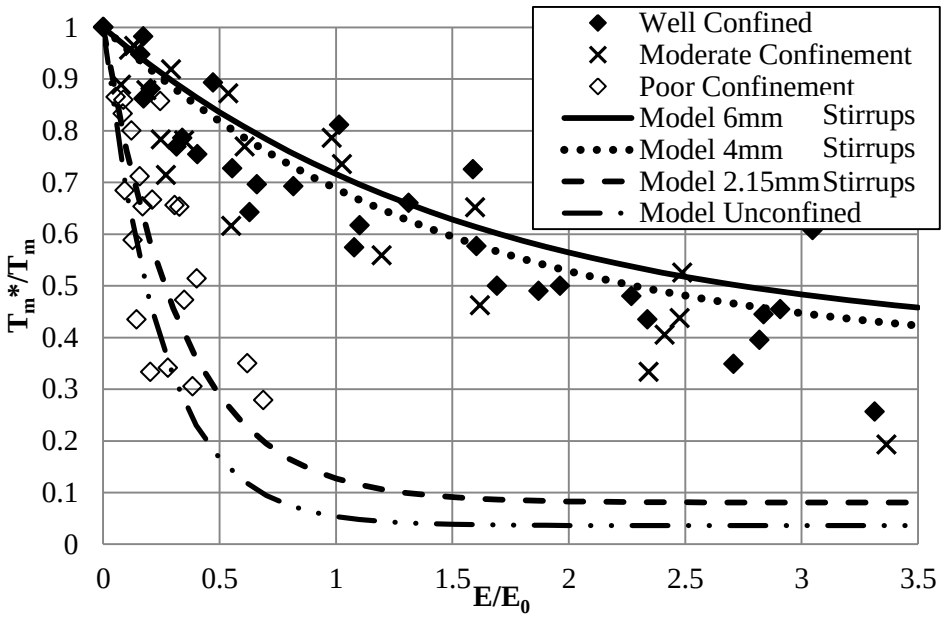

Figure 4-31: Comparison between damage-energy model including confinement factors and experimental results.

4.5 Summary of Experimental Model

A number of strong relationships were found between corrosion level, confinement and bond performance under monotonic and cyclic loading. These relationships have been represented by a series of formula shown in Table 2-1.

Table 4-2: Summary of developed experimental model (Continued over page)

Description	Symbol	Equation
Monotonic backbone curve	T_m	$T_m = \begin{cases} T_R \left(\frac{Slip}{S_R}\right)^n & 0 \le Slip < S_R \\ T_R & S_R \le Slip < S_P \\ T_R + \frac{\left(T_f - T_R\right)}{\left(S_f - S_P\right)}(Slip - S_P) & S_P \le Slip < S_f \\ T_f & S_f \le Slip \end{cases}$
Reduction in bond rupture stress due to corrosion	$\frac{T_{R,K}}{T_{R,0}}$	$\frac{T_{R,K}}{T_{R,0}} = 1.2e^{-0.076K} \le 1.0$
Reduction in frictional stresses due to corrosion	$\frac{T_{f,K}}{T_{R,K}}$	$\frac{T_{f,K}}{T_{R,K}} = \begin{cases} 0.26 + 0.13K & 0\% \le K < 3\% \\ 0.65 & 3\% \le K < 13\% \\ 0.65 - 0.06(K - 13) & 13\% \le K < 20\% \end{cases}$

Description	Symbol	Equation
Slip at which bond stresses become purely frictional for corroded 20mm deformed reinforcing bars	S_f	$S_f = 4.5e^{-0.3K} + 7.5$
Slip at which bond rupture occurs	S_R	0.25mm-1.5mm (0.3mm)
Slip at which the rupture plateau finishes	S_p	~S_R + 0.5mm
Reduction in monotonic envelope due to cyclic loading of corroded bars	$\frac{T_m^*}{T_m}$	$\frac{T}{T_m} = \alpha_K e^{\beta_K \frac{E}{E_0}} + (1 - \alpha_K)$ $\alpha_K = 1 - \frac{T_{f,K}}{T_R,K} \quad 0 \le \alpha_K \le 1$ $\alpha_K = \begin{cases} 0.75 - 0.13K & 0\% \le K < 3\% \\ 0.35 & 3\% \le K < 13\% \\ 0.35 + 0.06(K - 13) \le 0.6 & 13\% \le K < 20\% \end{cases}$ $\beta_K = -0.58 - 0.046K$
Sliding bond stress relationship of corroded bars	$T_{s,K}$	$T_{s,K} = A(T_{f,K} \times Slipmax)e^{B(\frac{E_f}{E_{0f}})^C} \le T_{f,K}(\frac{T}{T_m})$ $A = 2.16e^{0.077K}$ $B = -0.22K - 3.1$ $C = 0.019K + 0.29$
Reduction in rupture stress from well confined conditions due to confinement level.	$\frac{T_{R,\Omega}}{T_{R,K}}$	$\frac{T_{R,\Omega}}{T_{R,K}} = 0.55 + 0.45(1 - e^{-65\Omega})$
Reduction in frictional stresses due to confinement level	$\frac{T_{f,\Omega}}{T_{R,\Omega}}$	$\frac{T_{f,\Omega}}{T_{R,\Omega}} = 0.29\left(1 - e^{-40(\Omega - 0.01)}\right) \quad \ge 0$
Adjustment factor to allow for reduced confinement when determining the damage-energy relationship	$\frac{\alpha}{\alpha_K}, \frac{\beta}{\beta_K}$	$\frac{\alpha}{\alpha_K} = 1.58 - 8\Omega \quad \ge 0.0$ $\frac{\beta}{\beta_K} = 6.4 - 180\Omega \quad \ge 1.0$

Close links were found between the monotonic performance and cyclic performance with altered resistance mechanisms, mechanical interlock, and friction varying with differing levels of corrosion. Understanding of the true mechanics underlying bond performance under differing levels of corrosion

has been improved, allowing for possible further, less empirical research in this field. The effect of adjusting some of the key parameters are shown in Figure 4-32 for ‘n’, Figure 4-33 for α and β, and Figure 4-34 for A, B and C.

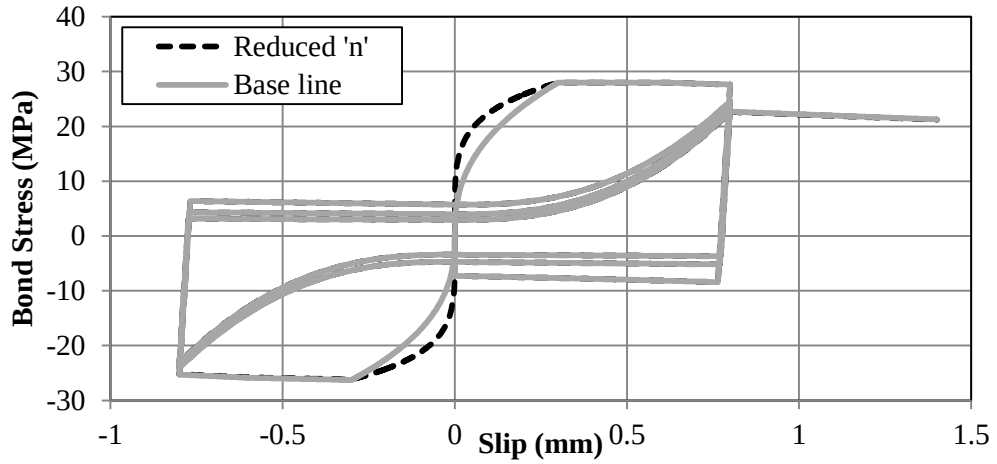

Figure 4-32: Bond-slip model showing effect of reduced 'n', initial loading prior to rupture.

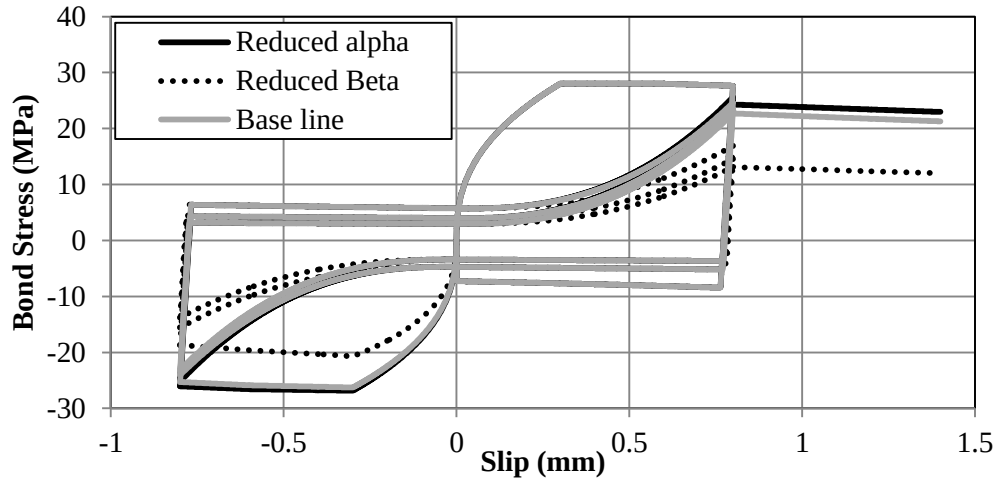

Figure 4-33: Bond-slip model showing effects of reduced α and β, damage to the monotonic envelope

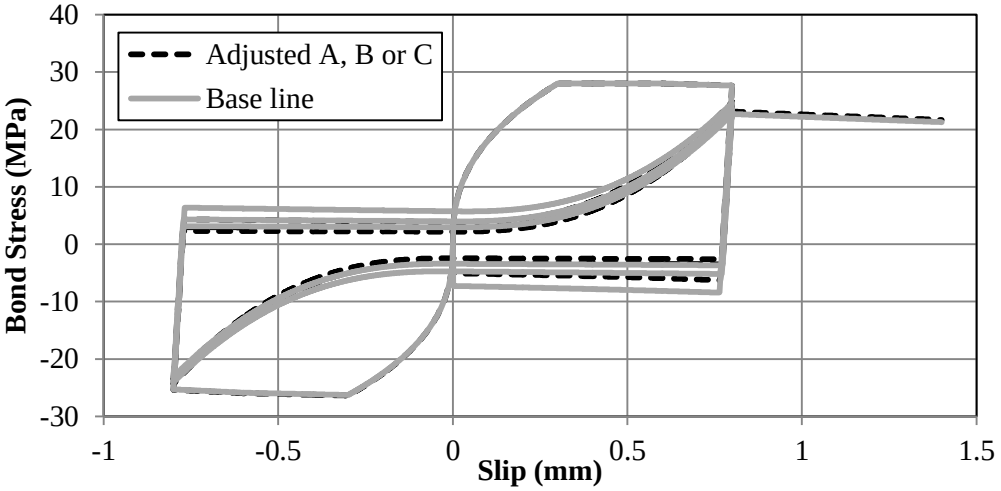

Figure 4-34: Bond-slip model showing effects of altered A, B and C, damage to sliding stresses. ‘A’ affects the initial sliding stress while ‘B’ and ‘C’ affect the rate at which sliding stress decays.

4.6 Comparison of Model with Experimental Results

Several representative experimental tests were selected and compared to modelled behaviour to determine the proposed cyclic model's effectiveness at portraying corroded bond-slip phenomena. Overall, the proposed model was very capable, matching observed behaviour. It can be seen in Figure 4-35 that the proposed model accurately recreated cycling damage along with sliding behaviour for uncorroded tests.

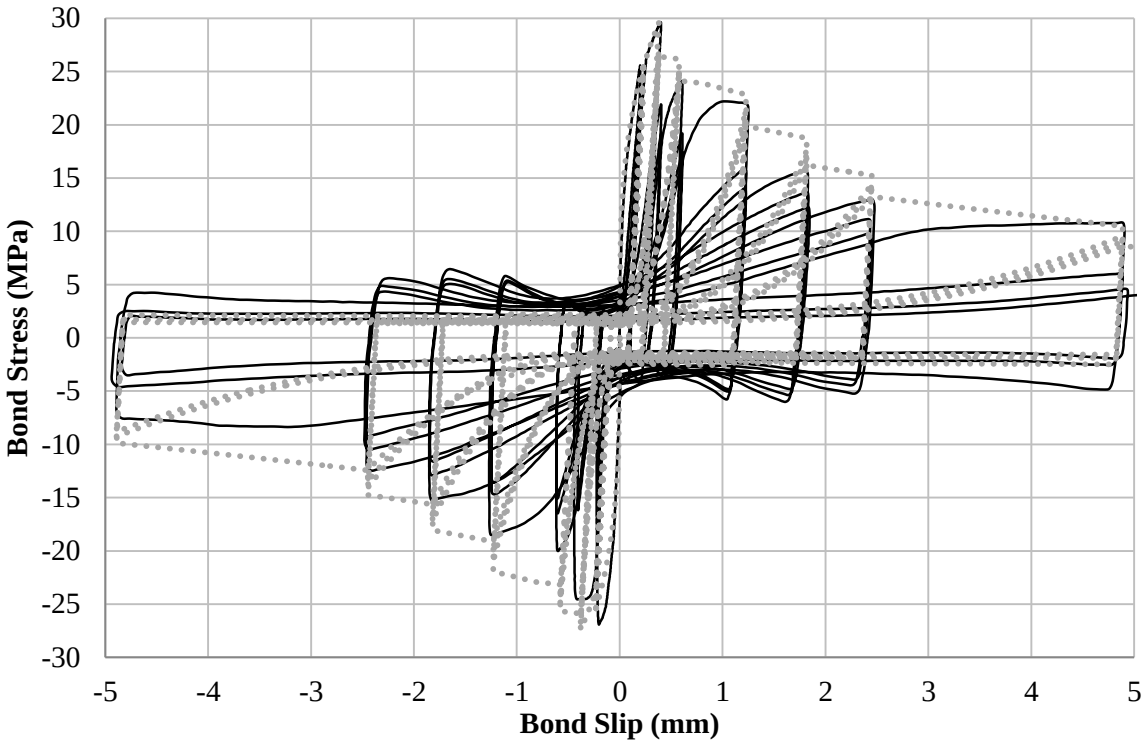

Figure 4-35: Comparison between experimental results at 0% corrosion (Solid) and the proposed numerical model at 0% corrosion (Dashed).

Figure 4-36 displays the models good accordance with experimental testing at 18.6% corrosion. Further comparisons at higher levels of corrosion have been made and show similar accordance with the uncorroded comparison, these are shown in Appendix G.

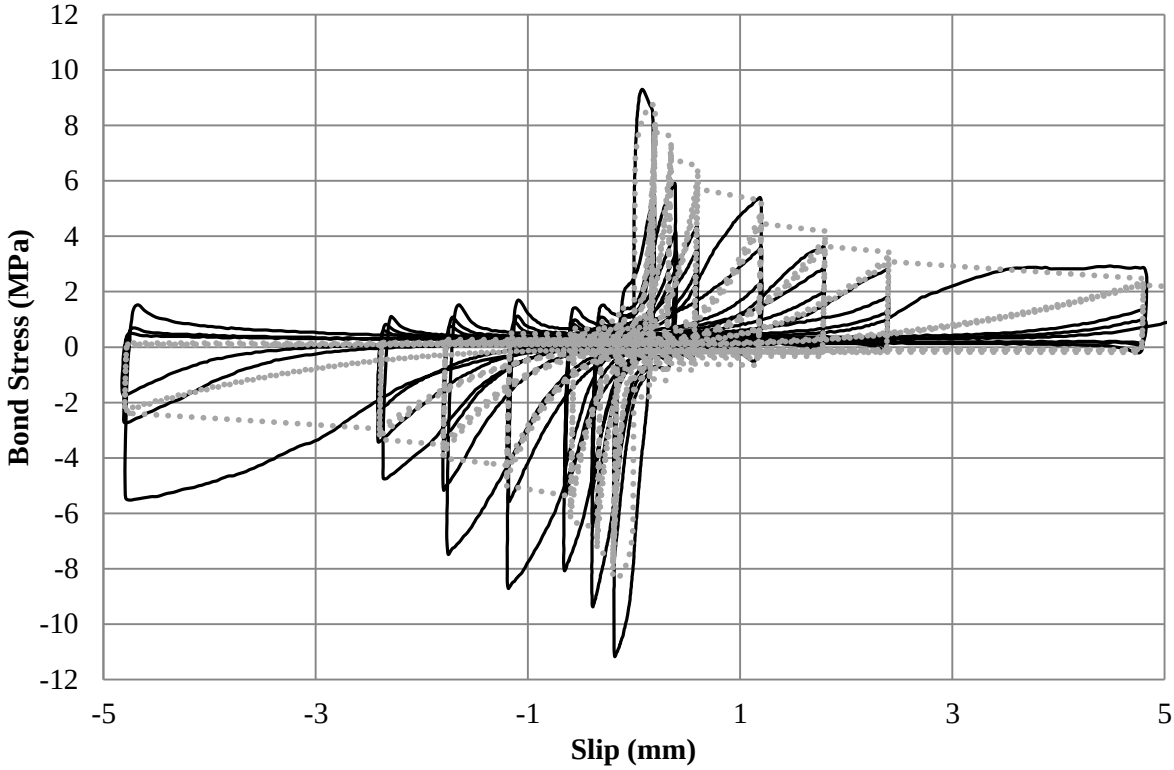

Figure 4-36: Comparison between experimental results at 18.6% corrosion (Solid) and the proposed numerical model at 18.6% corrosion (Dashed).

The proposed model did present some limitations though, with certain aspects not being recreated. One of these phenomena was associated with apparent differing bond performance depending on whether the reinforcing bar is in tension or compression. Since slip direction is not necessarily associated with a bar being in tension or compression it was deemed suitable by the author to treat compressive and tensile slip as equivalent. This simplification introduces possibility of errors in the order of 15% in some instances. Further investigation would be required to reduce errors associated with slip direction.

Unloading initially carried a very high stiffness as concrete elastically rebounded. After elastic rebound, unloading was represented by the value of damage affected sliding stress, T_s, within the current cycle. This provides some dissimilarity between the proposed model and experimental results, where experimentally a small peak was present, followed by a decaying curve until slip returned to approximately zero. The sliding stress value used in the model was taken to be the minimum of this curve which was seen to be accurate throughout testing.

A power function was used after sliding passed zero (reloading) so that when slip was equal to its maximum value, stress was equal to the damaged-reduced monotonic value. Experimentally monotonic behaviour did not return until slip had well exceeded the previous maximum slip increment, which is displayed in Figure 4-37. This caused the proposed model to overestimate stresses when slip is near to the previous maximum increment.

From Figure 4-37, the proposed model did not provide an exact match with experimental results, but it did provide a good representation of bond-slip behaviour. When experimental variations and errors were taken into account, its performance is more than suitable for use within finite element modelling, or similar, where an imperfect connection between steel and concrete elements is desired. Exact bond performance is dependent on factors regarding reinforcing and concrete properties, along with geometric layout. If these aspects are known, the proposed model and relationships allow for alteration of bond-slip behaviour due to the effects of corrosion deterioration and variations in confinement.

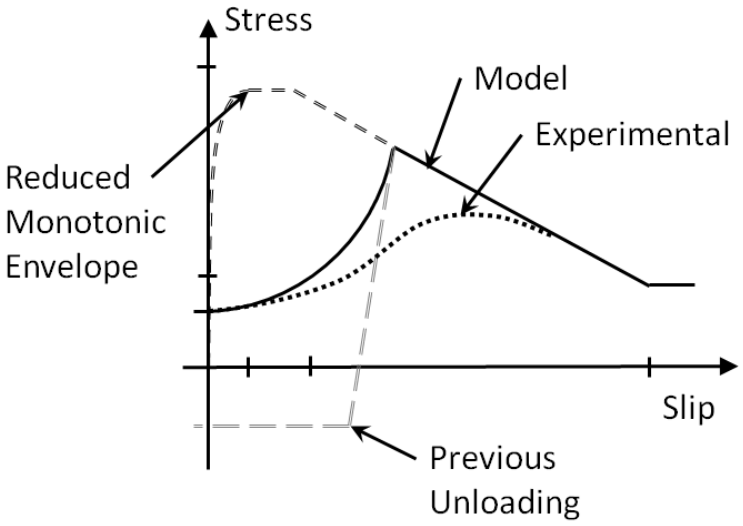

Figure 4-37: Diagram of the comparison between experimental results and the proposed model for cyclic bond slip showing reloading behaviour around maximum slip.

5 Multi-Spring Modelling

Data from experimental tests was used to develop a micro-model of corroded bond performance under different levels of corrosion, confinement, and cyclic loading. Following this, the model was implemented within a multi-spring representation of a bridge column and its moment curvature behaviour analysed under monotonic and cyclic loading. Lastly, a case study investigating the life cycle seismic performance of the New Brighton Pier was performed.

5.1 Multi-Spring Cyclic Pull-out Model

Results from experimental pull-out testing provided an indication of corroded bonding performance when bonded length was far less than development length. For seismic design, a ductile failure mechanism is essential in resisting seismic excitation. Reinforcement is designed to develop stresses over a much longer length than that tested experimentally. Ductile failure mechanism implies failure through yielding of steel reinforcement as opposed to bar pull-out due to bond failure.

5.1.1 Methodology

Corrosion has been shown to impact bond performance but its effects on reinforcement development were difficult to assess within the laboratory due to space and material constraints. In light of this, it was elected to extrapolate on experimental findings to determine the effects of corrosion on bond development using a numerical, multi-spring model. The selected model schematic is shown in Figure 5-1 below, where a series of steel spring elements are linked at equal intervals by bond spring elements connected to a fixed base.

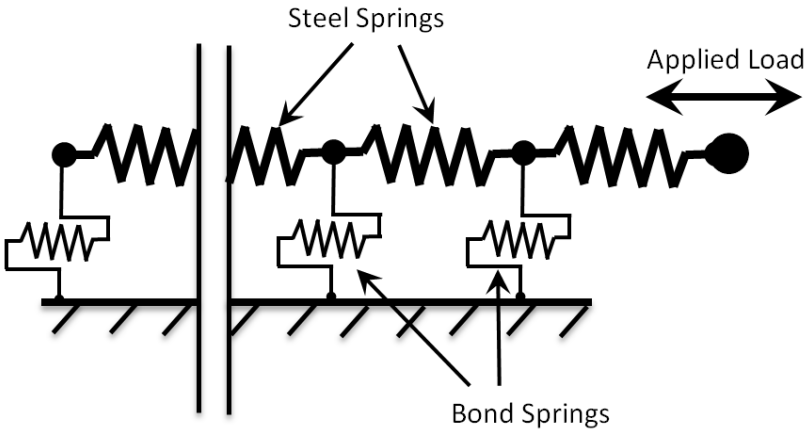

Figure 5-1: Diagram of multi-spring pull-out model.

This model was implemented within Ruaumoko 3D (Carr 2010b), a structural analysis program capable of performing inelastic dynamic structural analysis. Ruaumoko 3D includes numerous hysteretic models, two of which were used within the cyclic pull-out model. The first of these was the Dhakal steel hysteresis model (Carr 2010a). The Dhakal model (Dhakal and Maekawa 2002) was developed for specific use in modelling steel reinforcing and included allowance for post-yield plateau, strain hardening (3 models) and bar buckling. The second hysteretic model was proposed from experimental testing and analysis described in Chapter 3.

Using the same reinforcement used in experimental testing, HD20 (Grade500), along with a concrete strength of 65MPa (same as experimental 90 day results), Equation 5-1 from NZS3101:2006 determined that the development length was 620.2 mm.

$$L_{db} = \left(\frac{0.5\alpha_a f_y}{\sqrt{f_c'}}\right) d_b \qquad \text{Equation 5-1}$$

Where L_{db} is the required length of curtailment, α_a is either 1.0 or 1.3 depending on the depth of fresh concrete poured below the bar (assumed 1.0) and d_b is the reinforcement diameter. Based on this it was elected to use a bonded length of 625mm within the model, which consisted of 125, 5mm springs.

The loading protocol consisted of ten inelastic cycles of the steel reinforcing at 96.7% (205 kN) of bar overstrength (212.1 kN) (Standards New Zealand 2006), followed by increasing load until pull-out or bar rupture was achieved. The primary variables investigated for their effects on bond development were corrosion level, which ranged between 0% and 20%, and confinement, which was either fully confined ($\Omega = 0.071$) or unconfined ($\Omega = 0.0$). While a fully unconfined situation does not occur in the design of structures, complete section loss of confining steel due to corrosion is a viable possibility, providing a worst case scenario. This would result in poor confinement to bars in surrounding regions, even though developing bars may not suffer similar high levels of deterioration themselves.

From experimental results, the value of uncorroded, fully confined rupture stress: T_0, was found to be 30 MPa. This differed from values found in existing research where for similar arrangements and concrete strength, T_0 values were nearer to 20 MPa. In light of this models were run using T_0 values of 30 MPa and 20 MPa.

5.1.2 Results and Discussion

Within the model, 'pull-out' was defined as the point when dead-end bond-slip exceeds S_1 (0.3mm), at which point bond capacity can no longer increase and the bar will pull-out if loaded further. The 'dead-end' was defined as the end of reinforcing furthest from the loaded end. Figure 5-2 and Figure 5-6 show the relationship between dead end slip at rupture after 10 inelastic cycles and the corrosion level, for T_0 = 30 MPa and T_0 = 20 MPa, respectively. Values do not take into account reductions in

bar rupture strength as it has been shown that for corrosion levels less than 8%, there is little reduction in yield strength (Cairns et al. 2005). In heavily corroded bars, strength reduction was less than the reduction in section (Cairns et al. 2005). Bar strength reduction is likely to play some role in reducing applied forces, but its effect at higher levels of corrosion was poorly defined in literature and so was conservatively taken to be negligible.

5.1.2.1 T_0 = 30 MPa Model

When T_o = 30 MPa, as shown in Figure 5-2, the fully confined model did not display signs of pull-out within the range of 0% to 20 % corrosion. Based on the general behaviour observed in other models it would be expected that pull-out would occur at ~25% corrosion.

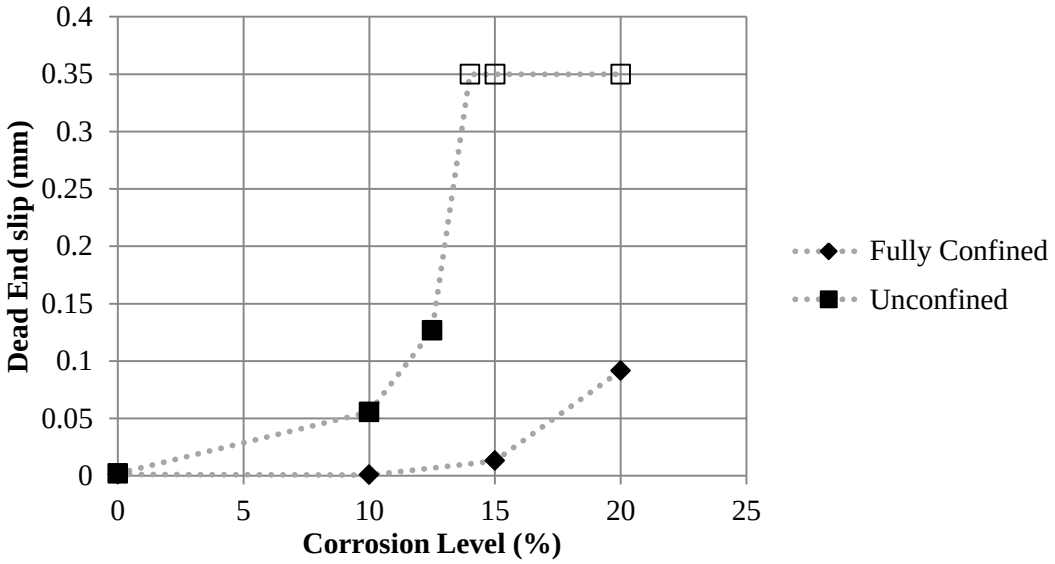

Figure 5-2: Comparison between dead end slip at rupture and corrosion level for fully confined and unconfined models using T_0 = 30 MPa, hollow makers indicate pull-out of reinforcement.

Effects of confinement were very pronounced with a sizeable shift in the dead end slip curve. It can be seen in Figure 5-2 that after 10 inelastic cycles, pull-out occurred at 14% corrosion. This large change can be attributed to two of the effects of reduced confinement, the first being: reduced bond rupture strength, but more so the second: brittle splitting failure. Under splitting, immediate loss of bond capacity to its frictional level means that only bonded regions with slip values less than ~1.5S_p (S_p = S_R = 0.5mm, for unconfined) had any significant bonding capacity, as shown in Figure 5-3, limiting the region of bond that was able to be actively contributing at any one time.

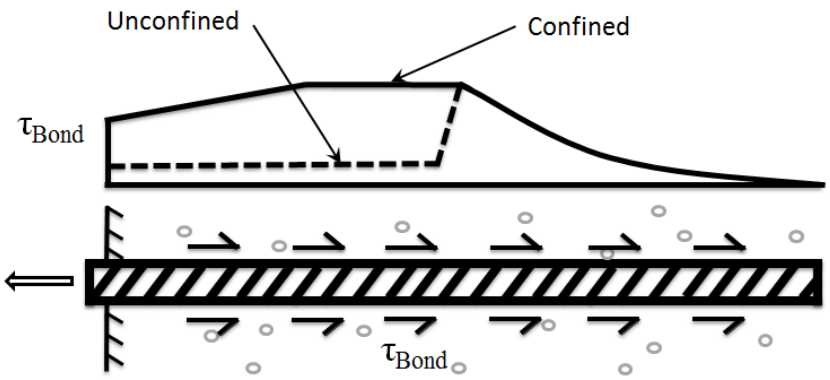

Figure 5-3: Comparison between confined and unconfined bond stresses along developing reinforcement

Slip profiles at rupture after 10 inelastic cycles are shown for fully confined and unconfined models in Figure 5-4 and Figure 5-5 respectively. Both models displayed an 'elbow' in the data, representing strain penetration into the bonded region. Strain penetration in unconfined models was found to be roughly double that of the confined models, this can be attributed to the same reasons that are displayed in Figure 5-3.

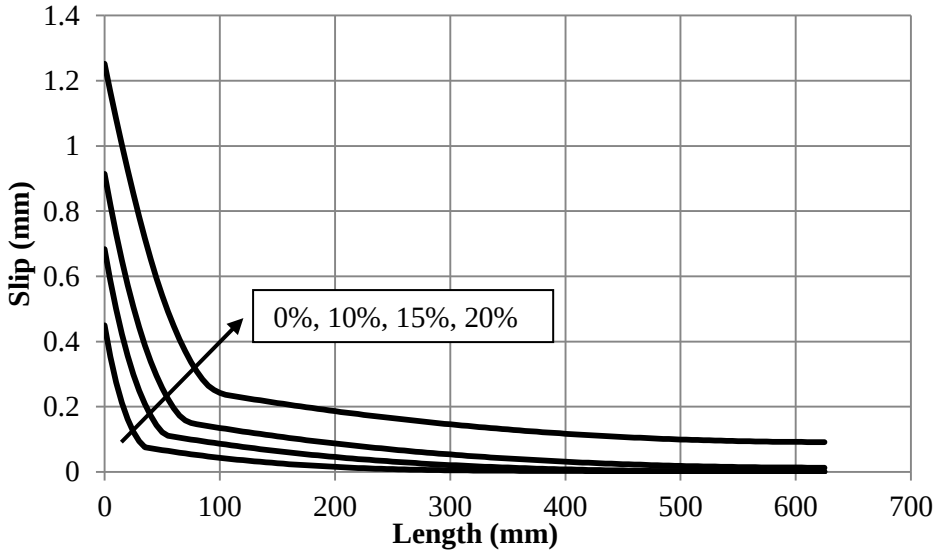

Figure 5-4: Bar slip along bar length at bar rupture after 10 inelastic cycles of loading, Fully Confined, T_0 = 30 MPa (Arrow show increasing level of corrosion).

It can be seen from the fully confined model that it was not until a corrosion level of 20% that there was a substantial slip at the dead-end. Even at 15% corrosion, with almost 0.9 mm slip at the loaded end, slip at the dead-end was negligible. The unconfined model displayed considerably larger slip beyond the strain penetration point. This was attributed to the inability for unconfined ruptured bond to contribute beyond frictional behaviour post rupture. As a result, cyclic loading causes a gradual bond 'unzipping' as frictional stresses are further degraded.

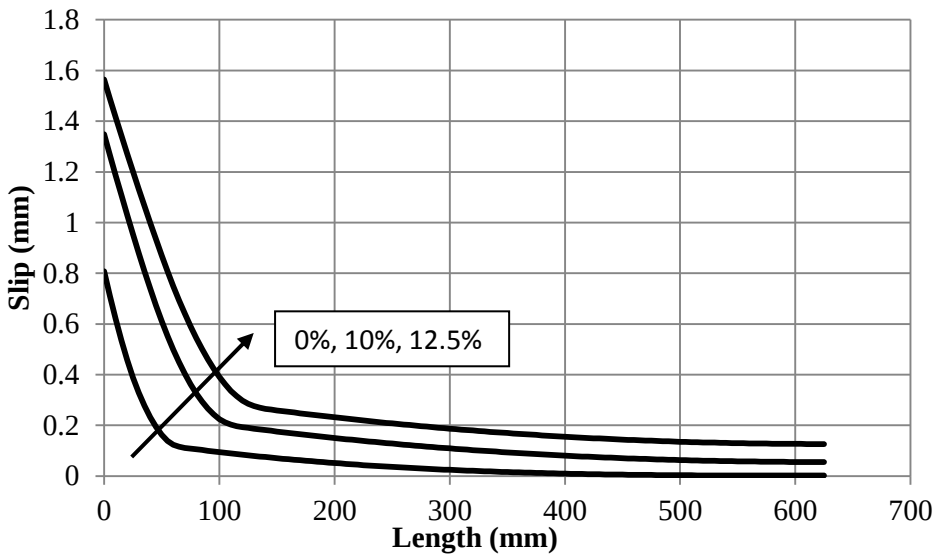

Figure 5-5: Bar slip along bar length at bar rupture after 10 inelastic cycles of loading, Unconfined, T_0 = 30 MPa. (Arrow show increasing level of corrosion).

5.1.2.2 T_0 = 20 MPa Model

When T_0 = 20 MPa, as shown in Figure 5-6, it can be seen that pull-out occurred in both the fully confined and unconfined models with the inclusion of high levels of corrosion. Under fully confined conditions, pull out occurred at a corrosion level of 18%, a decrease of ~25% from that expected for the model using T_0 = 30 MPa.

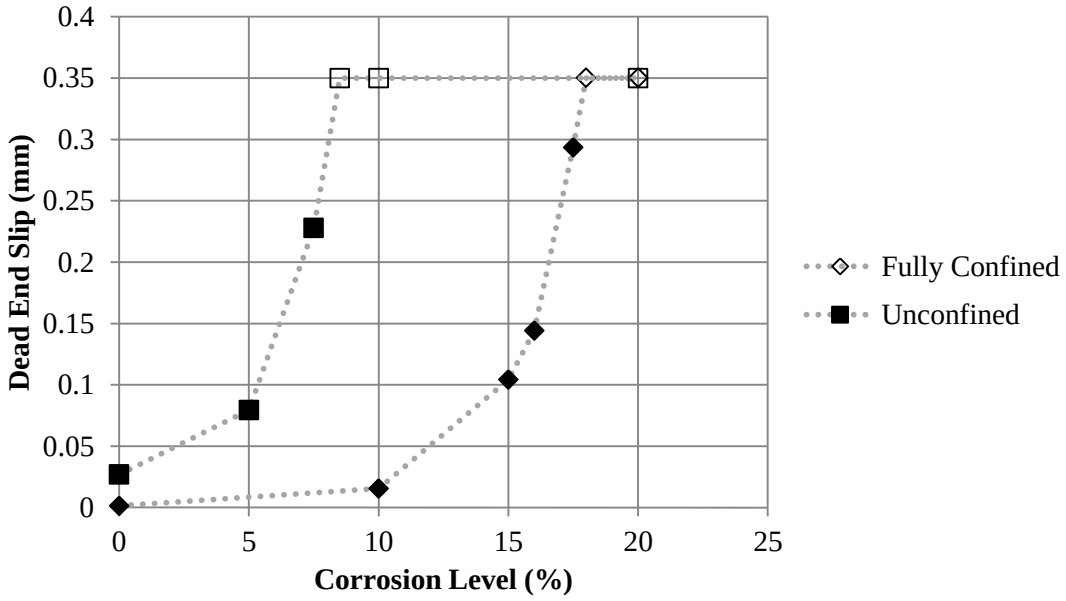

Figure 5-6: Comparison between dead end slip at rupture and corrosion level for fully confined and unconfined models using T_0 = 20 MPa. Hollow makers indicate pull-out of reinforcement.

The unconfined model displayed an even greater reduction in pull-out corrosion level, with pull-out occurring at a corrosion level of 8.5%. Deterioration at these levels is likely in corrosion affected structures and would also be accompanied by reductions in confinement. In older structures where seismic confinement detailing is not common place, already inadequate confinement may be further degraded by corrosive attack, leaving longitudinal reinforcement effectively unconfined.

The slip profiles at rupture for fully confined and unconfined models are shown in Figure 5-7 and Figure 5-8, respectively. General trends display similar behaviour to the T_0 = 30 MPa models with increasing strain penetration with increasing corrosion level. The 33% reduction in T_0 resulted in an approximately equal increase in loaded end slip for uncorroded fully confined specimens. For unconfined specimens a much larger loaded end slip increase of 75% was observed. This shows the higher importance of rupture stress in unconfined specimens when compared to their fully confined counterparts that are still aided by bond even when bar slippage has exceeded rupture slip in a given region.

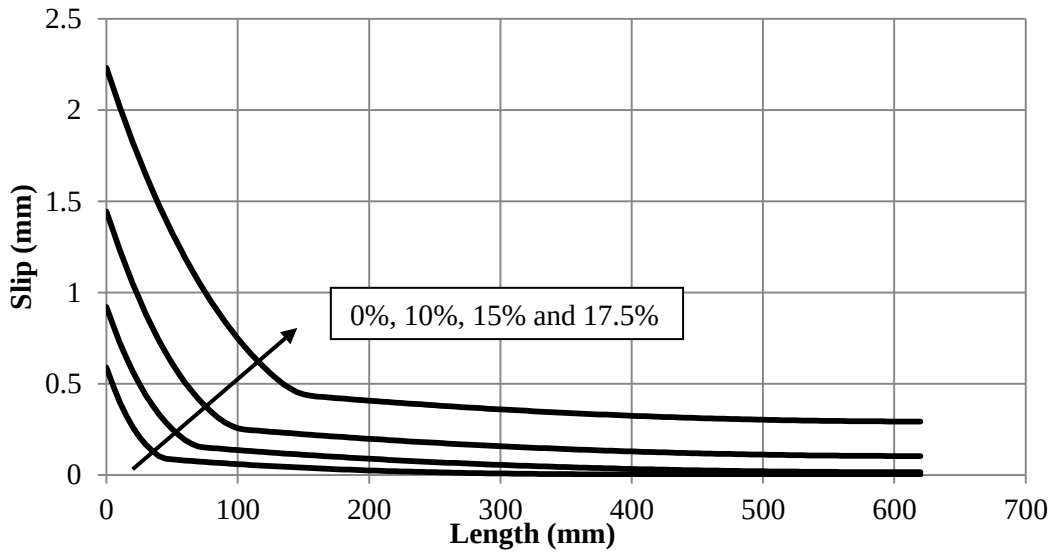

Figure 5-7: Bar slip along bar length at bar rupture after 10 inelastic cycles of loading, Fully Confined, T_0 = 20 MPa. (Arrow show increasing level of corrosion).

Increased corrosion levels also resulted in an increase in strain penetration in the T_0 = 20 MPa. Dead-end slip values at bar rupture were on the verge of pull-out at 17.5% corrosion for fully confined bonding and 7.5% corrosion for unconfined bonding.

From Figure 5-8 it can be seen that for unconfined reinforcement at the point of bar pull-out (the 7.5% corrosion curve) slip, and therefore stress along the non-strain penetrated section was approximately equal to the rupture slip/stress. When loading was continued, no further capacity was able to be generated through bonding, and rupture along the remaining length of non-strain penetrated reinforcing occurred.

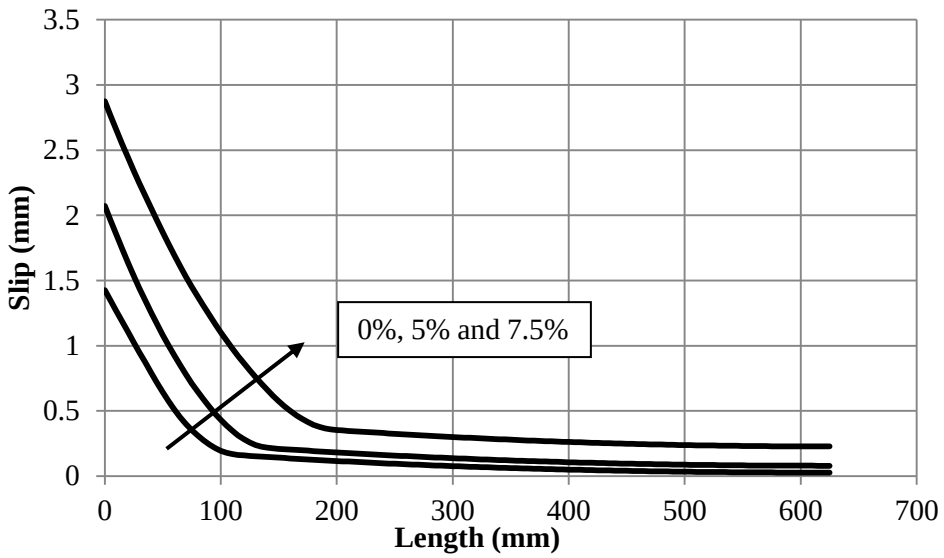

Figure 5-8: Bar slip along bar length at bar rupture after 10 inelastic cycles of loading, Unconfined, T_0 = 20 MPa (Arrow show increasing level of corrosion).

When comparing strain penetration values from all analyses, a common trend is seen between them, as shown in Figure 5-9. Effects of confinement are prominent and are most apparent in the 20 MPa, unconfined curve where strain penetration depths of nearly 200mm are present before rupture occurs.

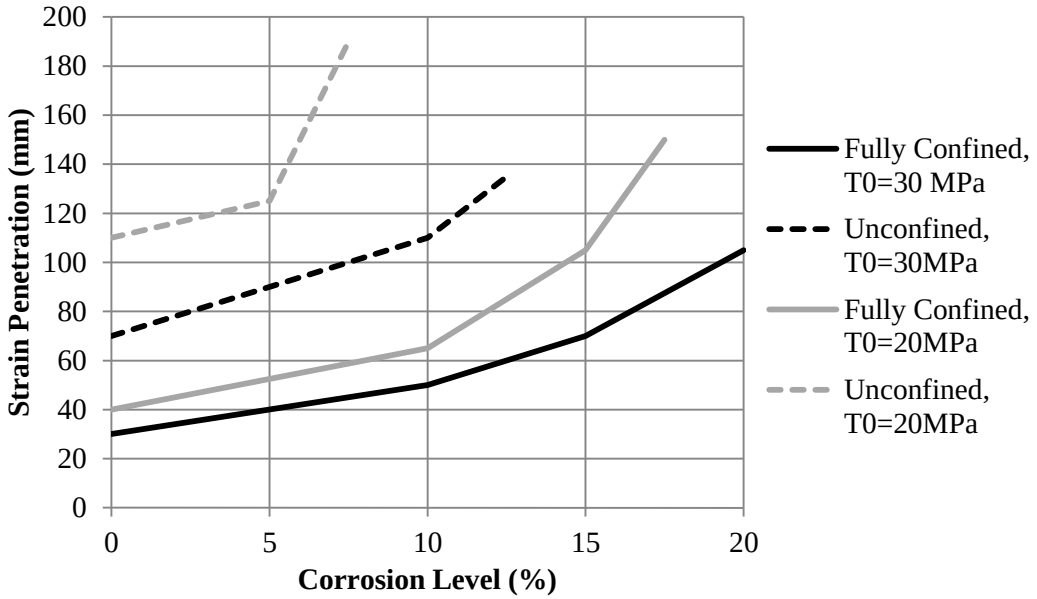

Figure 5-9: Strain penetration length after 10 inelastic cycles over 0% to 20% corrosion of HD20 reinforcing bar.

From Paulay and Priestley (1992), the Equation 5-2 was proposed for determining the amount of strain penetration in regards to extension of plastic hinge zones;

$$l_{sp} = 0.022 d_b f_y \qquad \text{Equation 5-2}$$

Using this equation, including a bar diameter (d_b) of 20 mm and yield strength (f_y) of 500 MPa, the theoretical strain penetration was calculated to be 220 mm for a HD20 bar. This value is significantly greater than those observed in these models in the order of two to four times. This could be attributed to:

- differing number of inelastic cycles performed,
- independence of concrete strength on strain penetration depth in the Paulay and Priestley equation,
- the Paulay and Priestley model being derived for plastic hinge length purposes and so while applicable to plastic hinge length, may not be the same length as has been defined within these models,
- possible conservatism in the '0.022' factor.

Regardless of the reasons for differences, values produced from numerical modelling are of the same rough order of magnitude, giving confidence to the models accuracy.

5.2 Multi-Spring Moment-Curvature Model

5.2.1 Methodology

The multi-spring models (Spieth et al. 2004) were developed to model the plastic hinge region of a bridge column under various levels of deterioration. In essence, the models were fibre models that allowed for bond-slip at the interface between steel and concrete fibres. Factors included in the analysis were the level of corrosion in longitudinal reinforcing (%), level of confinement allowing for any reductions induced through corrosion of confining steel and reduced member dimension associated with spalling of cover concrete due to corrosive expansion of steel or general damage.

A series of diagrams displaying the concept of this model are shown in Figure 5-10. The model consisted of two main sections. The first of these was the ridged frame to which axial load and imposed moment are applied. This section was allowed to rotate and move vertically, moving as a ridged body as shown in Figure 5-10a. The second section was the fixed base which mirrored the rigid frame but was restrained in all directions. Using this arrangement, an overturning moment was applied to the rigid frame section causing rotation.

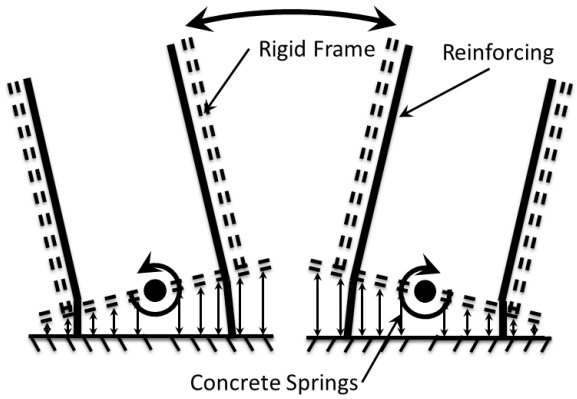

(a)

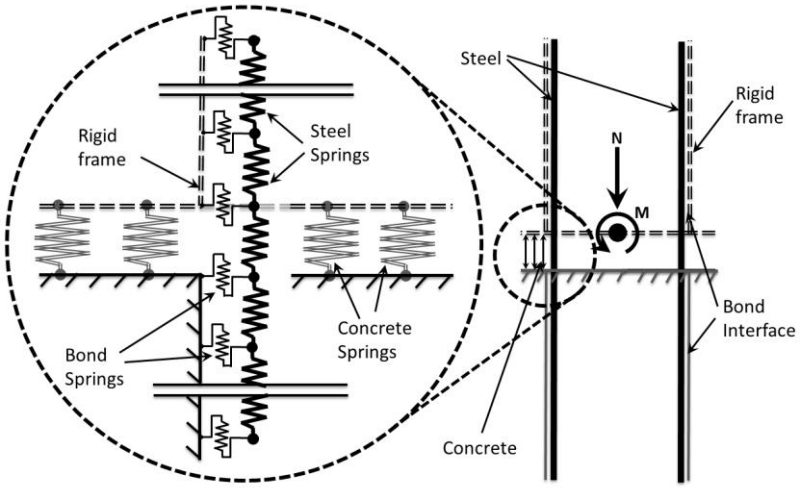

(b)

Figure 5-10: Diagram of Multi-spring plastic hinge model for determining moment-curvature behaviour. a) Deformed model behaviour subjected to cyclic loading, b) Excerpt (left) and overall pier base model (right)

As can be seen in Figure 5-10 'b', bond spring elements were used to connect steel spring elements at the interface between the ridged frame and also the fixed base in order to allow for imperfect bonding. Concrete springs elements were used between the rigid frame and ridged base. Applied moments were resisted through the couple formed between the applied axial load, reinforcing springs, and concrete springs.

This model was implemented within Ruaumoko 3D (Carr 2010b). In addition to Dhakal Steel Hysteresis and the Bond-slip Model for Connectors, Brian Peng Concrete Hysteresis was used to model concrete behaviour at the interface between the rigid frame and fixed base sections. Examples taken from the Ruaumoko 3D manuals (Carr 2010b) shown in Figure 5-11 display the general hysteretic behaviour of these hysteretic rules.

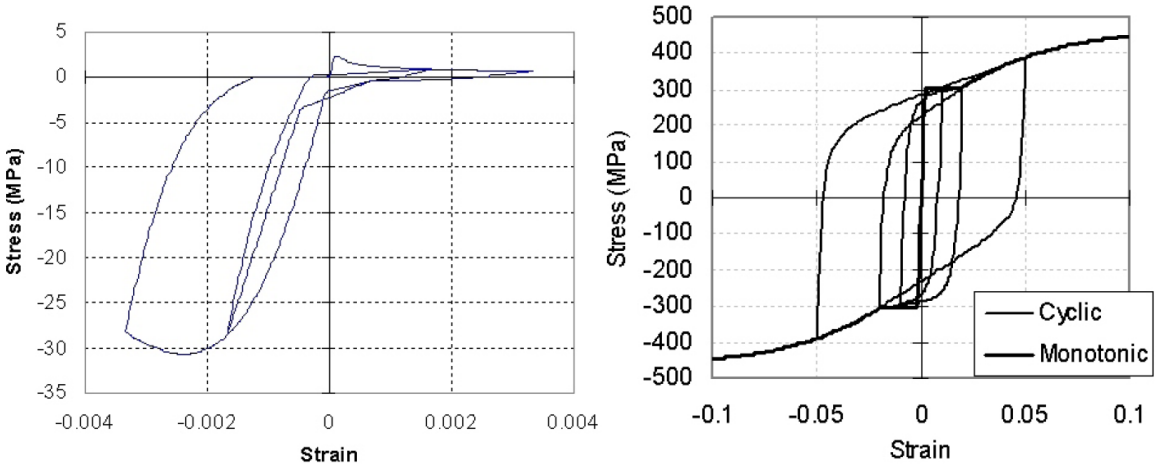

Figure 5-11: a) Brian Peng Concrete Hysteresis model, b) Dhakal Steel Hysteresis model (Carr 2010a).

5.2.2 400mm × 400mm Section Model

The first model was a 400 mm × 400 mm column, as shown in Figure 5-12. This was selected as a simplified example section to allow for rapid analysis in determining generalised effects of bond deterioration due to corrosion. Confinement was varied for bond purposes, as discussed earlier, though for concrete stress-strain behaviour all regions were assumed confined.

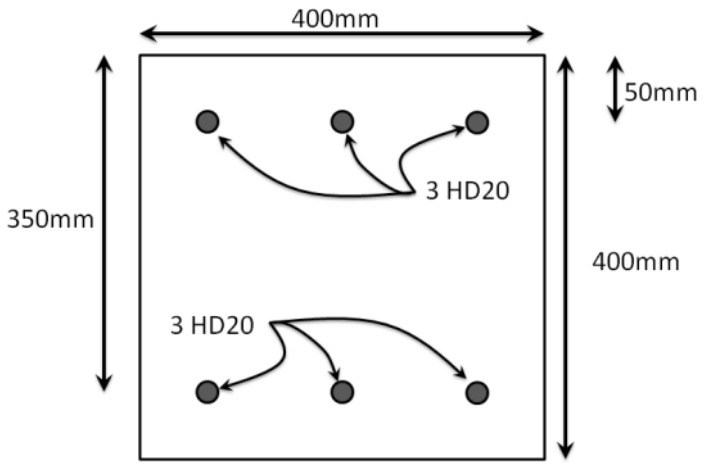

Figure 5-12: Section layout for the 400mm x 400mm section model.

Using the same reinforcement used in experimental tests, HD20 (Grade500), along with a concrete strength of 65MPa (same as experimental 90 day results), NZS3101:2006 determined that the development length was 620.2 mm. Based on this, it was elected to use a bonded length of 640mm within the model for both the rigid and fixed steel lengths. This consisted of 32 40mm springs for each row of steel, with 211 springs used in total.

The primary variables investigated for their effects on bond development were corrosion level, which ranged between 0% and 20%, and confinement, which was either fully confined (Ω = 0.071) or unconfined (Ω = 0.0). Curvature was calculated as rotation of the rigid frame (radians) divided by the

interface gap (40 mm). The interface gap was required to maintain strain-continuity between steel and concrete.

5.2.2.1 Model Validation

Validation of the multi-spring model was performed by comparing results with the section and member analysis program Response2000 (Bentz 2001). The concrete stress-strain relationship used was based on Popovic/Thorenfeldt/Collins for the base curve, Vecchio-Collins (1986) for compression softening, and tensile strength was assumed to be zero. General material characteristics and dimensions were identical to those used in the Ruaumoko3D (Carr 2010b) model, as shown in Figure 5-13 .

Table 5-1: Material characteristics used in modelling 400x400 section in Response2000 (Bentz 2001) and Ruaumoko3D (Carr 2010b).

Concrete		**Steel (Rebar)**	
Characteristic	**Value**	**Characteristic**	**Value**
Crushing Strength, f'_c	65 MPa	Stiffness, E	200,000 MPa
Crushing Strain, ε_c	0.003	Yield Stress, f_y	585 MPa
Tensile Strength, f'_t	0 MPa	Ultimate Stress, f_u	675 MPa
		Strain at beginning of strain hardening	0.006
		Rupture Strain, ε_u	0.100

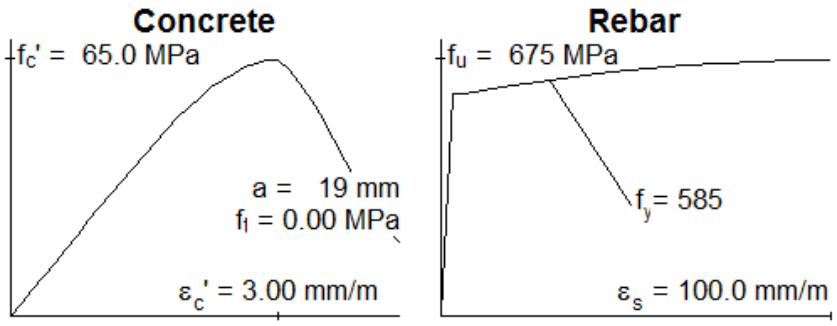

Figure 5-13: Material characteristic curves for concrete and reinforcing used within Response2000 model (Bentz 2001).

Comparisons between the models analysed under monotonic loading are shown in Figure 5-14.

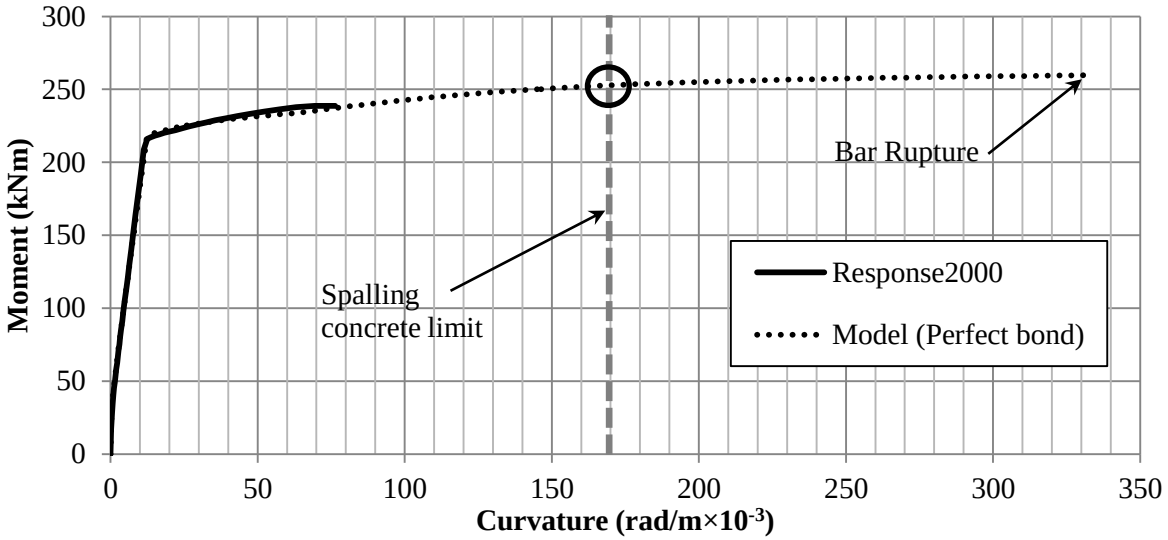

Figure 5-14: Model validation comparison with Resposne2000 (Bentz 2001) using perfect bonding and allowance for bond slip.

Response2000 (Bentz 2001) does not include allowances for bond-slip within its analysis, so initially the multi-spring model was run using perfect bonding. From Figure 5-14 it can be seen that the multi-spring model follows the behaviour exhibited in the Response2000 analysis extremely well up until curvature ductility approximately equals 10 (10 times yield curvature). Beyond this point a reduction of strength occurs, associated with concrete spalling within the Response2000 model. This strength reduction was not mirrored within the multi-spring model in spite of crushing occurring within the Brian Peng concrete hysteretic model used in concrete springs. Due to errors in the imposed displacement algorithms in the current (2011) version of Ruaumoko3D (Carr 2010a), imposed rotation could not be applied to the model which meant that instead of applying a rotation and recording the corresponding resistance provided by the model, moments were applied and the deformation recorded. This is the likely cause of inconsistencies beyond ultimate capacity and is the reason for no strength degradation being displayed by the Ruaumoko3D model.

Concrete strains were checked within the model and if spalling occurred prior to bar rupture this value was taken as the ultimate capacity and curvature. Using equivalent stress block values determined from NZS3101(Standards New Zealand 2006) of α=0.81 and β=0.65 in conjunction with a concrete spalling strain of 0.0064 (Mander et al. 1988), it was determined that at approximately 170×10^{-3} rad/m spalling of concrete would occur. This was determined under the assumption that all reinforcing had yielded which resulted in the maximum capacity occur at this curvature when spalling onset. From this, ultimate curvature was taken to be. 170×10^{-3} rad/m. This value has been used to limit the curvature determined from multi-spring modelling. While within the model this was accounted for already, aforementioned errors at the time of analysis within Ruaumoko3D (Carr 2010b) meant that this methodology had to be adopted. Using these assumptions and conditions the model provided a good representation of pre and post yield behaviour.

Inclusion of bond-slip saw a significant reduction in the model's elastic stiffness, as can be seen in Figure 5-15. This can be purely attributed to strain penetration of bond at the interface. It also resulted in increased yield strength, along with post-yield strength. This is attributed to an increased curvature requirement in order to develop yield due to strain penetration, which in turn increases the lever arm between the higher concrete compression centroid and reinforcement. With both sections having similar ultimate curvatures due to concrete crushing governing the ultimate failure mechanism, inclusion of bond-slip caused a reduction in the section ductility from μ=13 to μ=4.25.

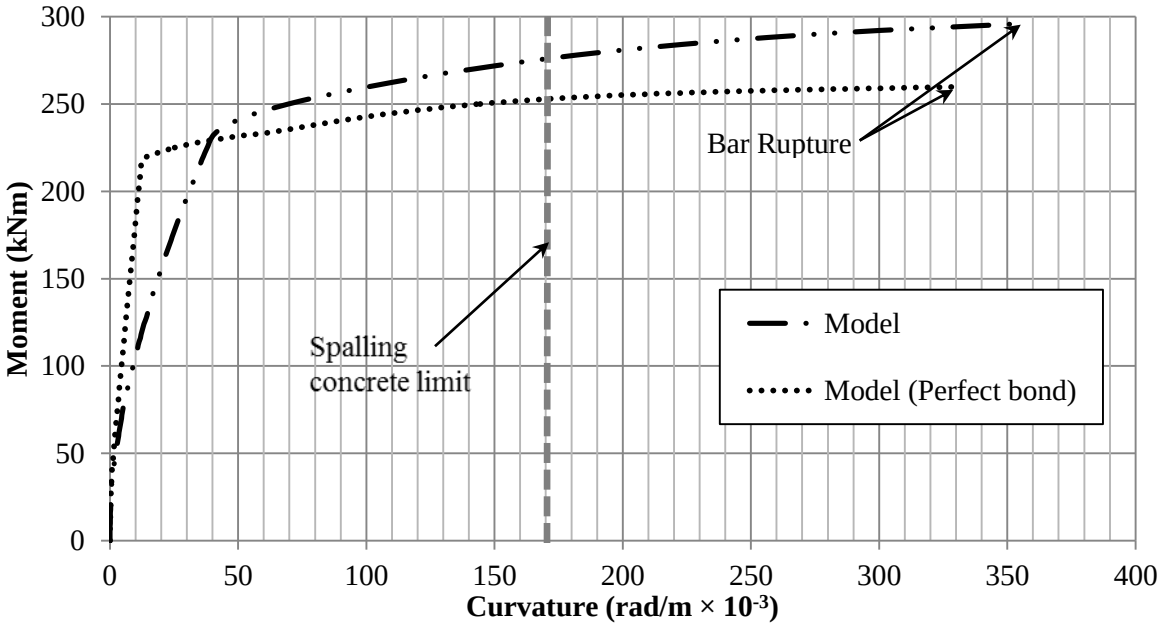

Figure 5-15: Model validation comparison with Response2000 (Bentz 2001) using perfect bonding and allowance for bond slip.

5.2.2.2 Push-over Results

Monotonic push-over analyses were performed using an axial load of 250 kN (1.56 MPa over section). Again these were carried out using T_0 = 20 MPa and 30 MPa at a range of corrosion levels between 0% and 20% under fully confined or unconfined conditions. Within all of the 400mm × 400mm analyses the steel area was kept constant, ignoring any reduction in section due to corrosion. As mentioned in the pull-out models, corrosion has large effects on bar ductility for even low levels of deterioration, which is compounded at higher levels of deterioration by reduced strength (Cairns et al. 2005). These analyses only assessed impacts of bond deterioration due to corrosion of moment curvature behaviour and so reinforcement properties do not account for deterioration.

Figure 5-16 shows the moment-curvature relationship for the well confined, T_0 = 30 MPa models at three levels of deterioration (0%, 10% and 20% corrosion). It shows that the bond deterioration primarily affects section stiffness with yield curvature increasing from perfect bond conditions by 315% to 475% to 1000% through inclusion of bond slip and increasing corrosion levels of 0%, 10% and 20% respectively. Increased strain penetration associated with increasing corrosion levels caused

slight increases in yield strength. This was due to larger curvature requirements for development of yield strain within reinforcement increasing the height of the neutral axis. Elevating the neutral axis in the section increased the internal moment lever arm, increasing yield moment capacity. Delayed yield combined with constant ultimate capacity resulted in reductions in ductility from μ=4.25 at 0% corrosion to μ= 1.5 at 20% corrosion.

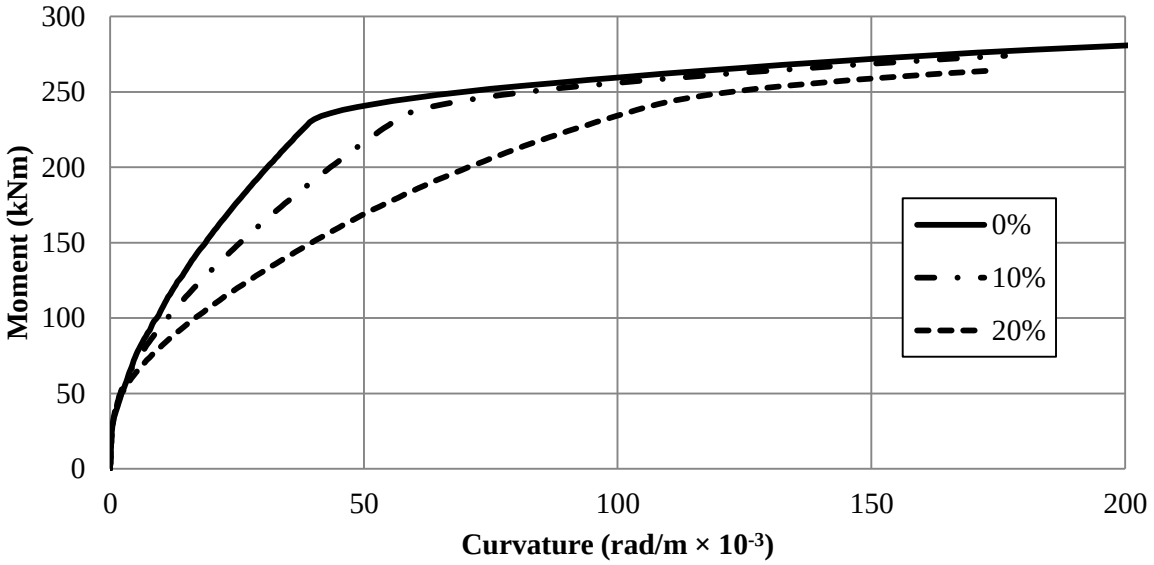

Figure 5-16: Push-over analysis of the 400mm × 400mm section using bond properties: T_0=30MPa, Ω=0.071 and corrosion levels of 0%, 10%, and 20 %.

To illustrate strain penetration effects, maximum strain in tensile reinforcing was plotted against curvature in Figure 5-17. A slight delay of yielding was observed at 10% corrosion. Increased strain penetration resulted in larger section curvature requirements with post yield behaviour similar between the 0% and 10% models with limited additional strain penetration occurring alter yield due to plastic behaviour in the reinforcing. However, significant delay of yield was observed at 20% corrosion, although similar initial post yield behaviour was observed.

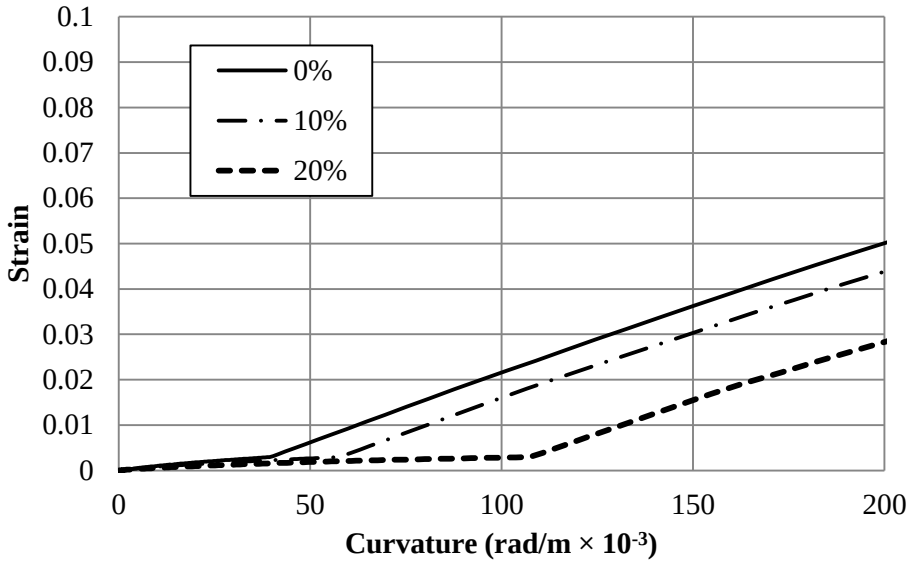

Figure 5-17: Reinforcement strain against curvature for T_0 = 30 MPa and fully confined conditions.

The moment-curvature behaviour of the 400mm × 400mm model using T_0 =30 MPa and unconfined bond is shown in Figure 5-18. This figure illustrates the effect that reduced confinement has on stiffness through impaired bonding. This can be seen when the two 0% corrosion series: fully confined and unconfined, are compared where yield curvature increased by 30% when unconfined bonding conditions were applied. Increased yield curvature was not accompanied by significant increases in the ultimate curvature, resulting in reduced ductility.

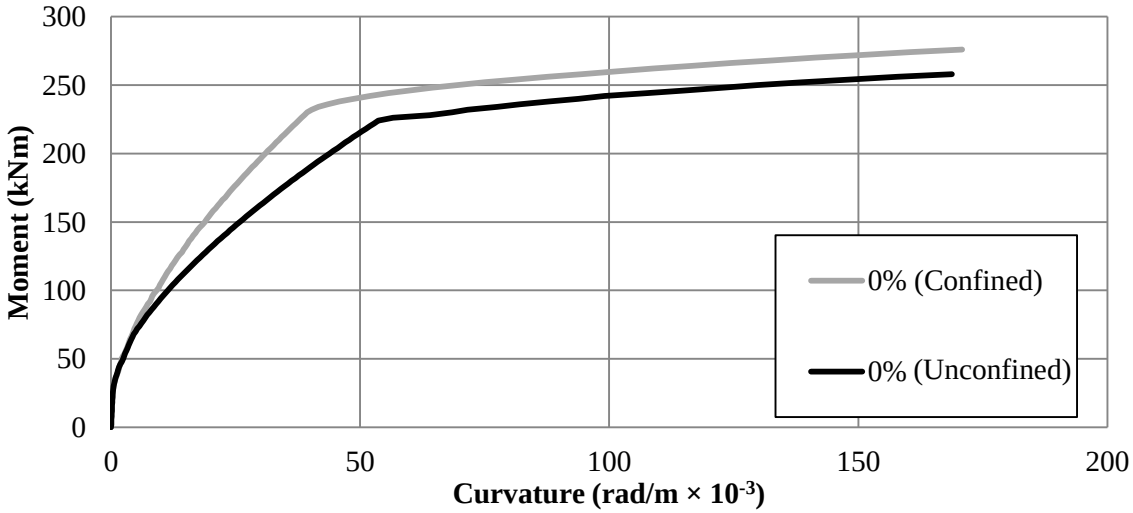

Figure 5-18: Push-over analysis of the 400mm × 400mm section using bond properties: T_0=30MPa, Ω=0.0 and corrosion level of 0% including comparison with Ω=0.071.

It was interesting to note in Figure 5-19 that at low levels of corrosion (5%), yield strength increased with only a minor reduction in stiffness. This was due to the instantaneous strength loss post-rupture typical of unconfined bond performance. After rupture occurred, instead of providing slightly reduced strength, unconfined conditions resulted in a rapid strength loss until reaching the sliding bond stress, T_s.

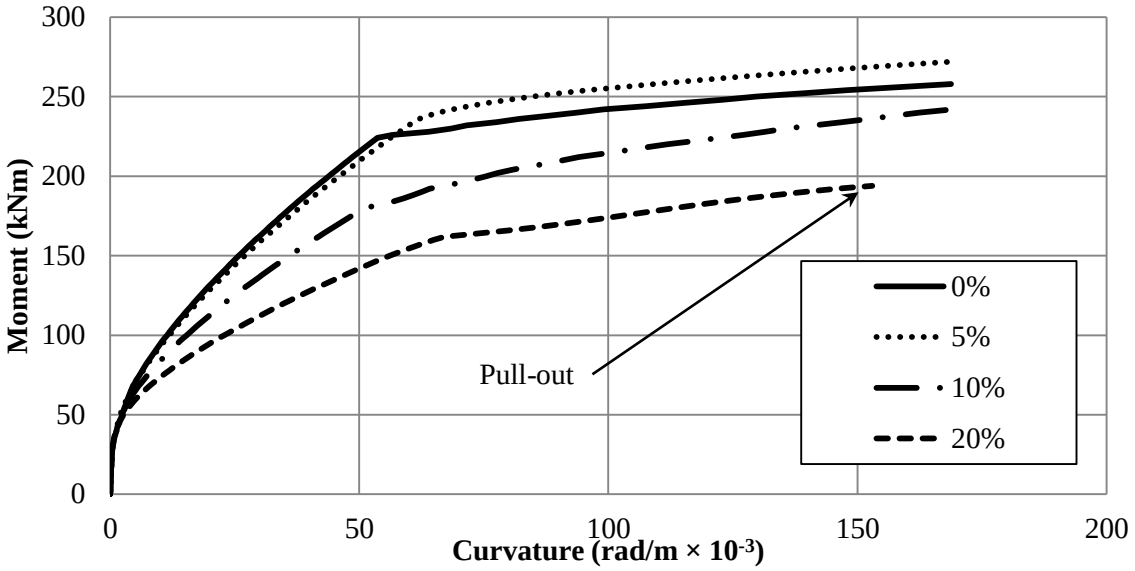

Figure 5-19: Push-over analysis of the 400mm × 400mm section using bond properties: T_0=30MPa, Ω=0.0 and corrosion levels of 0%, 5%, 10% and 20 %.

Experimental testing revealed that sliding stresses are increased by low levels of corrosion due to additional radial stresses on the reinforcing bar, thus in the strain penetrated regions where bond rupture had already occurred, 5% corroded bars will provide more resistance than uncorroded bars in unconfined cases. According to the model, post rupture bond stresses were 8.9 MPa of uncorroded bars, 11.7 MPa for 10% corrosion, but 14.4 MPa for 5% corrosion. Based on the proposed bond-slip model, ultimate frictional stresses that are closely related to sliding stress, are at their maximum between 3% and 7% corrosion in unconfined bonding conditions. However, this is reliant on surrounding concrete not being significantly cracked and is in the region of interpellation between the series of experiments conducted so should be treated with caution.

It was noted that crushing occurred in the outermost springs prior to yielding of reinforcement. This brittle behaviour was common in models where less robust bonding was provided due to reductions in confinement, increased corrosion, or lower T_0. These factors all increase strain penetration and so require increased curvature to induce yielding of reinforcement. Increasing yield curvature requires a higher neutral axis, reducing the area of compression concrete available, thus increasing stresses in compressed concrete.

Analyses using T_0 = 20 MPa were conducted and similar effects to T_0 = 30 MPa were observed with decreased stiffness and ultimate strength under increased corrosion, as shown in Figure 5-20 and Figure 5-21. Reducing the uncorroded, fully confined rupture stress resulted in increased bond pull-out failure occurring at lower levels of corrosion as was shown in Section 5.1. An example of this is the fully confined, 20% corrosion model failed through concrete spalling when T_0 = 30 MPa, but failed through bond rupture (pull-out) when T_0 = 20 MPa.

When looking at uncorroded fully confined behaviour in Figure 5-20, there is very little difference between 0% (confined, T_0=30MPa) and the uncorroded model using T_0 = 20 MPa, prior to pull-out failure occurring.

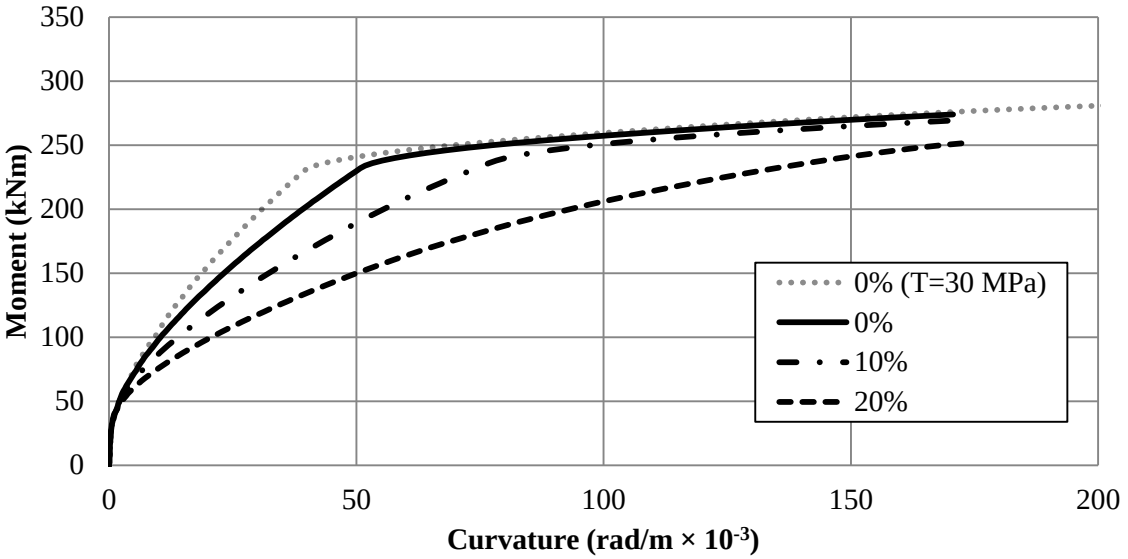

Figure 5-20: Push-over analysis of the 400mm × 400mm section using bond properties: T_0 = 20MPa, Ω=0.071 and corrosion levels of 0%, 10% and 20 %, including comparison with T_0 = 30MPa.

When comparing fully confined bonding (Figure 5-20) with unconfined bonding (Figure 5-21), the differences are far greater. Reduced confinement saw bar stresses reduce significantly due to increased strain penetration, reducing the yield moment capacities. Concrete spalling occurred before yield under 10% corrosion and bar pull-out occurred at 20% corrosion.

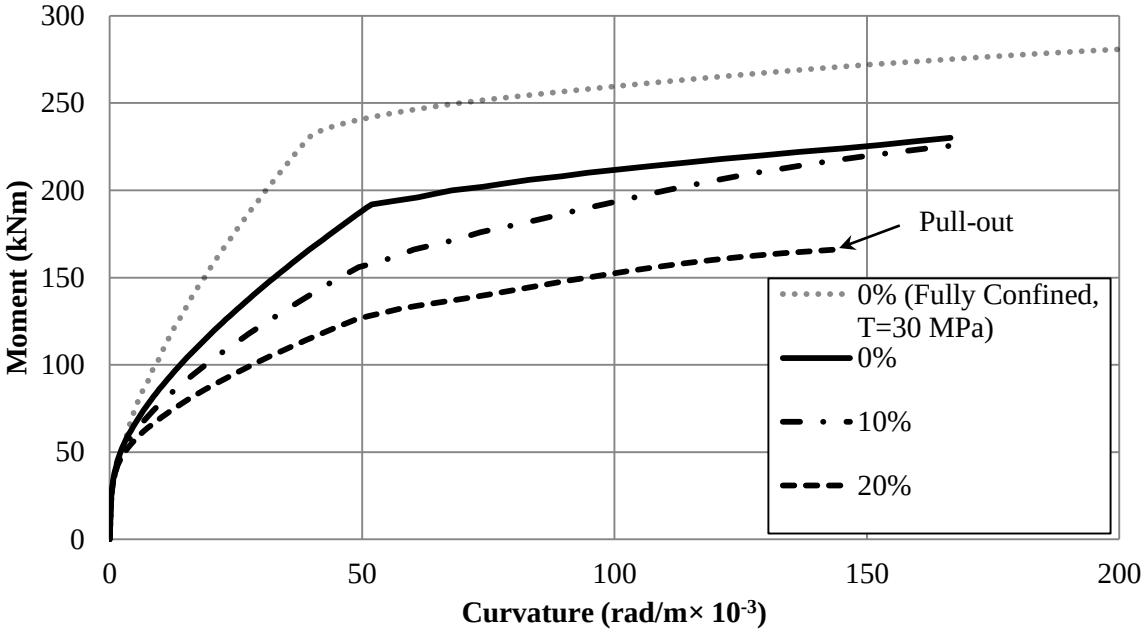

Figure 5-21: Push-over analysis of the 400mm × 400mm section using bond properties: T_0 = 20MPa, Ω=0.0 and corrosion levels of 0%, and 20 %, including comparison with T_0 = 30MPa, Ω=0.071.

5.2.2.3 Cyclic Push-over Results

Cyclic push-over analyses were performed using the multi-spring models to assess the effects of bond deterioration on hysteretic behaviour. Unfortunately, due to errors in the imposed displacement algorithms in the current (2011) version of Ruaumoko3D (Carr 2010a), the author was unable to apply a cyclic displacement protocol making results difficult to compare and interpret.

The effects are visible in Figure 5-22 where the hysteretic loop from the third loading cycle is displayed for 0%, 10% and 20% corrosion for the fully confined condition. Fully hysteretic loop are shown in Appendix H. Increasing bond deterioration saw a narrowing of the hysteretic loop inducing stiffness degradation. This was attributed to increased slippage of reinforcement due to decreases in bond stiffness, as well as increased strain penetration due to decreased bond strength. Both of these introduced slackness in reinforcement as it transitioned from compression into tension. Recentring behaviour was observed when loading was kept below yield level.

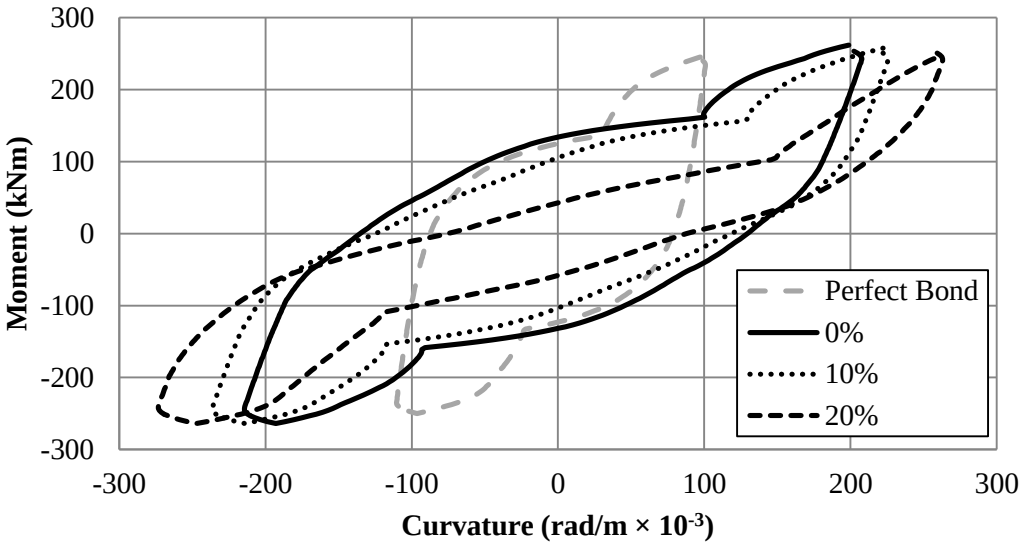

Figure 5-22: Third inelastic cycle hysteretic loop for corrosion levels between 0% and 20% T_0 = 30MPa, Ω=0.071, Including comparison with perfectly bonded condition.

Due to pull-out occurring at 20% corrosion and strength reduction at lower levels of corrosion, it was not possible to determine cyclic behaviour using the same load regime for all models. In spite of this, clear differences in hysteretic behaviour were visible and can be seen in Figure 5-23.

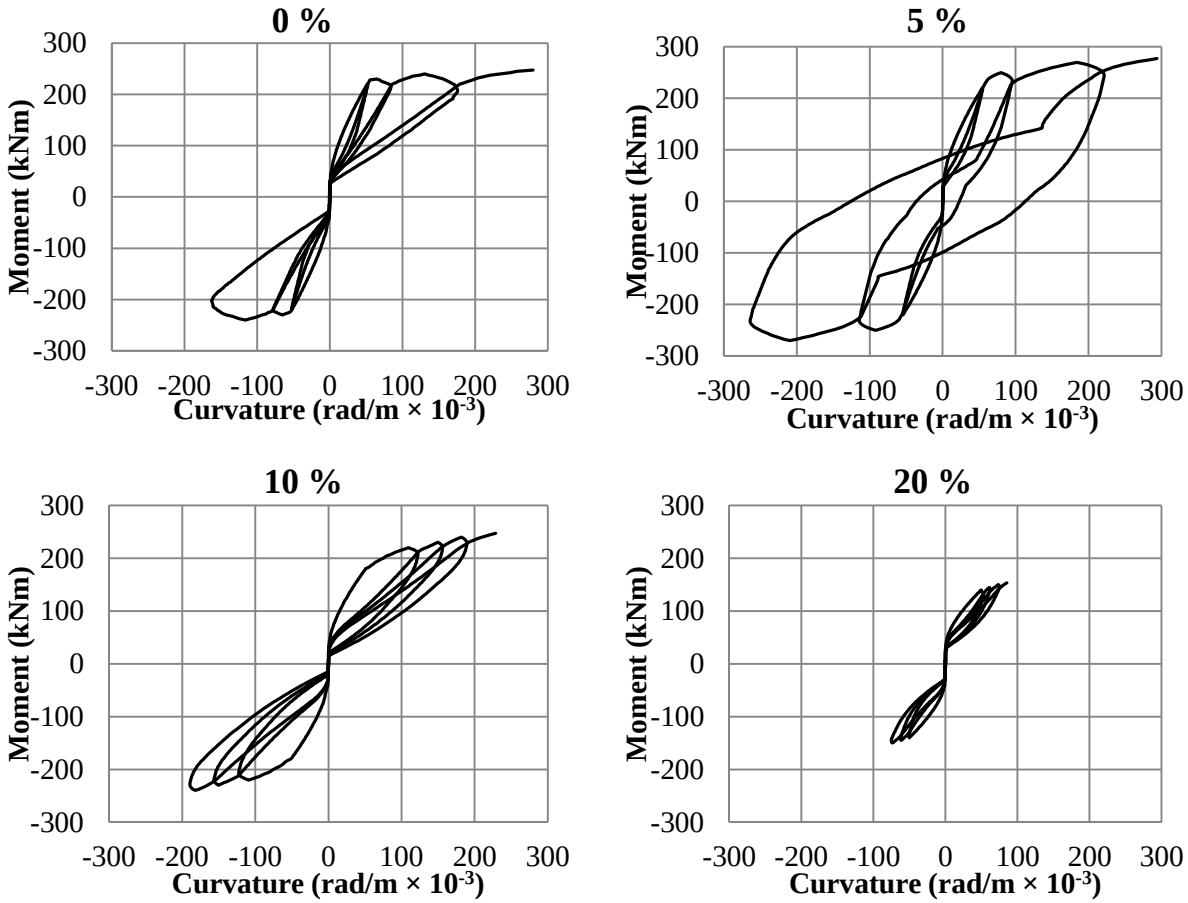

Figure 5-23: Degraded moment-curvature hysteretic behaviour of 400mm × 400mm multi-spring model for bond degradation between 0% and 20 % corrosion using unconfined conditions.

5% corrosion provided the best performance, with similar hysteretic properties to confined specimens. A strong theme shown in Figure 5-23 is recentring due to axial load with flag shaped hysteretic loops most commonly seen in hybrid post-tensioned rocking systems. This can be attributed to strain penetration into the bonded length of reinforcement acting in a similar manner to the deboned region present in hybrid post-tensioned rocking systems (Spieth et al. 2004).

Recentering behaviour was not observed past yield at 5% deterioration. This was attributed to the combination of comparatively high rupture stress (T_R=12.5 MPa), combined with high sliding stresses post bond rupture. Figure 5-24 shows how at 5% corrosion, sliding stress was over twice that of the uncorroded situation. Increase in post-rupture stress, which is proportional to sliding stress when unconfined behaviour is assumed, is responsible for the improved hysteretic behaviour at 5% deterioration. This is because, when ruptured, bond resistance is over double that seen in the uncorroded case, therefore more bond is developed within the strain penetrated section.

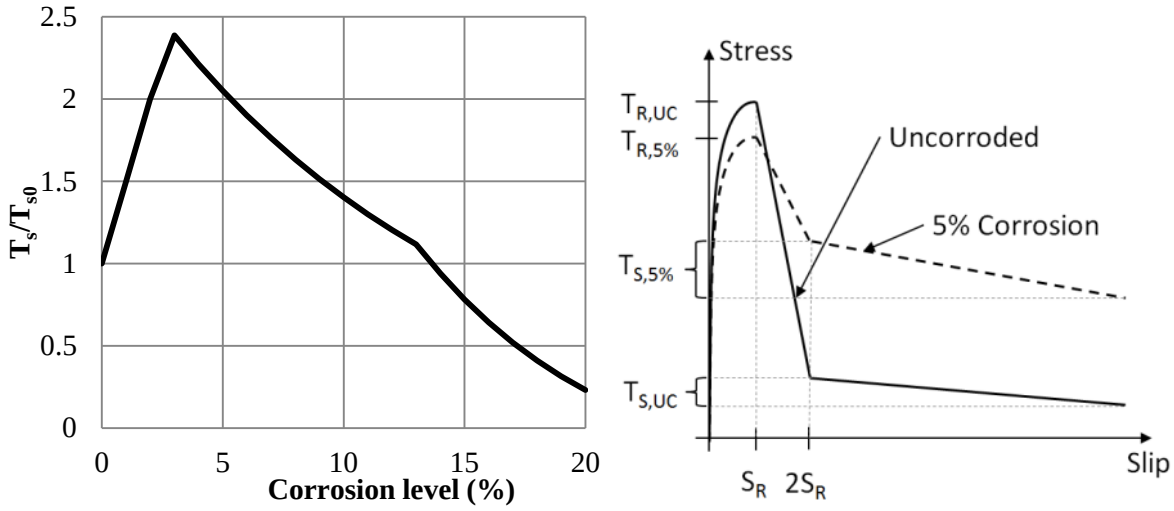

Figure 5-24: Left: Normalised initial sliding stresses with increasing level of corrosion. Right: Comparison between uncorroded unconfined performance and 5% corroded unconfined performance.

Validity of the unconfined, moderate to heavily corroded portion of the implemented bond-slip model is unclear as sliding stresses were determined based on confined specimens with 0% - 20% corrosion and unconfined/partially confined specimens with 0% - 2% corrosion. Performance bonding at higher levels of corrosion (> 2%) with no or low confinement was inferred from confined testing. Increased sliding stresses at moderate levels of corrosion (3%-13%) are reliant on additional radial stresses, that in turn are reliant on surrounding concrete and steels ability to resist them through confinement. Splitting of concrete surrounding the reinforcing bar allows relief of radial stresses, reducing sliding stresses, which was not accounted for within the proposed bond-slip model.

5.3 Case Study: New Brighton Pier

5.3.1 Introduction

The New Brighton Pier (-43° 30’ 20.55”, 172° 43’ 52.76’) is a structure design using modern design philosophies that sustained damage through cracking and spalling in the Christchurch earthquakes. Furthermore, its location on the New Brighton beach exposes it directly to a harsh natural environment where, without full protection from it now damaged cover concrete, the pier is at risk of accelerated corrosion deterioration. Because of these factors it is a prime candidate of a more in depth assessment of its lifecycle performance.

5.3.2 Description

The New Brighton Pier is situated in the suburb of New Brighton, Christchurch New Zealand. It was constructed in 1997 and extends from the beach front, 300m into the Pacific Ocean as can be seen in Figure 5-25. The structure consists of 15 20 m long, simply supported prestressed beams making up the deck with a viewing platform situated at the seaward end. These are supported by 17 reinforced concrete circular piers which taper from ϕ = 2600 mm at the deck down to ϕ = 1200 mm over their upper 2.75m. Sketches of the pier section can be seen in Figure 5-26.

Figure 5-25: Image of New Brighton Pier

Modern seismic design philosophies were adopted with hinging of piers expected to occur near to their interface with the sand level. Given the uncertainty of this exact location due to varying sand levels, columns were detailed with R16 stirrups at 125mm to account for hinging at any location above the steel encased concrete piles. Elastomeric bearings allow for thermal movement of the super structure, allowing limited seismic isolation.

Direct interaction with a marine environment places the pier exposure in class 'C' under NZS1170:2006. Due to this aggressive environment, concrete used in the pier was specified to have a 28 day strength of 50 MPa (assume 0.38 w/c) using a high slag blend (65% GGBS:ground blast furnace slag, Duracem- Holcim Cement), and all reinforcement was afforded 70 mm cover, which meets current standards.

In September 2010, Christchurch city felt the effects of the Darfield earthquake, M_w 7.1, epicentre approximately 50 km from the New Brighton Pier. Moderately strong shaking was felt through-out Christchurch with peak ground acceleration at New Brighton of 0.192g. This resulted in the formation of minor cracks in the piers. In following months, thousands of aftershocks occurred in the wider Christchurch area, with several of similar shaking intensity to the main event.

These were a precursor to the February 22nd 2011, Christchurch earthquake, M_w 6.3, centred 9 km south of New Brighton Pier. The February event resulted in the loss of 185 lives and widespread devastation in Christchurch city. Peak accelerations were measured at 2.2g with accelerations at the New Brighton Pier likely to have been between 1.0g and 1.9g. While the magnitude and duration of the February event was less than that of September 2010, its close proximity to Christchurch city, higher accelerations, and production of several strong aftershocks, left the New Brighton Pier with heavy damage (Palermo et al. 2012), as shown in Figure 5-27.

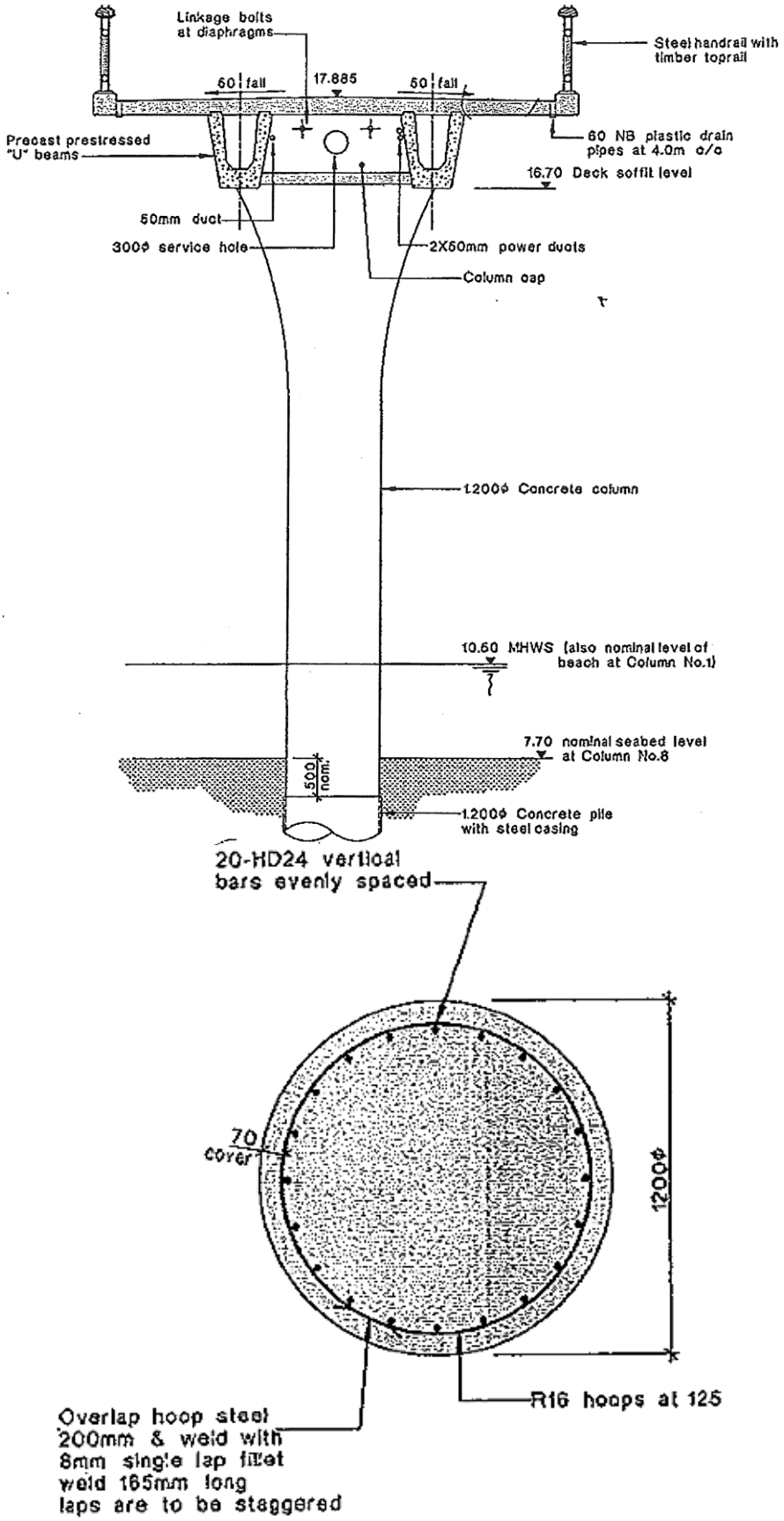

Figure 5-26: Top: Standard column layout with deck section atop; Bottom: Column section at soil interface (CCC 1995).

Inspection of piers following the February event was limited to a visual inspection of the first seven piers. This inspection revealed a trend of increasing damage further out to sea, with minor cracking becoming accompanied by major spalling in plastic hinge regions, as shown in Figure 5-27. Security video recorded from the western end of the pier showed significant movement of the deck resulting in pounding damage and movement of bearing pads.

Figure 5-27: Spalling, revealing transverse reinforcement of Pier 7 of New Brighton Pier.

Damage of this severity negates the ability of concrete to protect reinforcement, exposing reinforcing directly to the harsh tidal marine environment. As the pier serves no functional use, it is a low priority for repair for the Christchurch City Council and so is unlikely to be repaired for a number of years, especially in regions below the low tide line. Spalling, combined with flexural cracking further up the piers, will accelerate deterioration and allow for initiation and propagation of corrosion in damaged regions. This structure, designed for a 50 year design life in accordance with current design provisions, may be in serious distress within the next 10 years. Corrosion of transverse reinforcement was already apparent only a month after the February 2011 event.

In light of the apparent reduced durability of the New Brighton Pier, several existing models were used to predict its likely level of deterioration over the next 50 years. The models and processes that were implemented are explained in detail in the following section.

5.3.3 Degradation Parameters

The rate of degradation due to corrosion varies over time requiring different approaches to be taken depending on whether cover concrete is intact, cracked or spalling, as shown in Figure 5-28.

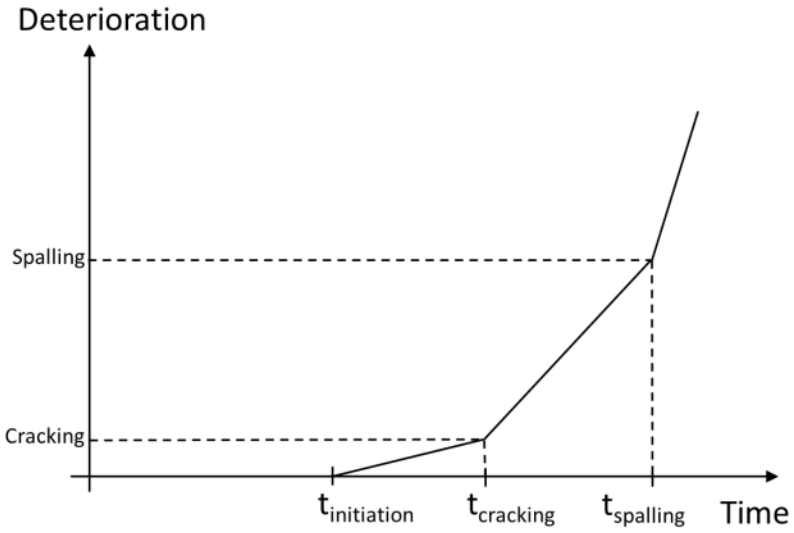

Figure 5-28: General damage propagation model

5.3.3.1 Chloride Ingress Models

Measurement of chloride ingress is the most common method of determining time to initiation of corrosion. Most methods utilise Fick's 2nd law of diffusion to determine the concentration of chlorides by mass at the depth of reinforcing. The general solution for this is shown below in Equation 5-3, where $n(x,t)$ can be taken to be the concentration at depth x at time t, $n(0)$ is the surface concentration, D is the diffusivity and *erfc* is the error function.

$$n(x,t) = n(0)erfc(\frac{x}{2\sqrt{Dt}}) \qquad \text{Equation 5-3}$$

Research into corrosion initiation chloride concentration using a 65% ground granulated blast furnace slag mix (Reddy 2001) found values ranging from 0.22% to 0.51% chloride ions by mass of binder. The concentration at which initiation of corrosion occurs was taken to be 0.3% chloride ions by mass of binder.

Dhir et al. (1996) and Mohammed et al. (2002), both investigated diffusion properties of GGBS mixes from tidal exposure. The values presented for diffusion of chlorides were 0.56×10^{-12} m^2/s and 0.486×10^{-12} m^2/s respectively, whereas for surface concentration their findings were 3.25% and 4.12% of binder mass, respectively. Based on these results, the value used for D was 0.52×10^{-12} m^2/s and surface concentration was 3.7% of binder mass for uncracked concrete. When these values were applied, it was found that it would take 50 years before initiation of corrosion occurred for the structure if it were in its undamaged condition as shown in Figure 5-29.

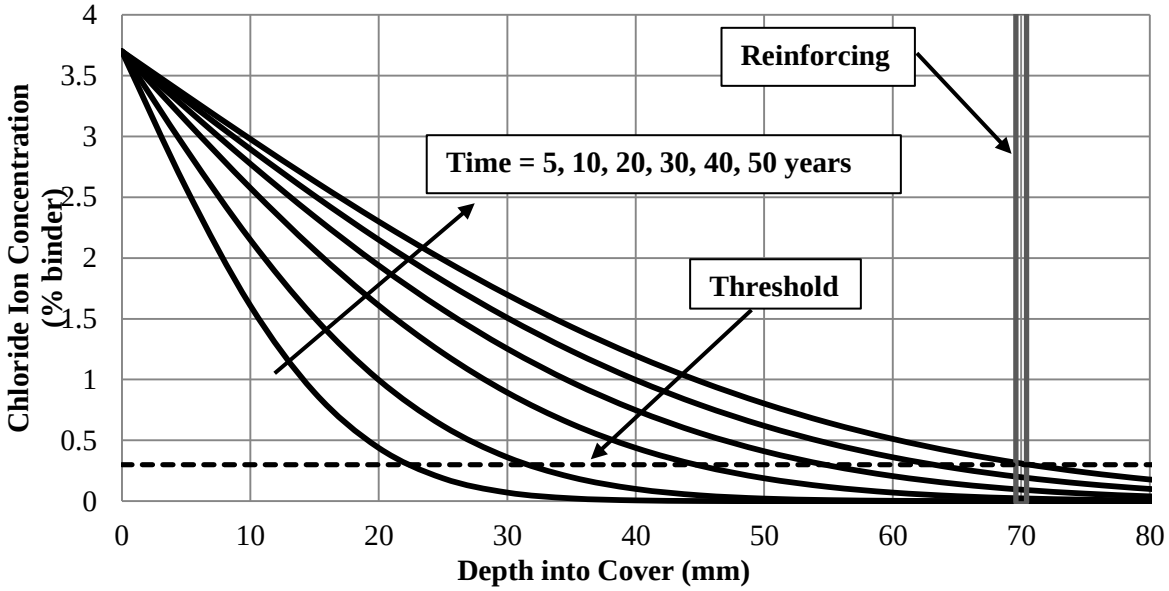

Figure 5-29: Chloride Ingress over 50 years for Undamaged condition

Cracking occurred in piers as a result of earthquake shaking. Cracking effects diffusion of chlorides and oxygen through concrete. Cracks ranged from hairline widths in areas far from the plastic hinge regions to ~0.3mm adjacent to plastic hinge regions. Ragueneau et al. (2006) and Djerbi et al. (2008) assessed effects of craking on chloride diffusion for various concrete mixes. Findings from their experimental programme showed crack width negated the effects of improved microstrcuture that high performance concrete provided once cracking exceeded ~0.065mm, this can be seen from Figure 5-30.

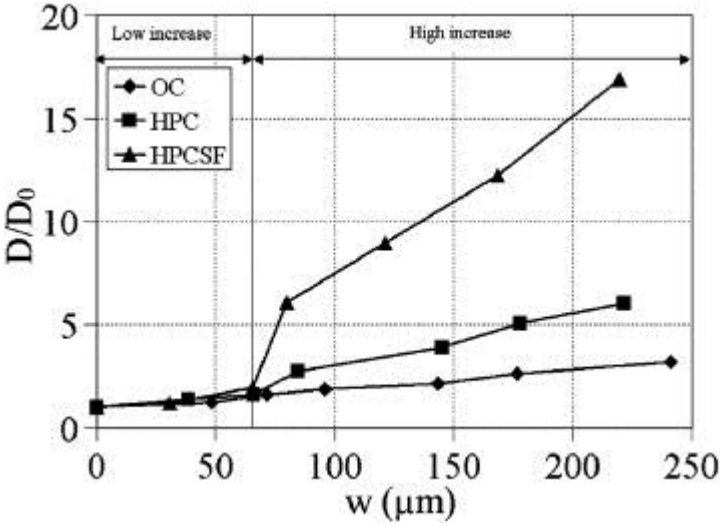

Figure 5-30: Relationship between crack width and increased chloride diffusion in Ordinary Concrete (OP), High Performance Concrete (HPC) and High Performance concrete using Silica Fume (HPCSF) (Djerbi et al. 2008).

As crack widths in the piers were of the order of 0.1mm, the chloride diffusion constant, *D*, was taken as 7.5 times the initial diffusion coefficient, making $D = 3.9 \times 10^{-12}$ m^2/s. This increase in diffusion allowed for accelerated ingress of chlorides and when the time to initiation was recalculated, it was found that initiation would likely occur within five to ten years of cracking as shown in Figure 5-31.

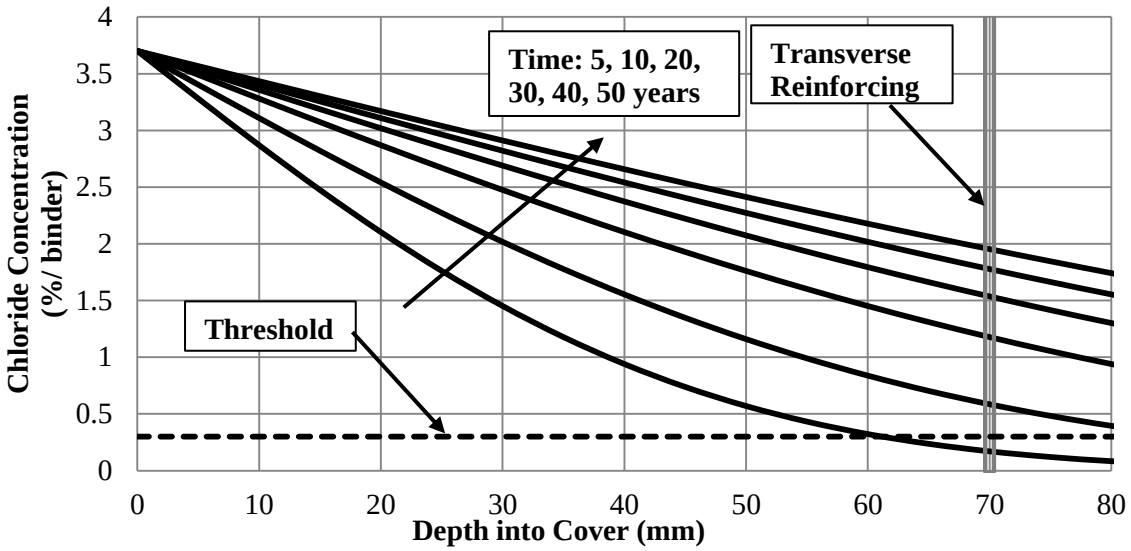

Figure 5-31: Chloride ingress over 50 years for damaged condition (0.1mm crack width).

5.3.3.2 Steel Damage

Once corrosion has been initiated, propagation of damage becomes a function of oxygen, water, and ion transport mechanisms (Melchers et al. 2008). This is dependent on concrete quality and cover and information on the effects of these on such phenomena is limited (Vu and Stewart 2000). As with chloride ions, ease of movement of oxygen and water is increased by cover cracking. Using the same adjustment as for chloride ion diffusion, it was assumed that cracking increased oxygen diffusion by 7.5 times. This was then applied to the Equation 5-4 proposed by Vu and Stewart (2000) through an increase in corrosion rate by 7.5 times.

$$i_{corr}(1) = \frac{37.8\,(1-\frac{w}{c})^{-1.64}}{cover} \qquad (\frac{\mu A}{cm^2}) \qquad \text{Equation 5-4}$$

1μA/cm^2 is approximately equivalent to a corrosion loss of 0.011 mm/yr. Thus for New Brighton Pier, the rate of deterioration in its cracked state will be 0.098 mm/year. This gives the depth of corrosion on the bar surface and so loss of diameter was taken as 0.196 mm/year once initiation of corrosion occurs. This was based on some simplified assumptions but provides an indication of likely deterioration.

It is noted by Vu and Stewart (2000) that corrosion rates tend to decrease with time due to build-up of corrosion products on the surface of reinforcement. To account for such behaviour Equation 5-5 (Vu and Stewart 2000) was used where t_p is time after initiation in years.

$$i_{corr}(t_p) = (i_{corr}(1) \times 0.85t_p)^{-0.29} \qquad (\frac{\mu A}{cm^2}) \qquad \text{Equation 5-5}$$

The model does not take into account effects of concrete spalling or effects of increased crack widths due to expansive corrosion pressures. These phenomena are very difficult to quantify but would increase the rate of deterioration by allowing increased exposure of reinforcing to oxygen and water. Assumptions have already been made regarding the corrosion rate where cracking was deemed to increase the rate of corrosion by 7.5 times that of uncracked conditions. It was assumed that this would account indirectly for effects of further cracking and spalling. Using these parameters, degradation of reinforcement over a 50 year life-time is shown in Figure 5-32, continuing this trend would see the level of corrosion reach 29% after 100 years of service if repairs were not undertaken.

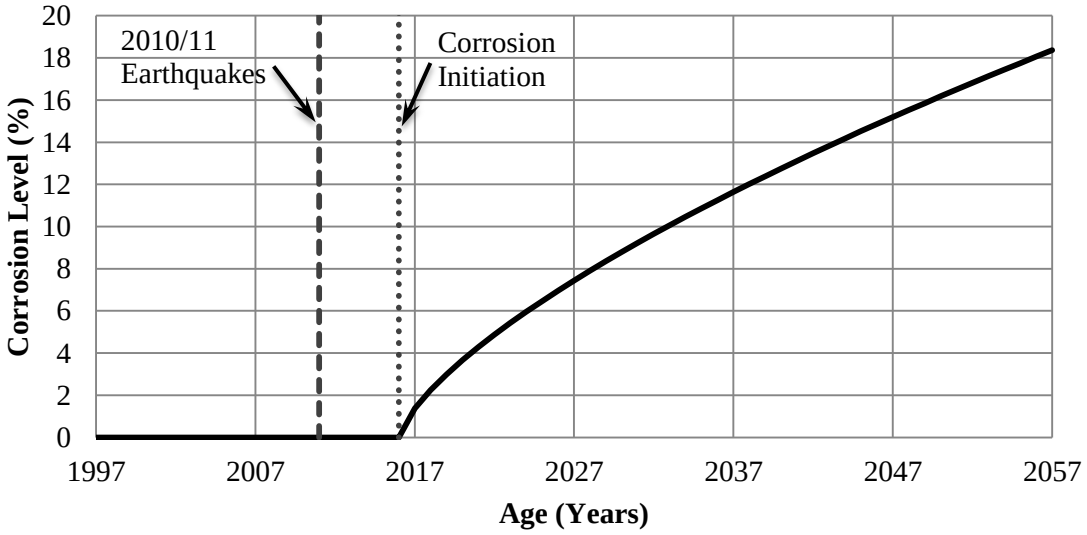

Figure 5-32: Predicted steel deterioration over time of New Brighton Pier due to corrosion

5.3.3.3 Reinforcement Mechanical Properties

The effects of corrosion on mechanical properties of reinforcement are highly variable. This is due to variation in the severity of corrosion even in small sections of reinforcing. Apostolopoulos and Papadakis (2008) found that for chloride induced corrosion, non-uniformity of mass loss resulted in only minor reductions in yield strength for corrosion levels less that ~8%. Apostolopoulos and Papadakis (2008) also found that the relationship was roughly proportional, although again there was much scatter. Corrosion was found to have its largest effects on ductility. These finding were further validated by Cairns et al. (2005) who presented their findings in visual form, as shown in Figure 5-33. This was used to determine the characteristics of corroded reinforcement within the model.

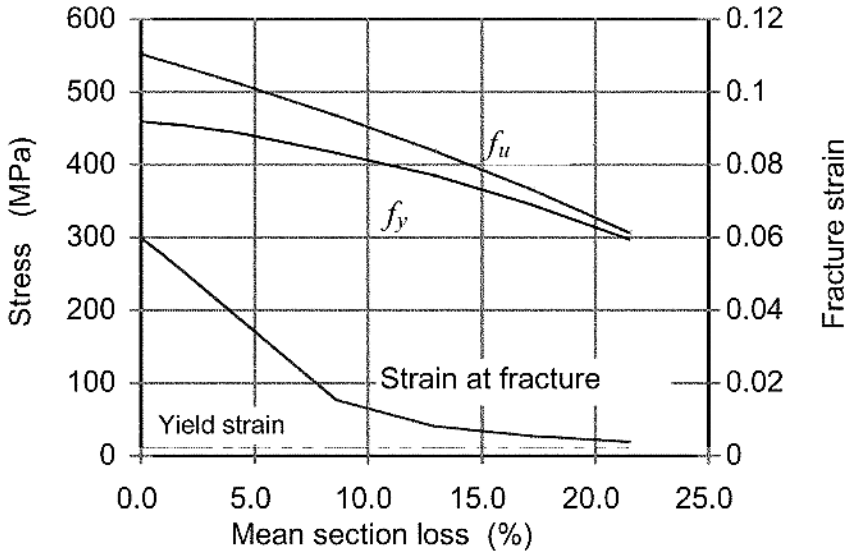

Figure 5-33: Yield, Ultimate and Elongation behaviour of reinforcement corroded to various levels. (Cairns et al. 2005).

5.3.3.4 Confinement

Prior to deterioration, the steel confinement index, Ω, determined using the equation proposed by Plizzari et al. (1998), was calculated to be 0.0066. This was reduced in accordance with the overall level of corrosion. It was assumed that bonding would behave in a 'well confined' manner and would not split following bond rupture. This assumption was able to be made due to close stirrup spacing (125 mm) and large cover depths (70 mm).

5.3.3.5 Summary of Analysis Inputs

Once the level of deterioration was determined, the values to be used within the corrosion dependent bond slip model that was developed in Chapter Corrosion Dependent Bond-Slip Model4 were calculated. Table 5-2 and Table 5-3 show these values used in modelling bond performance and reinforcement degradation in the New Brighton Pier over 50 years following damage sustained in the Canterbury earthquakes.

Table 5-2: Bond parameters used in New Brighton Pier model

Year	Corrosion Level (%)	T_R (MPa)	T_F (MPa)	S_R (mm)	S_p (mm)	S_f (mm)	n	α	β	A	B	C
0	0	21.2	7.8	0.3	0.5	12.0	0.4	1.13	-3.02	2.16	-3.1	0.29
10	4.3	18.4	16.8	0.3	0.5	16.8	0.4	0.53	-4.05	3.01	-4.05	0.37
20	9.2	12.6	11.6	0.3	0.5	11.6	0.4	0.53	-5.23	4.39	-5.12	0.46
30	13.1	9.4	8.6	0.3	0.5	8.6	0.4	0.54	-6.16	5.92	-5.98	0.54
40	16.5	7.3	4.5	0.3	0.5	4.5	0.4	0.86	-6.98	7.7	-6.73	0.60
50	19.5	5.8	2.1	0.3	0.5	2.1	0.4	0.92	-7.7	9.69	-7.39	0.66

Table 5-3: Reinforcing parameters used in New Brighton Pier Model, (Based on Cairns et al. (2005))

Year	Corrosion Level (%)	f_u (MPa)	f_y (mm)	ε_f
0	0	550	470	0.06
10	4.3	505	440	0.035
20	9.2	460	405	0.015
30	13.1	410	375	0.008
40	16.5	375	350	0.006
50	19.5	330	315	0.004

Degradation of concrete with time was not included within the models. It was assumed that spalling did not occur and that cracking damage induced by corrosion did not affect the concrete strength. While degradation of cover concrete due to high levels of corrosion is likely, determining when in the lifecycle of the structure this would occur was difficult with no suitable models found in literature.

5.3.4 Multi-Spring Model

A similar model set up as shown earlier in Figure 5-10 was used in modelling pier moment curvature behaviour. All steel spring were linked to the rigid frame with bond spring elements. 911 steel, concrete, and bond springs were used in total to represent the section. The circular piers were represented through a series of adjacent rectangular regions as shown in Figure 5-34.

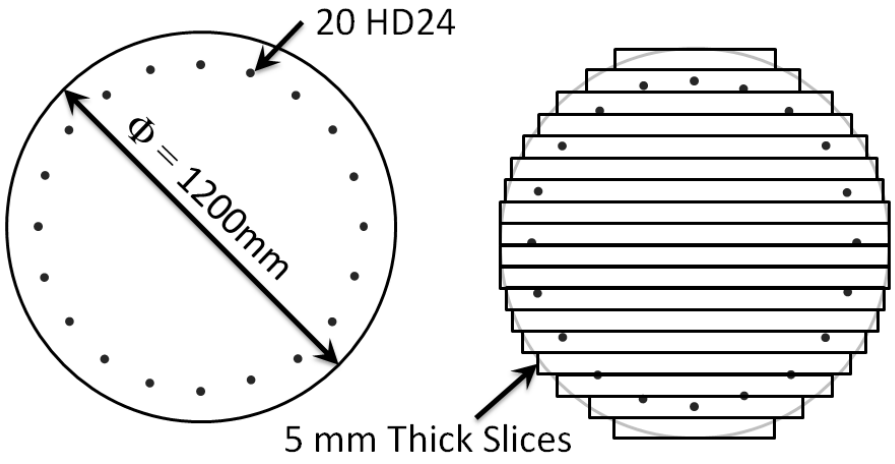

Figure 5-34: Left: Section layout for the piers of New Brighton Pier, Right: Model representation of the section using 5mm slices (not to scale)

In all, the multi-spring model consisted of 240 5mm concrete slices. To reduce the number of concrete spring properties required, concrete springs were grouped into fives, where all five springs received the average of the given regions characteristics. The weight of the structure was calculated in accordance with the tributary area of each pier. As the structure is only intended to be accessed by pedestrians, no live loading was included in modelling. Based on this, the axial load acting on the section was calculated to be 2100kN.

Figure 5-35 shows the comparison between the model and Response2000 (Bentz 2001) moment-curvature behaviour when using both 'perfect bonding' conditions within the model (no bond-slip) and when bond-slip is allowed for. When the assumption of perfect bonding is made, the model displays many similarities with Response2000 in both initial stiffness and yield strength. Post yield, the model using perfect bonding slightly overestimated moment capacity along with ultimate curvature. When bond-slip was introduced a decrease in pre-yield stiffness was observed although ultimate moment capacity was closer to that provided by Response2000. Inclusion of bond-slip also caused reduction in ductility, though exact values were difficult to determine due to sequential yield of reinforcement situated through the depth of the section.

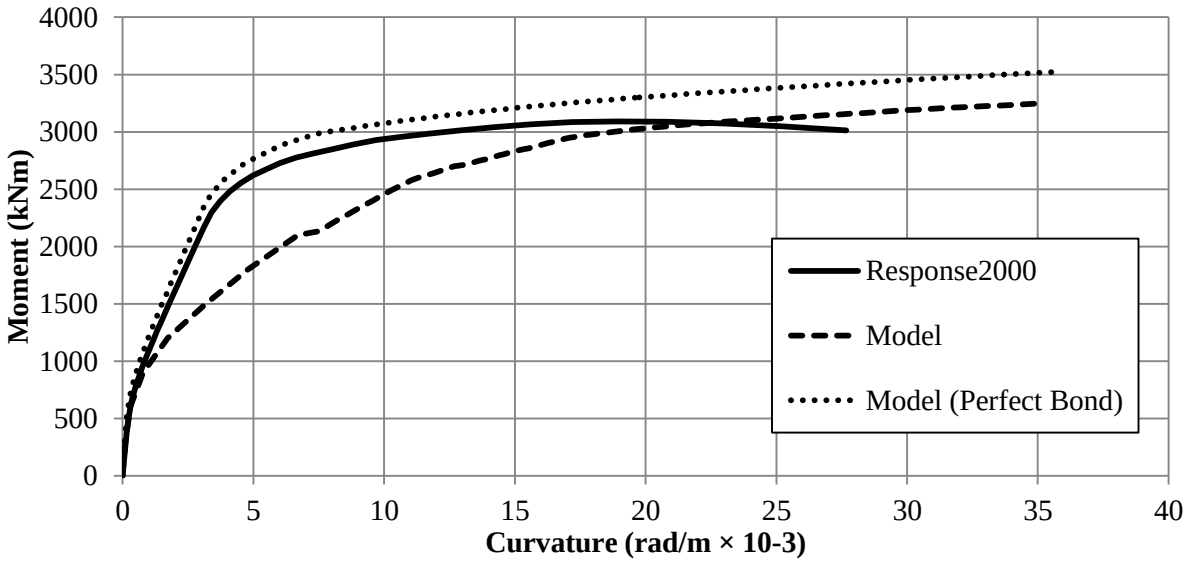

Figure 5-35: Validation of multi-spring model against Response2000 moment curvature behaviour.

5.3.5 Monotonic Push-over Analysis

No bond rupture was observed within monotonic testing, even at the same corrosion levels used in Section 5.1. This can be attributed to three things:

1. use of lower grade steel (Grade 430 as opposed to Grade 500),
2. monotonic loading as opposed to cycling before pull-out, and
3. reduced steel spring properties to account for loss of section in reinforcing, which was ignored in the earlier models.

It can be seen from the slip profiles shown in Figure 5-36 that bond rupture of the first bond spring (slip > 0.3mm) did not occur until after 20 years of damage with no bar slippage occurring at the non-loaded end even after 50 years deterioration.

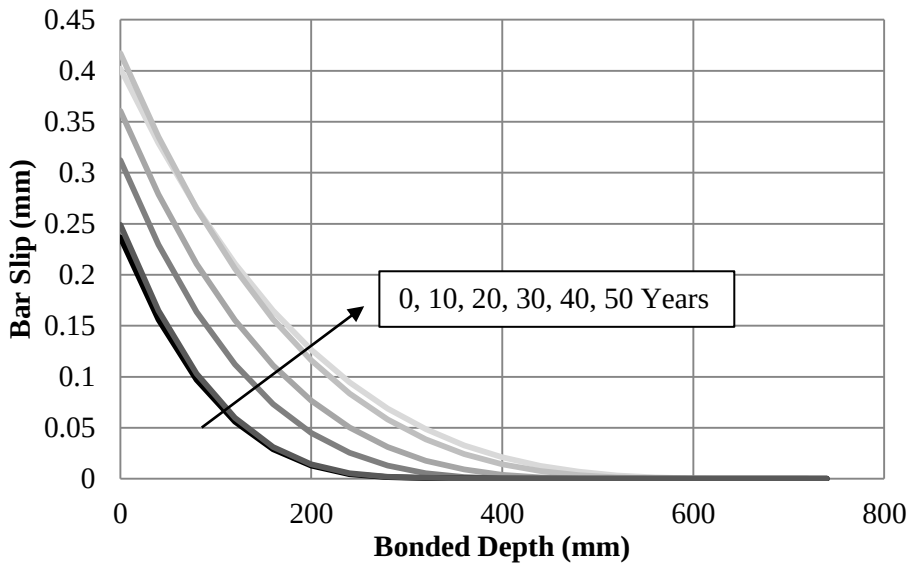

Figure 5-36: Slip profile of HD24 (Grade 430) reinforcing at rupture from the New Brighton Pier multi-spring model.

The push-over moment-curvature behaviour observed from the models over 50 years following the Canterbury earthquakes is shown in Figure 5-37. Unlike the 400mm × 400mm section previously analysed, it could not be assumed that the spalling curvature would be constant at all levels of deterioration due to the geometry of the columns and reductions in reinforcement properties. The spalling curvature was determined directly from the model at a concrete strain of 0.0064 (Mander et al. 1988), values for which are shown in Table 5-4. Increase in spalling curvature equated to only 10% over 50 years of deterioration. Such a minor difference in this example gives confidence in the assumption made in analysing the 400mm × 400mm section in Section 5.2.2.

Table 5-4: Curvature at spalling of the New Brighton Pier over 50 years of deterioration.

Year	Spalling Curvature (rad/m x10^{-3})
0	35.1
10	36.0
20	36.8
30	37.5
40	38.2
50	38.8

Effects of degradation were seen through significant reductions in stiffness after cracking occurred. Reduced stiffness resulted in increased displacements which when subjected to a moment of 2500 kNm leads to over double the curvature in the section. Large reductions in stiffness such as these introduce secondary effects that could increase moment demands and impair the stability of the structure. The ductility of the structure is also affected by deterioration though the geometric layout of the section making it difficult to give a value to ductility reduction.

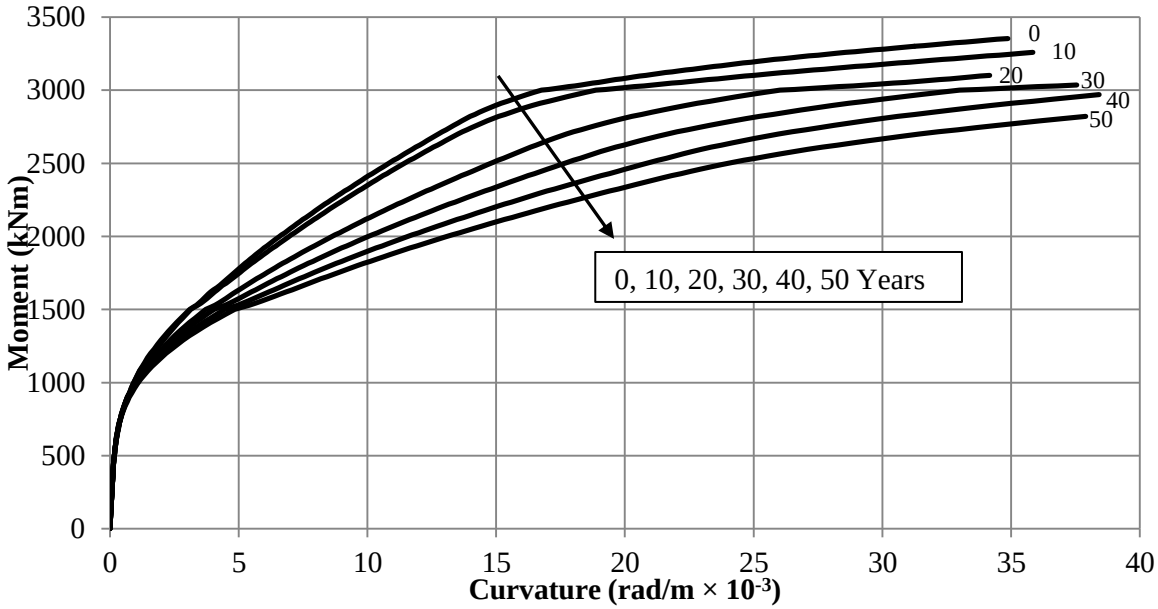

Figure 5-37: Push-over analysis of New Brighton Pier multi-spring model over 50 years of post-earthquake degradation.

The 20 year curve provides the most interesting phenomena; it is the only level of deterioration where bar rupture governs the ultimate capacity of the section. This was attributed to a 75% reduction of original steel rupture strain due to corrosion, which was unable to be counteracted by increased strain penetration associated with bond deterioration. In essence, the reduction in reinforcing elongation capacity due to its corrosion was greater than the increase in strain penetration due to corrosion. Reinforcement and bond elongation at rupture was combined to determine the total elongation capacity which is shown in Figure 5-38. This shows that the minimum elongation capacity occurred at 20 years, matching the decrease in curvature ductility displayed in Figure 5-37 at the same age.

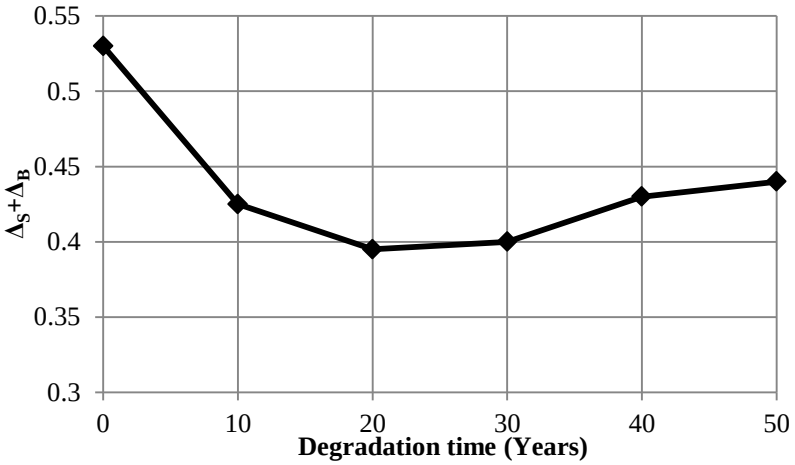

Figure 5-38: Variation in rupture deformation over time including components from reduced bar rupture strain (Δ_S) and bond slippage (Δ_B).

5.3.6 Cyclic Push-over Analysis

Using the same model set up, cyclic push-pull analyses were undertaken to determine effects of deterioration on hysteretic properties. Due to errors in the imposed displacement algorithms in the current (2011) version of Ruaumoko3D (Carr 2010a), cyclic loading to a prescribed displacement regime could not be performed. Instead, cyclic loading was undertaken using a forced based push-pull analysis. Three loading cycles were applied to the model before being increased incrementally until ultimate capacity was reached.

Hysteretic behaviour when perfect bonding was assumed is shown in Figure 5-39. Unloading stiffness was not affected by the level of maximum curvature and it was noted that there was a self-centring phenomena at elastic curvatures. As there is no bond slip included within this model it was unexpected to see pinching in its hysteretic behaviour and extension of the unloading plateau past zero curvature after the first cycle. This is shown within the circle in Figure 5-39.

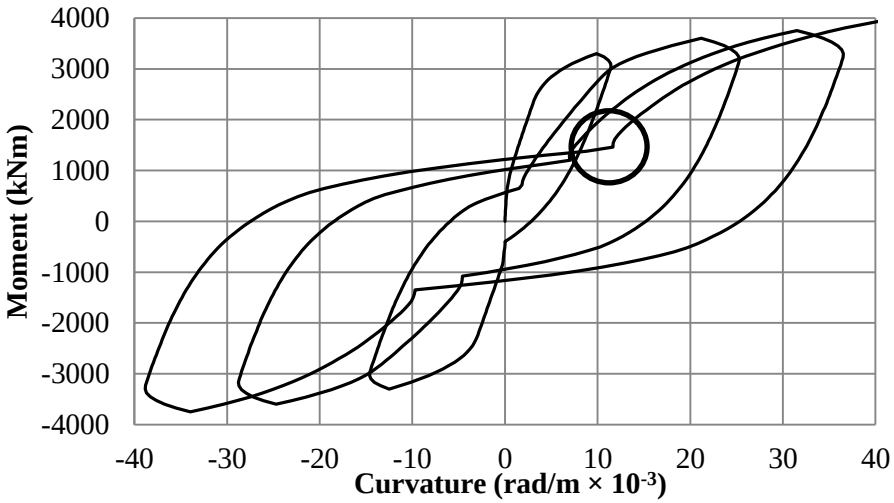

Figure 5-39: Hysteretic behaviour of the multi-spring model using 'Perfect Bond' condition.

On closer inspection it was revealed this that was due to use of Brian Peng concrete hysteresis (Carr 2010a), shown in Figure 5-40. Circled within Figure 5-40 is the region where after the first cycle of loading, stiffness is reduced beyond zero curvature before instantaneously increasing. This coincides with the sharp increase in stiffness in moment curvature behaviour, an example of which is circled in Figure 5-39. This feature of Brian Peng concrete hysteresis could not be disabled and is an accurate representation of concrete hysteresis. It is unfortunate that it resulted in hysteretic behaviour within the multi-spring resembling that of bar-slip, even when this was not present.

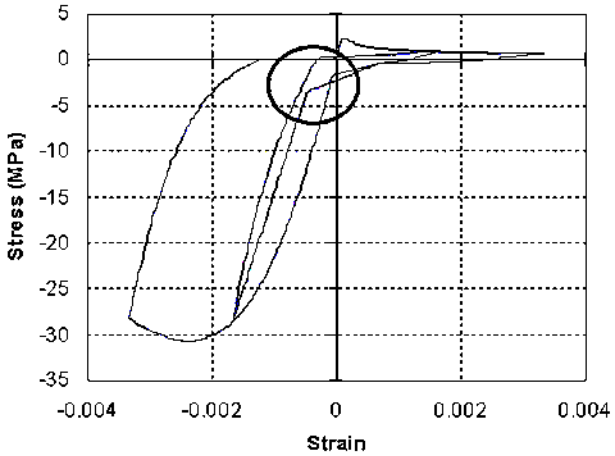

Figure 5-40: Brian Peng concrete hysteresis modified from Ruaumoko3D-Appendix B. (Carr 2010a)

When allowances for bar slippage were made, alterations to hysteretic behaviour in line with monotonic behaviour were seen with decreased loading stiffness, as shown in Figure 5-41. Prior to yield, hysteretic behaviour displayed recentring characteristics due to axial loading. Inclusion of bond slippage resulted in a reduction of unloading stiffness from ~540 kNm/rad/km to ~170 kNm/rad/km, roughly equal to 33% which matches the reduction in loading stiffness from monotonic push-over analysis. These actions combined with degrading stiffness resulted in decreased hysteretic energy dissipation for a given curvature.

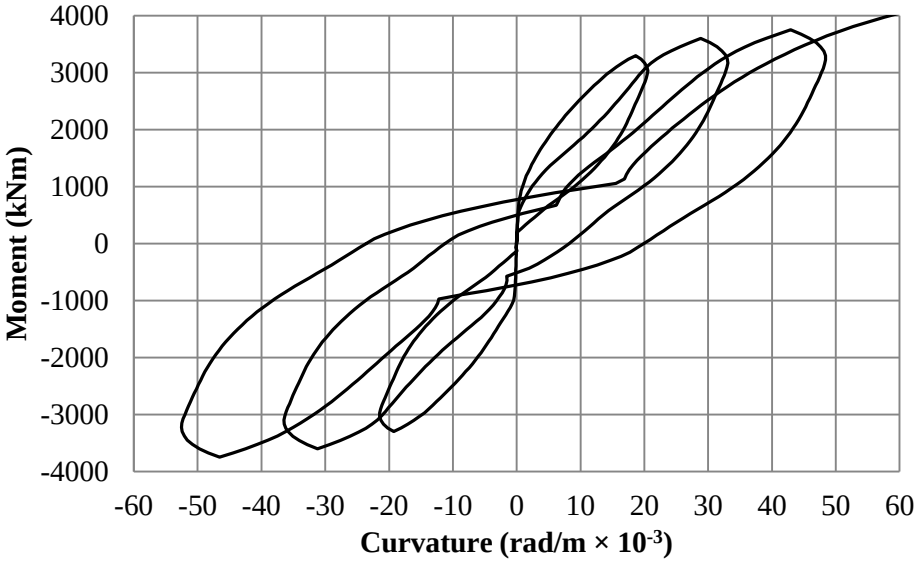

Figure 5-41: Incrementally increasing cyclic behaviour for the model at 0 years

Analyses were run using degraded properties between 0 and 50 years following the Christchurch earthquakes. All models were subjected to the same loading regime taking them through three inelastic cycles. From Figure 5-42 it can be seen that over 50 years there are significant increases in curvature that in turn resulted in increased stiffness degradation. In addition to this there was an increase in required curvature before steel previously yielded in compression to comes into tension due to bond sliding. Full graphs of cyclic behaviour are shown in Appendix I.

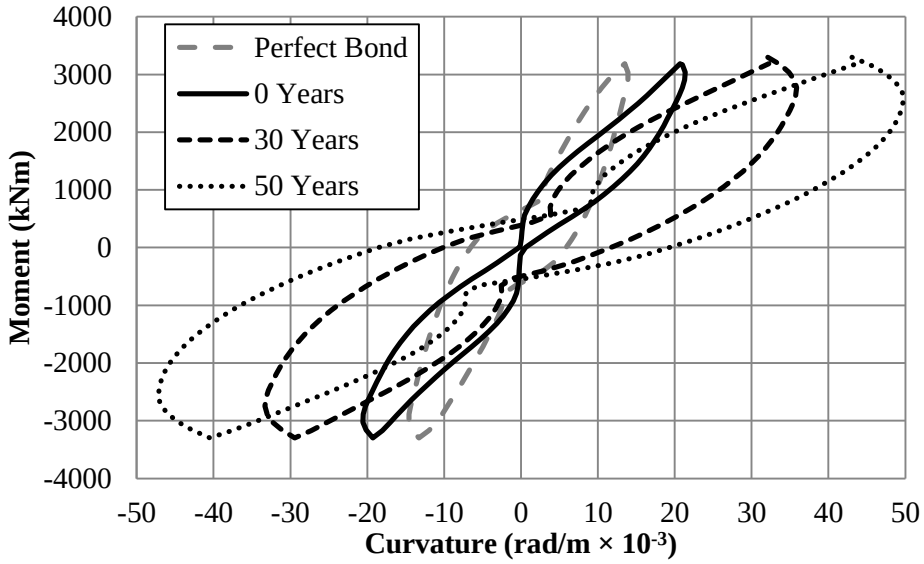

Figure 5-42: Comparison between hysteretic behaviour after two inelastic cycles for the New Brighton Pier model over 50 years of degradation.

5.4 Summary

Analyses showed that poorly confined reinforcing embedded in accordance with NZS3101:2004 was likely to fail through pull-out, as opposed to rupture, at as little as 8.5% corrosion. When adequate confinement was provided within analyses the level of corrosion require for pull-out failure rose to 18%. Results showed that impaired bonding due to loss of confinement has a greater impact on moment curvature behaviour than build-up of corrosion products on deteriorated columns.

From analysis on the doubly reinforced 400mm × 400mm column and the New Brighton Pier, reductions in stiffness associated with bond deterioration and its increase in strain penetration present two points of concern for seismic applications. The first of these is increased displacement demand, resulting reduced stability. Secondly, increased strain penetration effects energy dissipation, due to members yielding at larger curvatures.

Delay of yield not only reduces energy dissipation but impacts of member ductility. With spalling of concrete governing the ultimate section capacity in most cases analysed, ultimate curvature was largely unaffected by deterioration if spalling due to corrosion is ignored. Constant ultimate curvature combined with increased yield curvature due to strain penetration resulted in reduced section ductility. Ductility is a critical requirement for earthquake resilience, so reductions can have significant effects on seismic structural performance. In severe cases bar pull-out occurred, through pull-out only occurred when poor confinement was combined with moderate to high levels of corrosion.

Under cyclic loading, increases in deterioration were found to cause hysteretic energy dissipation to reduce through narrowing of the hysteretic loop. Reduced bond performance under reversing actions lead to strain penetration creating the equivalent of debonded conditions either side of the upper and

lower model interface resulting in pinching of the hysteretic curve. Cyclic analyses also displayed similar traits as their monotonic counterparts with reduced secant stiffness of roughly the same order displayed with increased deterioration.

5.5 Limitations

The 400mm × 400mm model was intended to solely show effects of bond deterioration on moment-curvature behaviour in a simplified concrete section. For this reason, a number of factors that would exist in a realistic representation of similarly dimensioned and deteriorated columns have been excluded. The first exclusion was effects of spalling due to corrosion. Spalling results in loss of cover concrete. Decreased section area in turn reduces section moment capacity due to removal of compression concrete. In addition to this, a lower neutral axis may induce brittle behaviour within the member.

Corrosion's most obvious effect is reduction in reinforcing cross-sectional area which was ignored for the 400mm × 400mm model. Reduction in area reduces strength and stiffness, though the magnitude of reduction is debated in literature (Cairns et al. 2005; Papadopoulos et al. 2007; Apostolopoulos 2008; Apostolopoulos et al. 2008; Apostolopoulos and Papadakis 2008). Conservatively all reinforcing used within the 400mm × 400mm model was assumed to have had unaffected mechanical properties.

Buckling of reinforcement in compression was assumed to not occur. In well confined regions, such as plastic hinge zones, buckling resistance through confinement is a key design parameters and so it would be expected that this assumption remains true. However, in unconfined models, buckling would be expected to be a common failure mechanism (Dhakal and Maekawa 2002).

In analyses it was assumed that reinforcement was detailed as to develop from both ends such that only at the interface it would be fully developed. Such regions do not exist in a real structure where reinforcement runs through plastic hinge regions and is anchored well outside them. This may have resulted in amplified reductions in stiffness within the multi-spring model

Modelling of likely degradation of the New Brighton Pier was based on a number of assumptions and factors taken from literature. Precise investigations into these factors through material testing of the Pier was not undertaken, this meant that many values were inferred from literature where investigations into similar materials were undertaken. Corrosion prediction is a highly variable process, dependent on numerous factors that, even when know precisely, may not produce an accurate prediction. The damage propagation model described within the case study was meant only as an indicative prediction of degradation. This can be highlighted by the use of 0.1mm cracking assumed when in some regions of the structure complete spalling was observed following the 2011 earthquake. Cracks are likely to increase in width as corrosion occurs, further accelerating deterioration. The

prediction also assumes that no maintenance is performed on the structure over the 50 year period which is highly unlikely.

The final limitation was associated with the distance between the rigid frame and fixed base. This was assumed to be 40 mm to maintain strain continuity between reinforcing and concrete. Also adjacent bond springs covered 20 mm from each side of the gap, providing complete bonding in the gap region. Curvature was determined by division of rigid frame rotation by the 40 mm gap used in the model. Issues arise when including bond-slip, which ranged from 0.4 mm to 2.9 mm at the loaded end. If a larger gap was used, the effect of slip would be reduced due bar strain being calculated over a longer length, thus when slippage occurred, strain reductions would be lessened. When combined with strain penetration, which ranged from 30 mm to 200mm, it can be seen that the gap portion of the strain penetrated length is substantial. A 40 mm gap was selected as it provided the correct bonding for the gap region when using 40 mm bond springs within the model. In addition to this, use of very small gaps resulted in computational errors which were unable to be overcome, even through use of small time-steps (0.00001 s) with large number of iterations per time-step (~25).

6 Conclusion

This thesis investigated the effects of bond deterioration due to corrosion on the seismic performance of reinforced concrete structures. Initially, an experimental investigation was used to develop a corrosion and confinement dependent bond-slip model. This was based on the results of 60 monotonic and cyclic pull-out tests of corroded reinforced concrete specimens, with corrosion levels ranging from 0% to 25% corrosion level, and steel confinement indices between $\Omega = 0.0$ and $\Omega = 0.071$. Multi-spring modelling of embedded reinforcing pull-out and of reinforced concrete foundation connection was performed at the full range of deterioration with allowance for bond slippage. Findings from this investigation are outlined in the following paragraphs.

The adopted electrochemical accelerated corrosion technique proved to be a suitable method of recreating bar deterioration within a reasonable timeframe. Discrepancies were observed between the electrochemically corroded products and those seen in natural corrosion, with electrochemically produced products being approximately 15% less expansive than naturally produced products. This is likely to have provided some discrepancies between reproduced radial pressures and equally corroded natural bars. This difference was assumed to be negligible though it will have had some minor influence on performance.

Corrosion was found to have a significant influence on the bonding performance of steel reinforcing in concrete. Under monotonic loading a 50% reduction in bond rupture strength was observed at a corrosion level of 11%, and continued to decrease following an inverse exponential trend. When the level of corrosion reached 12%, a change in the failure mechanism from rupture, to a gradual sliding was observed that was accompanied by reduced stiffness at failure and loss of a clear bond rupture location. Sliding failure was attributed to loss of mechanical interlock due to removal or smoothing of reinforcement ribs, as well as damage to concrete surrounding reinforcement due to expansive pressures induced by corrosion products. Initial stiffness was largely unaffected by corrosion. At very high levels of corrosion (>20%) there was an appreciable reduction in stiffness where it was believed that build-up of corrosion products provided a lubricating effect. No clear relationship was found between corrosion level and rupture slip which was attributed to non-uniform and erratic deterioration. The slip at which monotonic behaviour become purely frictional was found to decrease with increasing levels of corrosion.

Cyclic loading was found to significantly reduce maximum bond stresses due to damage induced by repeated loading. Reduction of in cyclic bond capacity was found to increase further with the inclusion of corrosion. These findings highlight the importance of accounting for cyclic degradation when modelling corroded bond subjected to seismic loading. Similar behaviour was observed for sliding stresses, with reductions occurring with continued cycling. Initial sliding stresses under cyclic loading

were found to be dependent on maximum slip and level of corrosion. Initial sliding stresses were found to be related to the ultimate frictional stress found from monotonic testing which increased significantly under low to moderate levels of corrosion (3% to 13%). Reduction of these stresses due to cycling was far more rapid with increased corrosion and declined to close to zero after several cycles in highly corroded (>15%) specimens.

Reduced confinement at low levels of corrosion was found to markedly increase splitting cracks within specimens prior to, and after testing. In specimens with low or no confining steel, these cracks ranged up to 4 mm in width, even at low corrosion levels (1% to 2%). Large longitudinal cracks were found to adversely affect bond performance through reduction of initial stiffness and loss of a defined bond rupture location. Rupture of unconfined or poorly confined specimens was abrupt if concrete was still intact, with an instantaneous loss of strength accompanied by a slip of approximately 1.0 mm. Beyond rupture, behaviour was similar to that seen in specimens split prior to testing due to internal corrosion pressure.

Results from sixty experimental tests were used to create a corrosion and confinement dependent cyclic bond model. The model followed a similar form to the model proposed by Eligehausen (1983) with some basic adjustments and allowances for altered performance at differing levels of corrosion and confinement. Relationships between corrosion level, level of confinement, and monotonic and cyclic behaviour were developed. When modelling cyclic bond performance, dimensionless energy was used as a key parameter in determining bond damage. Cyclic bond behaviour differed substantially from monotonic behaviour. Damage rates, even when non-dimensionalised, varied depending on the level of corrosion and confinement, with corrosion increasing stress in some cases, such as in cyclic sliding stresses. From this process, a model for well-confined bars and corrosion level between 0% and 20% was developed. This was combined with confinement-dependent model parameters to produce a corrosion and confinement-dependent bond-slip model.

The developed bond-slip model was first implemented in determining cyclic pull-out behaviour of reinforcing detailed to NZS3101 bond development conditions. Reinforcing in the model was subjected to ten inelastic cycles and then loaded until rupture of reinforcing or bond. Bond rupture under fully confined conditions did not occur until bond deterioration reached a corrosion level of 18%. However, under unconfined bonding conditions bond pull-out before bar rupture occurred at corrosion levels as low as 8.5%. In addition to the change in failure mechanism, significant increases in strain penetration were observed. Brittle post-rupture behaviour, displayed under poorly confined conditions, had greater influence on increased strain penetration and diminished reinforcement development, than level of corrosion.

Moment-curvature behaviour was assessed using multi-spring models of reinforced concrete sections, allowing for degraded bond-slip performance along the development length of reinforcement. Bond

deterioration was found to have two primary effects; firstly, stiffness of the section was reduced as deterioration increased, secondly, reinforcement strains at ultimate curvature were significantly reduced. Stiffness reduction was attributed to loss of strain compatibility due to strain penetration and bond slippage. Strain penetration was also responsible for reductions in reinforcement strains at ultimate curvature. As strain-penetrated length increased; increased geometric elongation was required to reach the ultimate strain of reinforcing. Concrete spalling governed the section's maximum ultimate curvature, meaning that decreased strain was experienced by reinforcement with the increased strain penetration produced due to increased corrosion level. Some multi-spring models displayed recentring behaviour. Recentring occurred in cases where yielding of steel was insufficient to overcome moments induced due to axial loads, primarily when curvature remained in the elastic region. Moreover, recentring behaviour was prevalent when low bond sliding stresses occurred in strain penetrated regions, generally associated with low levels of confinement. These low bond sliding stresses were generally associated with poorly confined conditions. Delayed yield due to increased strain penetration combined with concrete spalling determining ultimate curvature resulted in severe reductions in section ductility. In extreme cases, concrete spalling occurred prior to yield of reinforcement resulting in brittle failure of the section. Ductile behaviour is crucial in earthquake resistant design and reduced ductility can have serious implications on seismic structural performance.

It is anticipated that results from this investigation will allow for better prediction and assessment of the seismic performance of reinforced concrete structures throughout their lifetime. Bond deterioration due to corrosion was found to have significant impacts on structural behaviour, primarily affecting structural stiffness and ductility. These aspects are integral in producing stable, robust structures that are capable of withstanding the punishing requirements placed on them by earthquakes.

6.1 Future Research

Further investigation into corrosion effects on seismic performance is currently in progress at the University of Canterbury. An investigation is underway looking at Discrete Element Modelling (DEM) (Hentz et al. 2004)of corrosion-affected bond based on the experimental results from this thesis.

Further experimental validation of the proposed cyclic bond-slip model would be desirable, especially into the 8%-15% corrosion level where only a hand full of specimens were able to be produced. In addition to this, corroded bond performance in poorly confined condition was only assessed at low levels of deterioration.

Buckling of reinforcement under axial and flexural loads is a common failure mechanism in poorly detailed regions. Deterioration of transverse steel has been shown in literature to be more aggressive than longitudinal bars (Saito et al. 2007). Loss or reduction of confinement results in increased

buckling length for longitudinal reinforcement, heightening bar buckling risk, which would also be increased by reduced section properties for the deteriorated longitudinal reinforcement. Effects of premature bar buckling would likely affect flexural ductility and axial capacity of reinforced concrete members.

Numerical modelling, particularly Finite Element Modelling (FEM), of corroded plastic hinge regions is essential in verifying results found using multi-spring models. Further investigation into the influence of section shape on diminished bond behaviour could be undertaken.

In addition to plastic hinge regions, FEM modelling of exposed beam-column joints in frame structures may also provide areas for further investigation. Combination of plastic hinge region modelling and beam-column joint modelling could be applied to determine effects of non-uniform degradation on global performance. This occurs in situations where one side of a building is seaward and the other is protected. Reduced stiffness associated with bond deterioration would introduce torsional behaviour. Additional torsional behaviour has the potential to impact global behaviour in a similar way to that shown by Berto et al. (2009). Studies into the global structural performance may reveal an entire change in the deformation mechanism, such as that found by Biondini et al. (2011) with particular importance focused on bridges and wharf structures which are highly susceptible to degradation through corrosion.

References

Al-Hammoud, R., K. Soudki, et al. (2010). "Bond analysis of corroded reinforced concrete beams under monotonic and fatigue loads." Cement and Concrete Composites **32**(3): 194-203.

Almusallam, A. A. (2001). "Effect of degree of corrosion on the properties of reinforcing steel bars." Construction and Building Materials **15**(8): 361-368.

Almusallam, A. A., A. S. Al-Gahtani, et al. (1996). "Effect of reinforcement corrosion on bond strength." Construction and Building Materials **10**(2): 123-129.

Apostolopoulos, C. A. (2008). "The effect of ribs on the mechanical behavior of corroded reinforcing steel bars S500s under low-cycle fatigue." Materials and Structures **41**(5): 991-999.

Apostolopoulos, C. A., D. Michalopoulos, et al. (2008). "The corrosion effects on the structural integrity of reinforcing steel." Journal of Materials Engineering and Performance **17**(4): 506-516.

Apostolopoulos, C. A. and V. G. Papadakis (2008). "Consequences of steel corrosion on the ductility properties of reinforcement bar." Construction and Building Materials **22**(12): 2316-2324.

Ashtiani, M. S., R. Dhakal, et al. (2011). Bond Properties of Reinforcement in High-Strength Self-Compacting Concrete. 9th Symposium on High Performance Concrete. Rotorua, New Zealand.

ASTM-C78-09 (2009). ASTM C78 - 09. Standard Test Method for Flexural Strength of Concrete (Using Simple Beam with Third-Point Loading). , American Society for Testing and Materials.

ASTM-C469-02e1 (2002). ASTM C469 - 02e1 Standard Test Method for Static Modulus of Elasticity and Poisson's Ratio of Concrete in Compression, American Society for Testing and Materials.

ASTM-C873/C873M-04el (2004). ASTM C873 / C873M -04el. Standard Test Method for Compressive Strength of Concrete Cylinders Cast in Place in Cylindrical Moulds, American Society for Testing and Materials.

Au, E. (2010). The mechanics and design of a non-tearing floor connection using slotted reinforced concrete beams. Department of Civil and Natural Resources Engineering. Christchurch, University of Canterbury. **Master of Engineering**.

Bentz, E. (2001). Response-2000. Toronto, Canada, University of Toronto, Department of Civil Engineering**:** Reinforced Concrete Sectional Analysis using the Modified Compression Field Theory.

Berto, L., R. Vitaliani, et al. (2009). "Seismic assessment of existing RC structures affected by degradation phenomena." Structural Safety **31**(4): 284-297.

Bhargava, K., A. K. Ghosh, et al. (2007). "Corrosion-induced bond strength degradation in reinforced concrete--Analytical and empirical models." Nuclear Engineering and Design **237**(11): 1140-1157.

Biondini, F., F. Bontempi, et al. (2004). "Cellular Automata Approach to Durability Analysis of Concrete Structures in Aggressive Environments." Journal of Structural Engineering **130**(11).

Biondini, F., A. Palermo, et al. (2011). "Seismic performance of concrete structures exposed to corrosion: Case studies of low-rise precast buildings." Structure and Infrastructure Engineering **7**(1-2): 109-119.

Cabrera, J. G. (1996). "Deterioration of concrete due to reinforcement steel corrosion." Cement and Concrete Composites **18**(1): 47-59.

Cairns, J., Y. Du, et al. (2008). "Structural performance of corrosion-damaged concrete beams." Magazine of Concrete Research **60**(5): 359-370.

Cairns, J., G. A. Plizzari, et al. (2005). "Mechanical properties of corrosion-damaged reinforcement." Aci Materials Journal **102**(4): 256-264.

Carr, A. J. (2010a). Ruaumoko 3D: Manual - Appendix B. **3**.

Carr, A. J. (2010b). Ruaumoko Manual, Volume 3: User Manual for the 3:Dimensional Version, Ruaumoko3D.

CCC, C. C. C. (1995). Construction drawings for Christchurch Pier: D.4906.

Chung, L., S. H. Cho, et al. (2004). "Correction factor suggestion for ACI development length provisions based on flexural testing of RC slabs with various levels of corroded reinforcing bars." Engineering Structures **26**(8): 1013-1026.

Chung, L., J.-H. Jay Kim, et al. (2008). "Bond strength prediction for reinforced concrete members with highly corroded reinforcing bars." Cement and Concrete Composites **30**(7): 603-611.

Coronelli, D. and M. G. Mulas (2001). "Local-global approach in the seismic analysis of R/C frames including bond slip effects." Engineering Structures **23**(8): 911-925.

Costa, A. and J. Appleton (2002). "Case studies of concrete deterioration in a marine environment in Portugal." Cement and Concrete Composites **24**(1): 169-179.

Darmawan, M. S. (2010). "Pitting corrosion model for reinforced concrete structures in a chloride environment." Magazine of Concrete Research **62**(2).

Dhakal, R. P. and K. Maekawa (2002). "Path-dependent cyclic stress-strain relationship of reinforcing bar including buckling. ." Engineering Structures **24**: 1383-1396.

Dhir, R. K., M. A. K. El-Mohr, et al. (1996). "Chloride binding in GGBS concrete." Cement and Concrete Research **26**(12): 1767-1773.

Djerbi, A., S. Bonnet, et al. (2008). "Influence of traversing crack on chloride diffusion into concrete." Cement and Concrete Research **38**(6): 877-883.

Du, Y. G., L. A. Clarkt, et al. (2005). "Effect of corrosion on ductility of reinforcing bars." Magazine of Concrete Research **57**(7): 407-419.

Eligehausen, R., E. P. Popov, et al. (1983). Local bonds stress-slip relationships of deformed bars under generalized excitations. Earthquake Engineering Research Centre. Berkeley, University of California, Berkley. **83:** 169.

Fang, C. (2006a). Bond-slip behavior of corroded reinforcing steel in concrete bridges, Porto, Portugal, Taylor and Francis/Balkema.

Fang, C. (2006b). "Bond strength of corroded reinforcement under cyclic loading." Magazine of Concrete Research **58**(7): 437-446.

Fang, C., K. Gylltoft, et al. (2006a). "Effect of corrosion on bond in reinforced concrete under cyclic loading." Cement and Concrete Research **36**(3): 548-555.

Fang, C., K. Lundgren, et al. (2004). "Corrosion influence on bond in reinforced concrete." Cement and Concrete Research **34**(11): 2159-2167.

Fang, C., K. Lundgren, et al. (2006b). "Bond behaviour of corroded reinforcing steel bars in concrete." Cement and Concrete Research **36**(10): 1931-1938.

Filippou, F. C., E. V. Popov, et al. (1983). "Effects of Bond Deterioration on Hysteretic Behaviour of Reinforced Concrete Joints." UCB/EERC **92/19**: 191.

Hansson, C. M., A. Poursaee, et al. (2006). "Macrocell and microcell corrosion of steel in ordinary Portland cement and high performance concretes." Cement and Concrete Research **36**(11): 2098-2102.

Hentz, S., F. V. Donzé, et al. (2004). "Discrete element modelling of concrete submitted to dynamic loading at high strain rates." Computers & Structures **82**(29–30): 2509-2524.

Kivell, A., A. Palermo, et al. (2011a). Effects of Bond Deterioration Due to Corrosion in Reinforced Concrete. Ninth Pacific Conference on Earthquake Engineering. Auckland, New Zealand.

Kivell, A., A. Palermo, et al. (2011b). Monotonic and Cyclic Bond Testing of Heavily Corroded Reinforcing High Strength Concrete. 9th International Symposium on High Performance Concrete Rotorua, New Zealand.

Kwak, H.-G. and S.-P. Kim (2001). "Bond–slip behavior under monotonic uniaxial loads." Engineering Structures **23**(3): 298-309.

Lee, C., J. F. Bonacci, et al. (2000). "Accelerated corrosion and repair of reinforced concrete columns using carbon fibre reinforced polymer sheets." Canadian Journal of Civil Engineering **27**(5): 941-948.

Lee, H.-S., T. Noguchi, et al. (2002). "Evaluation of the bond properties between concrete and reinforcement as a function of the degree of reinforcement corrosion." Cement and Concrete Research **32**(8): 1313-1318.

Leung, H. K. (2011). Discrete Element Modelling of Corroded Bond. Christchurch, New Zealand, University of Canterbury.

Lundgren, K. (2007). "Effect of corrosion ont the bond between steel and concrete: an overview." Magazine of Concrete Research **59**(6): 447-461.

Mander, J. B., M. J. N. Priestley, et al. (1988). "Theoretical stress-strain model for confined concrete." Journal of Structural Engineering **114**(8): 1804-1826.

Melchers, R. E., C. Q. Li, et al. (2008). "Probabilistic modeling of structural deterioration of reinforced concrete beams under saline environment corrosion." Structural Safety **30**(5): 447-460.

Mohammed, T. U., N. Otsuki, et al. (2003). "Corrosion of Steel Bars in Cracked Concrete under Marine Environment." Journal of Materials in Civil Engineering **15**(5): 460-469.

Mohammed, T. U., T. Yamaji, et al. (2002). "Chloride diffusion, microstructure, and mineralogy of concrete after 15 years of exposure in tidal environment." Aci Materials Journal **99**(3): 256-263.

O'Flaherty, F. J., P. S. Mangat, et al. (2010). Influence of steel reinforcement corrosion on the stiffness of simply supported concrete beams. Bridge Maintenance, Safety, Managemnet and Life-Cycle Optimization. Frangopol, Sauae and Kusko.

Oliveira, R. S., M. A. Ramalho, et al. (2008). "A layered finite element for reinforced concrete beams with bond–slip effects." Cement and Concrete Composites **30**(3): 245-252.

Ou, Y.-C., L.-L. Tsai, et al. (2010). Cyclic behaviour of reinforced concrete beams with corroded reinforcing bars. Life-cycle of Civil Engineering Systems. Chen, Frangopol and Ang. Taipei, Taiwan.

Palermo, A., L. Wotherspoon, et al. (2012). "Seismic performance of concrete bridges during Canterbury earthquakes." Structural Concrete **13**(1): 14-26.

Palermo, A., L. Wotherspoon, et al. (2011). "Lessons Learnt from 2011 Christchurch Earthquakes: Analysis and Assessment of Bridges." Bulletin of the New Zealand Society for Earthquake Engineering **44**(4).

Papadopoulos, M. P., C. A. Apostolopoulos, et al. (2007). "Effect of salt spray corrosion exposure on the mechanical performance of different technical class reinforcing steel bars." Materials & Design **28**(8): 2318-2328.

Park, R. and T. Paulay (1975). Reinforced Concrete Structures, John Wiley & Sons.

Paulay, T. and M. J. N. Priestley (1992). Seismic Design of Reinforced Concrete and Masonry Buildings, John Wiley & Sons.

Plizzari, G. A., M. A. Deldossi, et al. (1998). "Transverse reinforcemnet effects on anchored deformed bars." Magazine of Concrete Research **50**(2): 161-177.

Ragueneau, F., N. Dominguez, et al. (2006). "Thermodynamic-based interface model for cohesive brittle materials: Application to bond slip in RC structures." Computer Methods in Applied Mechanics and Engineering **195**(52): 7249-7263.

Raupach, M. (1996). "Chloride-induced macrocell corrosion of steel in concrete - theoretical background and practical consequences." Construction and Building Materials **10**(5): 329-338.

Reddy, B. (2001). Influence of the steel–concrete interface on the chloride threshold level. London, University of London. **PhD Thesis**.

Rehm, G. (1968). "The Basic Pricipals of Bond Between Steel and Concrete." Cement and Concrete Association **134**: 66.

Rinaldi, Z., S. Imperatore, et al. (2010). "Experimental evaluation of the flexural behavior of corroded P/C beams." Construction and Building Materials.

Saito, Y., E. M. Oyado, et al. (2007). Structural Performance of Corroded RC Column under Seismic Load. Protect 2007. Whistler Canada.

Sánchez, P. J., A. E. Huespe, et al. (2010). "Mesoscopic model to simulate the mechanical behavior of reinforced concrete members affected by corrosion." International Journal of Solids and Structures **47**(5): 559-570.

Scott, A. and M. G. Alexander (2007). "The influence of binder type, cracking and cover on corrosion rates of steel in chloridecontaminated concrete." Magazine of Concrete Research **59**(7): 495-505.

Semchenkov, A., V. Meshkov, et al. (2009). "Bond to concrete action of reinforcing bars with different deformation patterns." Structural Concrete **10**(4): 203-209.

Spieth, H. A., A. J. Carr, et al. (2004). Modelling of post-tensioned precast reinforced concrete frame structure with rocking beam-solumn connections. NZSEE Conference. Rotorua, New Zealand.

Standards New Zealand (2006). NZS3101: Reinforced Concrete Construction. Wellington, New Zealand, Standards New Zealand.

Stanish, K., R. D. Hooton, et al. (1999). "Corrosion effects on bond stength in reinforced concrete." ACI Structural Journal **96**(6): 915-921.

Tang, D. L., T. C. K. Molyneaux, et al. (2007). The influence of chloride induced corrosion cracks on the strength of reinforced concrete. Progress in Mechnaics of Structures and Materials, Christchurch, New Zealand, Taylor & Francis Group, London.

Tsai, W.-P., H.-J. Chen, et al. (2008). The accelerated method for estimating corrosion of reinforced concrete structure in seawater, Vancouver, BC, Canada, American Society of Civil Engineers.

Val, D. V. and P. A. Trapper (2008). "Probabilistic evaluation of initiation time of chloride-induced corrosion." Reliability Engineering and System Safety **93**(3): 364-372.

Verderame, G. M., P. Ricci, et al. (2009). "Cyclic bond behaviour of plain bars. Part I: Experimental investigation." Construction and Building Materials **23**(12): 3499-3511.

Vu, K. A. T. and M. G. Stewart (2000). "Structural reliability of concrete bridges including improved chloride-induced corrosion models." Structural Safety **22**(4): 313-333.

Weizhong, G., M. Raupach, et al. (2010). " Corrosion products and their volume factor created by corrosion of steel in concrete (Korrosionsprodukte und Deren Volumenfaktor bei der Korrosion von Stahl in Beton)." Beton- und Stahlbetonbau **9**(105).

Yamakawa, T. (1998). Seismic Behaviour of R/C Columns Damaged Under Exposure test. Concrete Under Severe Conditions 2: Environment and Loading. O. E. Gjorv, K. Sakai and N. Banthia. Tromso, Norway.

Yankelevsky, D. Z. (1985). "Analytical model for bond-slip behavior under monotonic loading." Building and Environment **20**(3): 163-168.

Yingshu, Y., J. Yongsheng, et al. (2007). "Comparison of two accelerated corrosion techniques for concrete structures." ACI Structural Journal **104**(3): 344-347.

Zhang, W., X. Wang, et al. (2006). "Comparative study on structural performance of reinforced concrete beams subjected to natural corrosion and accelerated corrosion." Dongnan Daxue Xuebao (Ziran Kexue Ban)/Journal of Southeast University (Natural Science Edition) **36**(SUPPL. 2): 139-144.

Zhao, Y., H. Ren, et al. (2011). "Composition and expansion coefficient of rust based on X-ray diffraction and thermal analysis." Corrosion Science **53**: 1646-1658.

Appendix A: Steel Reinforcement Testing Results

PACIFIC STEEL GROUP

CERTIFICATE OF TEST

PACIFIC STEEL
PO Box 22 201, Otahuhu
Auckland
New Zealand

Ph: 64 9 276 1849
Fax: 64 9 276 1947
www.steelreinforcing.co.nz
A FLETCHER BUILDING LTD COMPANY

Customer Number:	317500
Customer Name:	FENWICK REINFORCING LTD
Delivery Address:	76 MAGDALA PLACE CHRISTCHURCH
Cast Number:	69668-02
Specification:	AS/NZS 4671 GRADE 500
Product:	ROUND M 20 SEISMIC 500 DEF 10M
Method of Manufacture:	MA 500
Certificate Number:	366484
Issue Date:	09/02/2011

Chemical Analysis (% by mass)

C (%)	Mn (%)	Sl (%)	S (%)	P (%)	Ni (%)	Cr (%)	Mo (%)	Cu (%)	Sn (%)	V (%)	Ceq (%)
0.18	1.32	0.38	0.027	0.030	0.08	0.15	0.018	0.26	0.037	0.086	0.48

Mechanical Tests

Mass/m (Kg/m)	Yield Strength Re (MPa)	Ultimate:Yield Rm/Re	Uniform Elong. Agt(%)	Bend Test
2.445	555	1.20	12.6	Passed
2.450	575	1.22	10.6	Passed
2.450	584	1.20	12.9	Passed

Geometric Properties

Rib Height (h) (mm)	Σ Gap (mm)	Longitud. Sp (c) (mm)	Proj Rib Area (fr)	Mass/m (Kg/m)
1.150	8.500	12.700	0.078	2.450

We certify that the above information is in accordance with the records of the company and conforms to the specifications as stated.

Pacific Steel Authorised Signatory:

Patrick Scanlon
Quality Manager

CERTIFICATE OF TEST

PACIFIC STEEL GROUP

PACIFIC STEEL
PO Box 22 201, Otahuhu
Auckland
New Zealand

Ph: 64 9 276 1849
Fax: 64 9 276 1947
www.steelreinforcing.co.nz
A FLETCHER BUILDING LTD COMPANY

Customer Number:	317500
Customer Name:	FENWICK REINFORCING LTD
Delivery Address:	76 MAGDALA PLACE CHRISTCHURCH
Cast Number:	68689-03
Specification:	NZS 3402:89 GRADE 300
Product:	ROUND S 6 GRADE300 PL 6M
Method of Manufacture:	G300
Certificate Number:	363095
Issue Date:	06/11/2010

Chemical Analysis (% by mass)

C (%)	Mn (%)	Si (%)	S (%)	P (%)	Ni (%)	Cr (%)	Mo (%)	Cu (%)	Sn (%)	V (%)	Ceq (%)
0.16	0.54	0.15	0.022	0.016	0.07	0.06	0.004	0.27	0.032	0.002	0.29

Mechanical Tests

Yield Strength Re (MPa)	Uniform Elong. Agt(%)	Bend Test
389	13	Passed

Geometric Properties

We certify that the above information is in accordance with the records of the company and conforms to the specifications as stated.

Pacific Steel Authorised Signatory:

Patrick Scanlon
Quality Manager

Appendix B: Experimental Results - Monotonic Testing, 6mm Confinement

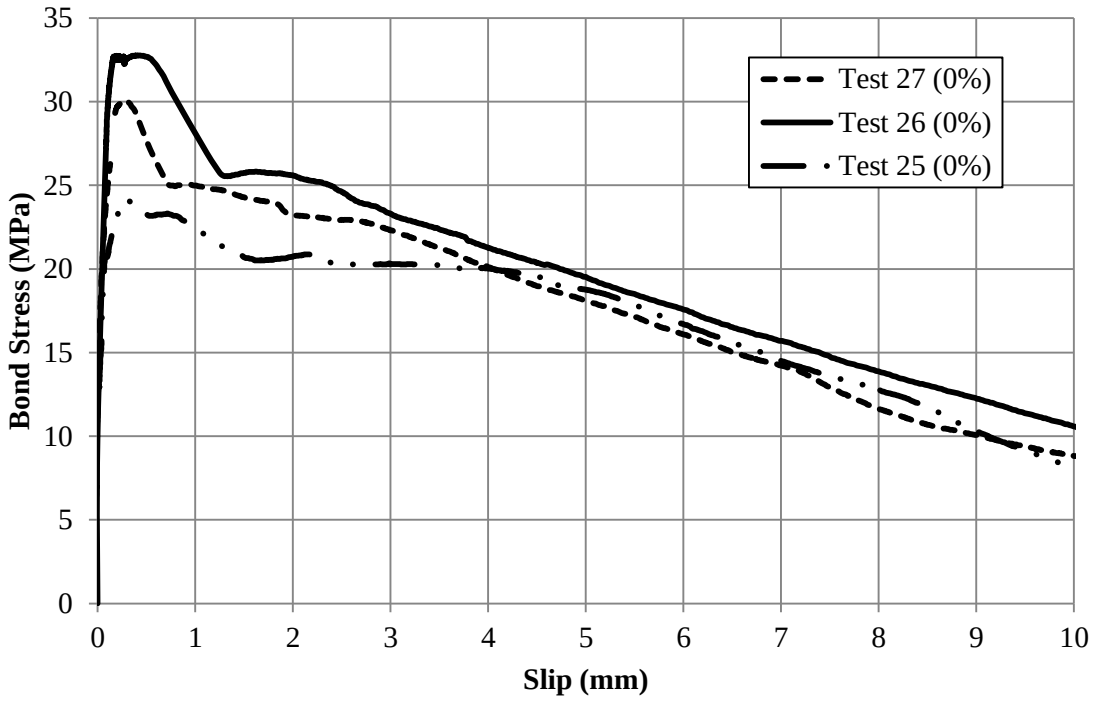

Figure B-0-1: Monotonic Pullout 0% corrosion 6 mm confinement

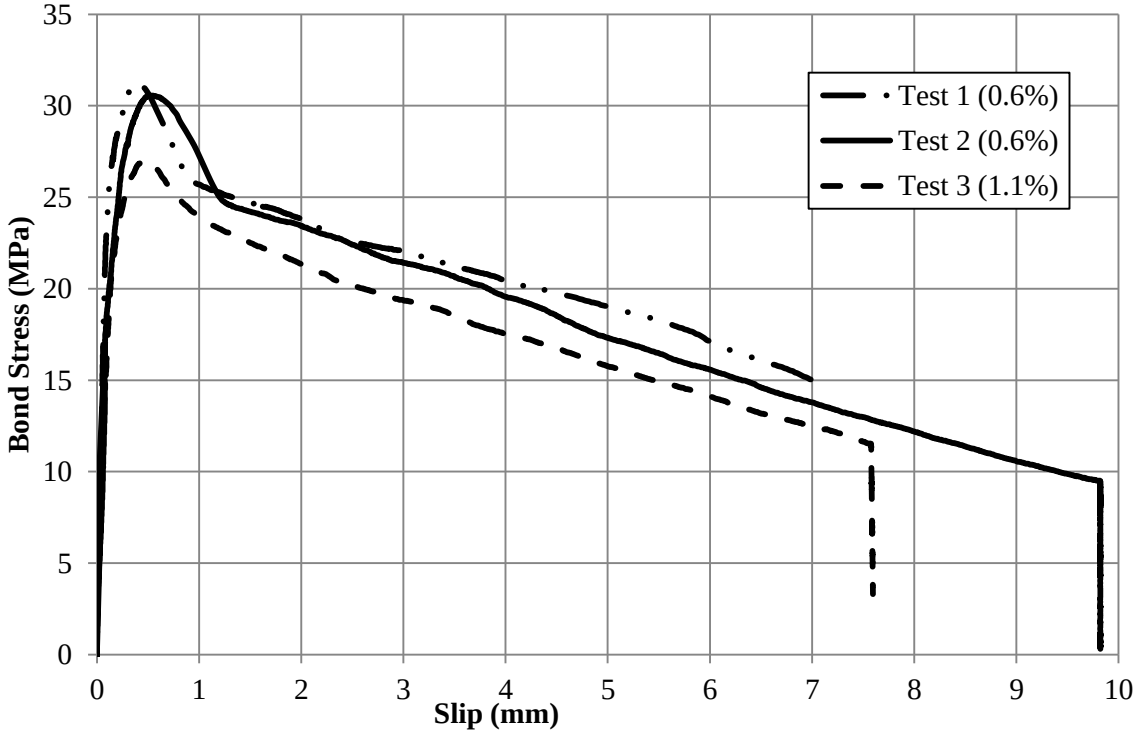

Figure B-0-2: Monotonic Pullout, 1% Corrosion, 6 mm Confinement

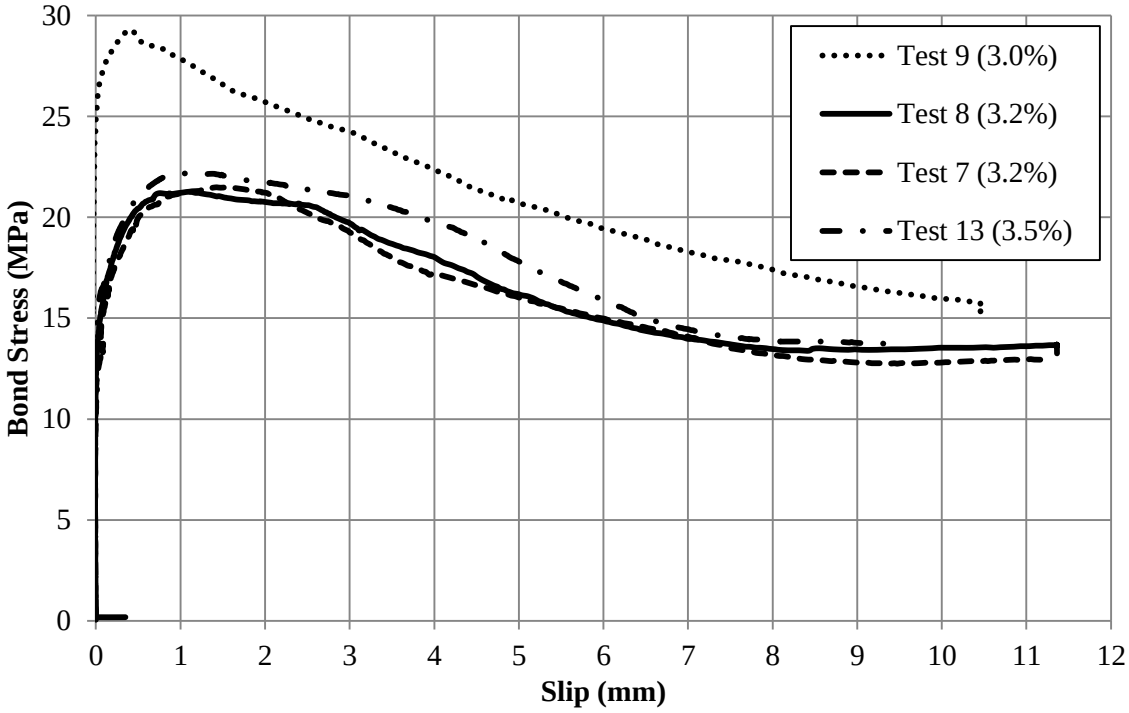

Figure B-0-3: Monotonic pullout, 3% Corrosion, 6 mm confinement

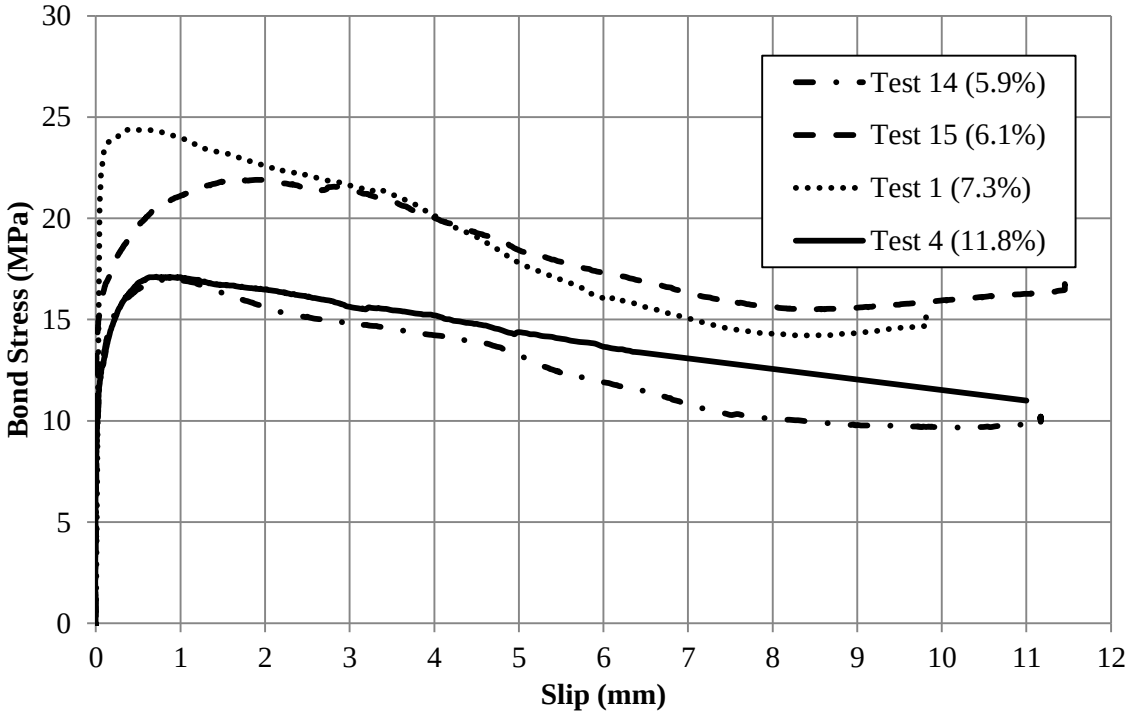

Figure B-0-4: Monotonic pullout, 6%-12% Corrosion, 6 mm confinement

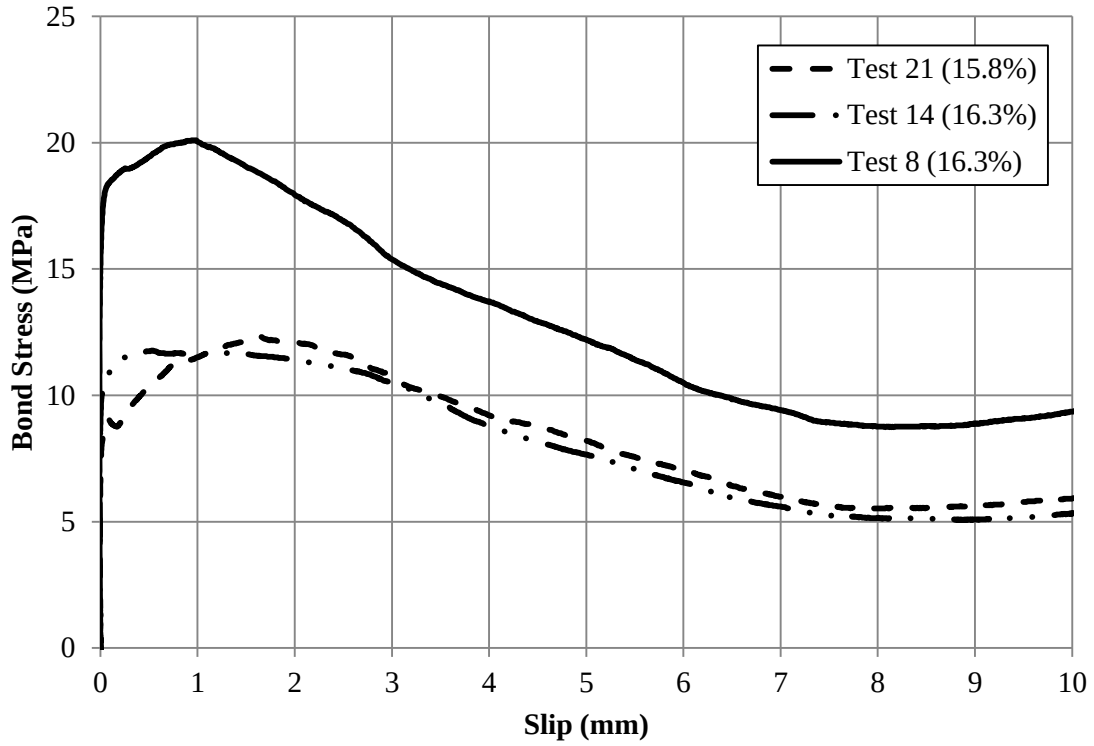

Figure B-0-5: Monotonic pullout, 15% Corrosion, 6 mm confinement

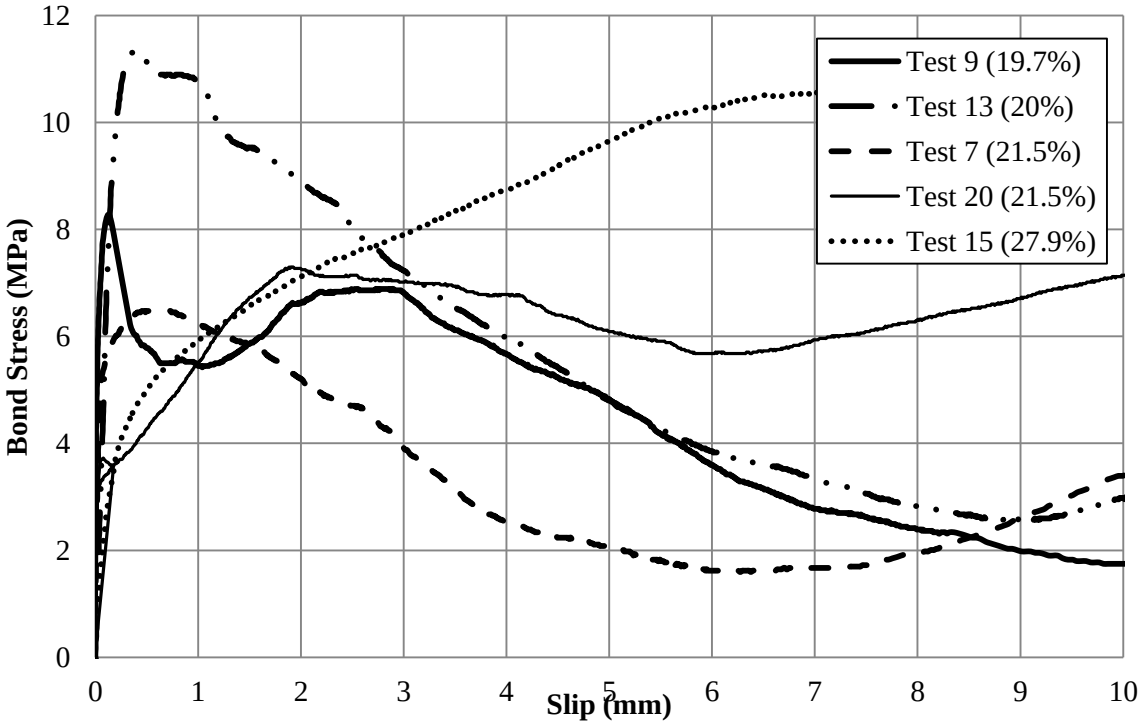

Figure B-0-6: Monotonic pullout, 20% corrosion and greater, 6 mm confinement

Appendix C: Experimental Results - Cyclic Testing, 6mm confinement

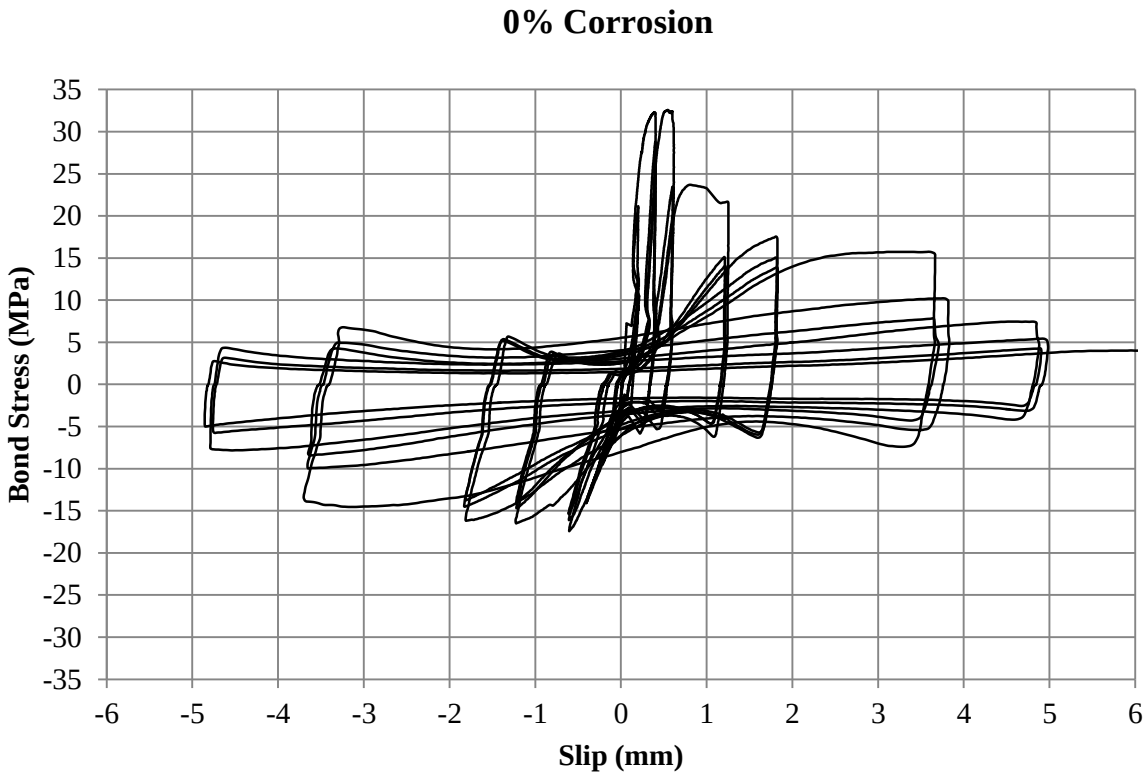

Figure C-0-1: Test 28 - Cyclic pullout, 0% corrosion, 6 mm confinement

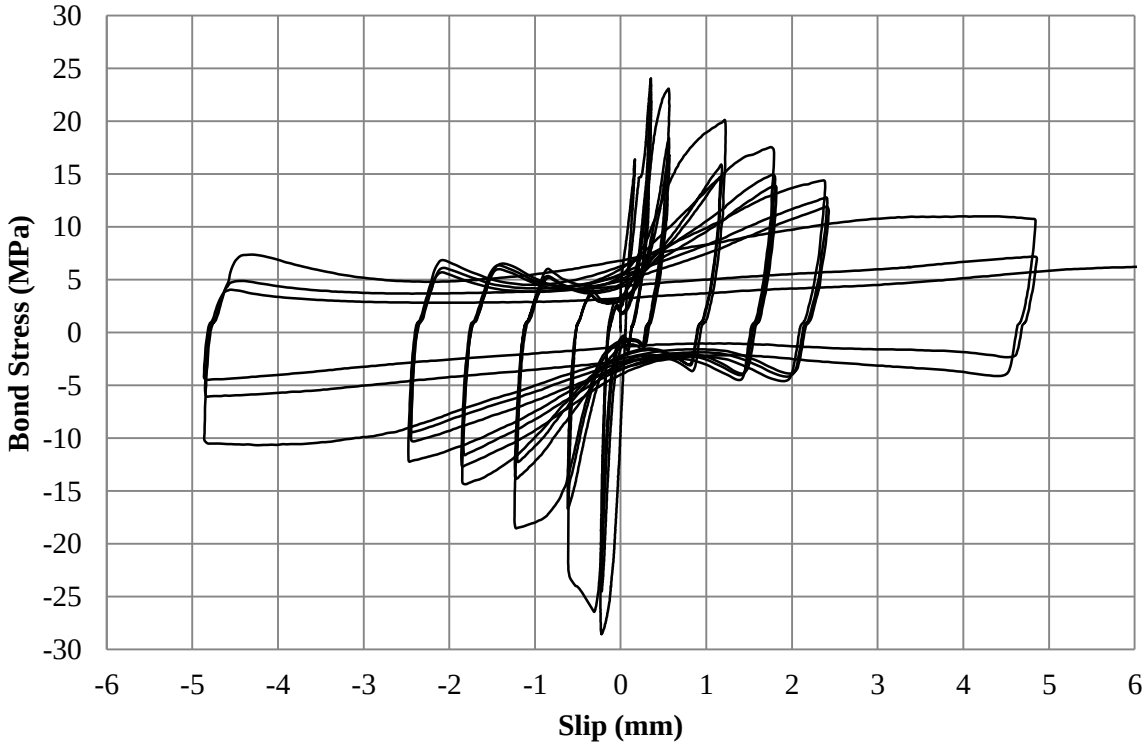

Figure C-0-2: Test 29- Cyclic pullout, 0% corrosion, 6 mm confinement

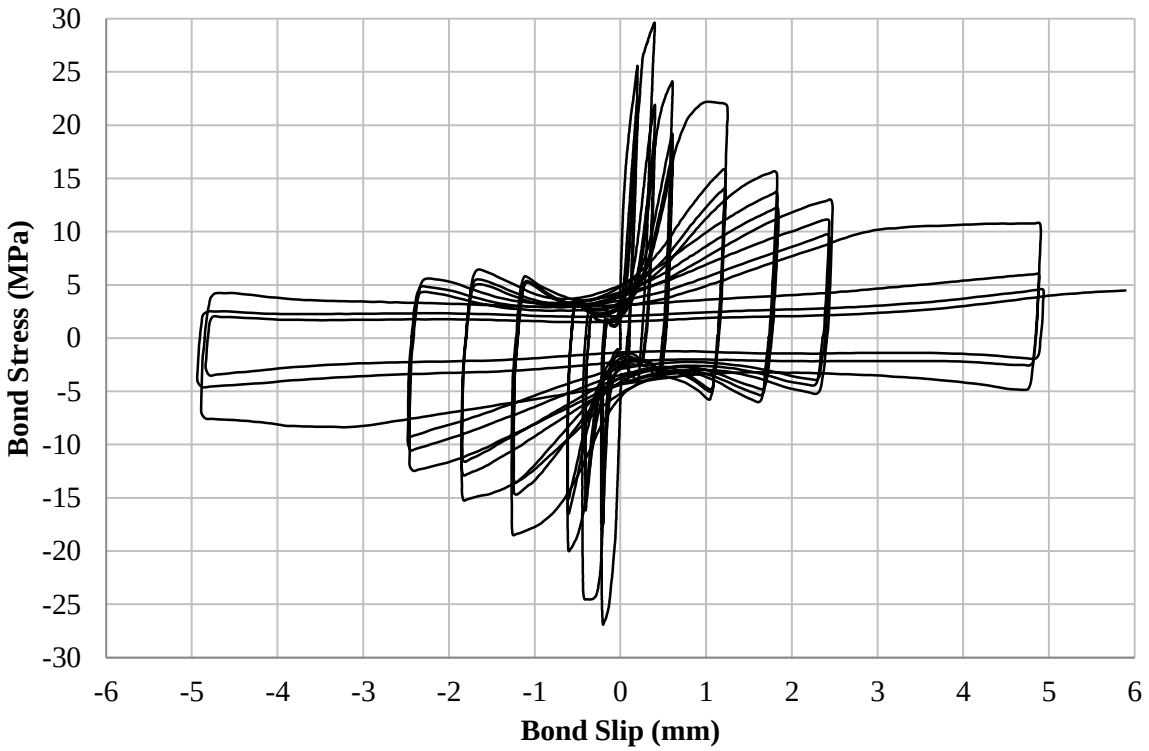

Figure C-0-3: Test 30 -- Cyclic pullout, 0% corrosion, 6 mm confinement

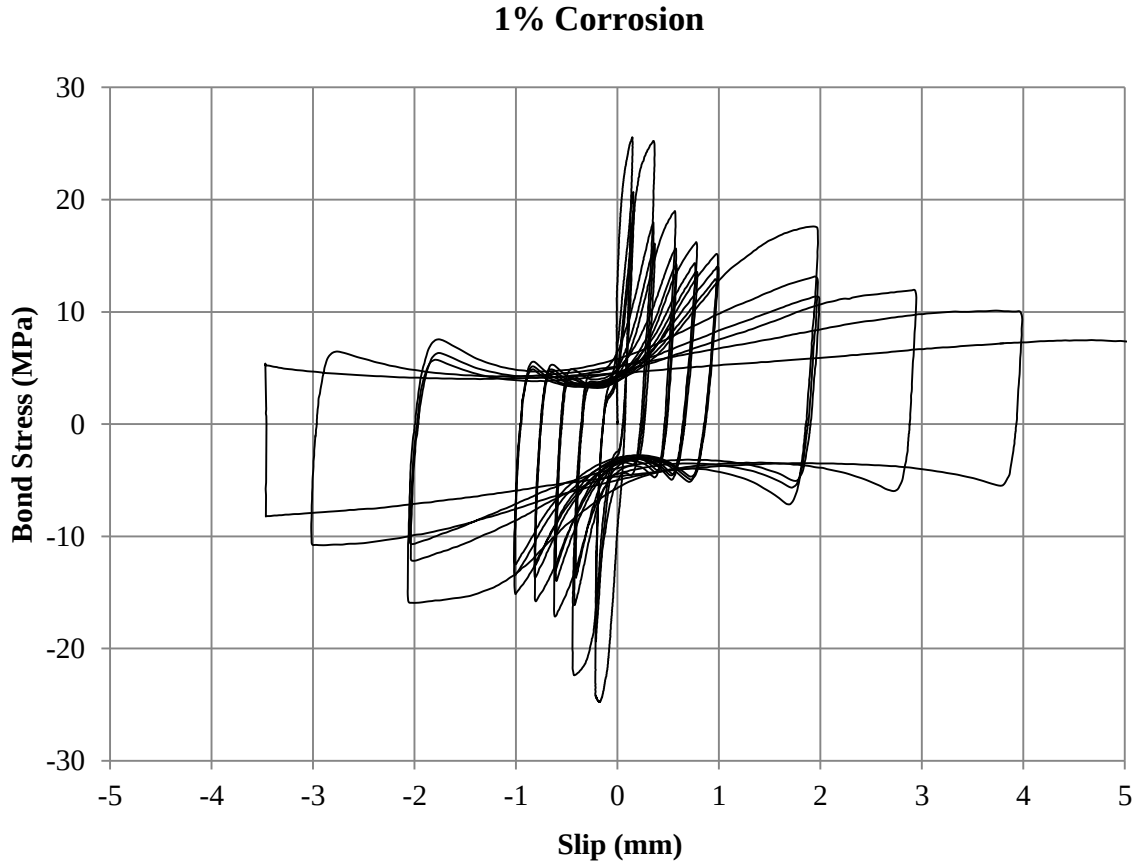

Figure C-0-4: Test 4- Cyclic pullout, 0.5% corrosion, 6mm Confinement

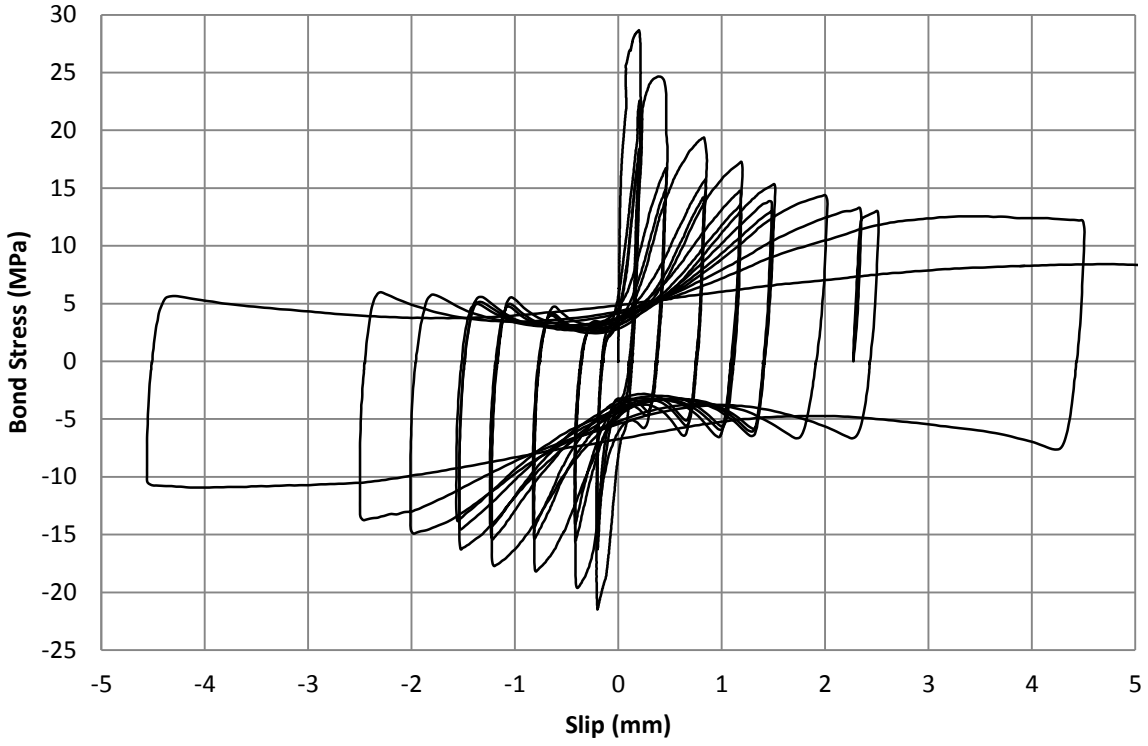

Figure C-0-5: Test 6- Cyclic pullout, 0.6% corrosion, 6 mm confinement

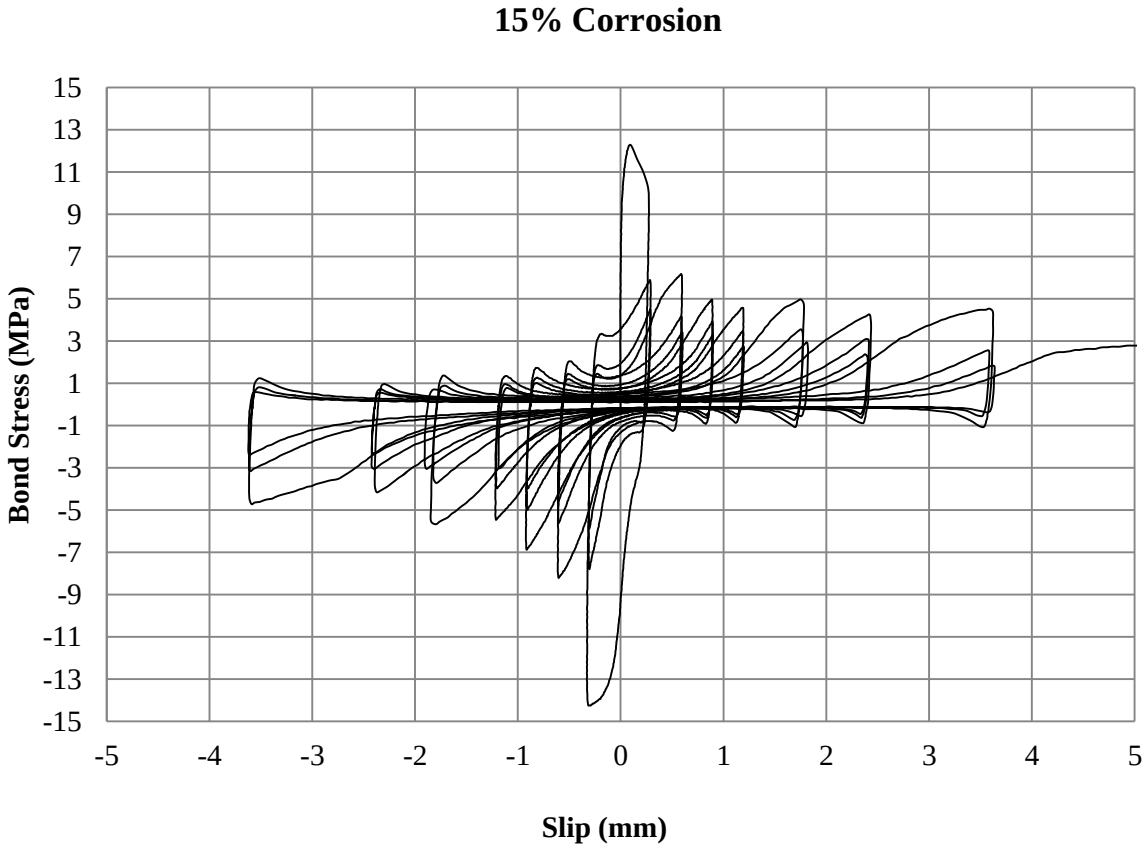

Figure C-0-6: Test 22- Cyclic pullout, 14.6% corrosion, 6 mm confinement

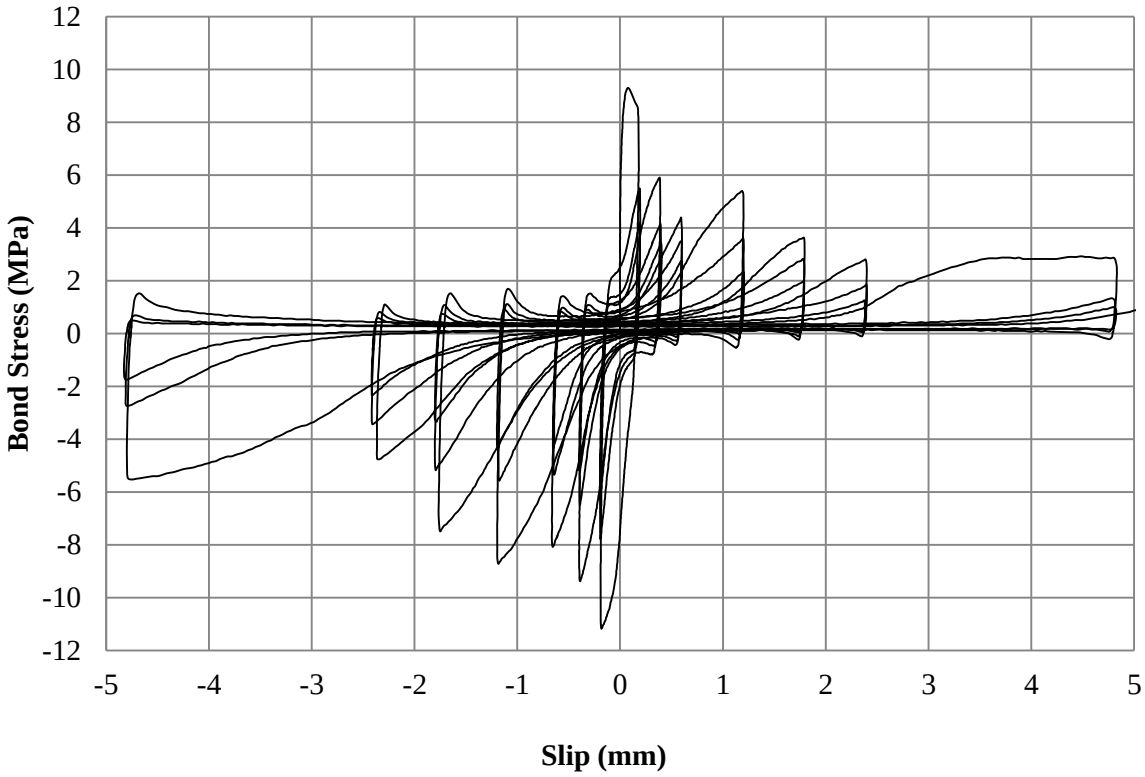

Figure C-0-7: Test 23- Cyclic pullout, 18.6% corrosion, 6 mm confinement

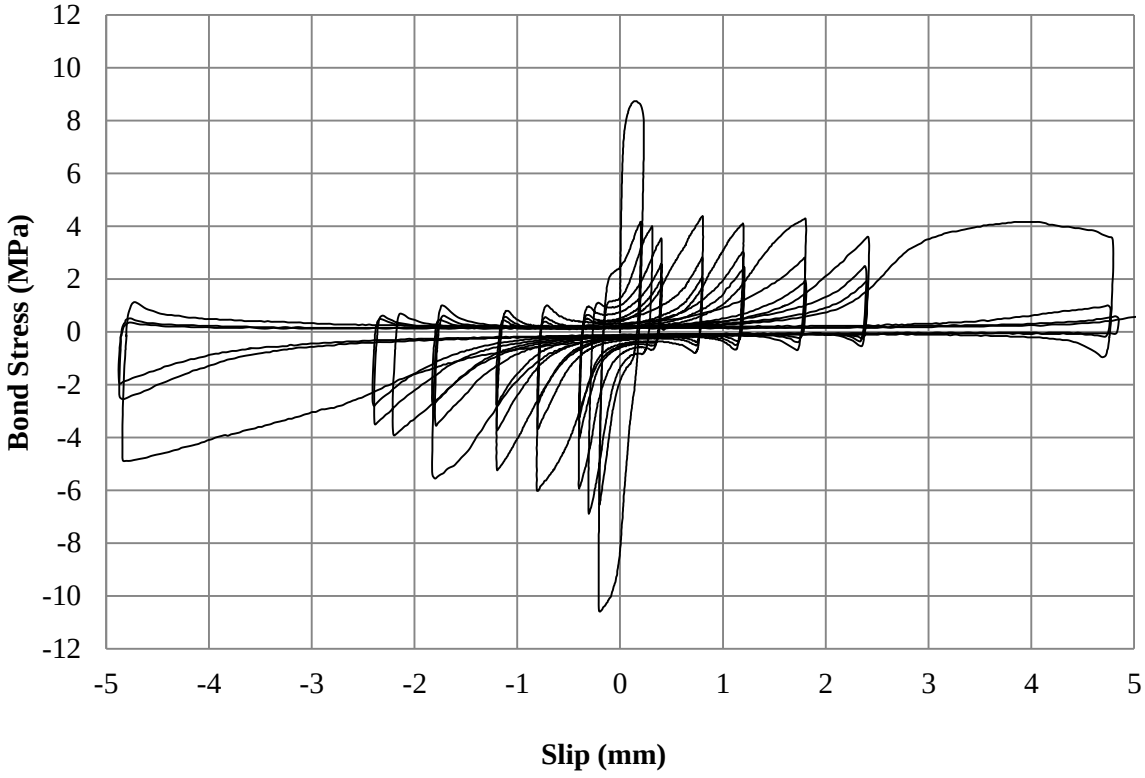

Figure C-0-8: Test 24- Cyclic pullout, 18.6% corrosion, 6 mm confinement

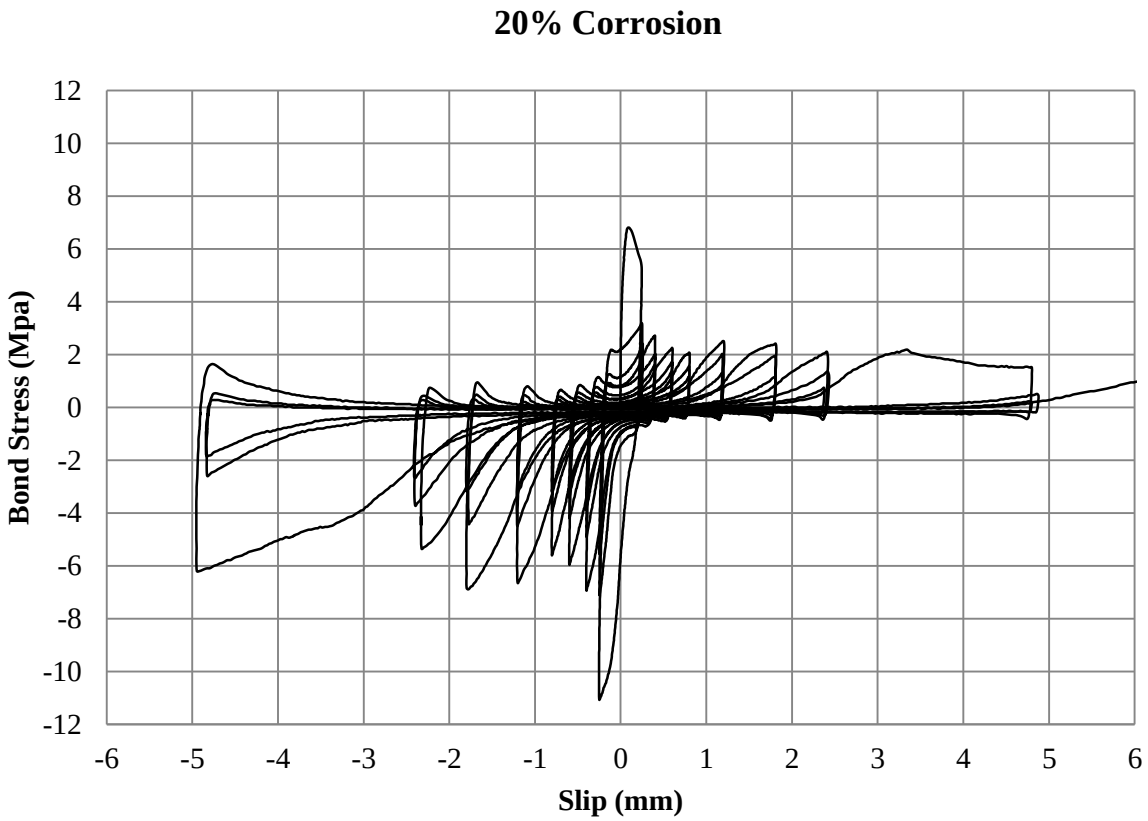

Figure C-0-9: Test 10- Cyclic pullout, 20.3% Corrosion, 6mm Confinement

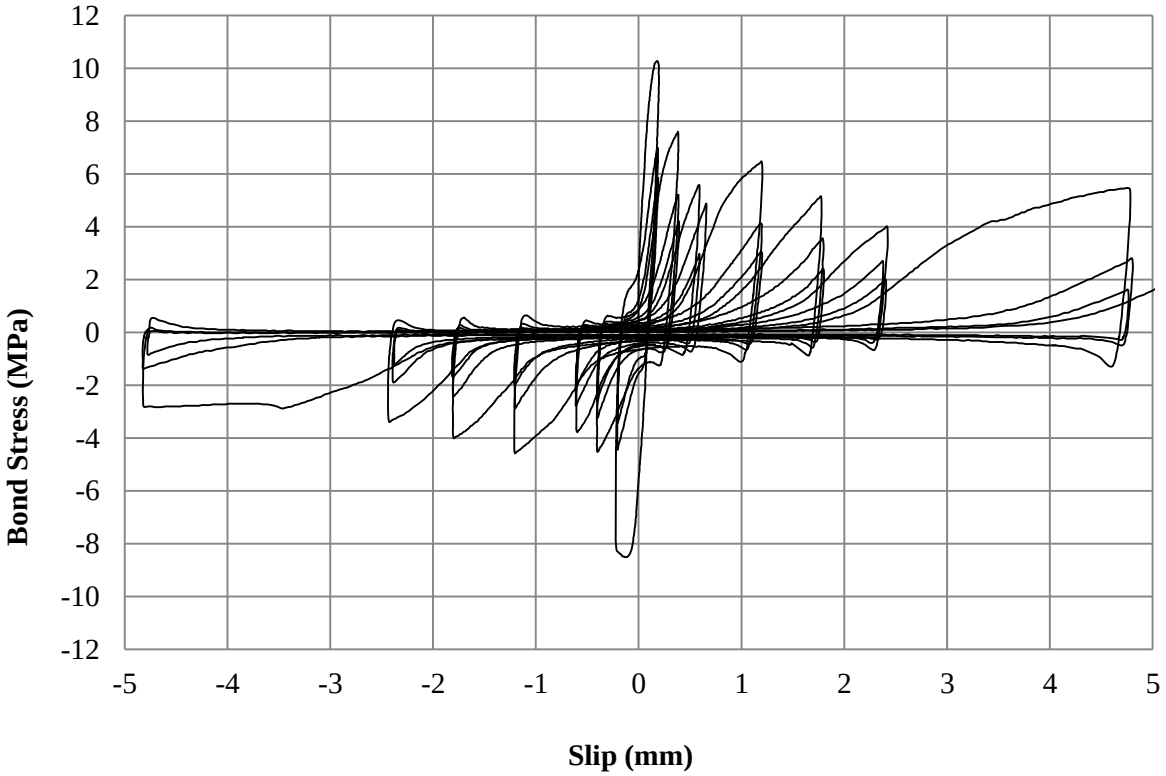

Figure C-0-10: Test 11- Cyclic pullout, 21.6% Corrosion, 6 mm confinement

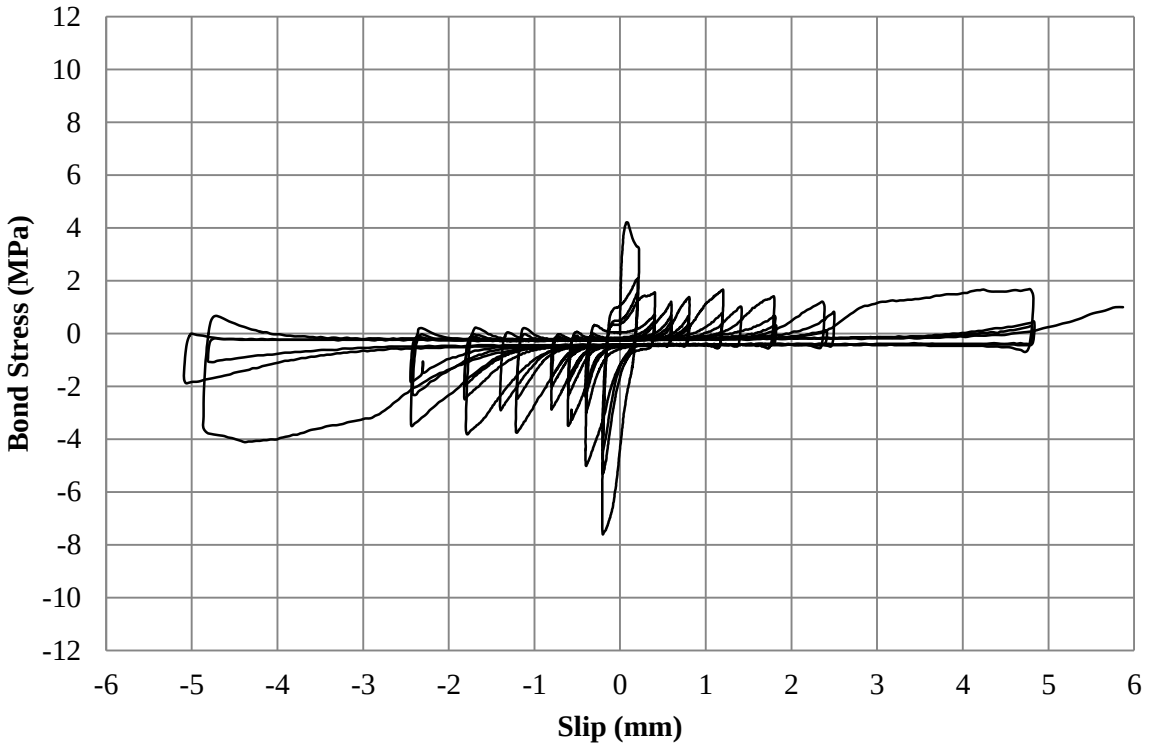

Figure C-0-11: Test 12 - Cyclic pullout, 20.6% corrosion, 6 mm confinement.(Suspected to have been damaged by twisting)

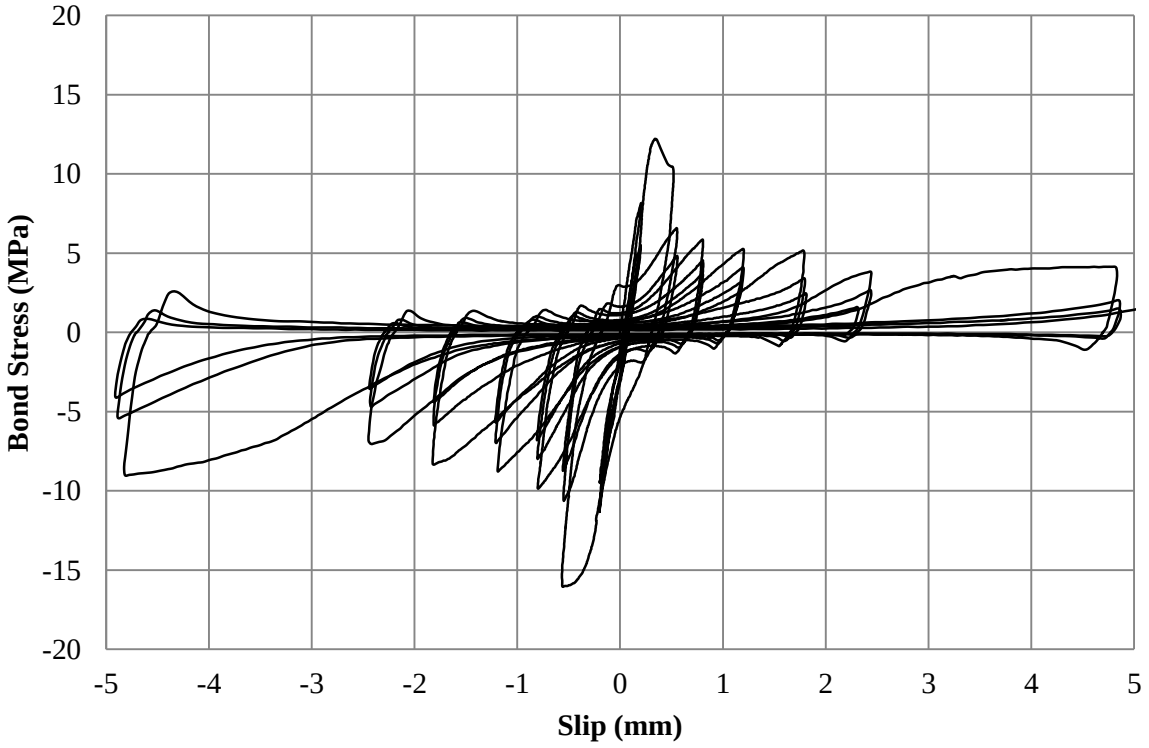

Figure C-0-12: Test 16- Cyclic pullout, 21.6% Corrosion, 6 mm confinement

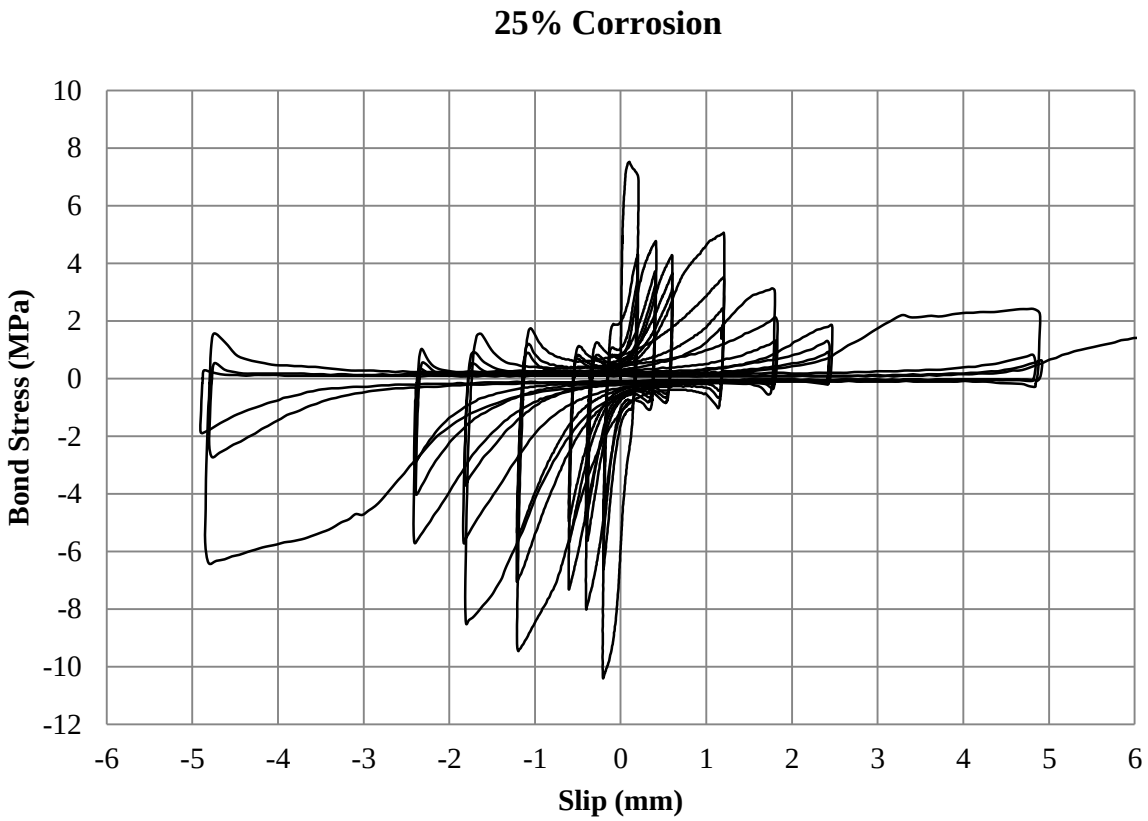

Figure C-0-13: Test 17- Cyclic pullout, 23% corrosion, 6 mm confinement

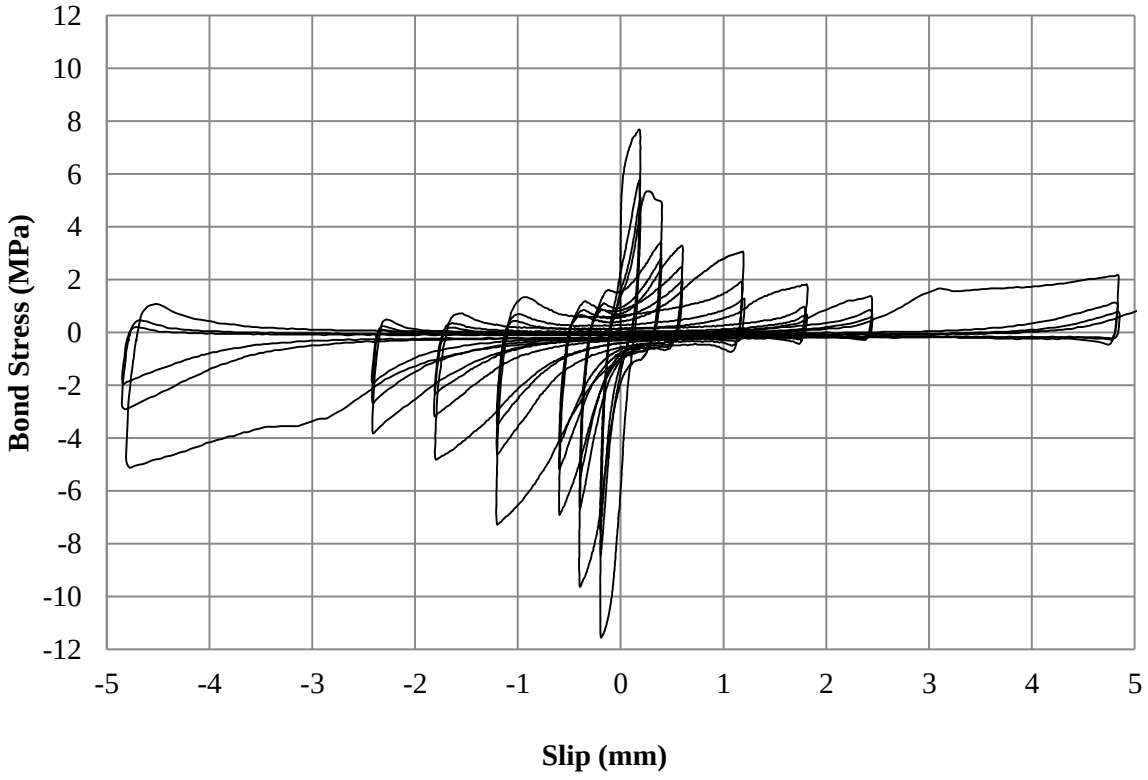

Figure C-0-14: Test 18 - Cyclic pullout, 26.5% Corrosion, 6 mm confinement

Appendix D: Experimental Results - Monotonic Testing, Variable Confinement

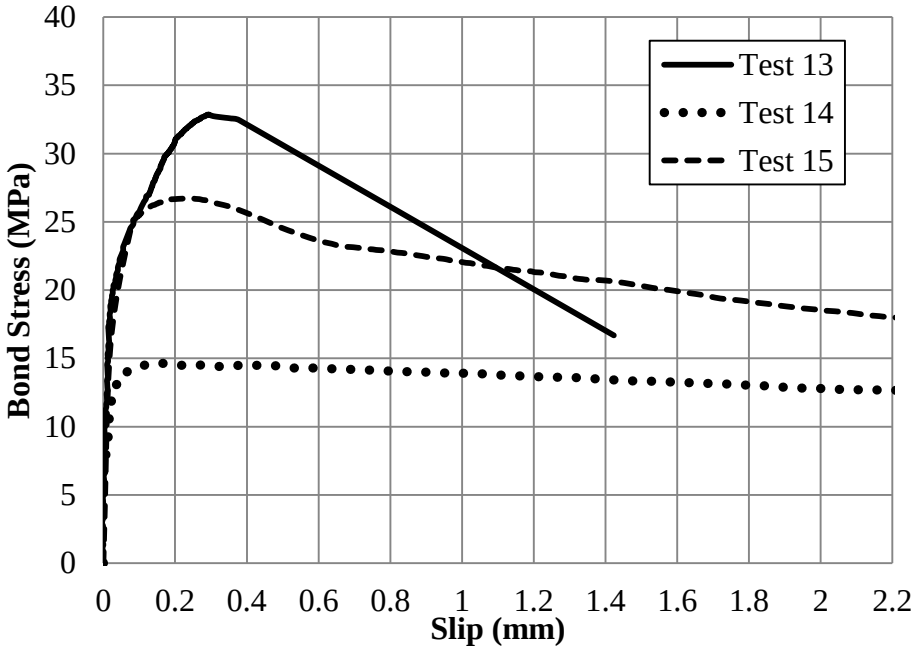

Figure D-0-1: Monotonic Pullout test results for 4.0 mm confinement, Test 13` 0.2%, Test 14 `6.4% , Test 15`2.8%.

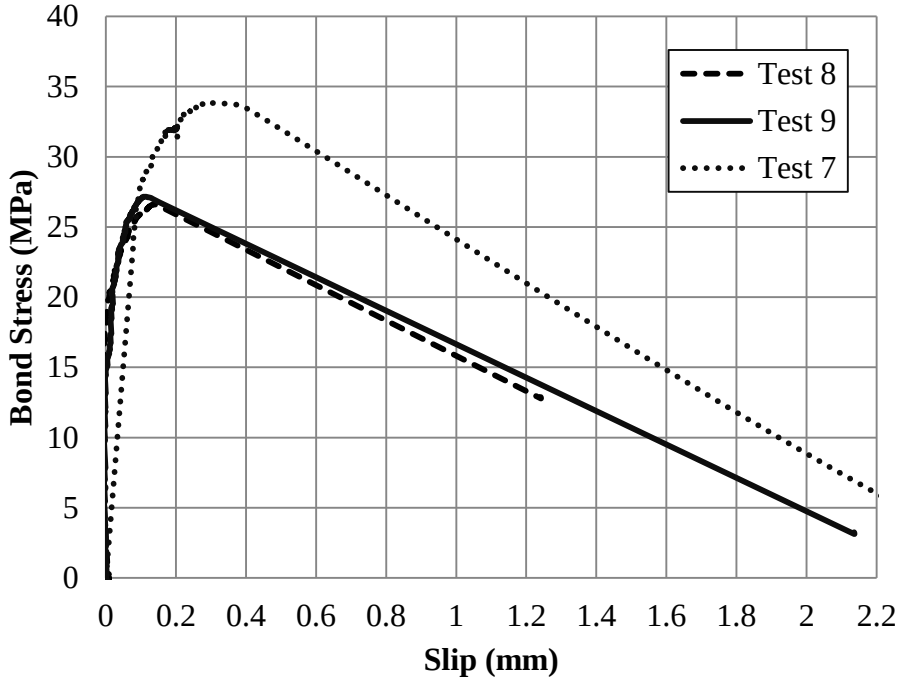

Figure D-0-2: Monotonic Pullout test results for 2.15 mm confinement, Test 7 – 0.7%, Test 8- 0.2%, Test 9 `0.5%.

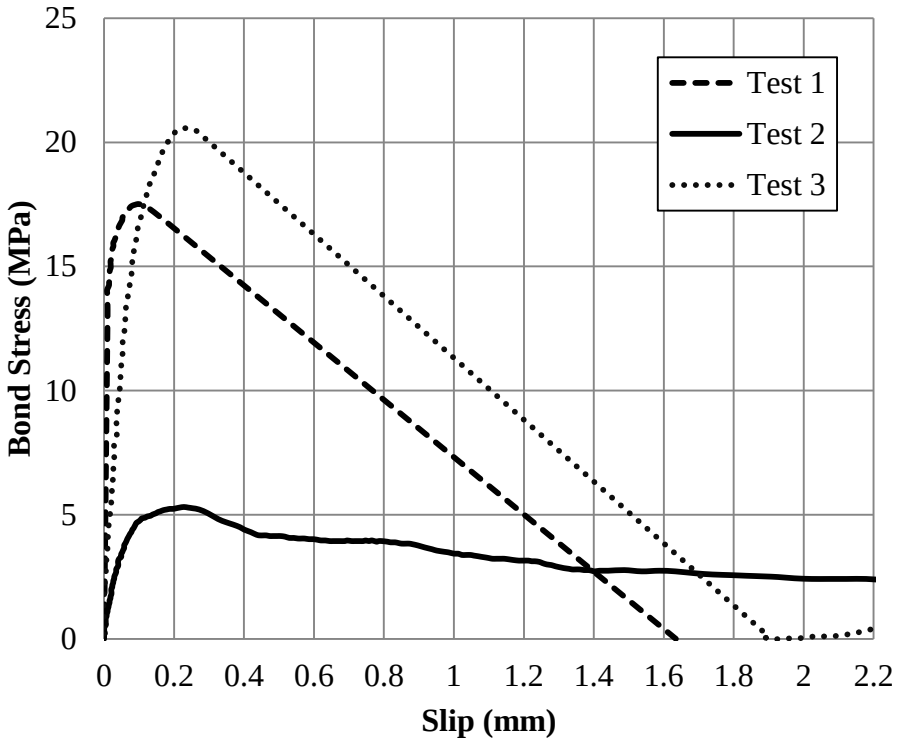

Figure D-0-3: Monotonic Pullout test results for Unconfined, Test 1 -0.4%, Test 2-3.1% and Test 3- 0.8%.

Appendix E: Experimental Results - Cyclic Testing, Variable Confinement

Unconfined

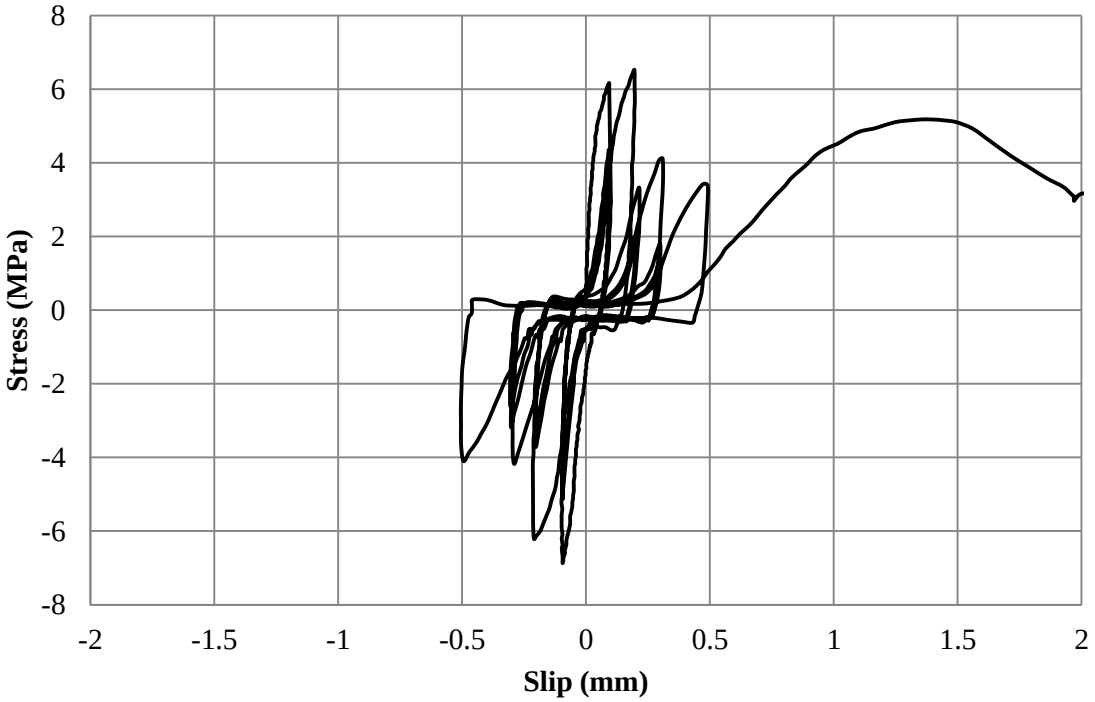

Figure E-0-1: Test 4- Cyclic pullout, 0.8% Corrosion, unconfined

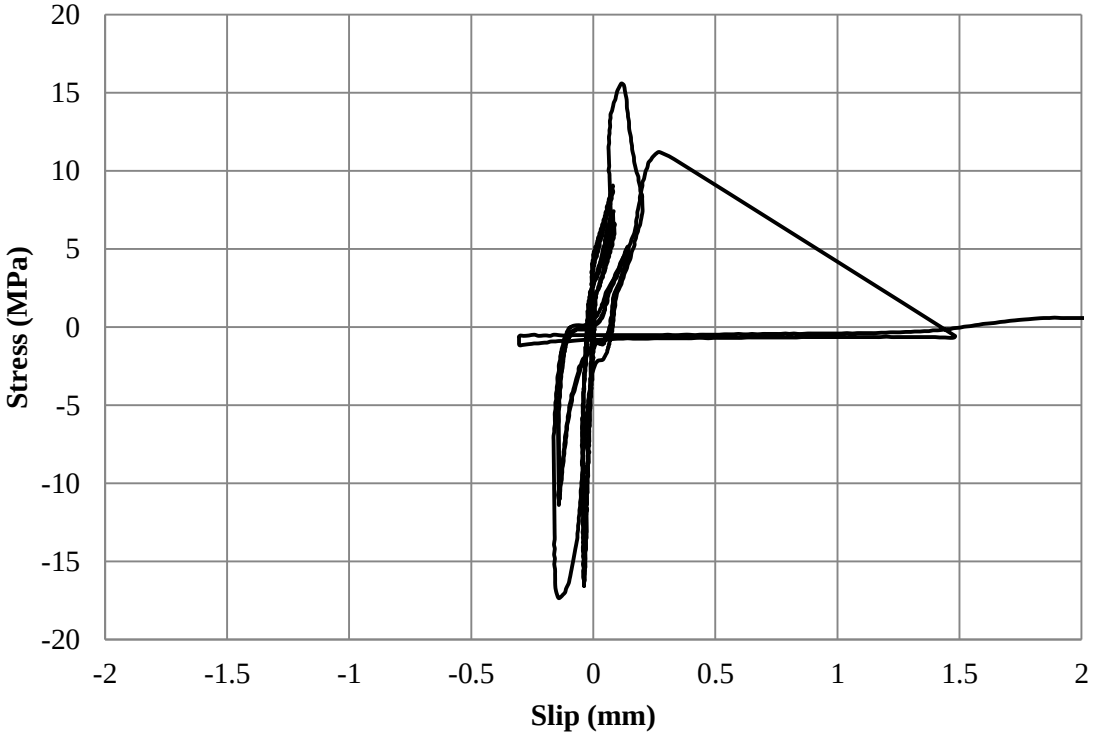

Figure E-0-2: Test 5- Cyclic pullout, 0.2% Corrosion, unconfined

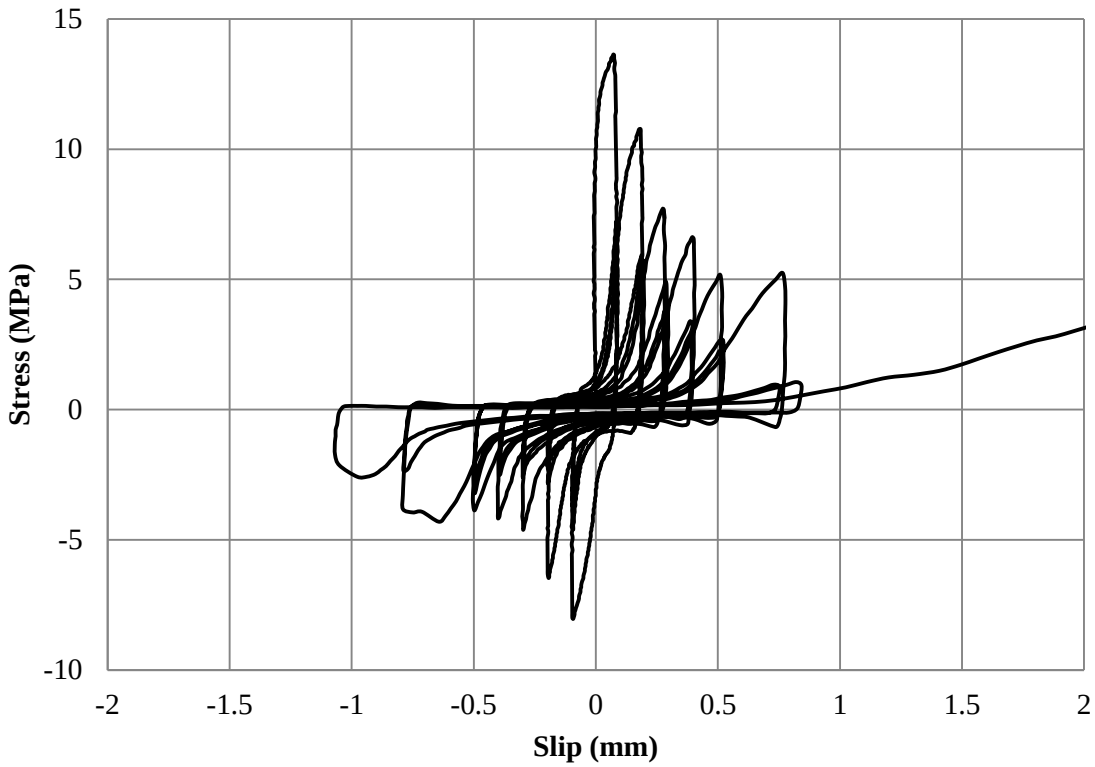

\

Figure E-0-3: Test 6- Cyclic pullout, 1.2% Corrosion, unconfined

2.15mm Stirrups

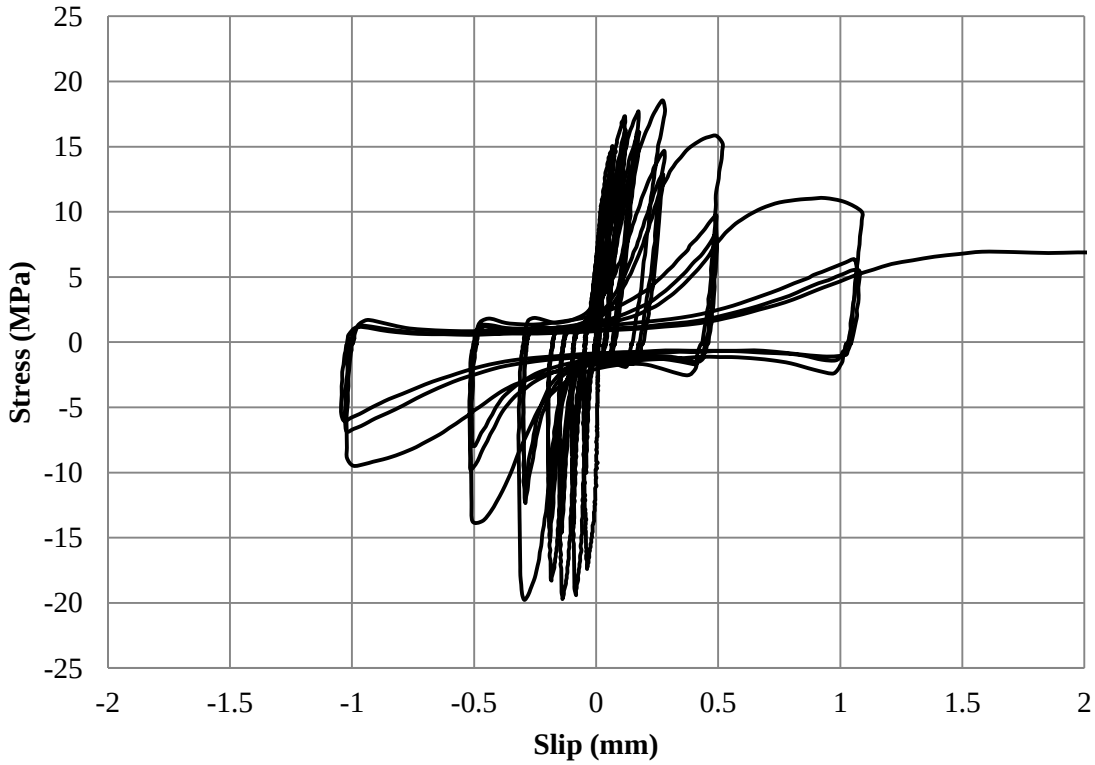

Figure E-0-4: Test 10- Cyclic pullout, 0.7% Corrosion, 2.15mm confinement

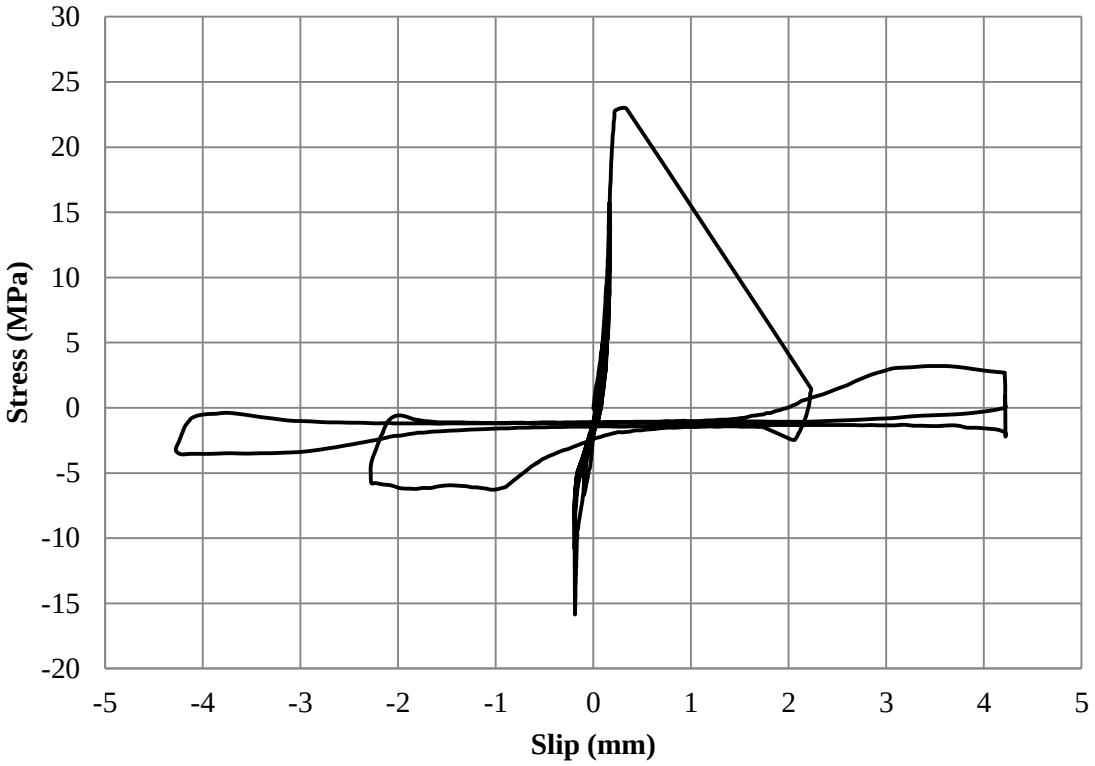

Figure E-0-5: Test 11- Cyclic pullout, 0.1% Corrosion, 2.15mm confinement

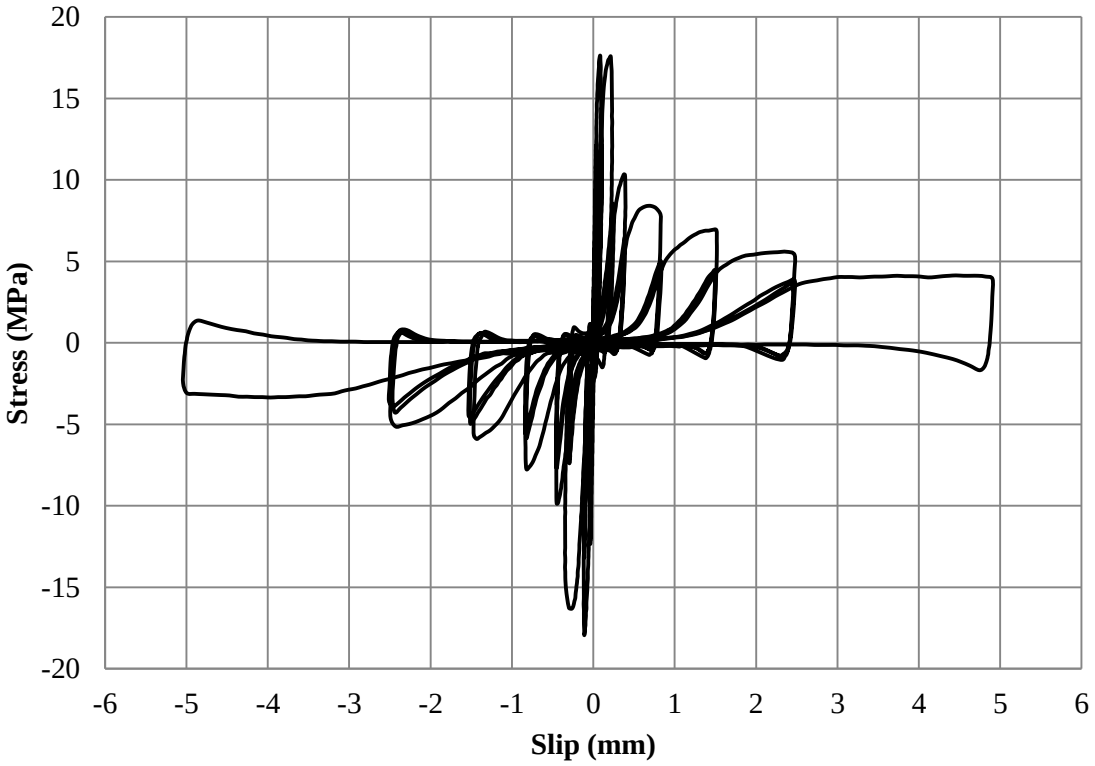

Figure E-0-6: Test 12- Cyclic pullout, 0.6% Corrosion, 2.15mm confinement

4.0mm Confinement

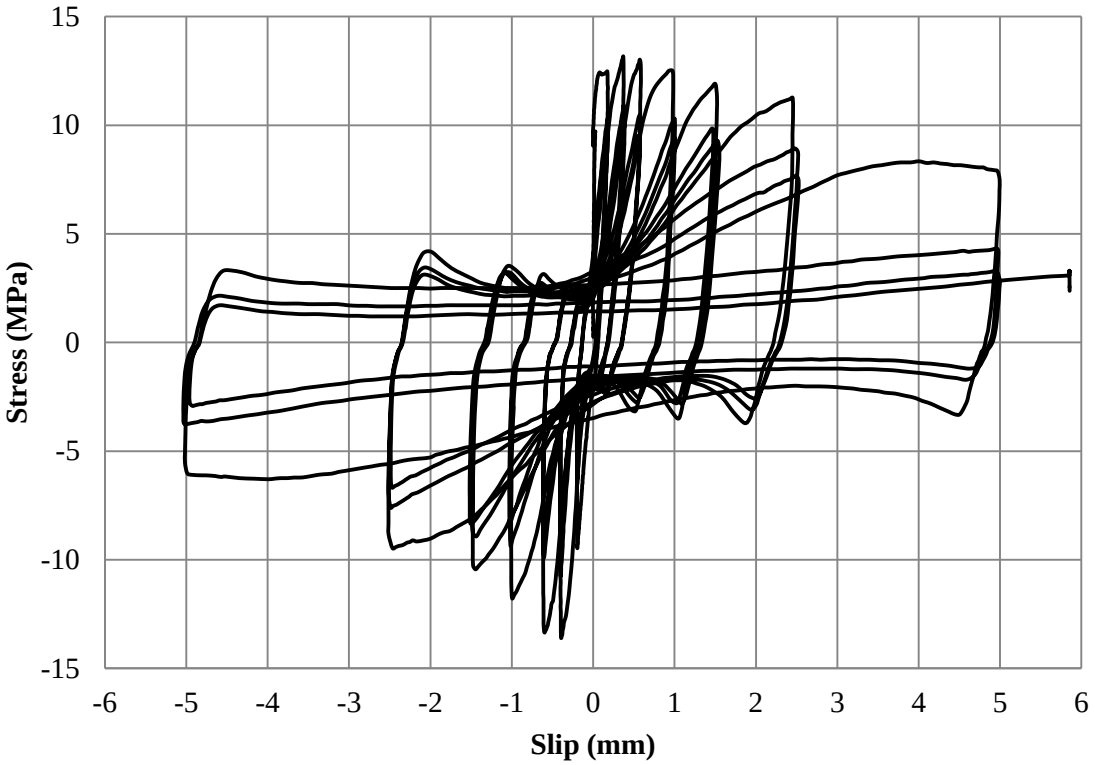

Figure E-0-7: Test 16- Cyclic pullout, 4.5% Corrosion, 4.0mm confinement

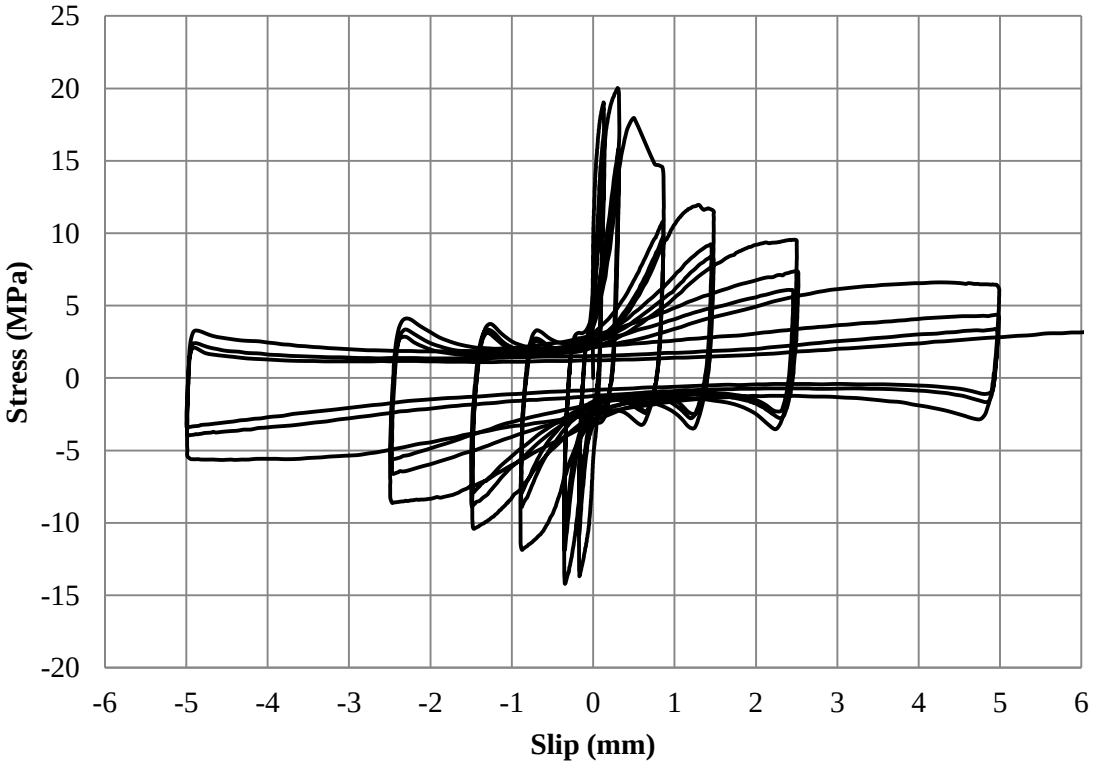

Figure E-0-8: Test 17- Cyclic pullout, 3.6% Corrosion, 4.0mm confinement

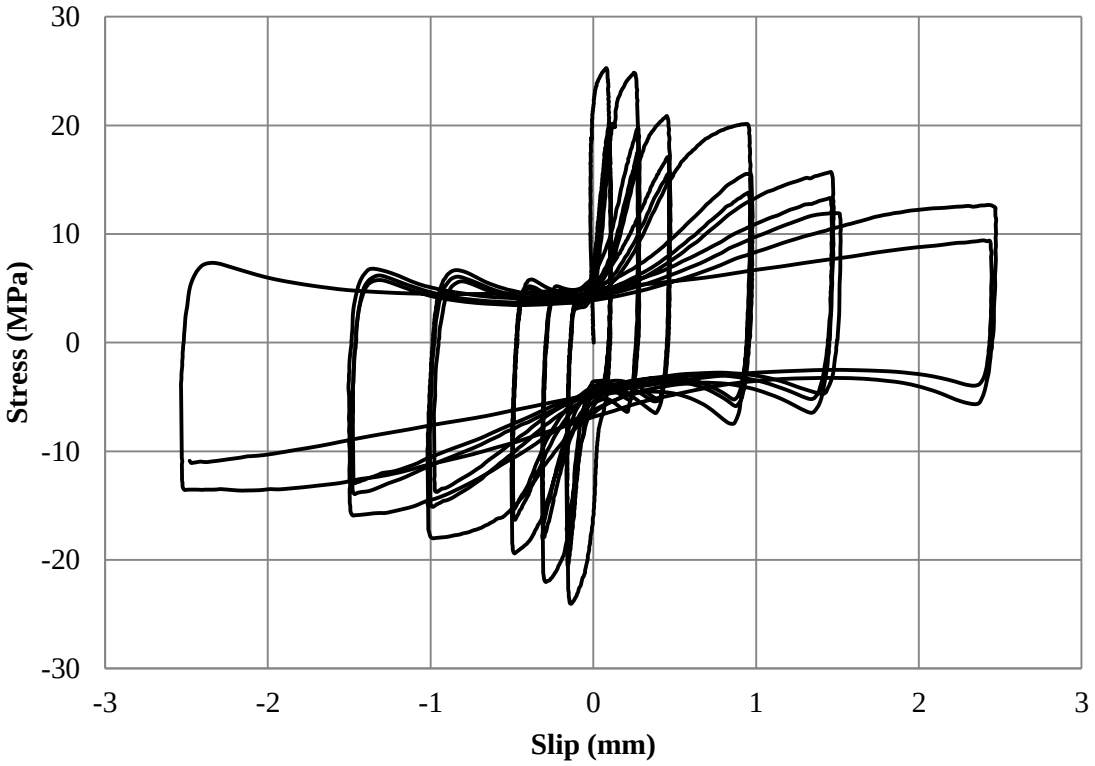

Figure E-0-9: Test 18- Cyclic pullout, 4.0% Corrosion, 4.0mm confinement

Appendix F: Numerical Model Damage-Energy Relationships

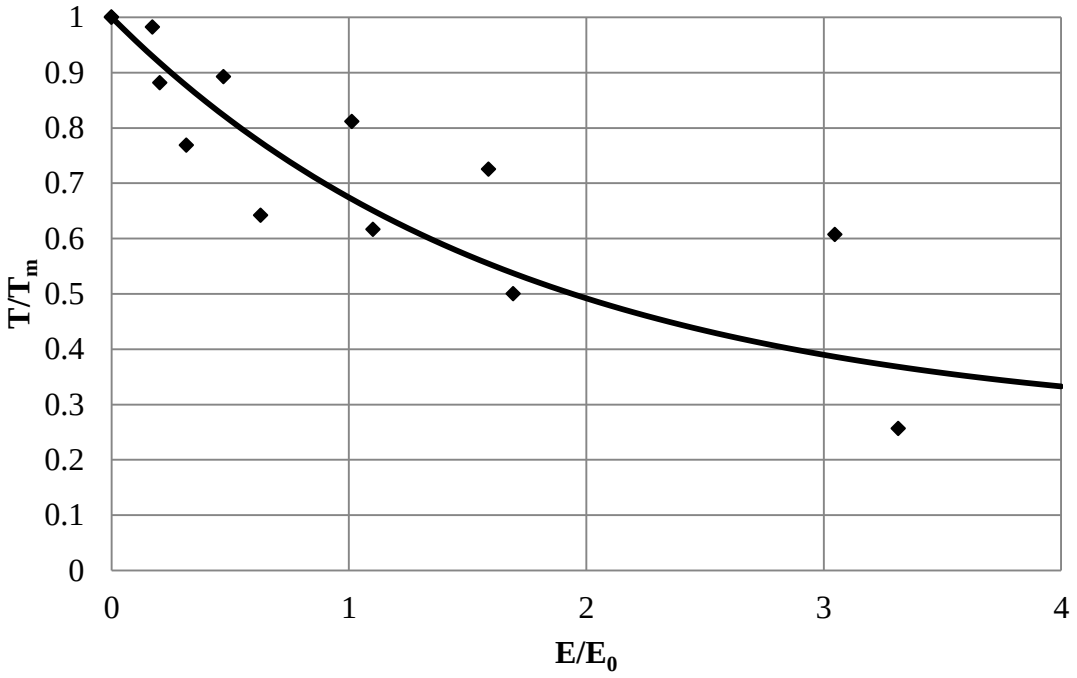

Figure F-0-1: Damage-energy relationship for 0% corrosion, Model and experimental data.

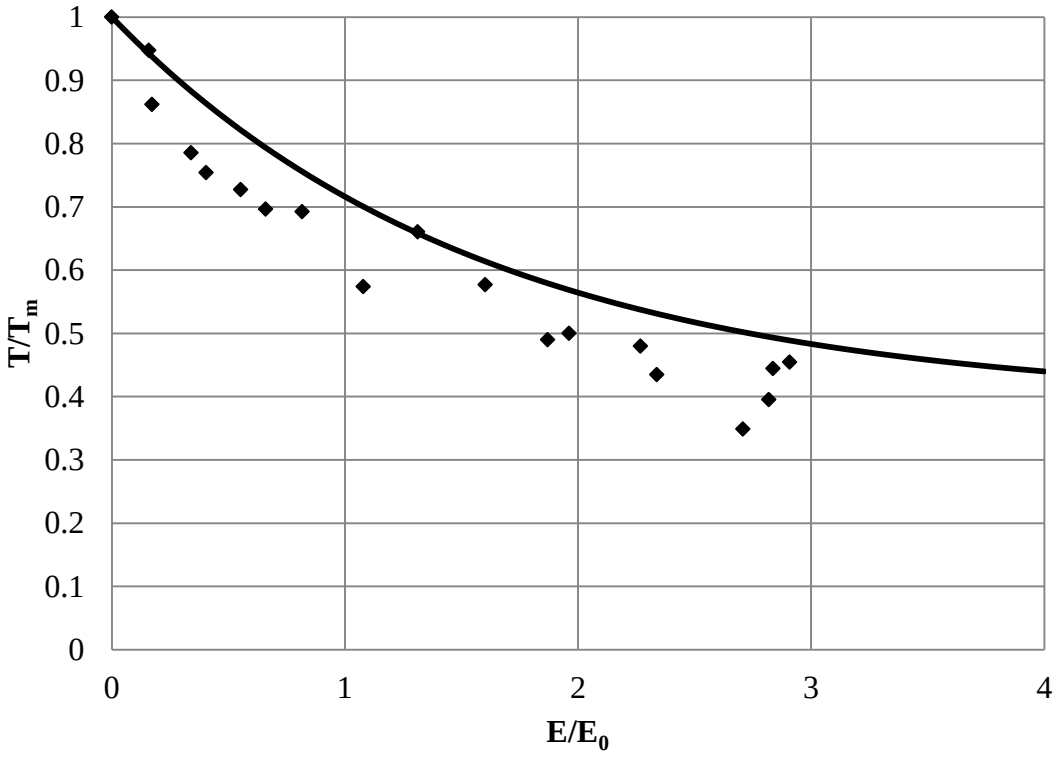

Figure F-0-2: Damage-energy relationship for 1% corrosion, Model and experimental data.

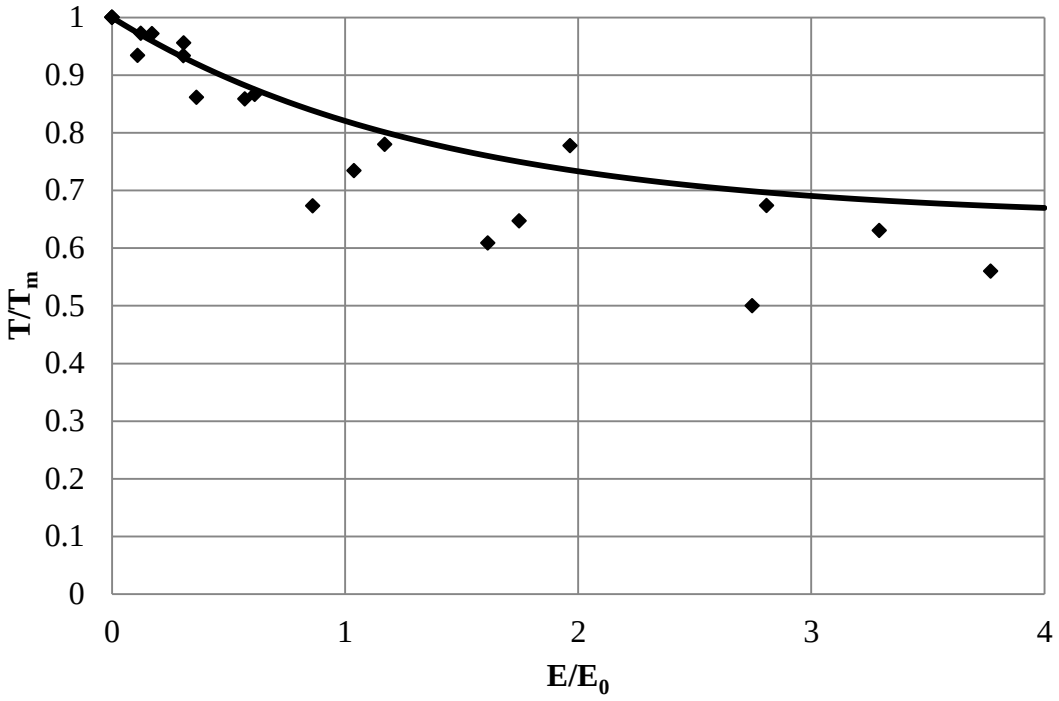

Figure F-0-3: Damage-energy relationship for 3% corrosion, Model and experimental data.

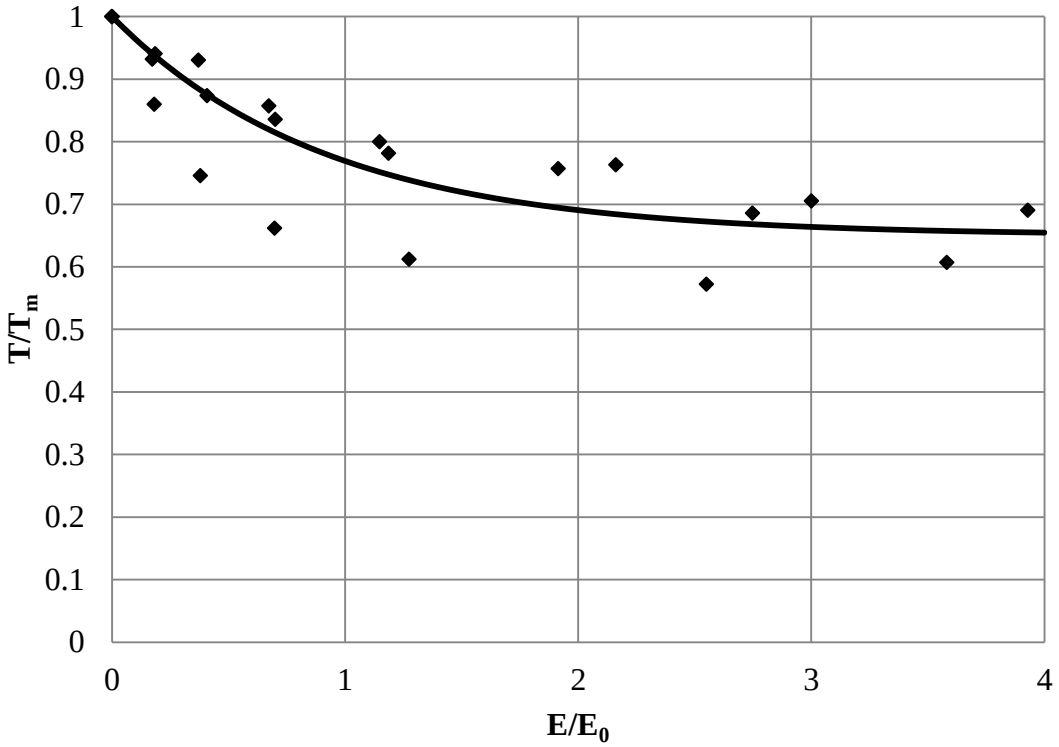

Figure F-0-4: Damage-energy relationship for 7% corrosion, Model and experimental data.

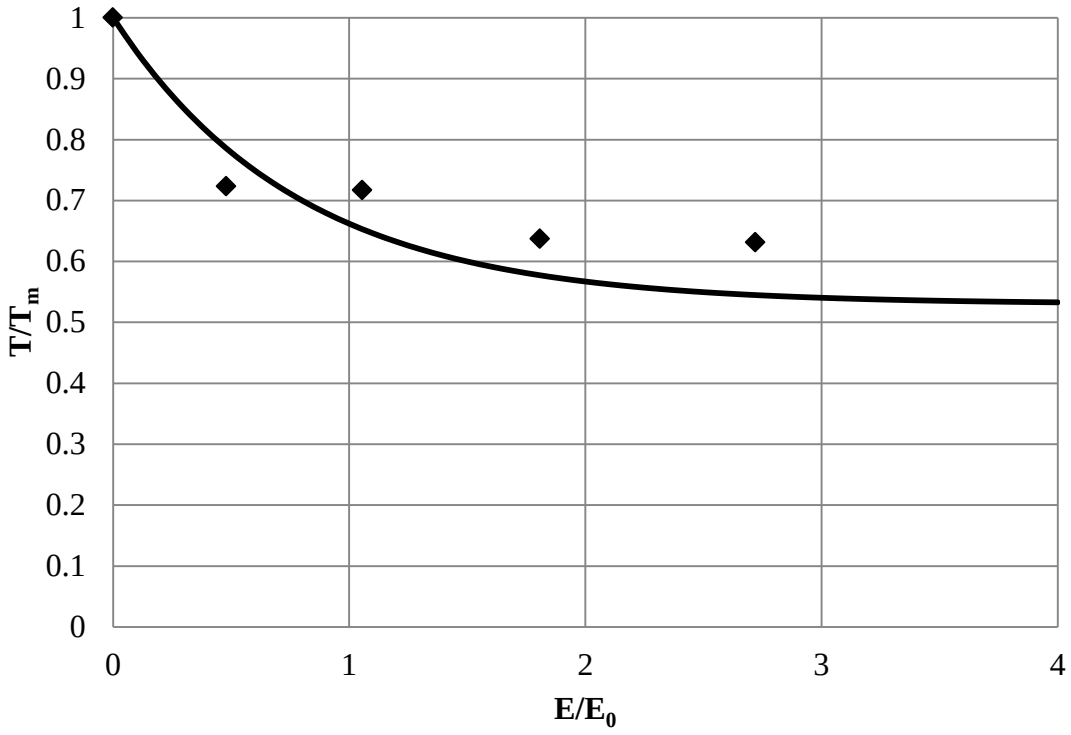

Figure F-0-5: Damage-energy relationship for 15% corrosion, Model and experimental data.

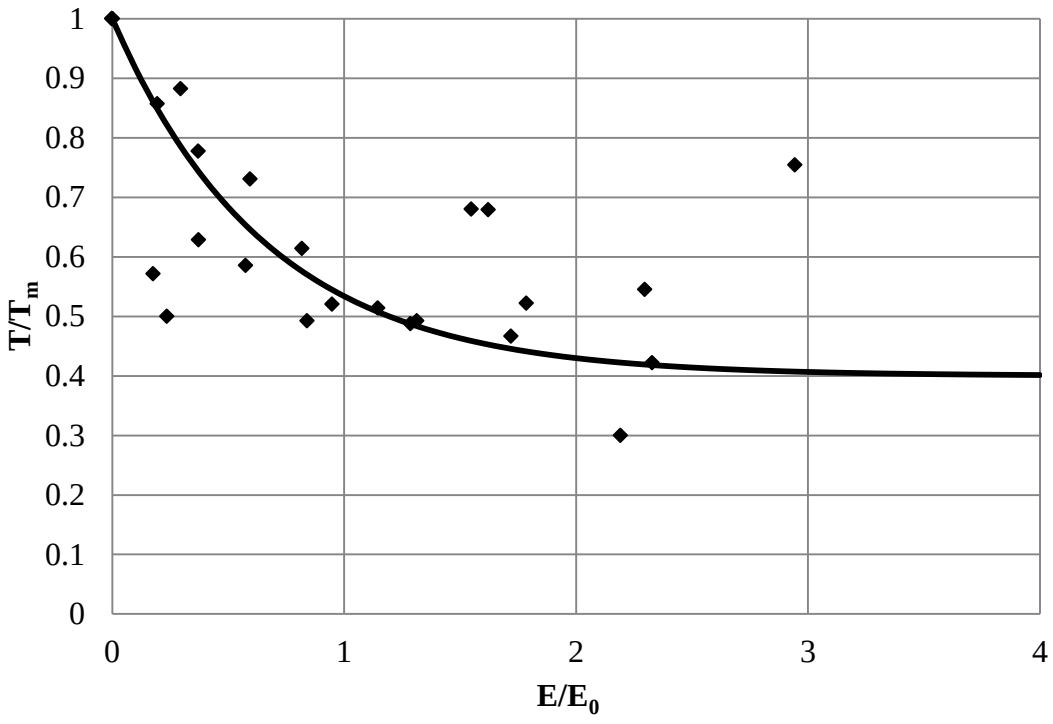

Figure F-0-6: Damage-energy relationship for 20% corrosion, Model and experimental data (using α=0.6).

Appendix G: Numerical Bond-Slip Model Coding for Ruaumoko3D

```
      SUBROUTINE BOND20(LNP,N,TAG,H,IERROR)
C
C     ****************************************************************
C     ANTON KIVELL BOND-SLIP MODEL
C
C     LNP      = Logical Unit No. Printer(input)
C     N        = Number of Actions       (input)
C     TAG      = Label for each action   (input)
C     H        = Hysteresis data array   (output)
C     IERROR   = Error Flag (0=no error) (output)
C
C     PROGRAMMED BY :  ATHOL J.CARR
C     DATE/VERSION  :  04-AUG-2010/1.0
C                      04-FEB-2011/1.1 A.Kivell
C                   01-SEP-2011/1.2 A.Kivell
C     ****************************************************************
C
      INTEGER          LNP,N,IERROR,I,J
      REAL             FCLVAL
CS    REAL             H(11,N)
CD    DOUBLE PRECISION H(11,N)
      LOGICAL          CMATCH
      CHARACTER        TAG(N)*12,LABEL*25,NOTE*20,CCLVAL*20
      EXTERNAL         FCLVAL,CCLVAL,CMATCH
      DATA LABEL       /'1Component =              '/
C
      CALL CLSHOW('1Anton Kivell Bond-Slip Hysteresis    : ')
      DO 10 I=1,N
         LABEL(14:25) = TAG(I)
         CALL CLSHOW(LABEL)
         CALL CLREAD(' Post Yield Parameters ? [Default]  : ',
     *     '1 POST YIELD CONCRETE PROPERTIES:
     *     &&    Default values are in MPa and mm units
     *     && T3R   = Ultimate Friction Stress Ratio   (Default= 0.3)
     *     && S1R   = Slip Ratio at Rupture S1=S1R*DY  (Default= 2.0)
     *     &&         where DY=(+Yield_action)/(Member_Stiffness)
     *     && S2R   = Slip Ratio at End of Plateau     (Default= 3.0)
     *     && S3R   = Slip at End of Friction Slip     (Default= 40.0)
     *     && ALPHA = Initial Slip Slope Parameter     (Default= 0.4)
     *     && EALPHA= Energy-Damage Factor, alpha      (Default= 0.75)
     *     && EBETA = Energy-Damage Factor, Beta       (Default= -0.58)
     *     && AFRIC = Frictional modification factor A (Default= 2.16)
     *     && BFRIC = Frictional modification factor B (Default= -3.1)
     *     && CFRIC = Frictional modification factor C (Default= 0.29)
     *     && AREA  = Scale Factor                     (Default= 1.0)
     *     &&         (scale factor between T units program units)
     *     ')
         IF(CMATCH(CCLVAL(1),'Default')) THEN
            H( 1,I) = 0.3
            H( 2,I) = 2.0
            H( 3,I) = 3.0
            H( 4,I) = 40.0
            H( 5,I) = 0.4
            H( 6,I) = 0.75
          H( 7,I) = -0.58
          H( 8,I) = 2.16
          H( 9,I) = -3.1
          H(10,I) = 0.29
          H(11,I) = 1.0
```

```
         ELSE
            H( 1,I) =  ABS(FCLVAL( 1))
            H( 2,I) =  ABS(FCLVAL( 2))
            H( 3,I) =  ABS(FCLVAL( 3))
            H( 4,I) =  ABS(FCLVAL( 4))
            H( 5,I) =  ABS(FCLVAL( 5))
            H( 6,I) =  ABS(FCLVAL( 6))
            H( 7,I) = -ABS(FCLVAL( 7))
            H( 8,I) =  ABS(FCLVAL( 8))
            H( 9,I) =  ABS(FCLVAL( 9))
            H(10,I) = -ABS(FCLVAL(10))
            H(11,I) =  ABS(FCLVAL(11))
            IF(H( 1,I).LT.0.01) H( 1,I) =  0.3
            IF(H( 2,I).LT.0.01) H( 2,I) =  2.0
            IF(H( 3,I).LT.0.01) H( 3,I) =  3.0
            IF(H( 4,I).LT.0.01) H( 4,I) =  40.0
            IF(H( 5,I).LT.0.01) H( 5,I) =  0.4
            IF(H( 6,I).LT.0.01) H( 6,I) =  0.75
          IF(H( 7,I).GT.0.00) H( 7,I) = -0.58
          IF(H( 8,I).LT.0.01) H( 8,I) =  2.16
          IF(H( 9,I).GT.0.00) H( 9,I) = -3.1
          IF(H(10,I).LT.0.01) H(10,I) =  0.29
          IF(H(11,I).LT.0.01) H(11,I) =  1.0
         ENDIF
         WRITE(LNP,60) I,TAG(I),(H(J,I),J=1,11)
   10 CONTINUE
      WRITE(LNP,61)
      RETURN
C
   60 FORMAT(4X,40HANTON KIVELL BOND-SLIP Model - Component,I2,1X,A12/
     *       4X,25HUltimate Friction Ratio =,1PE11.3,
     *       4X,25HSlip Ratio at Rupture . =,  E11.3/
     *       4X,25HSlip Ratio End Plateau. =,  E11.3,
     *       4X,25HSlip Ratio End Friction =,  E11.3/
     *       4X,25HInitial Slope ALPHA . . =,  E11.3,
     *       4X,25HDamage-Energy Alpha . . =,  E11.3/
     *       4X,25HDamage-Energy Beta. . . =,  E11.3,
     *       4X,25HFrictional AFRIC. . . . =,  E11.3/
     *       4X,25HFrictional BFRIC. . . . =,  E11.3,
     *       4X,25HFrictional CFRIC. . . . =,  E11.3/
     *       4X,25HArea Scale factor . . . =,  E11.3)
   61 FORMAT(1X)
C
      END
      SUBROUTINE BOND21(FORCE,SLIP,STEP,XS,F,STIFF,YP,T3R,S1R,S2R,S3R,
     *                  ALPHA,EALPHA,EBETA,AFRIC,BFRIC,CFRIC,AREA,SMAX,
     *                  SMIN,E,EF,DAMAGE,IPLOT,LPU,IERROR)
C
C     ****************************************************************
C     ANTON KIVELL BOND-SLIP MODEL
C
C      This function performs the stress-slip procedure for bond-slip
C      between reinforcing bars and concrete in reinforced concrete
C      based on the model developed by Eligihausen, Popov and Bertero,
C      1983, but modified to include additional damage alteration
C      variables with the intended use in modelling effects of
C      corrosion on bond-slip behaviour (Kivell,2011).
C
C      FORCE    = Force
C      SLIP     = slip
C      STEP     = Slip step,
```

```
C      XS       = Excess Force,
C      F        = Stiffness reduction factor,
C      STIFF    = Unload-Reload Stiffness,
C      YP       = Maximum stress (bond rupture)
C      T3R      = Ultimate frictional stress Ratio,
C      S1R      = Slip Ratio of linear Rupture deformation,
C      S2R      = Slip Ratio at end of plateau,
C      S3R      = Slip Ratio at fully frictional slip,
C      ALPHA    = Initial slip slope parameter,
C      EALPHA   = Damage-Energy Alpha,
C      EBETA    = Damage-Energy Beta,
C      AFRIC    = Frictional modification factor,A,
C      BFRIC    = Frictional modification factor,B,
C      CFRIC    = Frictional modification factor,C,
C      AREA     = Bond area of spring scale ratio
C      SMAX     = Maximum positive slip experienced
C      SMIN     = Maximum negitive slip experienced
C      E        = energy(total),
C      EF       = frictional energy,
C      DAMAGE   = damage flag,
C      IPLOT    = Plot Flag  1: Elastic
C                            2: Non-linear Positive
C                            3: Non-linear negative
C                            4: Slipping
C
C      SOLD = Slip at previous timestep
C      TOLD     = Stress from previous step
C      E0   = Energy normaliser
C      EOF  = Frictional energy normaliser
C      D    = Damage factor
C      T        = Stress,
C      TF   = Frictional stress
C      TX,TM      = Monotonic stress envelope
C      K    = Unload-Reload stiffness
C      FORCE    = Force applied
C
C     PROGRAMMED BY :  ATHOL J.CARR (from Anton Kivell)
C     DATE/VERSION  :  31-AUG-2010/1.1
C     ***************************************************************
C
      INTEGER          DAMAGE,IPLOT,LPU,IERROR,POSNEG,DRCTN,TMFLAG
CS    REAL             FORCE,SLIP,STEP,XS,F,STIFF,YP,T3R,S1R,S2R,S3R
CS    REAL             ALPHA,EALPHA,EBETA,AREA,SMAX,SMIN,AFRIC
CS    REAL             T,TOLD,SOLD,K,E,EF,EOF,E0,D,DF,TF,TM,T1,T3
CS    REAL             S1,S2,S3,SLIPT,BFRIC,CFRIC,TMP
CS    REAL             ONE
CD    DOUBLE PRECISION FORCE,SLIP,STEP,XS,F,STIFF,YP,T3R,S1R,S2R,S3R
CD    DOUBLE PRECISION ALPHA,EALPHA,EBETA,AREA,SMAX,SMIN,AFRIC
CD    DOUBLE PRECISION T,TOLD,SOLD,K,E,EF,EOF,E0,D,DF,TF,TM,T1,T3
CD    DOUBLE PRECISION S1,S2,S3,SLIPT,BFRIC,CFRIC,TMP
CD    DOUBLE PRECISION ONE
      LOGICAL          DONE
      SAVE             DONE
      DATA ONE         /1.0/
C
      IERROR = 0
      TOLD   = FORCE/AREA
      T      = TOLD
      K      = STIFF/AREA
      SOLD   = SLIP
      SLIP   = SLIP+STEP
```

```
      XS     = FORCE+STIFF*F*STEP
      T1     = YP/AREA
      T3     = T1*T3R
      S1     = S1R*T1/K
      S2     = S1*S2R
      S3     = S1*S3R
      IF(.NOT.DONE) THEN
         WRITE(LPU,'(A,1PE11.3)') '     YP',YP
         WRITE(LPU,'(A,1PE11.3)') '     T1',T1
         WRITE(LPU,'(A,1PE11.3)') '     T3',T3
         WRITE(LPU,'(A,1PE11.3)') '     S1',S1
         WRITE(LPU,'(A,1PE11.3)') '     S2',S2
         WRITE(LPU,'(A,1PE11.3)') '     S3',S3
         WRITE(LPU,'(A,1PE11.3)') '  ALPHA',ALPHA
         WRITE(LPU,'(A,1PE11.3)') ' EALPHA',EALPHA
         WRITE(LPU,'(A,1PE11.3)') '  EBETA',EBETA
         WRITE(LPU,'(A,1PE11.3)') '  AFRIC',AFRIC
         WRITE(LPU,'(A,1PE11.3)') '  BFRIC',BFRIC
         WRITE(LPU,'(A,1PE11.3)') '  CFRIC',CFRIC
         WRITE(LPU,'(A,1PE11.3)') '   AREA',AREA
         WRITE(LPU,'(A,1PE11.3)') '      K',K
         DONE = .TRUE.
      ENDIF
C                *Determining MIN/MAX slip
      SMAX   = MAX(SLIP,SMAX)
      SMIN   = MIN(SLIP,SMIN)
C                *DETERMINING MONOTONIC
      TMFLAG = 0
      IF(SLIP.EQ.SMAX.OR.SLIP.EQ.SMIN) TMFLAG = 1
C                *POSITIVE OR NEGITIVE SLIP
      POSNEG = 0
      IF(SLIP.GE.0.0)      POSNEG = 1
C                *DIRECTION
      DRCTN  = 0
      IF(SLIP-SOLD.GE.0.0) DRCTN  = 1
C                    *Energy/Damage
      IF(DAMAGE.EQ.0) THEN
         IF(DRCTN.EQ.0.AND.SMAX.GT. 0.9*S1) DAMAGE = 1
         IF(DRCTN.EQ.1.AND.SMIN.LT.-0.9*S1) DAMAGE = 1
      ENDIF
      E0  = T1*S1/(ALPHA+1.0)+T1*(S2-S1)+(T1+T3)*0.5*(S3-S2)
      E   = E+ABS(STEP*T)
      D   = 1.0
      IF(DAMAGE.EQ.1) D = EALPHA*EXP(EBETA*ABS(E/E0))+(1.0-EALPHA)
C                    *Frictional limit
      EOF = T3*S3
      TMP = AFRIC*T3*MAX(SMAX,ABS(SMIN))*EXP(BFRIC*ABS(EF/EOF)**CFRIC)
      TF  = MIN(TMP,T3*D)
      EF  = EF+ABS(TF*STEP)
C                *MONTOTONIC TARGET
      IF(DRCTN.EQ.1) THEN
       SLIPT = SMAX
      ELSE
       SLIPT = ABS(SMIN)
      ENDIF
      IF(SLIPT.GE.S3) THEN
       TM    = T3
       F     = 0
      ELSEIF(SLIPT.GE.S2) THEN
       TM    = T1-((T1-T3)/(S3-S2))*(SLIPT-S2)
       F     = (T3-T1)/(S3-S2)
```

```
      ELSEIF(SLIPT.GE.S1) THEN
       TM    = T1
       F     = 0
      ELSE
       TM    = T1*(SLIPT/S1)**ALPHA
       F     = (ALPHA*T1/S1)*(ABS(SLIPT/S1))**(ALPHA-1.0)
      ENDIF
      IF(DRCTN.EQ.0) THEN
       TM    = -TM
      ENDIF
      IF(DAMAGE.EQ.1) TM = TM*D
C                 *MONOTONIC STRESS
      IF(TMFLAG.EQ.1) THEN
       T=TM
       IF(DRCTN.EQ.1.AND.TM.GT.T+10.0*K*STEP) THEN
          T = T+10.0*K*STEP
          F = 10.0*K
       ELSEIF(DRCTN.EQ.0.AND.TM.LT.T+10.0*K*STEP) THEN
          T = T+10.0*K*STEP
          F = 10.0*K
       ENDIF
C                 *CYCLING STRESSES
      ELSE
       IF(POSNEG.EQ.1.AND.DRCTN.EQ.0) THEN
          IF ((T+TF)/K.GT.SLIP)  K=MIN((T+TF)/SLIP,10.0*K)
          T = T+K*STEP
          F = K
          IF(T.LT.-TF) THEN
             T = -TF
             F = 0
           ENDIF
       ELSEIF(POSNEG.EQ.1.AND.DRCTN.EQ.1) THEN
          T = T+K*STEP
          F = K
          IF(T.GT.(TF+(TM-TF)*ABS(SLIP/SMAX)**2.5)) THEN
             T = TF+(TM-TF)*ABS(SLIP/SMAX)**2.5
             F = (2.5*(TM-Tf)/SMAX)*ABS(SLIP/SMAX)**1.5
          ENDIF
       ELSEIF(POSNEG.EQ.0.AND.DRCTN.EQ.0) THEN
          T = T+K*STEP
          F = K
          IF(T.LT.(-TF+(TM+TF)*ABS(SLIP/SMIN)**2.5)) THEN
             T = -TF+(TM+TF)*ABS(SLIP/SMIN)**2.5
             F = -(2.5*(TM+TF)/SMIN)*ABS(SLIP/SMIN)**1.5
          ENDIF
       ELSE
          IF ((T-TF)/K.LT.SLIP)  K=MIN((T-TF)/SLIP,10.0*K)
          T = T+K*STEP
          F = K
            IF(T.GT.TF) THEN
             T = TF
             F = 0
          ENDIF
       ENDIF
      ENDIF
C                 *Clean up
      F      = MIN(F,10.0*K)
      F      = F/STIFF
      FORCE  = T*AREA
      XS     = XS-FORCE
C                     *Plot Flag
```

```
      IPLOT = 1
      IF(F.LT.0.7.AND.T     .GT. 0.3*T1) IPLOT = 2
      IF(F.LT.0.7.AND.T     .LT.-0.3*T1) IPLOT = 3
      IF(F.LT.0.1.AND.ABS(T).LT. 0.1*T1) IPLOT = 4
C
  100 RETURN
      END
```

Appendix H: Comparison Between Experimental Results and Numerical Model.

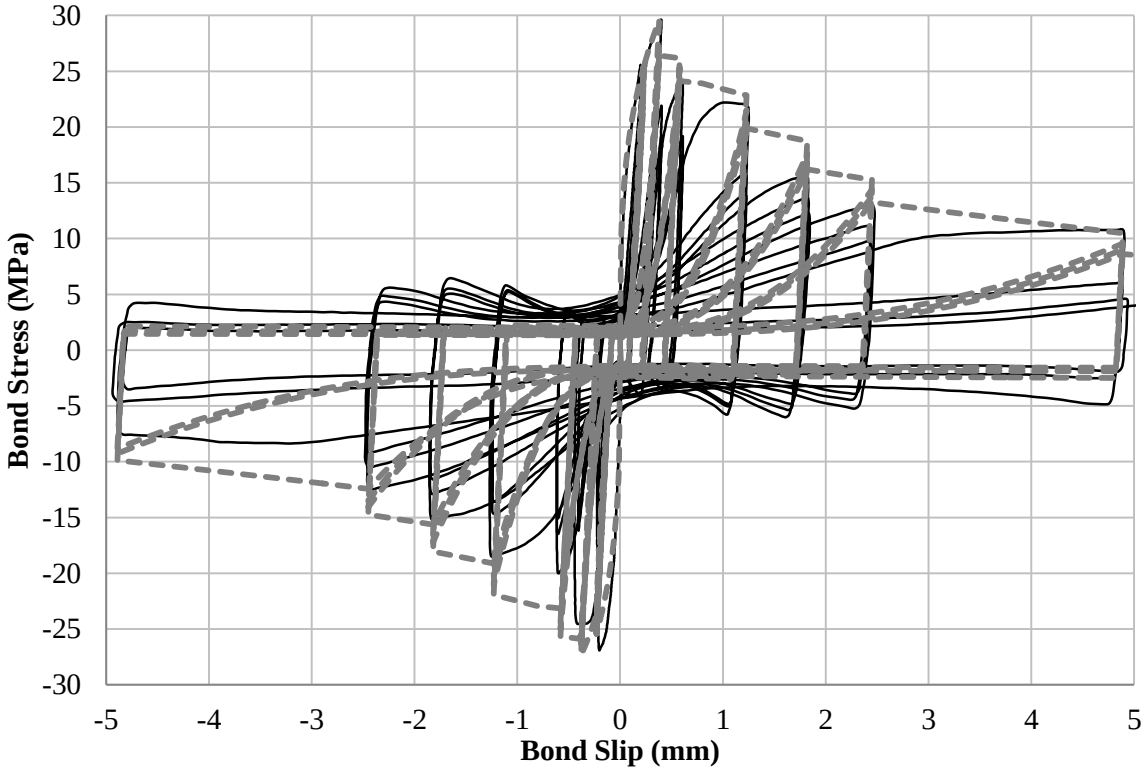

Figure H-0-1: Experimental/Numerical Comparison for 0% corrosion.

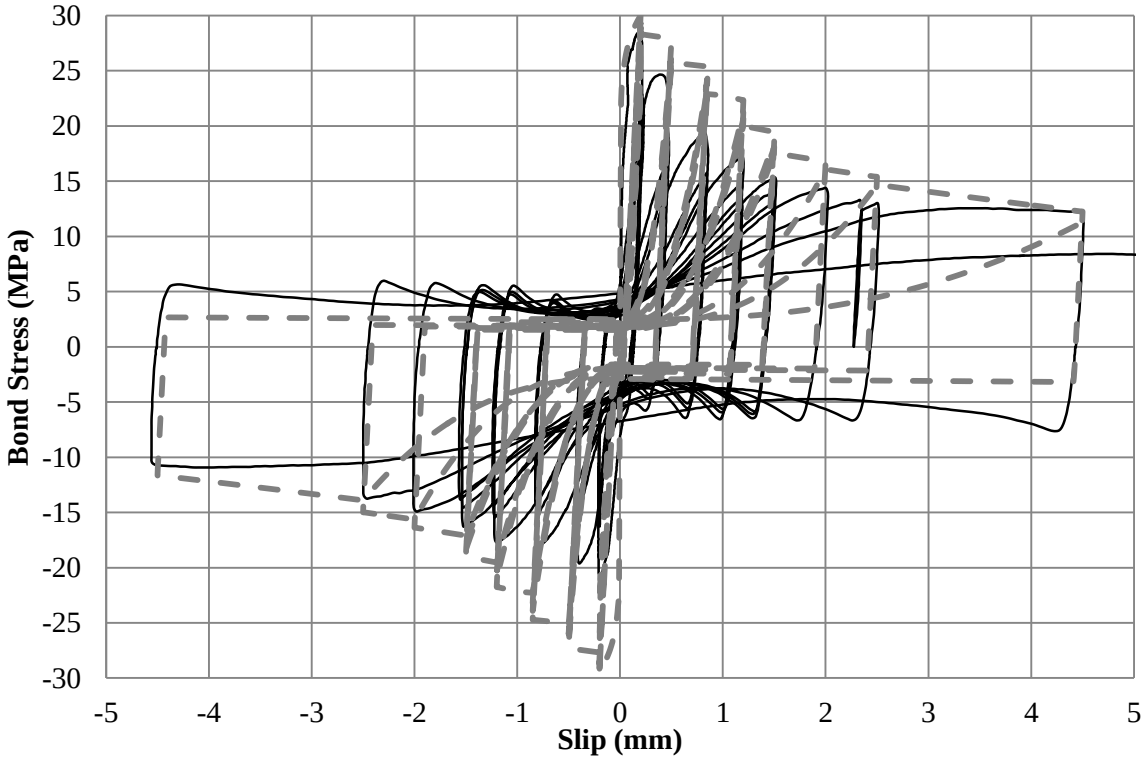

Figure H-0-2: Experimental/Numerical Comparison for 0.6% corrosion.

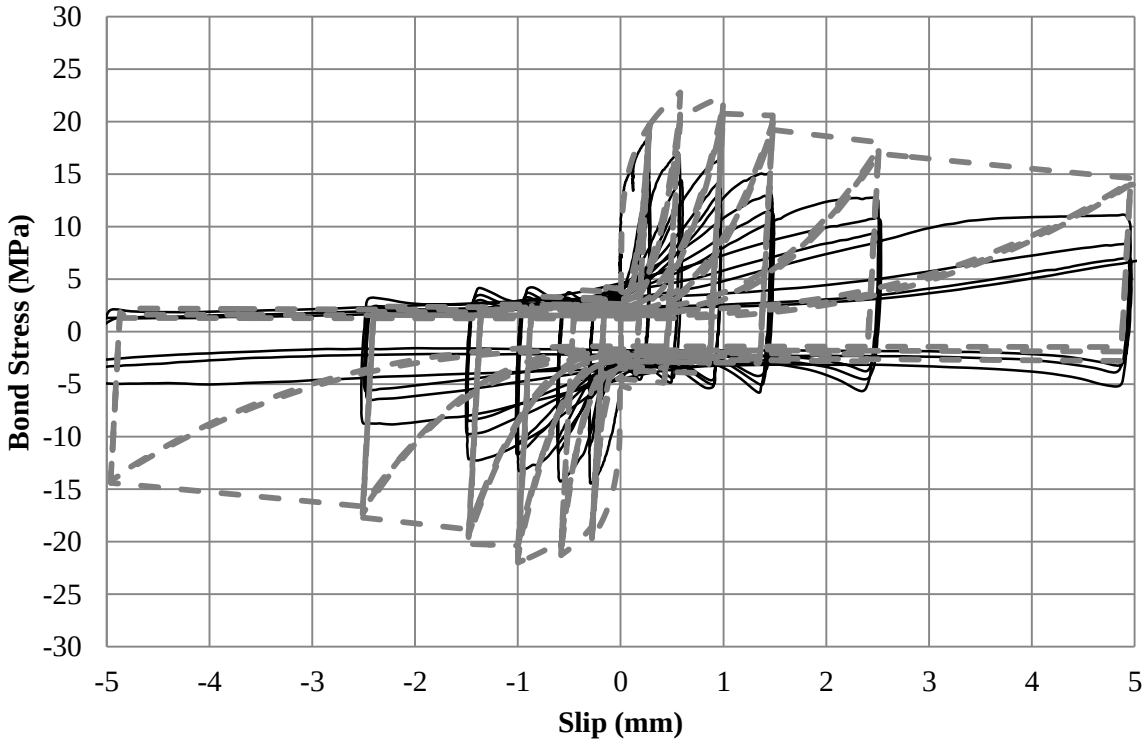

Figure H-0-3: Experimental/Numerical Comparison for 4.6% corrosion.

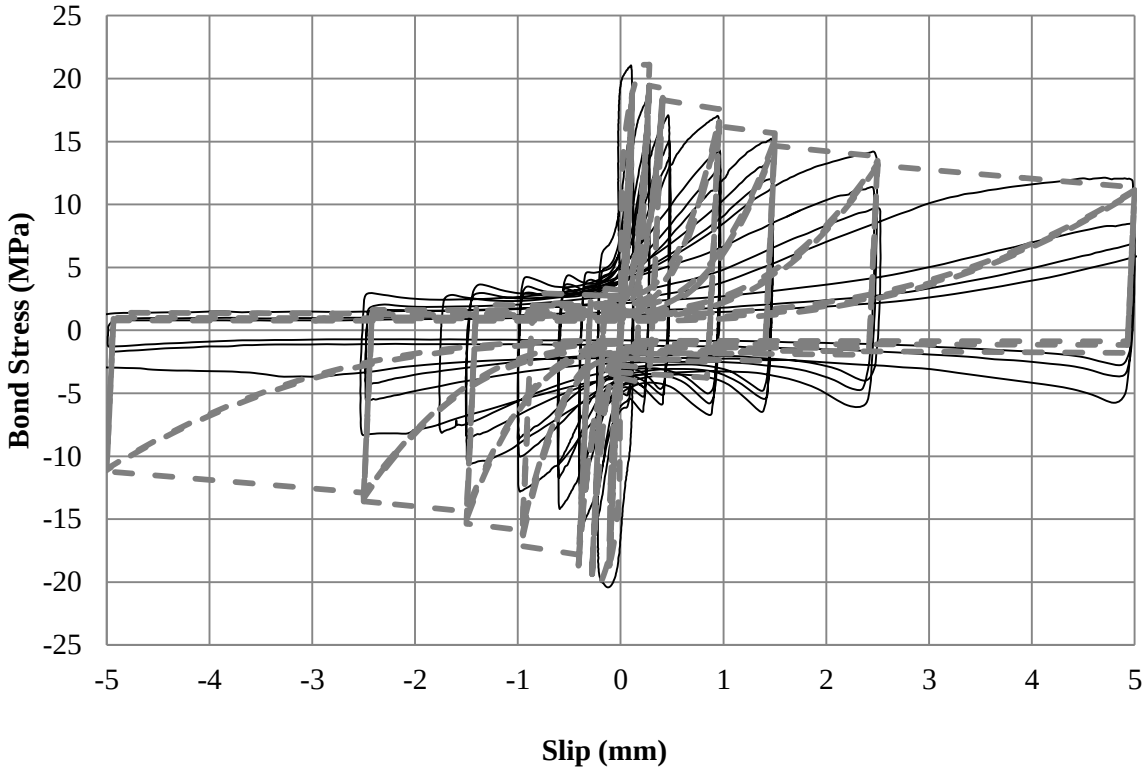

Figure H-0-4: Experimental/Numerical Comparison for 7.0% corrosion.

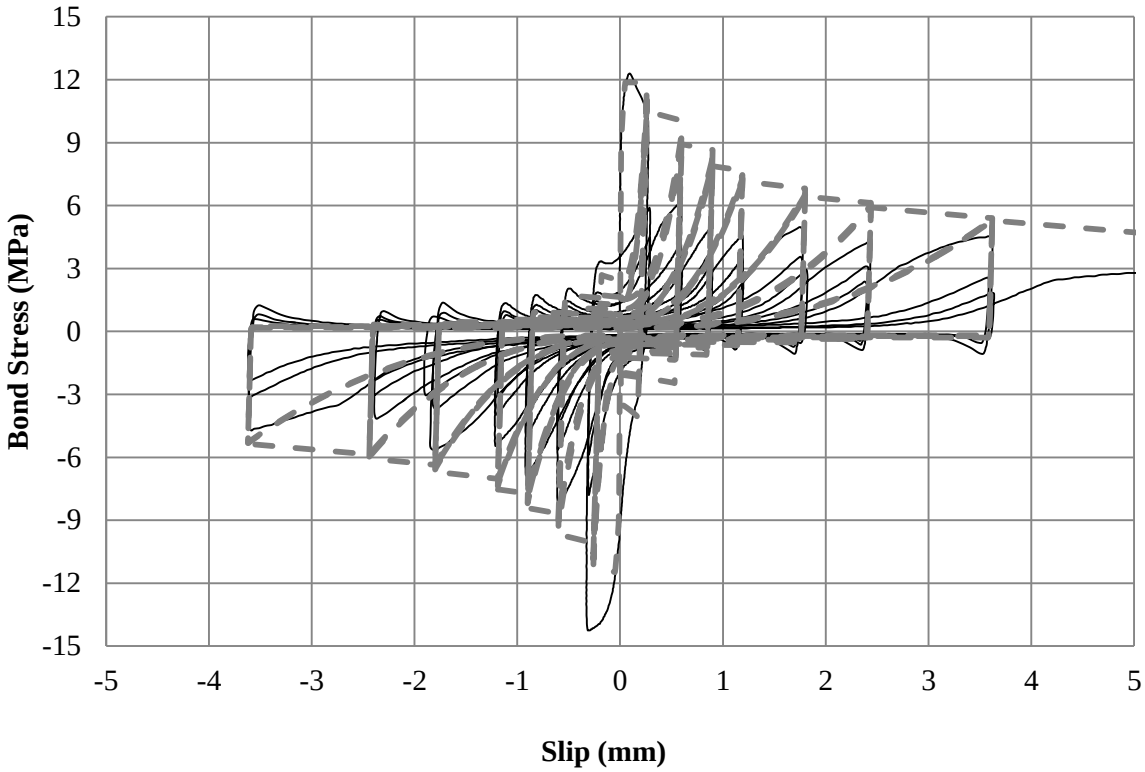

Figure H-0-5: Experimental/Numerical Comparison for 14.6% corrosion.

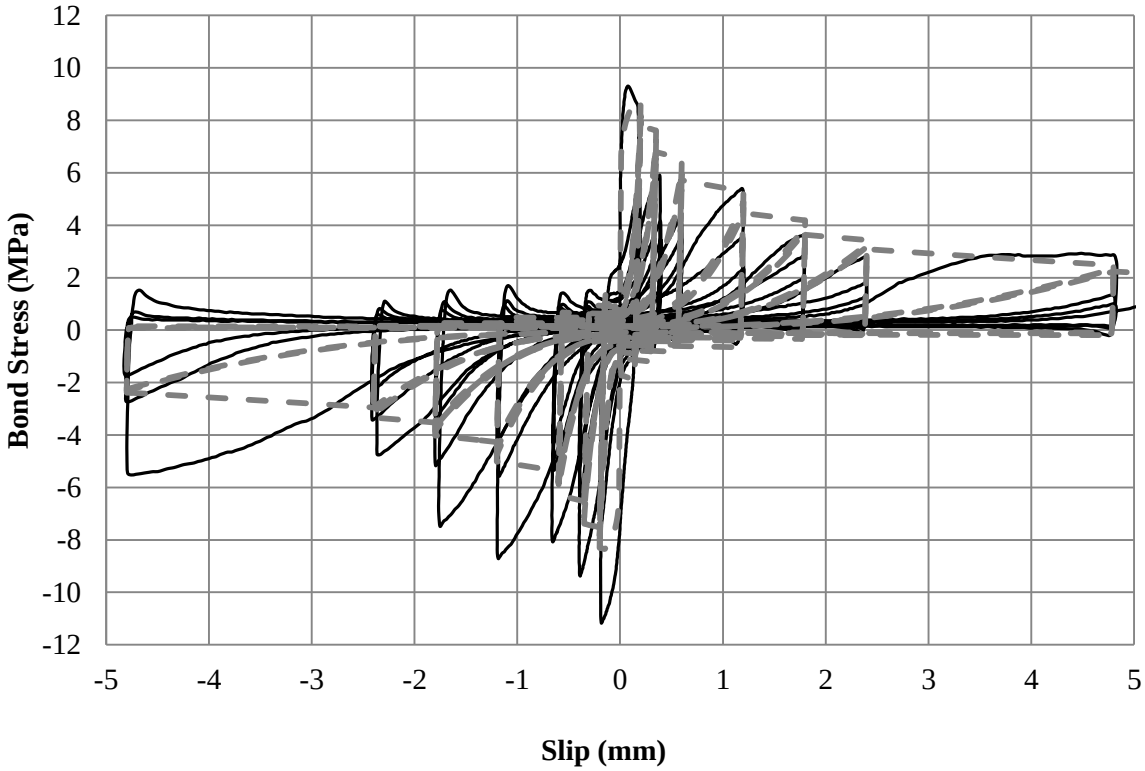

Figure H-0-6: Experimental/Numerical Comparison for 18.6% corrosion.

Appendix I: Cyclic Multi-Spring Behaviour (400 × 400 Column)

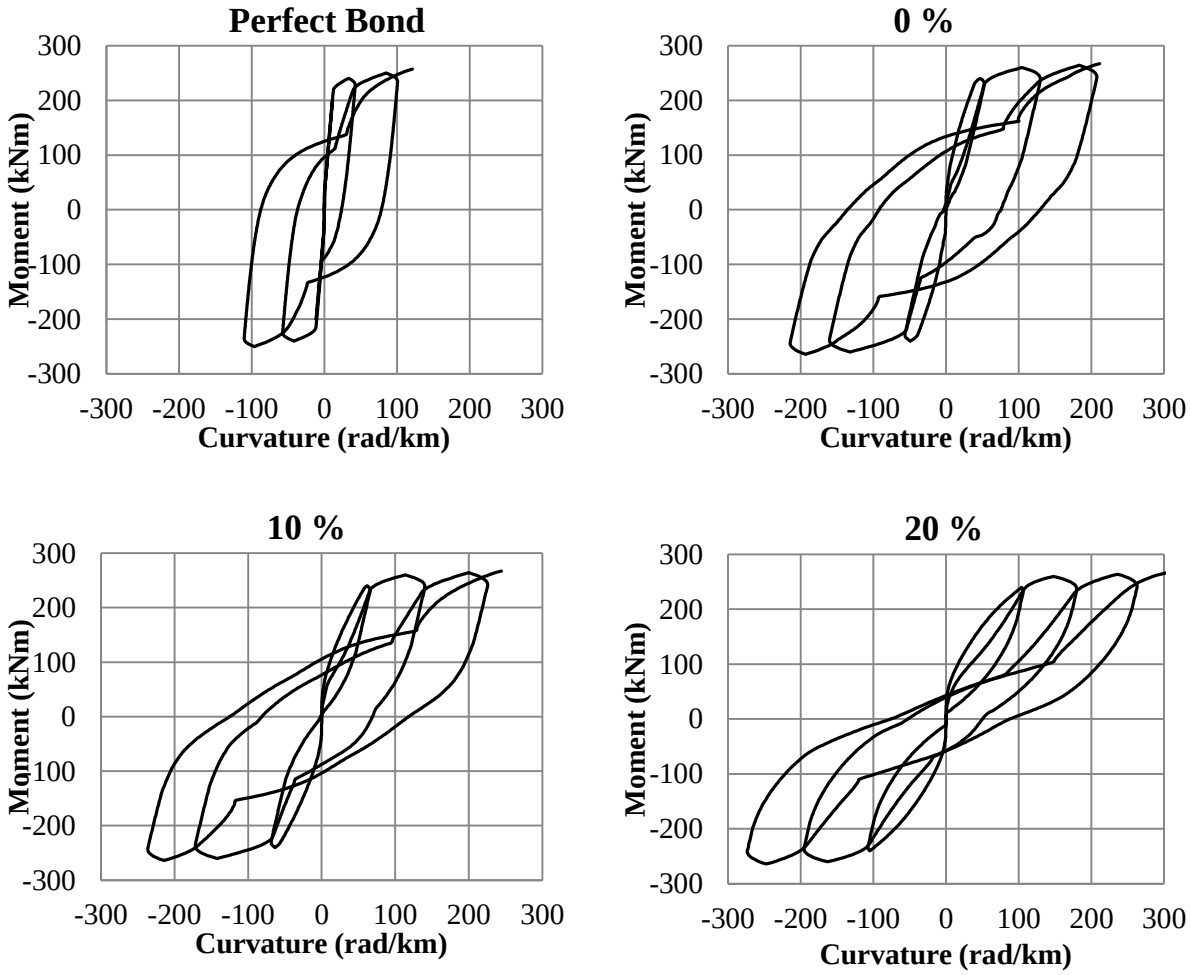

Figure I-0-1: Degraded moment-curvature hysteretic behaviour of 400mm × 400mm multi-spring model for bond degradation between 0% and 20 % corrosion using perfectly confined conditions.

Appendix J: Cyclic Multi-Spring Behaviour (New Brighton Pier)

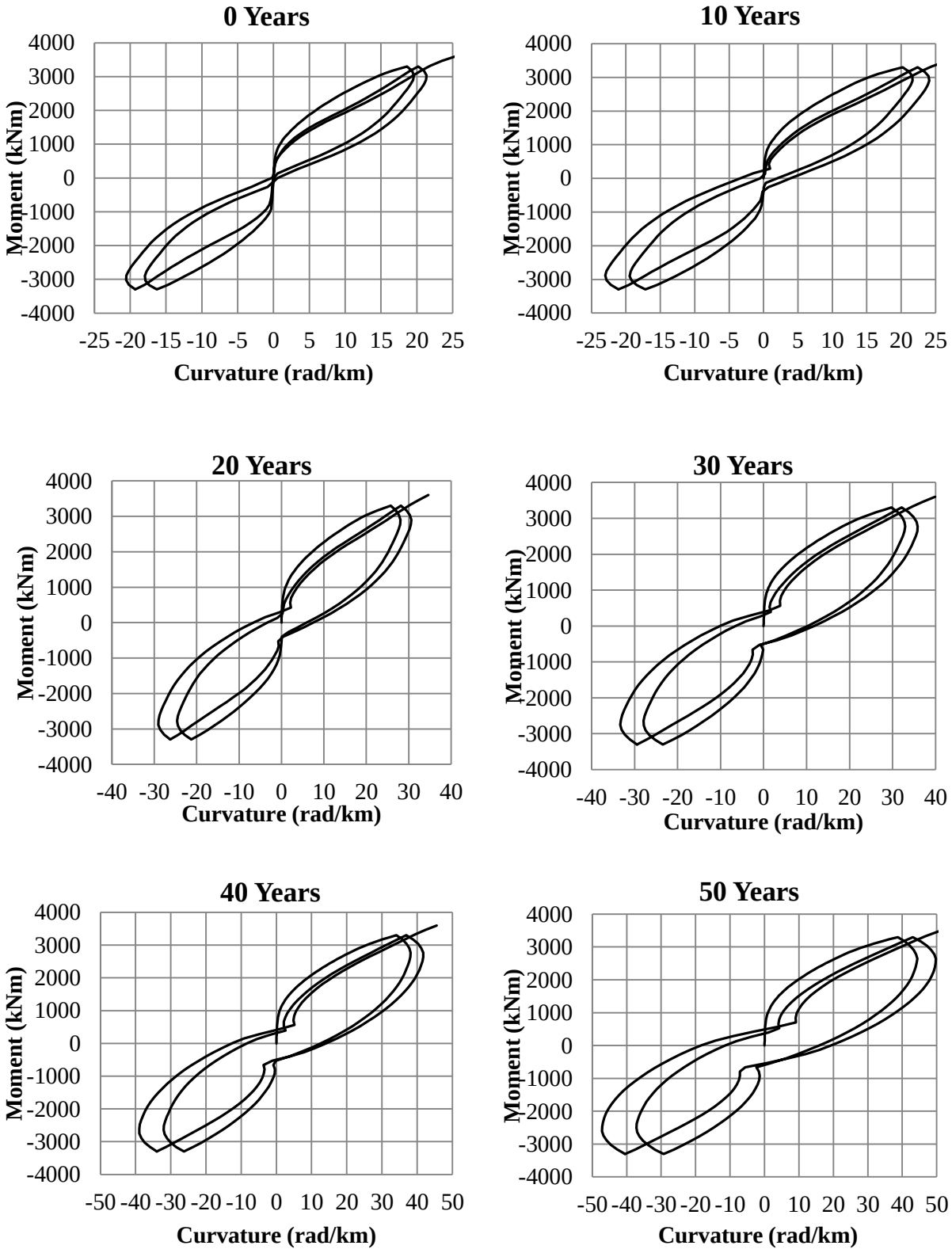

Figure J-0-1: Degraded moment-curvature hysteretic behaviour of the New Brighton Pier from multi-spring modelling over simulated 50 Years.